Some Nuclear Physics Aspects of the r-process Nucleosynthesis

Stephane Goriely

Wolfson College

A thesis submitted for the degree of

Doctor of Philosophy in the

University of Oxford

Trinity Term, 1991

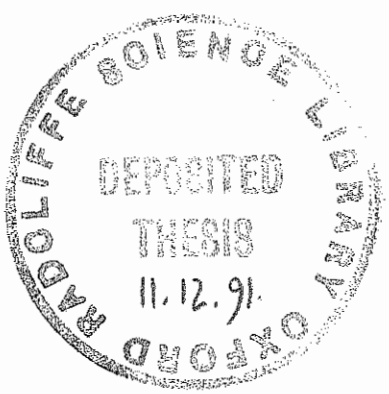

Some Nuclear Physics Aspects of the r-process Nucleosynthesis

Stephane Goriely

Wolfson College

Thesis submitted for the degree of Doctor of Philosophy
in the University of Oxford

Trinity Term, 1991

Abstract

Two aspects of the nuclear physics involved in calculations of the rapid neutron capture process (or r-process) are studied in an attempt to put the nucleosynthesis predictions on safer and sounder grounds. In considering the first aspect, we investigate the influence of nuclear mass models on the r-abundance distribution in the framework of the standard r-process model. Here the first r-process calculations, making use of a non-droplet type mass formulae, are performed. The r-abundance distribution obtained with the mass table based on the microscopic Extended Thomas-Fermi plus Strutinsky Integral method shows significant differences from the one using a droplet mass formula. The impact of the nuclear mass model on the final r-abundance profile is analysed in detail.

With the second aspect, another quantity of fundamental importance for the r-process calculations, the nuclear level density, is examined. In the framework of the statistical model, the analytical approximation to the spin-dependent level density is improved by introducing in a new way the shell and pairing effects. The semi-classical approximation to the single-particle state density is used to describe the influence of the nuclear shell structure on the energy dependence as well as on the spin distribution of the level density. To take the pairing effects on the level density into account, simple and accurate analytical expressions are derived from the BCS formulation. The new analytical level density formula appears to be in close agreement with both numerical shell-model calculations and experimental data. To prove the reliability of the adopted semi-classical shell description, a new formulation of the ground-state shell correction energy and of the ground-state pairing gaps is proposed and shown to give a good fit to the experimental data.

ACKNOWLEDGEMENTS

I am very grateful to my supervisor, Dr. P.E. Hodgson, for guiding and helping me over the last two years. He has always shown interest in my research and has been available to help and advise.

I would also like to thank many people who have helped me in one way or another to complete the present work, namely M. Arnould, M. Rayet, K. Takahashi, D. Brink, M. Pearson and Peter.

Lastly, I am grateful for the encouragement of those workers in the shadows who make things worthwhile. They know who they are.

CONTENTS

Some Nuclear Physics Aspects of the r-process Nucleosynthesis

Introduction: The r-process Nucleosynthesis

1. Nucleosynthesis of heavy elements by neutron capture

One of the major question Astrophysics has been trying to answer concerns the interpretation of the present composition of the Universe and its various constituents. The aim of nucleosynthesis models is to identify the diverse processes by which the different elements observed in nature could be synthesized. To that end, nucleosynthesis models have called for two broad classes of nuclear reactions: non-thermal nuclear transmutations (referred to as spallation reactions) and thermonuclear processes. The former are thought to occur in the interstellar medium (through interactions with galactic cosmic rays) and at the surface or surroundings of stars (through interactions with stellar energetic particles). Some models also show that spallation reactions could have taken place at a cosmological or pregalactic level. The thermonuclear processes, on the contrary, are known to occur inside stars during the galactic era as well as at a "primordial" level (Big Bang). Primordial nucleosynthesis is generally considered to be responsible for the production of the lightest nuclides, such as H, D, ^{3}He, ^{4}He and ^{7}Li; while spallation reactions formed ^{6}Li, (most of) ^{7}Li, Be and B. Yet it is now widely recognized that the origin of the vast majority, if not all, of the elements in nature with mass numbers $A \geq 12$ can be explained through thermonuclear processes in stars, either during their non-explosive evolutionary phases or in supernova explosions. Quiescent as well as explosive charged-particle nucleosynthesis has succeeded in explaining the production of most

of the nuclides from ^{12}C to the iron group. Yet it failed to explain the origin of the so-called heavy elements, i.e. the nuclei more massive than the iron-group nuclei. Because the Coulomb barrier has to be overcome, the lifetime of a heavy nucleus against charged-particle reactions increases rapidly with increasing nuclear charge, soon exceeding the lifetime of the corresponding epoch of stellar evolution, so that at "moderate" temperatures no nuclear statistical equilibrium can be attained. At higher temperatures, however, a nuclear equilibrium can be reached, but these temperatures favor the production of the iron group nuclei characterized by the maximum binding energy per nucleon and this is more likely to occur either by fusion reactions on light nuclei or by photodisintegration of heavier nuclei. In both cases, however, no elements more massive than the iron-group nuclei can be produced by means of charged-particle processes.

Nucleosynthesis models, then, predict that the production of nuclei, heavier than the iron-group, must involve neutron capture reaction mechanisms for which there is no Coulomb repulsion. Heavy elements could, indeed, be synthesized at relatively low temperatures by exposing lighter nuclei to a neutron flux. The patterns of heavy element abundances characteristic of solar system matter have substantiated those models thanks to the strong correlation found between the observed abundance peaks and the nuclear systematics of neutron capture.

More precisely, the abundances of the different nuclear species seem to suggest that two quite distinct neutron capture processes contribute to the synthesis of heavy elements: the so-called s-process and the so-called r-process.†

The distinction between the s- and r-process is made on the basis of the relative lifetimes for neutron captures (τ_n) and beta decays (τ_β):

---

† A third process, known as the p-process, is currently used to explain the origin of the heavy proton-rich nuclei (known as p-nuclei) observed in the bulk solar system material. The p-nuclei are on the average a factor of 10^2–10^3 less abundant than the s- and r-isotopes. However, this process, which remains poorly understood will not be discussed in the present work.

(i) the s-process

The s-(for slow) process results from the production of neutrons and their captures by preexisting nuclei (mainly iron, assumed to be formed in previous stellar burning stages) on timescales long compared with the beta-decay lifetimes. If $\tau_n > \tau_\beta$, the β-unstable nuclei near the valley of β-stability decay before capturing a neutron. Therefore, the short β-decay timescales—short relative to the neutron capture timescales—constrain the flow to the vicinity of the valley of stability, as shown in Figure 1. For some nuclides, however, neutron capture may compete with β-decays, leading to local branches along the main path. The small neutron capture cross-section of closed shell nuclei at N=50, 82 and 126 forms bottle necks along the s-process path and gives rise to the pronounced abundance peaks at ^{88}Sr, ^{138}Ba and ^{208}Pb (see Fig. 2). Typical s-process flow paths are obtained for neutron densities N_n in the approximate $10^7 \mathrm{cm}^{-3} \leq N_n \leq 10^9 \mathrm{cm}^{-3}$ range.

The discovery of technetium lines in the atmosphere of a red-giant star by Merrill in 1952 (Merrill, 1952) demonstrates conclusively that the formation of heavy elements by neutron capture occurs in stars and is a continuing process (technetium is an unstable element with a half-life of less than a million years). However, free neutrons are not normally thought to be abundant in the major phases of nuclear burning. It now appears that neutrons are liberated mainly by secondary reactions (i.e. reactions which do not play an important role in the energy generation of the star), like $^{13}\mathrm{C}(\alpha,\mathrm{n})^{16}\mathrm{O}$ and $^{22}\mathrm{Ne}(\alpha,\mathrm{n})^{25}\mathrm{Mg}$ during the hydrostatic He or C burning phases. The precise identification of the astrophysical sites where these neutron producing reactions can take place is the other key aspect of the s-process modeling. Three main astrophysical sites have been shown to be good candidates for the s-process:

1. central He-burning in massive stars ($M \geq 10 M_\odot$) (e.g. Prantzos et al., 1987, 1988);
2. central C-burning in massive stars (Arcoragi et al., 1991);
3. shell He-burning in highly evolved (asymptotic giant branch) low and intermediate mass

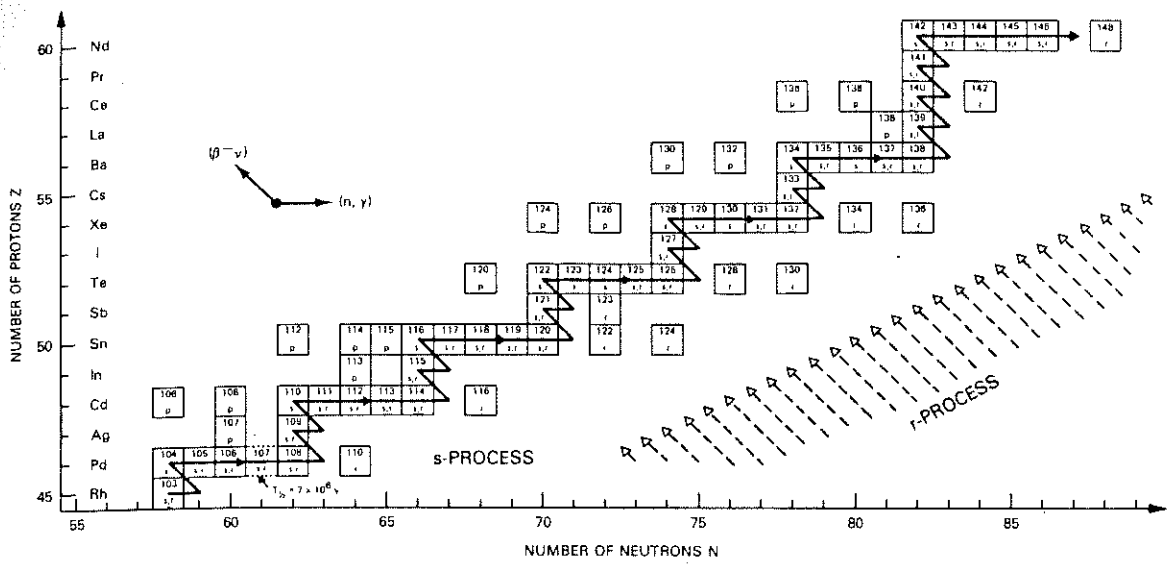

Figure 1. A section of the chart of nuclides and the s-process path (full line) through the elements in this mass region. The stable nuclei are represented by squares and their s-, r-, or p-character is indicated. Neutron-rich isotopes (r) formed by the r-process are bypassed by the s-process path which is constrained to the valley of stability. The r-process nuclei are the end products of an isobaric β-decay chain—the flow of which is indicated by the dashed arrows—from neutron-rich progenitors produced in an intense neutron flux (from Rolfs and Rodney, 1988).

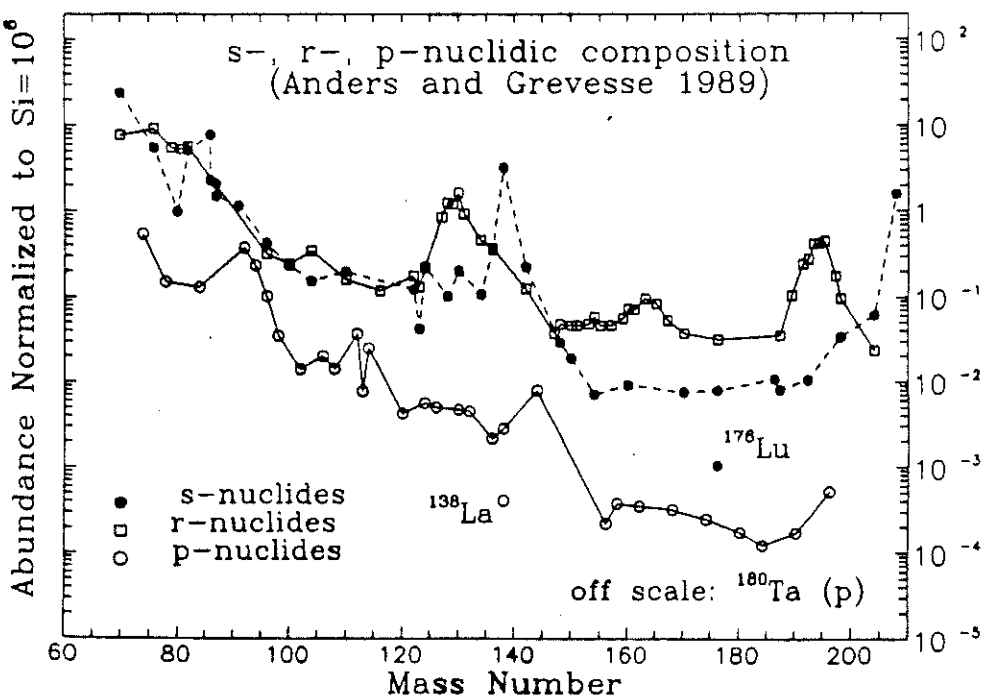

Figure 2. The solar system abundances of the s-, p- and r-nuclei resulting from the splitting of the solar system composition. The solar system abundances have been derived from Anders and Grevesse (1989). The nuclei which have a mixed sr-character are not shown. The abundances are normalized in such a way that the abundance of Si has the value 10^6 (from Arnould and Rayet, 1990).

($M \leq 10 M_{\odot}$) stars (e.g. Howard et al., 1986; Jorissen and Arnould, 1986, 1989). However, it has to be emphasized that the astrophysical scenarios underlying the s-process nucleosynthesis are still quite uncertain and that many uncertainties in the nuclear physics involved also remain. Despite those difficulties, the s-process is by far the best understood mechanism for the production of nuclides heavier than iron.

In particular, quite good fits to the solar system s-nuclei abundance curve have been obtained by means of parametrized models requiring a specific combination of temperatures, densities and superposition of neutron exposures (e.g. Käppeler et al., 1989). Even if the astrophysical models still cannot reproduce the conditions required for achieving such a fit, this parametric approach has the virtue of enabling a separation between the contribution of the s- and r- processes to the production of each isotope. After the s-abundance curve has been defined for pure s-process nuclei, it can be used to determine the s-process contributions for all other sr-nuclei and consequently to provide a more or less reliable estimate of the r-process abundance contributions.

Details of the nuclear physics and astrophysics aspects of the s-process can be found in Bao and Käppeler (1987), Käppeler et al. (1989) or Prantzos (1989).

(ii) the r-process

In contrast to the s-process, the r-(for rapid) process assumes that neutron captures are more rapid than β-decays, so that successive neutron captures will proceed into the neutron-rich regions well off the β-valley of stability, before any β-decay can take place. This process encounters nuclei with decreasing neutron binding energies. At a certain point, the (γ,n) photodisintegration becomes fast enough to compete with the slowing down (n,γ) reactions. In such conditions, a (n,γ)-(γ,n) equilibrium (at least in a certain range of values for the temperature and neutron density) will be reached for each isotopic chain. Once such an isotopic equilibrium is established, the abundance flow can go from one isotopic chain to the next by β-decays and so drive material to higher and

higher Z values. As in the s-process, the particularly low neutron separation energy S_n just past a neutron magic number hinders the material flow to proceed to more neutron-rich species, so that β-decays drive the material closer to the valley of stability following a path with increasing Z at practically constant N. Consequently, the β-decays tend to slow down the nuclear flow and some material accumulates at nuclei with a magic number of neutrons. However, when the path gets closer to the stability line, the neutron binding energy finally becomes large enough to allow the process to break through the bottleneck and to resume the normal sequence of (n,γ)-(γ,n) events, until a new neutron magic number is reached and then passed. This accumulation of matter at neutron closed shell nuclei is held responsible for the observed peaks in the r-nuclei abundance distribution, as displayed in Fig. 2.

The nuclear flow towards increasing Z values is generally believed to be stopped by neutron-induced fission as well as β-delayed fission which lead to a cycling back of a portion of the material to lower Z values. After a certain time τ, the neutron irradiation is thought to disappear rapidly so that all nuclear reactions are suddenly frozen. At this stage, mainly β-decays, but also spontaneous and β-delayed fissions and single or multiple β-delayed neutron emissions, drive the neutron-rich matter towards the valley of stability. A typical r-process nuclear flow during the pre-freezing regime is shown in Fig. 3. A schematic post-freezing cascade flow is represented in Fig. 2 by the isobaric β-decay chains pouring down to the valley of stability.

The r-process has proved to be an important nucleosynthesis mechanism for a number of reasons:

1. it is the nucleosynthesis mechanism that produces approximately one half of the $A > 60$ stable nuclei observed in nature;

2. it is held responsible for the production of the long-lived nucleocosmochronometers relevant in the evaluation of the age of our galaxy, such as ^{232}Th, ^{238}U or ^{235}U;

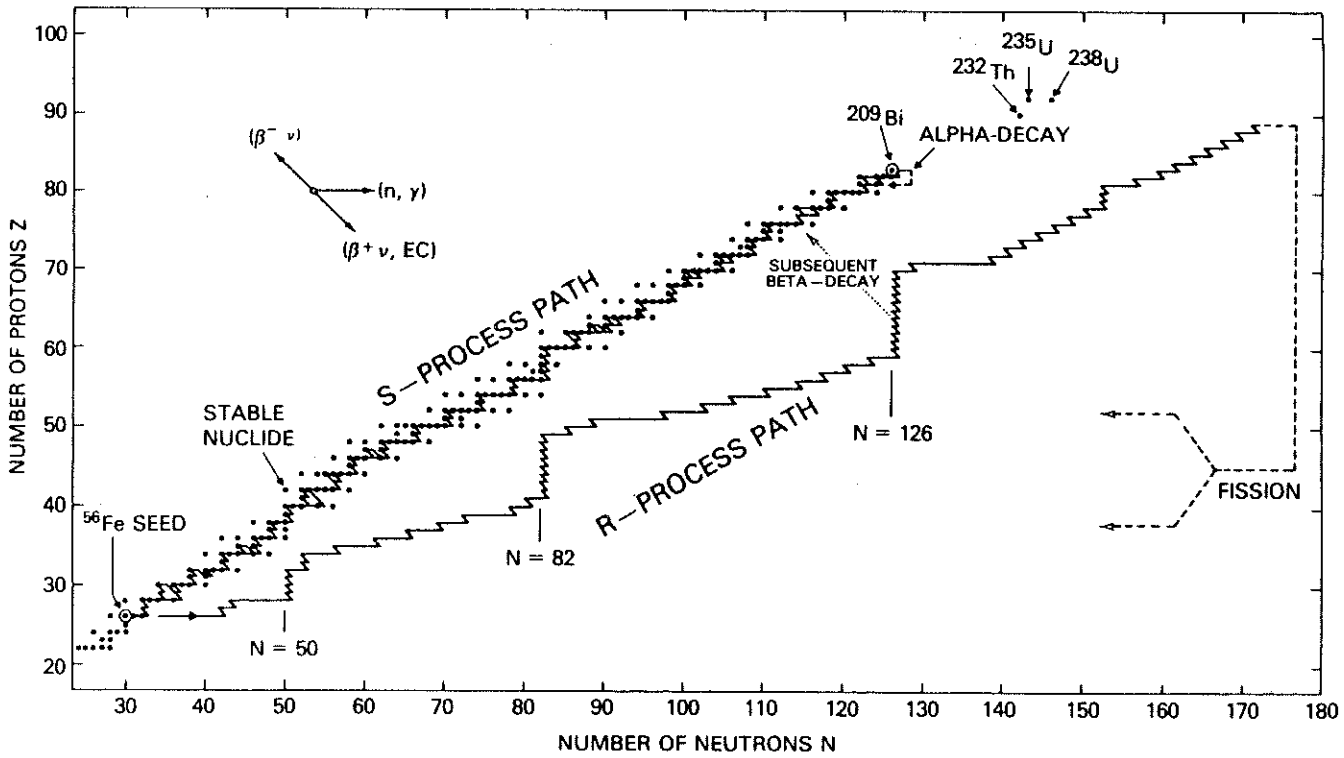

Figure 3. Neutron-capture paths for the s-process and the r-process in the (N,Z)-plane. The s-process follows a path along the stability line and terminates finally above ^{209}Bi via α-decay. The r-process path drives the nuclear matter far to the neutron-rich side of the stability line until β-delayed fission and neutron-induced fission occur (from Rolfs and Rodney, 1988).

3. it provides an interesting probe of the astrophysical conditions in explosive events which contain highly neutronized matter.

The currently available models for the r-process are, however, far from being firmly established either from the astrophysical or from the nuclear physics point of view.

2. Astrophysical scenarios proposed for the r-process

Unlike the s-process, which is usually associated with the earlier, largely hydrostatic phases of stellar evolution, the r-process is believed to develop in explosive environments, like supernovae. One of the conditions required for the r-process is high neutron densities to drive the heavy seed nuclei (essentially iron nuclei) into the very neutron rich region of the chart of nuclides, between the valley of stability and the neutron drip line. The high temperatures as well as the very short timescales (typically of the order of 1 second) associated with such high neutron fluxes have for some times suggested an explosive astrophysical origin of the r-process.

Proposed models for r-process nucleosynthesis are usually grouped into two broad classes:

- those involving the expansion and cooling of neutron rich matter;
- those concerned with the passage of supernova shock waves through the stellar carbon and helium burning layers.

Originally, the r-process was thought to take place at the base of the material ejected during a type II supernova explosion—i.e. just outside the supernova residue (Burbidge et al., 1957; Seeger et al., 1965; Hillebrandt et al., 1976). These models are, however, dependent on the still unsolved type II supernova explosion mechanism and are, therefore, at best provisional particularly because of the uncertainties about the description of the layers located at the mass cut between the supernova residue and remnant. Only when reliable predictions of the astrophysical conditions (like temperature, density and initial abundance distribution) at the mass cut can be made, will it be possible to put the r-process nucleosynthesis calculation in supernovae environment on more

reliable ground. Moreover, none of the currently available predictions are yet able to reproduce the solar system r-nuclei abundance under physically plausible conditions.

The problems associated with the supernova models led to other suggestions for r-process scenarios, such as the neutronized "jets" ejected from the collapse of rotating and/or magnetized stellar cores (Leblanc and Wilson, 1970; Symbalisty et al., 1985). Rotation of the supernova core may cause jet-like ejections of neutron-rich material at its pole from the core into the stellar envelope. Once again the very large rotation rates, as well as the extremely high magnetic fields required to eject the r-process material from the core, raise the question of the possible efficiency of such a mechanism. Furthermore, the actual composition of the ejected matter remains to be determined. Recent developments in supernova core-collapse theory have also suggested the so-called hot bubbles as a plausible site for the r-process nucleosynthesis (Mayle and Wilson, 1988). The interesting scenario of the hot bubbles might lead to the production of heavy elements as well as to a successful supernova explosion, via late-time neutrino heating. The modelisation of such sites remains, however, problematic and requires further studies.

More exotic astrophysical sites for the r-process have also been proposed, such as the interaction between a neutron star and a black hole in a close binary system (Lattimer and Schramm, 1974, 1976) or between two neutron stars (Symbalisty and Schramm, 1982). These models suffer from many difficulties and require further investigation to check their validity as sites for the r-process.

Because of the numerous difficulties encountered by supernova core models, other environments have been suggested like the exploding He-rich layers of massive stars (Thielemann et al., 1979, for example). As a result of the shock wave, high temperatures and densities can lead to an important neutron production through (α,n) reactions, such as ^{22}Ne(α,n)^{25}Mg, ^{13}C(α,n)^{16}O or ^{18}O(α,n)^{21}Ne. But this so-called He-driven r-process is also problematic. In particular, the neu-

tron flux produced in the He-zone during the explosion is lower than that produced in the classical r-process model (where typically $N_n \gtrsim 10^{20}\mathrm{cm}^{-3}$). This too low neutron concentration allows a competition between β-decays and neutron captures. The study of the r-process synthesis in such conditions requires techniques which are different from those commonly used in the so-called canonical r-process model (see Chapter I.1). The fuller theoretical understanding of this intermediate process, generally called the n-process (because it is characterized by an intermediate neutron density between the one required for an s-process and an r-process) is impeded not only by astrophysical difficulties but also by nuclear physics input data especially about the neutron-rich region the reliability of which is far from being established (see Section 4). Moreover, the most consistent studies (Thielemann et al., 1979; Cowan et al., 1983) lead to heavy elements abundances that do not reproduce the solar system distribution, mainly because of the lack of available neutrons to produce the total solar system content of r-nuclei.

Other similar sites have been proposed, such as C-rich zones of a massive star undergoing a supernova explosion or the He-core of low mass ($M \leq 2M_\odot$) stars, in which He starts burning more or less violently (He-flash). The production of some r-nuclei in those astrophysical sites cannot be excluded, but appears unlikely to account for the bulk solar system r-process, at least at the present stage of modelisation.

In conclusion, the astrophysical sites of the r-process, at least the ones responsible for the bulk solar system r-abundances, are still unknown: none of the postulated scenarios are unproblematic. At the present time, too little is known about the general set of initial conditions (like temperature, density, neutron sources, chemical composition) required to produce the r-process nuclei and to locate the r-process at a specific site. The remaining uncertainties on the nuclear physics treatment of the r-process also hinder a more plausible determination of the astrophysical site(s).

3. The r-process calculation

Ideally, the r-process should be considered as a dynamical process, taking place in a specific astrophysical environment. A full nucleosynthesis network should, therefore, be coupled with the system of equations used to describe the astrophysical conditions (mainly the evolution over time of the temperature, density and neutron abundance) in which the r-process develops. Yet such a task is often too complex to be practically feasible and other techniques are generally used.

One of these techniques separates the dynamical process into two parts. The first one follows the time dependence of the thermodynamical quantities corresponding to the chosen site as well as the abundances of a few nuclei which will be relevant to a later r-process calculation. This includes for example, for an He-driven r-process, a charged-particle network responsible for the production of neutrons, particularly as a result of (α,n) reactions on light nuclei. Having determined the temperature, total density and neutron density as a function of time, the abundances of the heavy nuclei can be evaluated by means of a second network, as described later. This procedure, however, does not allow any feedback (Hillebrandt et al., 1976) between the two networks and might introduce uncertainties concerning the mass conservation or the precise number of neutrons captured at any given time. It also assumes that the astrophysical conditions are sufficiently well known to be properly modelized.

This technique has been widely used to describe the dynamical r-process during the passage of supernova shock waves through the carbon and helium shells (e.g. Thielemann et al., 1979). More sophisticated calculations have merged the two separate reaction networks in order to couple stellar evolution to nucleosynthesis (Cowan et al., 1983). Such a procedure, even if more consistent, still suffers from the numerous astrophysical uncertainties as well as the nuclear physics ones and still raises the question of its plausibility. These models will not be discussed in the present work.

Since so many unknowns remain, other r-process calculations have performed parametric stud-

ies by using many different values of the parameters such as temperature, density, chemical composition and characteristic timescales. This approach has the advantage of being independent of the still inconsistent astrophysical models which are meant to describe the r-process sites and has helped to give information about the plausible astrophysical sites. The range of parameters that reproduced the observed r-process abundance distribution could be compared with those evaluated for each of the proposed sites. In so doing, the number of possible sites might be reduced. However, to explore the large parameter space will require a considerable amount of computer time. This approach, even if still subject to the nuclear physics uncertainties, seems more appropriate to the r-process calculation because it is more manageable and because it avoids the remaining astrophysical difficulties. The range of initial data should, however, be chosen so that the physical conditions remain plausible from an astrophysical point of view. Such an approach will be followed in this work since we want to deal with the nuclear physics uncertainties only.

The problem raised by the r-process calculations clearly appears to be two-sided. On the one hand, phenomenological approaches with simple models (like the so-called canonical model) have been successful in providing some ideas about the astrophysical conditions most appropriate for explaining the observed solar system abundance distribution. However, these conditions still remain astrophysically unrealistic because no astrophysical environments that fulfill such optimal conditions have been found yet. On the other hand, more realistic astrophysical sites which might lead to r-process nucleosynthesis have been considered, but the agreement between the computed and solar abundances is too poor to allow definite conclusions on the validity of such sites.

A nuclear reaction network described by a system of coupled differential equations is used to calculate the changes in abundance of the heavy nuclei as a result of the r-process. The network includes all strong, electromagnetic and weak interactions governing the nuclear transformations of all nuclei with $Z \geq Z_0$ and situated between the valley of stability and the neutron drip line.

Here, Z_0 describes the astrophysical boundary conditions and depends on the site in which the r-process occurs. Although the liberated neutrons can be captured by any element present in the considered site, most of them will be captured by the iron-group nuclei, which correspond to the last major abundance peak synthesized without the aid of neutron capture. Therefore, most of the parametric r-process calculations consider that the seed nuclei are the iron-group nuclei assumed to have been produced in the previous stellar generations.

The chosen set of nuclear species are coupled by a set of reactions which involves neutron captures, photodisintegrations, β-decays, fissions and β-delayed processes. The rate of change in the abundance of the nucleus (Z, A) can be written as:

$$\begin{aligned}\frac{dN(Z,A)}{dt} &= N_n N(Z,A-1) < \sigma v >_{Z,A-1} + N(Z,A+1)\lambda_{\gamma,n}^{Z,A+1} + N(Z-1,A)\lambda_{\beta}^{Z-1,A} \\ &- N(Z,A)\left[N_n < \sigma v >_{Z,A} + \lambda_{\beta}^{Z,A} + \lambda_{\gamma,n}^{Z,A} + \lambda_{n}^{Z,A} + \lambda_{2n}^{Z,A} + \lambda_{3n}^{Z,A} + \lambda_{f}^{Z,A} + \lambda_{\beta f}^{Z,A}\right] \\ &+ N(Z-1,A+1)\lambda_{n}^{Z-1,A+1} + N(Z-1,A+2)\lambda_{2n}^{Z-1,A+2} + N(Z-1,A+3)\lambda_{3n}^{Z-1,A+3} \\ &+ \sum_f q_{Z_f,A_f}(Z,A)\left[\lambda_f^{Z_f,A_f} N(Z_f,A_f) + \lambda_{\beta f}^{Z_f-1,A_f} N(Z_f-1,A_f) + \lambda_{nf}^{Z_f,A_f-1} N(Z_f,A_f-1)\right]\end{aligned} \quad (1)$$

where $N(Z, A)$ is the number density of the nucleus (Z, A), N_n is the neutron number density, $< \sigma v >_{Z,A}$ is the Maxwellian-averaged (n,γ) reaction rate of nucleus (Z, A), $\lambda_{\gamma,n}^{Z,A}$ is the photodisintegration rate of nucleus (Z, A), $\lambda_{\beta}^{Z,A}$ is the β-decay rate of nucleus (Z, A) and $\lambda_{kn}^{Z,A}$ is the rate of β-decay followed by the emission of k delayed neutrons. The last terms reflect the feedback due to fissions of all synthesized heavy elements. The factor $q_{Z_f,A_f}(Z, A)$ is the probability for the fissioning nucleus (Z_f, A_f) at rate $\lambda_f^{Z_f,A_f}$ to produce a (Z, A)-fragment; the fission of nucleus (Z_f, A_f) can also be obtained by delayed fission at rate $\lambda_{\beta f}^{Z_f-1,A_f}$ of nucleus $(Z_f - 1, A_f)$ or by neutron induced fission at rate $\lambda_{nf}^{Z_f,A_f-1}$ of nucleus $(Z_f, A_f - 1)$. The possible α-decays have been neglected in expression (1). Fission of nuclei with $Z < 80$ does not play any role, so that neutron captures, photodisintegration and β-decays are predominant in expression (1) for those nuclei.

The complexity of such a reaction network can be avoided by simplifying assumptions, such as

the (n,γ)-(γ,n) equilibrium approximation. It constitutes the simplest form of the r-process model (see Chapter I.1). Another approximation, known as the steady flow approximation, has also been widely used over the last decade (see for example, Cameron et al., 1983a), but will not be discussed in this work.

4. Nuclear Physics of the r-process

In addition to the astrophysical difficulties, as discussed in Section 2 and 3, there are major nuclear physics problems with the r-process. To describe the neutron capture by the seed nuclei, and the consequent production of heavy nuclei, a detailed reaction network, as given by expression (1) and including all nuclei from the β-stability valley to the first neutron drip line is required. We are, therefore, left with the formidable task of providing the required nuclear properties of thousands of (mostly unknown) neutron-rich nuclei. Those properties include neutron capture cross-sections, photodisintegration rates, β-decay half-lives, rates of β-delayed single and multiple neutron emission, α-decay half-lives, fission barriers and β-delayed as well as neutron-induced fission probabilities. Given the lack of experimental data on very heavy neutron-rich nuclei, theoretical studies of nuclear properties in this region of the nuclides chart are of fundamental importance for the r-process calculations.

Furthermore, in most of the cases, the nuclear physics models still suffer from many uncertainties and sometimes only crude treatments are available. For example, the neutron capture cross-section calculation of nuclei with small neutron binding energies still raises many difficulties. Compromises also have to be made between using the best available theories in all their complexities and the need to calculate a great number of cases. As already emphasized, the r-process calculations involve some thousands of nuclei. Limitations due to the large amount of computer time (as well as human time) required to predict theoretically so many nuclear properties often render some of the most reliable studies of no practical use. Yet we should stress at this point that

such reliable, but complex models, might be of great value as soon as the final results are highly sensitive to the nuclear properties of specific key nuclei. In particular, application of the r-process calculation to the evaluation of production ratios of radionuclides of cosmochronological interest often requires an accurate knowledge of some of their nuclear properties.

Among the different nuclear models available for practical purposes, the one having the most reliable predictive power far from the stability region is to be preferred. As a matter of fact, it is essential to be confident about the model's ability reliably to extrapolate its results to regions where no experimental information is available. Clearly, it is the model with the better theoretical foundation which should be chosen. However, this statement, which might seem trivial, should not be followed in some cases. Meyer et al. (1989a) have pointed out the importance of computing the different nuclear properties consistently within the same model. Since a number of different quantities are needed in the r-process calculations, it is generally not possible to extract all of them from one single model. Yet it is of great importance to use a consistent set of data and not a mixed set. The use of the best available models without regard to this rule of consistency, has been shown to lead to significant discrepancies (Cowan et al., 1991). In particular, it is well known that a quantity of fundamental importance in the r-process calculations is the nuclear mass. Many nuclear properties have to be deduced from a nuclear mass formula, for example neutron separation energies, β-decay Q-values or fission barriers. It has been shown (Meyer et al., 1989a) that the use of two mass formulae to evaluate two different quantities, like Q_β-values and fission barrier heights, can have drastic consequences and can, for example, overestimate the β-delayed fission probabilities. Therefore, we want to stress here that the r-process calculations require to compute the different nuclear quantities, such as ground-state masses, deformations, fission barriers, β-strength functions consistently within the same model.

Due to the great difficulties raised by such calculations, simplifying assumptions are generally

made. In its simplest form, for example, the so-called canonical r-process assumes that temperature, density and neutron concentration remain constant over the whole timescale τ during which the neutron irradiation and the photodisintegrations occur. Moreover, neutron captures are assumed to be always faster than β-decays. In such conditions, an (n,γ)-(γ,n) equilibrium will be attained for each isotopic chain. Under the assumption of an (n,γ)-(γ,n) equilibrium, the knowledge of the neutron capture cross-sections is not required. It does considerably facilitate the calculations and this is definitely the main reason why the equilibrium condition has been so widely used. Even if in quite a number of cases this approximation remains valid, this canonical model has been misused too often.

The numerous remaining inconsistencies faced by the r-process calculations, on the astrophysical as well as on the nuclear physics side, call for a much deeper study of each of the input data before rushing into numerical results. This should be kept in mind especially when applications of the r-process calculation to cosmochronology are considered. Two aspects of the nuclear physics involved in the r-process calculations have, therefore, been worked out in order to put the nucleosynthesis predictions on safer and sounder grounds. The first one investigates the influence of nuclear masses on the r-abundance distribution in the framework of the canonical model (Part I). Nuclear masses are known to have the most decisive influence on the distribution of the nuclei produced by the r-process. All r-process calculations have so far made use of droplet-type mass formulae only, whose reliability along the r-process path (i.e. far off the experimentally known region) remains very uncertain. A new mass table based on a microscopic theory of the nucleus is now available for the first time. New r-process calculations have been performed in the framework of the canonical model to analyse the impact of the adopted nuclear mass model on the final r-abundance profile.

When the often non-valid assumption of an (n,γ)-(γ,n) equilibrium is removed, a detailed

knowledge of the nuclear properties like neutron capture cross-sections or photodisintegration rates is required. In these conditions, use is generally made of the Hauser-Feshbach statistical model, even if its reliability remains sometimes doubtful. Consequently, Part II will be devoted to the level density prediction which remains so far the weakest point in the current procedure used in the evaluation of cross-sections. In the framework of the analytical approximation to the statistical model, we have tried to improve the description of the spin-dependent level density by introducing in a new way the shell and pairing effects. Such an approach is believed to be more reliable than the level density models used at present.

Part I

The influence of nuclear masses on the r-abundance distribution

I.1 The canonical r-process model

The simplest and most widely used form of the r-process model, referred to as the canonical model, assumes that the neutron density and temperature not only remain constant over the whole time scale τ of the neutron irradiation, but also that they are high enough, so that strong and electromagnetic interactions can occur in a much faster time scale than the weak interactions. Under such conditions, an (n,γ)-(γ,n) equilibrium can be reached for each isotopic chain, before any β-decay can take place. This approximation allows us to neglect the small β-decay rates to the first order, so that the abundance equation for the nucleus (Z, A) becomes (if we assume that only the (n,γ) and (γ,n) reactions play an important role during the neutron irradiation):

$$\frac{dN(Z,A)}{dt} = \lambda_{\gamma,n}^{Z,A+1} N(Z,A+1) - < \sigma v >_{Z,A} N(Z,A-1) N_n \qquad (2)$$

As soon as the equilibrium is established, $\frac{dN(Z,A)}{dt} = 0$ and the abundance ratio of two isotopes is determined by the ratio of the two nuclear rates:

$$\frac{N(Z,A+1)}{N(Z,A)} = \frac{< \sigma v >_{Z,A}}{\lambda_{\gamma,n}^{Z,A+1}} N_n \qquad (3)$$

Expression (3) has the interesting advantage of not requiring a detailed reaction rate calculation. It involves the ratio of two inverse reactions, which thanks to the principle of time-reversal invariance

can be rewritten in terms of the temperature T of the gas and the neutron separation energies S_n (e.g. Rolfs and Rodney, 1988)

$$\frac{<\sigma v>_{Z,A}}{\lambda_{\gamma,n}^{Z,A+1}} = \frac{G(Z,A+1)}{2G(Z,A)} \left(\frac{A+1}{A}\right)^{3/2} \left(\frac{2\pi\hbar^2}{m_u kT}\right)^{3/2} \mathrm{e}^{\frac{S_n(Z,A+1)}{kT}} \quad (4)$$

where $G(Z,A)$ is the partition function of nucleus (Z,A) for the considered temperature T and m_u is the nuclear mass unit.

Inserting (4) in equation (3), the abundance ratio of two isotopes can be quite simply expressed in terms of T, N_n and S_n, leading to the well known Saha equation:

$$\log \frac{N(Z,A+1)}{N(Z,A)} = \log \frac{G(Z,A+1)}{G(Z,A)} + \log N_n - 34.075 - \frac{3}{2} \log\left(\frac{A}{A+1} T_9\right) + \frac{5.04}{T_9} S_n(Z,A+1) \quad (5)$$

where T_9 denotes the temperature expressed in billion of degrees, S_n the neutron separation energy in MeV and N_n the neutron number density in cm^{-3}. Expression (5) explains why this approximation is also called the waiting point approximation. Because of the exponential dependence on S_n, the abundance ratios (5) in each isotopic chain will vary sharply around a particular value of the neutron separation energy. At maximum, $N(Z,A) \sim N(Z,A+1)$ and the corresponding S_n determined by equation (5) will in turn depend on the thermodynamic conditions, i.e. the temperature and the neutron density. These peaks for each element constitute what is called the r-process path. For each isotopic chain, the nucleus with maximum abundance (the "waiting point") must then wait for the slower β-decay to take place.

The relative isotope abundances in each Z-chain can be obtained from equation (5) and characterized by the coefficients

$$P(Z,A) = \frac{N(Z,A)}{N(Z)} \quad (6)$$

where $N(Z) = \sum_A N(Z,A)$ is the total abundance in the isotopic chain Z.

The abundance flow from one isotopic chain to the next is governed by β-decays and can be described, omitting the fission feedback, by the set of differential equations

$$\frac{dN(Z)}{dt} = N(Z-1)\sum_A P(Z-1,A)\lambda_\beta^{Z-1,A} - N(Z)\sum_A P(Z,A)\lambda_\beta^{Z,A} \qquad (7)$$

This means that instead of solving a system of differential equations for all nuclei involved, it is sufficient to solve a system which contains only as many equations as the number of Z-chains. This feature constitutes the main reason for the popularity of the waiting point approximation. It is, however, important to stress that this approximation is valid only if either the temperature or the neutron number density of the gas is very high ($N_n > 10^{20}\mathrm{cm}^{-3}$ and/or $T_9 > 1$) (Cameron et al., 1983b). Otherwise β-decay rates are fast enough to compete with the (n,γ) and (γ,n) reactions and steadily to deplete the isotopic chain before an equilibrium can be ensured. A full reaction network, involving the reaction cross-section calculation is then required (see Part II).

The neutron capture process followed by the β-decay is assumed to take place over a time τ, which if not fixed by a definite astrophysical model, plays the role of a fourth parameter (the three others being the temperature, the neutron number density and the initial chemical composition). After the time τ, the temperature is assumed to fall to zero and the neutron flux is annihilated. The neutron-rich nuclei then undergo successive β-decays towards the valley of β-stability. No neutron capture is usually assumed to occur anymore. However, β-delayed neutron emission has to be taken into account because of its important influence on the final abundance distribution (Kodoma and Takahashi, 1973). It has been shown that the even-odd fluctuations of the mass abundance curve are extremely smoothed out when the possible emission of delayed neutrons is included in the post-freezing cascade process.

Other nuclear transformations like α-decays (in the $A > 210$ region), spontaneous or β-delayed fissions also contribute to the final abundance distribution and should be included in any calculation which tries to explain the observed solar abundances.

I.2 Influence of nuclear masses on the nuclear properties of interest for the r-process calculation

In order to evaluate the influence of the nuclear masses on the r-abundance distribution, we have performed calculations in the framework of the canonical r-process model. Among the nuclear properties of interest for the r-process, nuclear masses clearly have the most decisive influence. They not only determine the position of the neutron drip line, the value of the neutron separation energies and the β-decay Q-values, but also indirectly modify the rates for fission and β-delayed processes. More precisely, equation (5) shows that the position of the r-process path in the (N, Z) nuclear chart critically depends on the neutron separation energies. Consequently, the resulting abundance distribution may be strongly affected by the uncertainties of the model used to calculate the nuclear masses. Since very few (if any) binding energies are actually known along the r-process path, all r-process nucleosynthesis calculations have to make use of the available theoretical nuclear mass formulae.

The r-process requirements, however, concern the masses of several thousands of nuclei, many of which deformed. Mass predictions for these have nowadays only been obtained through droplet-type mass formulae. The droplet model is based on an expansion of the nuclear mass in powers of $A^{-1/3}$ and on the neutron excess $I = (N - Z)/A$. This average macroscopic contribution to the mass originates from the classical liquid drop model (von Weizsäcker, 1935) and has further been corrected by the so-called microscopic term which essentially describes the nuclear shell contribution to the total nuclear mass. Further parameters have been introduced in the liquid drop part, such as the nuclear symmetry energy J, the incompressibility coefficient K, etc. (see Myers and Swiatecki, 1974) although the droplet model makes no attempt to extract these parameters from first principles and instead fits them to the experimentally known masses. If an important effect is not included in the general formula, one hopes that it has been artificially introduced

through other parameters. Yet this procedure has the dangerous consequence that extrapolation into the experimentally unknown regions is made very uncertain. The sensitivity of the mass formula to extrapolations away from the valley of stability can be seen in Fig. 4 which shows the difference between the theoretically calculated droplet masses and the experimental ones as a function of the distance from the valley of stability, i.e. the neutron surplus ΔN.† The droplet masses are derived from von Groote et al. (1976) and the purely experimental masses are taken from the Wapstra et al. (1988) mass table. These theoretical masses correspond to one of the most reliable fits among the presently available droplet mass formulae and have been extensively used in r-process calculations. However, Fig. 4 shows the danger of using such a formula, namely that the theoretical evaluation gets less accurate for nuclei far from stability. Even if the mean value is approximately zero, neutron-rich nuclei seem to be essentially too well bound ($M_{cal} - M_{exp} < 0$), compared with the stable nuclei (i.e. for a neutron surplus $\Delta N = 0$).

Experimental masses concern nuclei which remain close to the valley of stability, i.e. $\Delta N \lesssim 20$. Fits to such nuclei do not greatly restrict extrapolations of the mass values to the very neutron-rich region. As a matter of fact, two similar droplet-type formulae with the same accuracy of fit to experimental values can exhibit a completely different behaviour far away from stability. An example can be found in the comparison of von Groote et al. (1976) and Hilf et al. (1976) mass formulae. Both are based on exactly the same droplet model formula but correspond to two possible minimizations, relative to the parameter set. Their respective parameters lead to very similar root mean square deviations from experimental masses (of 756 and 774 keV, respectively on the 1440 experimental masses of Wapstra et al. (1988) corresponding to $20 \leq Z \leq 100$) but

† We define here for each isotopic chain Z, the neutron surplus of a nuclide (Z, A) by $\Delta N = N - N_s(Z)$ where for proton- (neutron-) rich isotopes, $N_s(Z)$ denotes the most proton- (neutron-) rich stable isotope of the element Z. If there is no stable isotope in the Z-chain, the isotope with the longest half-life is taken for $N_s(Z)$.

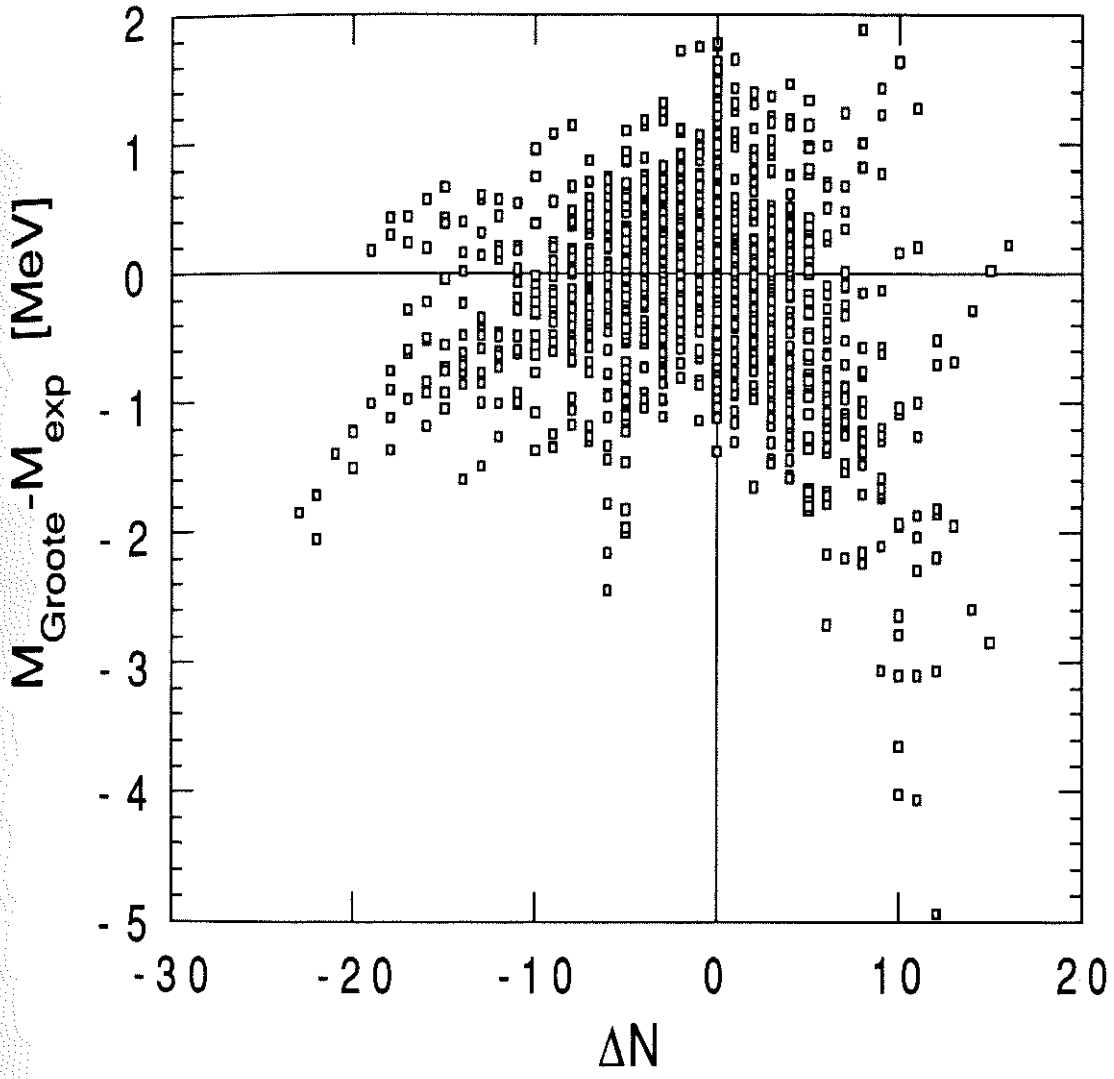

Figure 4. Deviation as a function of the neutron surplus ΔN of the masses calculated with von Groote et al. (1976) mass formula from the experimental masses taken from Wapstra et al. (1988).

lead to very different predictions for neutron-rich nuclei. The location of the neutron drip line is particularly affected by this. The neutron-rich region for $20 \leq Z \leq 100$ includes a 1050 more nuclei which are stable for neutron emission if use is made of von Groote et al. instead of Hilf et al. formula. Hilf et al. mass parabola is characterized by a much steeper slope relative to the von Groote et al. parabola. Extrapolations to neutron-rich regions of the nuclear chart are extremely sensitive to the asymmetry terms and consequently to the so-called nuclear symmetry energy J, the symmetry anharmonicity coefficient M or the effective surface stiffness Q. A modification of this parameter set does not affect significantly the fits to experimental masses but has drastic effects on the calculated masses of the very neutron-rich nuclei. Such an effect can be observed in Fig. 5. The two fits agree within 1 MeV for stable nuclei and within 6 MeV for known unstable neutron-rich nuclei ($\Delta N \leq 15$). However, they show complete disagreement as soon as predictions for unknown nuclei are concerned. Mass differences as large as 35 MeV appear indeed for nuclei close to Hilf et al. neutron drip line.

The very crucial question of the reliability of such models, therefore, remains when predictions far away from the valley of stability are required. In order to improve the droplet model consistency, the finite range droplet model (Möller et al., 1988) has been introduced. It corresponds to the most recent and sophisticated version of the macroscopic-microscopic approach, at the expense of an increasing number of parameters, which often makes the mass formula extremely cumbersome. However, no complete mass table is available yet in the literature.

Despite the increasing reliability of the macroscopic-microscopic models, two main criticisms are usually brought against these models and are based on

a) the danger of a premature truncation in the expansion of the mass in powers of $A^{-1/3}$ and I. Dutta et al. (1986a) showed that it could lead to errors as large as 15 MeV or more on the nuclear mass of the n-drip line nuclei;

b) the inconsistent treatment of the macroscopic and microscopic contributions as pointed out by Dutta et al. (1986b). The shell correction to the total mass constitutes a pure artificial contribution, which strongly depends on the coefficient adopted for the macroscopic part. The only link between the two terms results from fits to experimental data, and not from physical principles. Therefore, extrapolations to unknown regions of the nuclear chart become highly questionable.

Both these uncertainties can be avoided when the nuclear masses are calculated by the Hartree-Fock + BCS method, which represents the most fundamental approach to the mass formula. In this case, a suitable form of the effective nucleon-nucleon force is considered and then fitted to reproduce the different nuclear properties like masses and fission barriers. Recent fits with Skyrme-type forces have shown that the HF+BCS method can achieve an accuracy comparable to that of the droplet-model mass formulae (Tondeur, 1978, 1983).

However, even though the calculation for spherical nuclei can be performed in practice, the large amount of computer time required to treat deformation with this method prevents a least-square fit of the effective force to all nuclei. Moreover, even if the effective interaction were known, the computation of a complete set of nuclear masses, including the 6000 nuclei lying between the drip lines, is so far unrealizable in the HF+BCS formalism. An interesting compromise between the computationally fast but uncertain droplet model and the complex but highly reliable HF+BCS approach can be found in the Extended Thomas-Fermi plus Strutinsky Integral method (ETFSI) (Dutta et al. 1986b; Tondeur et al., 1987). This method is based on the extended Thomas-Fermi approximation to the HF method, using a Skyrme-type effective interaction. The ground state energy is derived by a minimization of the semi-classical approximation to the energy expressed as a parametrized functional of the nucleon densities, with respect to variations of the functional parameters (Brack et al., 1985). The resulting energy will, however, vary smoothly from one

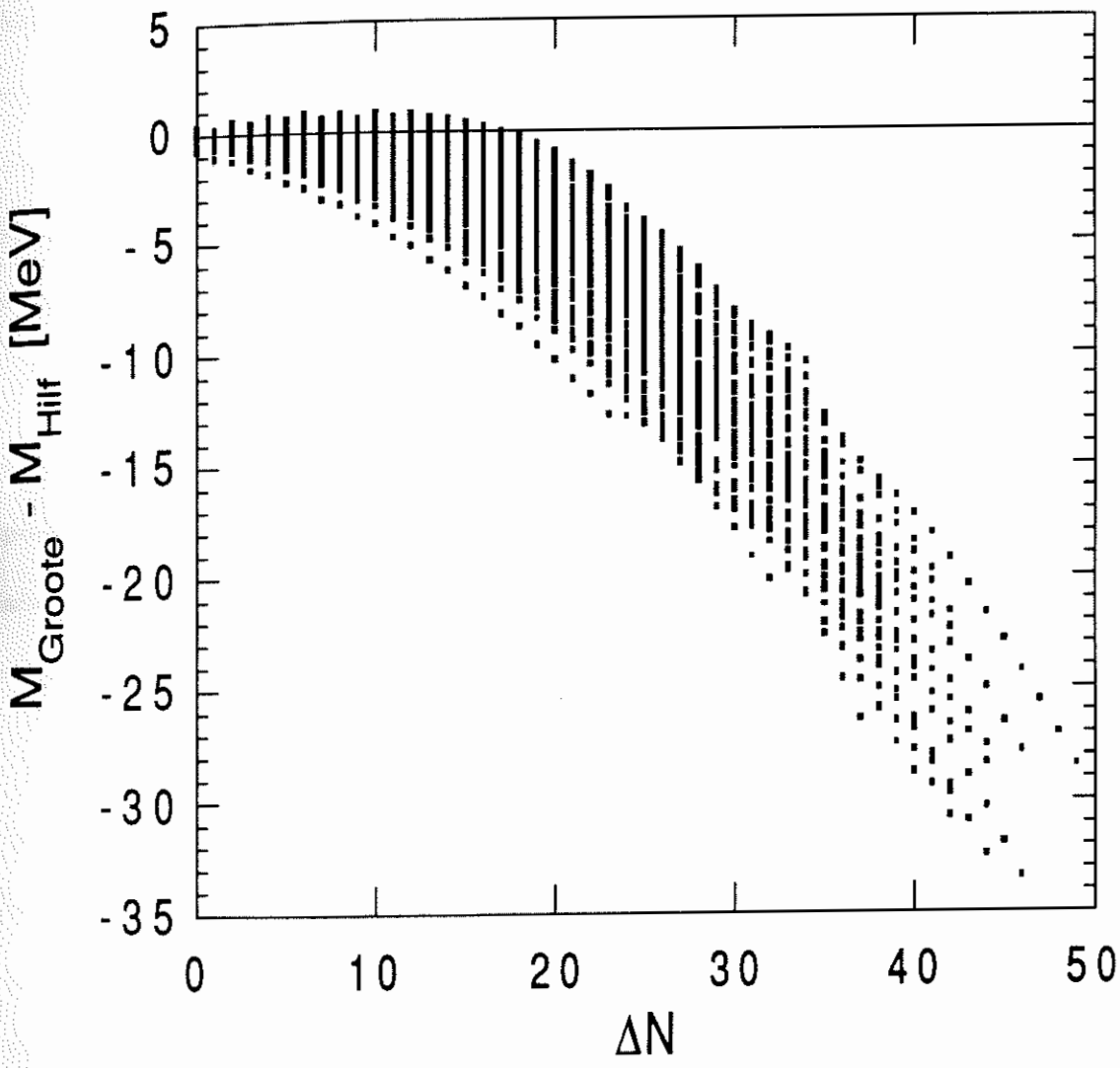

Figure 5. Difference as a function of the neutron surplus ΔN between von Groote et al. (1976) and Hilf et al. (1976) masses for all nuclei with $20 < Z < 100$ between the valley of stability and the Hilf et al. neutron drip line. Both predictions are based on exactly the same droplet mass formula but are characterized by a different set of parameters.

nucleus to another and should therefore be corrected by shell terms. The shell corrections can be calculated by different methods. One of them, the Strutinsky integral method (Chu et al., 1977), makes use of the single-particle potential obtained by one iteration of an HF calculation, which folds the same Skyrme-type force as the one involved in the macroscopic (ETF) part of the calculation. This technique is thus characterized by a high degree of coherence between the macroscopic and microscopic terms, the unifying factor being the Skyrme-type force that underlies both parts. It has been proved to be the only non-ambiguous approach for calculating the shell correction terms (Pearson et al., 1991).

Dutta et al. (1986b) and Tondeur et al. (1987) showed that, even out to the neutron drip line, the ETFSI method with a unique set of renormalized parameters for the effective interaction, can reproduce the HF+BCS binding energies to within less than 1 MeV. No other approach approximates the HF method so well. Moreover, the ETFSI method is an order of magnitude faster than the HF one and has the additional and very interesting advantage of permitting interpolations.

The ETFSI method expresses the total energy in terms of quantities that vary smoothly with respect to N, Z and the deformation parameters. The calculations can therefore be restricted to a limited number of key nuclei and key deformations. The results can then be interpolated on the others. This advantage enabled Aboussir et al. (1991) (see also Pearson et al., 1991) to generate for the first time a complete mass table based on a microscopic theory of the nucleus whose parameters concern only the nucleon-nucleon force. Without this possibility of interpolation, the amount of computer time required to calculate the few thousands of nuclei would have been prohibitive.

Compared with the droplet model, the ETFSI masses give comparable fits to the experimental data (characterized by a root mean square deviation of 714 keV from the same Wapstra et al. (1988) purely experimental masses as mentioned above). Yet they extrapolate differently: Fig. 6 shows the deviations of the ETFSI masses from the experimental masses, as a function of the

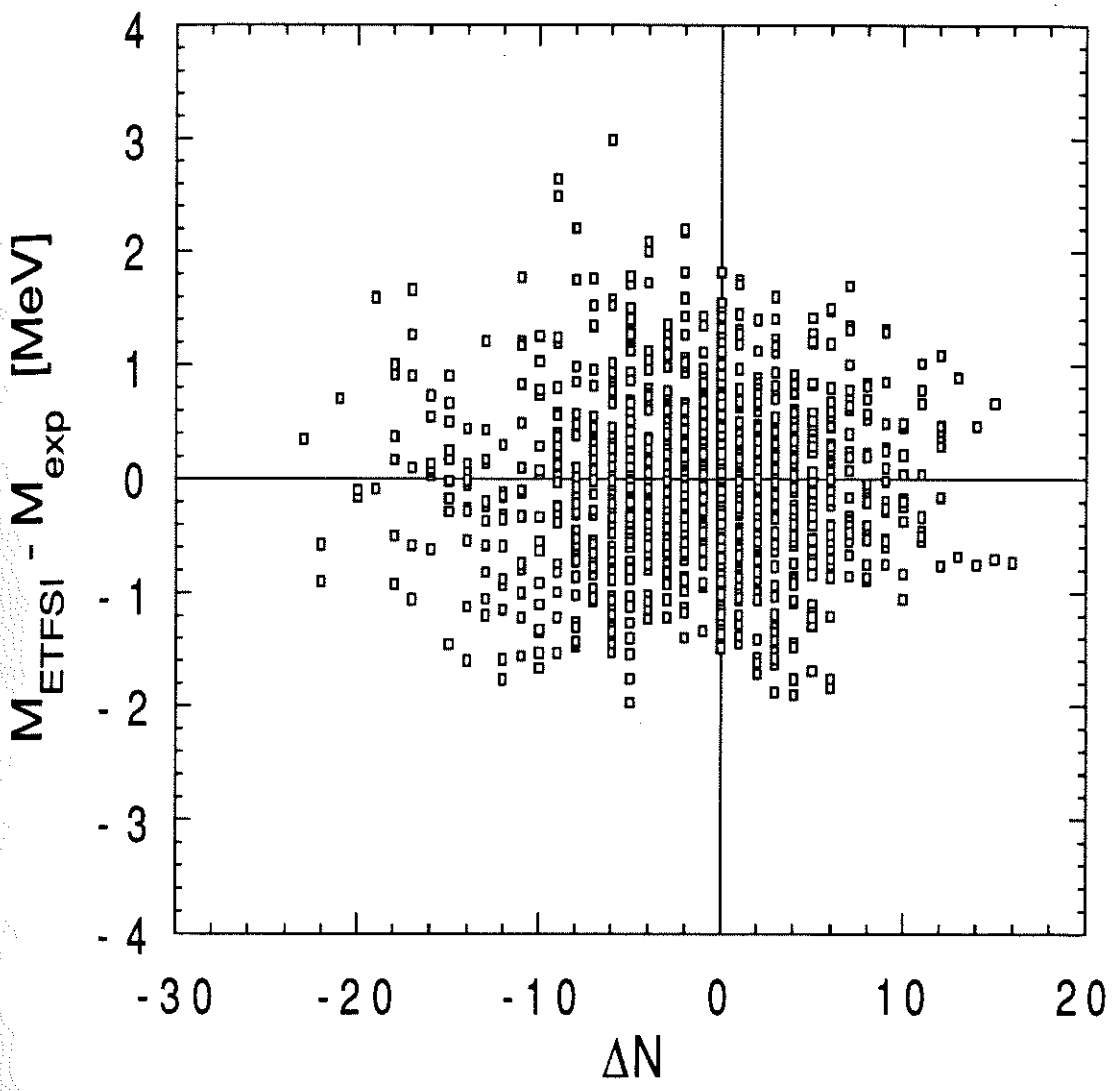

Figure 6. Deviation as a function of the neutron surplus ΔN of the ETFSI masses (Aboussir et al., 1991) from the experimental data (Wapstra et al., 1988).

neutron surplus. In comparison with Fig. 4, the ETFSI deviations seem to have a much more uniform distribution with an average deviation much closer to zero than in the case of the droplet model which tended to bind neutron-rich and proton-rich nuclei too strongly. The mass differences between the ETFSI and the droplet model (DM) of von Groote et al. is displayed in Fig. 7 for all nuclei with $20 \leq Z \leq 100$ between the valley of stability and the ETFSI neutron drip line (the ETFSI mass parabola being characterized by a steeper slope). Differences as large as 23 MeV can be expected out at the n-drip line. Fig. 7 also shows the important effects resulting from the differences in the shell correction treatment. The droplet shell effects at neutron magic numbers appear to be clearly underestimated relative to the ETFSI model (except at N=50). The largest differences observed concern very neutron-rich nuclei. Such differences are worrying since many useful properties (like neutron separation energies or β-decay rates) are related to nuclear masses and might be affected. Yet the effect of such discrepancies might be reduced since nuclear quantities of importance for the r-process calculations generally involve only nuclear mass *differences.*

Let us discuss briefly the influence of the adopted mass formula on two main quantities of importance for the r-process calculations, i.e. the neutron separation energy and the β-decay rate.

(i) Effect of the mass formula on the neutron separation energy

The neutron separation energy S_n is a quantity of fundamental importance for r-process calculations since the ratio of the (n,γ) to the (γ,n) rate depends exponentially on S_n at a given temperature (see expression (4)). Under the steady flow conditions discussed in Chapter I.1, the r-process-path is specified by the equi-neutron-separation-energy contour

$$S_n^0 = \left(34.075 - \log N_n + \frac{3}{2}\,\log T_9\right)\frac{T_9}{5.04} \tag{8}$$

This is derived from equation (5) by assuming that for each isotopic chain, $N(Z,A+1) = N(Z,A)$ at the waiting point, and by neglecting the term $\log\left[\left(\frac{A+1}{A}\right)^{3/2}\frac{G(Z,A+1)}{G(Z,A)}\right]$ (a typical value being

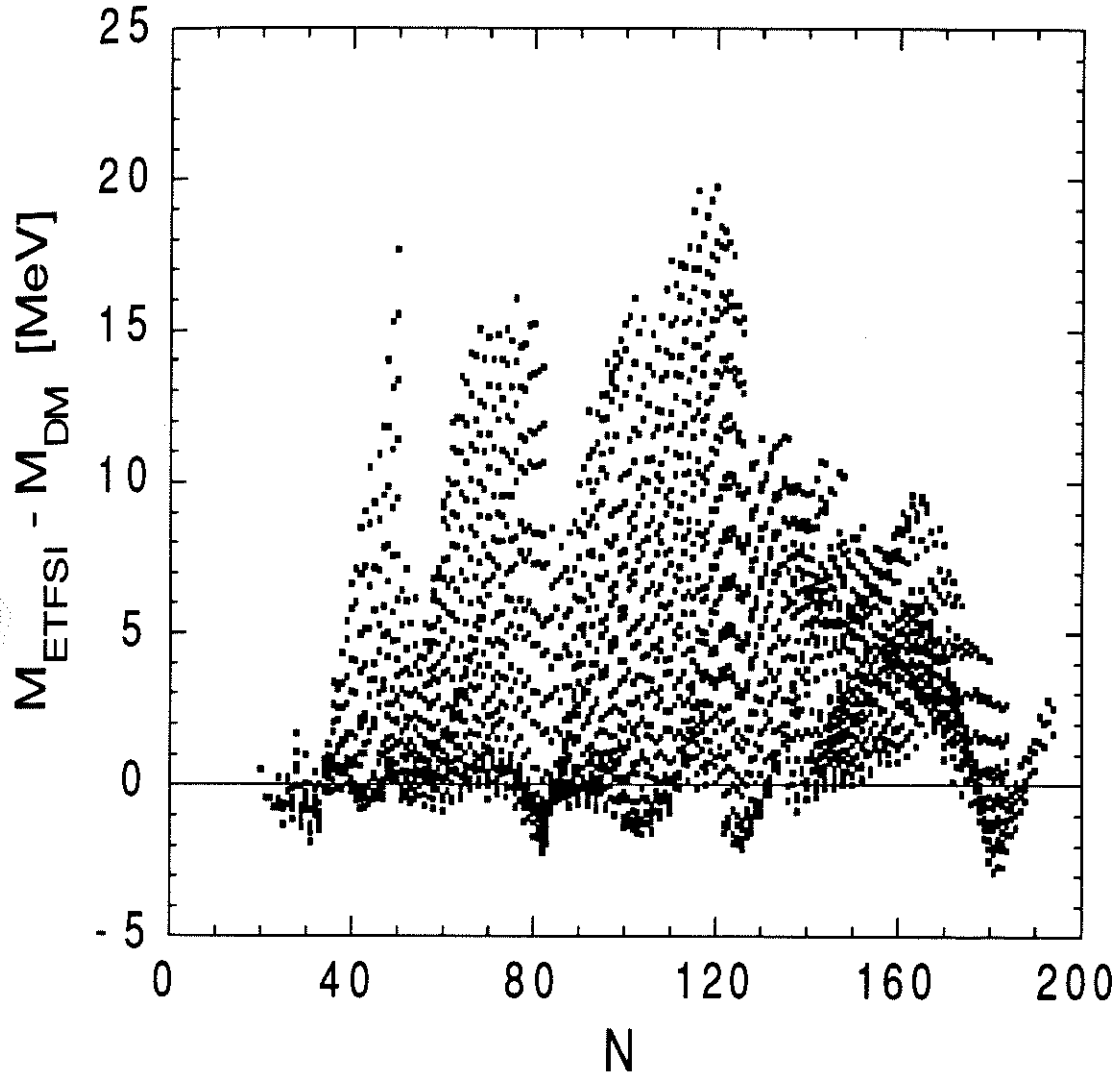

Figure 7. Difference as a function of the neutron number N between ETFSI masses (Aboussir et al., 1991) and DM masses (von Groote et al., 1976) for all nuclei with $20 < Z < 100$ between the valley of stability and the DM neutron drip line.

~ 0.1). At a given temperature and neutron density, all abundance maxima in each isotopic chain will be characterized by the same neutron separation energy S_n^0. The r-process path in the steady flow conditions, as well as the resulting abundance curves, are often classified according to S_n^0 instead of the parameter set (T_9, N_n). Expression (8) also shows that two sets of parameters (T_9, N_n) can lead to the same path (and therefore globally to the same abundance distribution) although the path width might still differ according to the non-equal N_n- and T_9-dependences of the abundance ratio, as given by equation (5).

Another quantity of interest that we have introduced in our discussion, and which characterizes the r-process path in a similar way, is the even-odd-averaged neutron separation energy

$$S_a(Z,A) = \frac{S_n(Z,A) + S_n(Z,A-1)}{2} \tag{9}$$

Since $S_a(Z,A)$ is not affected by the odd-even effects, it is a smooth function of the neutron excess $I = (N-Z)/A$ and can be expressed in its simplest droplet form by

$$S_a(Z,A) \approx a_v - \frac{2}{3} a_s A^{-1/3} - a_{sym} I + \frac{1}{2}\left[M_s(Z,A-2) - M_s(Z,A)\right] \tag{10}$$

where $M_s(Z,A)$ denotes the microscopic shell correction energy of the (Z,A) nucleus as defined in a macroscopic-microscopic droplet model; and a_v, a_s and a_{sym} the usual volume, surface and symmetry coefficients, respectively (e.g. Bohr and Mottelson, 1969). Far away from the magic numbers, $S_a(Z,A)$ is therefore a linearly decreasing function of I, which does not show the saw-tooth feature resulting from the pairing effect.

On the r-process path, $S_a(Z,A)$ also enables a more accurate determination of the waiting point. Saha equation (5) can be rewritten as

$$\frac{1}{2}\log\frac{N(Z,A)}{N(Z,A-2)} = \frac{1}{2}\log\left[\left(\frac{A}{A-2}\right)^{3/2}\frac{G(Z,A)}{G(Z,A-2)}\right] + \log N_n - 34.075 - \frac{3}{2}\log T_9 + \frac{5.04}{T_9} S_a(Z,A) \tag{11}$$

and in each isotopic chain at the abundance maxima, S_a takes the value

$$S_a(Z,A) = S_a^0 = \left(34.075 - \log N_n + \frac{3}{2}\,\log T_9\right)\frac{T_9}{5.04} \tag{12}$$

where this time $\frac{1}{2}\log\left[\left(\frac{A}{A-2}\right)^{3/2}\frac{G(Z,A)}{G(Z,A-2)}\right]$ can be neglected more safely than the corresponding factor in expression (8) since it does not show the strong odd-even effects that are sensitively present in the partition function. Yet despite these interesting features of S_a^0 in comparison with S_n^0, it should be mentioned that S_a^0 has never been used in previous studies to define the r-process path.

Expression (10) clearly shows the strong dependence of the r-process path on the droplet parameters and more precisely on the symmetry coefficient. It still remains quite difficult to determine unambiguously the symmetry energy terms of the droplet mass formula from fits to experimental masses since, in the vicinity of the valley of stability, their contributions are strongly reduced. Different mass formulae generally make use of different symmetry parameters. Therefore they will also lead to significantly different r-process paths. Fig. 8 compares the neutron drip lines ($S_n = 0$ MeV) and the equi-S_a^0 curve ($S_a^0 = 3$ MeV) corresponding to the droplet extrapolation (von Groote et al., 1976) and the ETFSI approximation. The softer slope of the droplet mass parabola is reflected by the fact that for each element a given S_n is encountered for a larger value of N (except at magic neutron numbers). Consequently the number of nuclei involved in the r-process calculation will also differ.

The $S_a^0 = 3$ MeV paths for the two nuclear models displayed in Fig. 8 can be readily understood by looking at expression (10). The symmetry coefficient can be expressed as

$$a_{sym} = J + a_{ss}\,A^{-1/3} \tag{13}$$

where J is the symmetry energy and a_{ss} the surface-symmetry coefficient given to first approximation by

$$a_{ss} = \left(\frac{2L}{K}a_s - \frac{9J^2}{4Q}\right)B_s \tag{14}$$

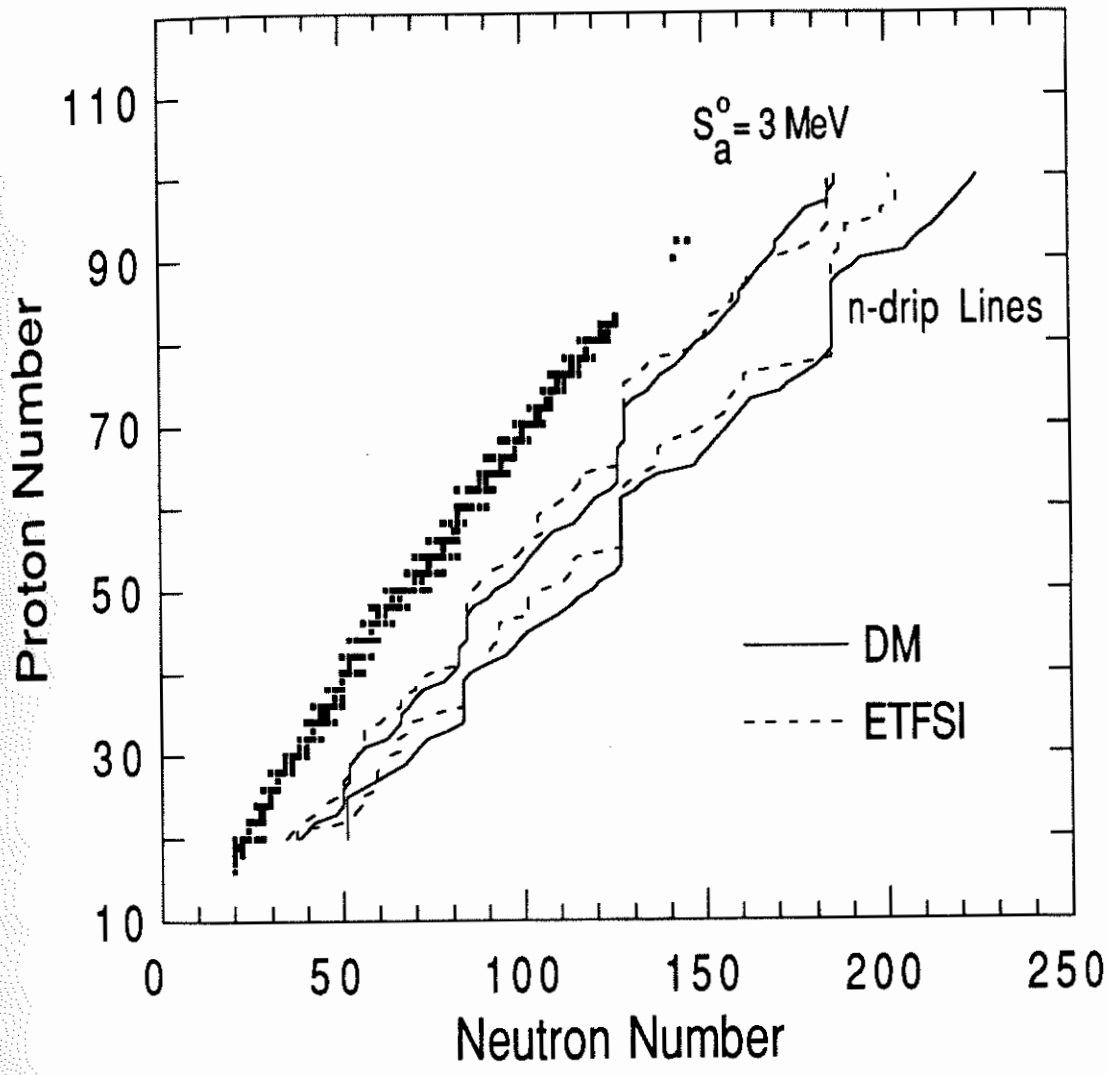

Figure 8. Comparison in the nuclear chart between the neutron drip line and the equi-averaged-neutron-separation-energy contour $S^0_a = 3\,\mathrm{MeV}$ obtained with the droplet mass formula of von Groote et al. (1976) (full line) and those derived from the mass table of Aboussir et al. (1991) (dashed line). Black squares correspond to stable nuclei.

where L, K and Q are the so-called density symmetry, incompressibility and effective surface stiffness coefficients, respectively. The factor B_s denotes the usual nuclear surface area relative to the spherical shape.

The droplet model of von Groote et al. (1976) leads to the parameter set $J = 38.2\,\mathrm{MeV}$ and $a_{ss} = -170\,\mathrm{MeV}$ which are to be compared with the corresponding macroscopic coefficients resulting from the ETFSI forces: $J = 27.0\,\mathrm{MeV}$ and $a_{ss} = -16\,\mathrm{MeV}$ (Aboussir et al., 1991). The higher ETFSI symmetry coefficient gives rise (for the same deformation) to a faster decrease of $S_a(Z,A)$ as a function of the neutron excess I, i.e. to a r-process developing in a less neutron-rich region than in the case of the droplet model of von Groote et al. The sudden fall-off of $S_a(Z,A)$ at the magic number—due to the last term of expression (10)—is, however, strong enough for both models to meet condition (12) at the same magic nucleus.

In summary, even if the accumulation points corresponding to the neutron magic numbers are globally the same for the two mass formulae, the r-process path differs significantly from one mass formula to the other one.

(ii) Effect of the mass formula on the β-decay rates

As regards the β-decay rates, the influence of the adopted nuclear mass table might be non-negligible. The β-decay half-lives, particularly for nuclei with magic neutron numbers, also enter into the calculations of the r-process abundance, and play a crucial role in the prediction of the amplitude as well as the location and width of the r-process abundance peaks. From the astrophysical point of view, they are the quantities which fix the duration of the nucleosynthetic process.

The β-decay rate λ_β is given in rough approximation by

$$\lambda_\beta \propto Q_\beta^5 \, M^2 \tag{15}$$

where Q_β is the effective β-decay energy and M^2 represents the squared matrix element involved in the β-decay (e.g. Rolfs and Rodney, 1988). Since the Q_β-values depend on the nuclear masses,

a modification of the latter can affect the β-decay rate significantly. However, the fact that Q_β is a mass difference:

$$Q_\beta = M(Z,A) - M(Z+1,A), \tag{16}$$

could greatly decrease the influence of the uncertainties inherent to the calculation of individual masses. We show in Fig. 9 the ratio of the ETFSI Q-values to the droplet (von Groote et al., 1976) Q-values as a function of the neutron surplus. The two Q_β evaluations appear to agree within a factor of two. The convergence of this ratio towards unity for very neutron-rich nuclei proves that although the two models extrapolate the nuclear masses quite differently (Fig. 7), the mass differences (16) can still be extrapolated in a similar manner. The discrepancies between the Q_β-values predicted by the two mass models for nuclei close to the stability valley can be explained as resulting mainly from the different treatment of the odd-even effects. Close to the valley of stability, the pairing correlation has a significant impact on the low Q_β-values; while, in the neutron-rich region, these values are predominantly influenced by the asymmetry effects. As expected, the steeper slope of the ETFSI mass parabola gives rise to higher Q_β-values. The high sensitivity of the β-decay rate (15) to the Q_β-value led us to an evaluation of the ratio of the two β-decay rates instead of the two Q_β-values.

The β-decay half-lives have been estimated in the gross theory formalism (Takahashi and Yamada, 1969; Takahashi et al., 1973), even if better treatment can be found in the recent quasi-particle RPA calculations (Möller and Randrup, 1990; Staudt et al., 1990). Yet the gross theory is accurate enough for our purpose, which is to discuss the influence of nuclear mass formulae. An accurate evaluation of the absolute β-decay rates is, however, of great importance when observed abundances are to be compared or when the time scale of the dynamical r-process synthesis is to be determined. Fig. 10 presents the ratio $\frac{\lambda_\beta(ETFSI)}{\lambda_\beta(DM)}$ in the neutron-rich region for all nuclei whose β-decay might be involved in the r-process, i.e. for which $\lambda_\beta \geq \frac{1}{\tau_{max}}$ (where τ_{max} represents an

upper limit to the characteristic time scale of the r-process, typically of the order of one minute). The two different Q_β-determinations give β-decay half-lives which agree within a factor of 10 and as expected from Fig. 9, the ETFSI masses lead to faster β-decays, due to higher Q_β-values. No drastic divergence between the two models can, however, be seen for nuclei lying close to the neutron drip line.

Therefore, it is clear that the influence of the nuclear mass model on the neutron separation energies, as well as on the β-decay rates, is far from being negligible. Another quantity which is also expected to be affected by the choice of the mass formula concerns the fission barriers. In the macroscopic-microscopic approximation, several methods are used to estimate the fission barriers. For example, Barashenkov et al. (1973) decomposed the fission barrier B_f into 3 parts:

$$B_f = B_f^0 - \Delta_{gs} + \Delta_{sad} \tag{17}$$

where B_f^0 describes the liquid drop part and Δ_{gs} and Δ_{sad} the shell plus pairing correction parts at the ground state and at the saddle point, respectively. Improvement of the fission barrier prediction followed improvement of the nuclear mass formula (Meyer et al., 1989b). Yet one of the main uncertainties in equation (17), as well as in all formulae based on the macroscopic-microscopic model, comes from the artificial shell correction which, as already discussed, is treated inconsistently in this approach. Although the reliability of the droplet-type formulae to predict fission barriers is far from being established, no other methods have been used in the r-process calculations. As in the case of nuclear masses, Hartree-Fock + BCS calculations can be used to predict fission barriers. In turn, the ETFSI approximation can give a reliable estimation of the HF prediction for a large number of nuclei. A complete set of barrier fission energies is now being generated in the ETFSI formalism (Tondeur, 1991) and should be available in the near future. For that reason, the comparison between droplet and ETFSI fission barriers will not be discussed in the present work and will be postponed to a later study.

I.3 Influence of the nuclear mass model on the r-process abundances

As described in the previous sections, the remaining uncertainties in the nuclear mass models affect in a non-negligible way the calculated values of the nuclear properties (mainly the neutron separation energy and the Q_β-value) of the neutron-rich nuclei. Here, we attempt to evaluate the influence of the nuclear masses on the abundances of nuclei produced by the r-process. A schematic r-process calculation has been performed for this purpose, making use of two nuclear mass models:

- the recently generated mass table of Aboussir et al. (1991) obtained in the ETFSI formalism;
- the droplet model of von Groote et al. (1976), extensively used in r-process calculations (in the following section, the droplet model (DM) refers to this mass formula).

The astrophysical conditions chosen in the present work correspond to those of the "canonical" r-process. The simple (n,γ)-(γ,n) equilibrium has the advantage of presenting a simplified and therefore clearer picture of the numerous mechanisms that occur during the r-process. The different nuclear physics aspects enter the calculation in a quite straightforward way which allows a much better understanding of the process than more sophisticated models would allow.

Yet the use of such a simple model implies that no premature conclusions concerning the output should be drawn. At this stage, we do not pretend to perform calculations which could reproduce the solar system abundance curve (Fig. 2) since our discussion centres strictly on the influence of the nuclear mass model on the abundance distribution. We will, however, be guided by the observed abundance distribution in order to restrict our calculations to a set of plausible astrophysical conditions.

In the (n,γ)-(γ,n) equilibrium approximation, the abundances are a function of three main parameters (in addition to the initial chemical composition and to the nuclear physics input): the neutron number density (N_n), the temperature (T) and the duration of the process (τ). These parameters are usually chosen to best reproduce the observed abundances and yet remain not

totally unrealistic from the astrophysical point of view. Ultimately, of course, these astrophysical conditions should be identified with a naturally occurring astrophysical scenario. The adopted set of parameters should also be checked to ensure that the waiting point approximation remains valid. An evaluation of this validity domain can be found in Cameron et al. (1983b).

Concerning the initial chemical composition, our calculations have been carried out assuming iron nuclei to be the only seed nuclei. The choice of iron seems a logical one since it has an abundance which is by far the largest one among the heavy nuclei which can be synthesized during previous stellar generations without the aid of neutron capture processes. Moreover, the relative isotopic abundances of the elements heavier than the seed nuclei will often be independent of this choice, since the choice of a starting point at a lower Z value would just modify the time scale of the process.

As soon as the astrophysical conditions are set, the calculation of the resulting r-nuclei abundances can be performed in the framework of the waiting point approximation. As described in Chapter I.1, the problem separates into two parts:

(i) the neutron irradiation during $0 < t < \tau$

Over the whole timescale τ during which the neutron irradiation takes place, the temperature and the neutron density number are kept constant. For each isotopic chain Z and at each timestep we calculate

- the relative isotopic abundances as given by equation (5) and (6).
- the abundance flow of β-decays resulting from the lower $Z-1$ isotopic chain and the abundance flow of the Z-chain towards the $Z+1$-chain, as given by equation (7).

This procedure enables a fast evaluation of each isotopic abundance $N(Z,A)$ at each time t. The nuclear physics input data required at this stage includes the partition functions, the neutron separation energies and the β-decay half-lives. If the neutron separation energy depends on the

nuclear mass formula only, the β-decay rate evaluation constitutes a new task to be modelled. The β-decay rates have been calculated by the gross theory of β-decay (Takahashi et al., 1973) with the use of the Q-values from the considered mass formula. Studies (Klapdor and Oda, 1980) have indicated that for heavy neutron-rich nuclei, the β-decay half-lives predicted by the gross theory were too long. However, the choice of the gross theory, as already explained in Chapter I.2, should not influence our conclusions concerning the influence of the mass formula. The absolute value of the β-decay rates essentially affects the timescale of the process which is, in any case, considered here as a free parameter.

The nuclear partition function $G(Z,A)$ appearing in equation (5) is defined by

$$G(Z,A) = \sum_i (2J_i + 1)\, \mathrm{e}^{-\frac{E_i}{kT}} \tag{18}$$

where E_i and J_i denote the excitation energy and the spin of the i-th nuclear state of the (Z,A) nucleus and k is the Boltzmann constant. The partition function strongly reflects the pairing, shell and deformation effects. We used the approximate empirical formula obtained by Kodoma and Takahashi (1975) for a constant temperature $kT = 200\,\mathrm{keV}$. Once again, this approximation is supposed to be accurate enough for our discussion and remains in any case within the much larger error bars associated with the estimation of the neutron separation energies and the β-decay rates.

It must be stressed that no fission has been introduced in our calculations. Normally as the synthesis advances up to the heavy nuclear mass region ($Z \gtrsim 80$), the neutron-induced fission as well as the spontaneous and β-delayed fissions recycle back a portion of the material to lower Z values. Two main considerations led us to neglect the fission processes. First, if fission is a crucial factor in the production of superheavy elements or elements of cosmochronological interest, its contribution to the abundances of the classical elements ($26 \leq Z \leq 83$) is much less important. The process duration τ associated with the hydrodynamical timescale is usually thought to be short enough for the r-process to terminate by the lack of free neutrons rather than by neutron-induced

(or β-delayed) fissions. Second, if fission is included in the calculation, a set of fission barriers is required. The use of droplet fission barriers, even if more realistic than the total neglect of fission processes, would not be consistent with the use of a ETFSI mass table, as discussed in the introduction (Section 3.). Therefore, it is our view that at this stage and while we are waiting for the new ETFSI fission barriers, it is reasonable not to include the fission processes in the nuclear reaction network.

(ii) the post-freezing phenomena: $t > \tau$

After the time interval τ, the temperature and the neutron density drop to zero, freezing all nuclear reactions suddenly. The neutron-rich nuclei then undergo β^--cascades towards the β-stability valley. However, another important process must be included because of its non-negligible contribution to the final abundance distribution. It concerns the single and multiple β-delayed neutron emissions. Without these β-delayed processes, the so-called frozen abundance curve is known to show very strong odd-even effects, which in turn reflect the zig-zag pattern of the relative abundances in each isotopic chain as given by the neutron separation energy dependence of expression (5). Kodoma and Takahashi (1973) showed the significant effect of the β-delayed neutron processes to smooth out the serrated frozen abundance curve.

The one, two and three β-delayed neutron emissions have therefore been introduced in the successive decays towards the β-stability region during the post-freezing processes. The emission rates have been estimated within the same model than the β-decay rates, i.e. in the gross theory of Kodoma and Takahashi (1975). For the same reason as explained previously, neutron-induced fission as well as β-delayed fission have been neglected. For simplicity, we also assumed that no neutrons are present any more after $t = \tau$ and in particular that no emitted β-delayed neutron would be captured by other nuclei. It should be noticed that the freezing-out of the neutron capture processes would probably not take place so suddenly in a realistic astrophysical site.

Comparison of abundance distributions

Figure 11 shows the abundance patterns obtained for the set of parameters ($T_9 = 1$, $N_n = 10^{24}\,\mathrm{cm}^{-3}$ i.e. $S_a^0 = 2\,\mathrm{MeV}$ and $\tau = 1\,\mathrm{s}$) with the canonical model making use of the von Groote et al. (full line) and the ETFSI (dashed line) mass formulae. The two abundance distributions show obvious differences. Although both exhibit the abundance peaks around A=126 and A=182 corresponding to the accumulation of material at the neutron shell closures N=82 and N=126, effects due to the different value of the neutron separation energies and Q_β-values are clearly apparent.

As regards the influence of the neutron separation energies, the steeper ETFSI mass parabola is expected to shift the peaks to a higher A-value. This is verified for the A=126 peak and to a lesser extent for the A=182 peak. This shift is, however, compensated by the DM underestimate (relative to the ETFSI approximation) of the shell correction at the magic numbers N=82, 126 and 184. We find, indeed, for these neutron numbers: $S_n(\mathrm{ETFSI}) \gtrsim S_n(\mathrm{DM})$, although far away from closed neutron shells, the inequality should be reversed. This characteristic is well described by Fig. 12 which shows the two different r-paths, corresponding to the equi-averaged-neutron separation energy $S_a^0 = 2$ MeV. The stronger ETFSI shell correction has two important effects on the abundance distribution and more precisely on the abundance peaks. The first affects the widening of the abundance peaks. The ETFSI r-process path extends to regions closer to the valley of stability before overcoming the barrier due to the neutron shell closure. The abundance peaks therefore tend to be not only shifted but also widened to higher A-values. The second effect is well displayed by the long "plateaus" appearing in the ETFSI path of Fig. 12. To such plateaus correspond a range of A-values for which nuclei will be very weakly produced after β-decays to the valley of stability. At "low" temperature (such as $T_9 = 1$), the r-process path is so strongly centred on the waiting point that nuclei lying between two distant waiting points might not be produced. To understand the profile of the abundance distribution, it is of interest to analyse the behaviour

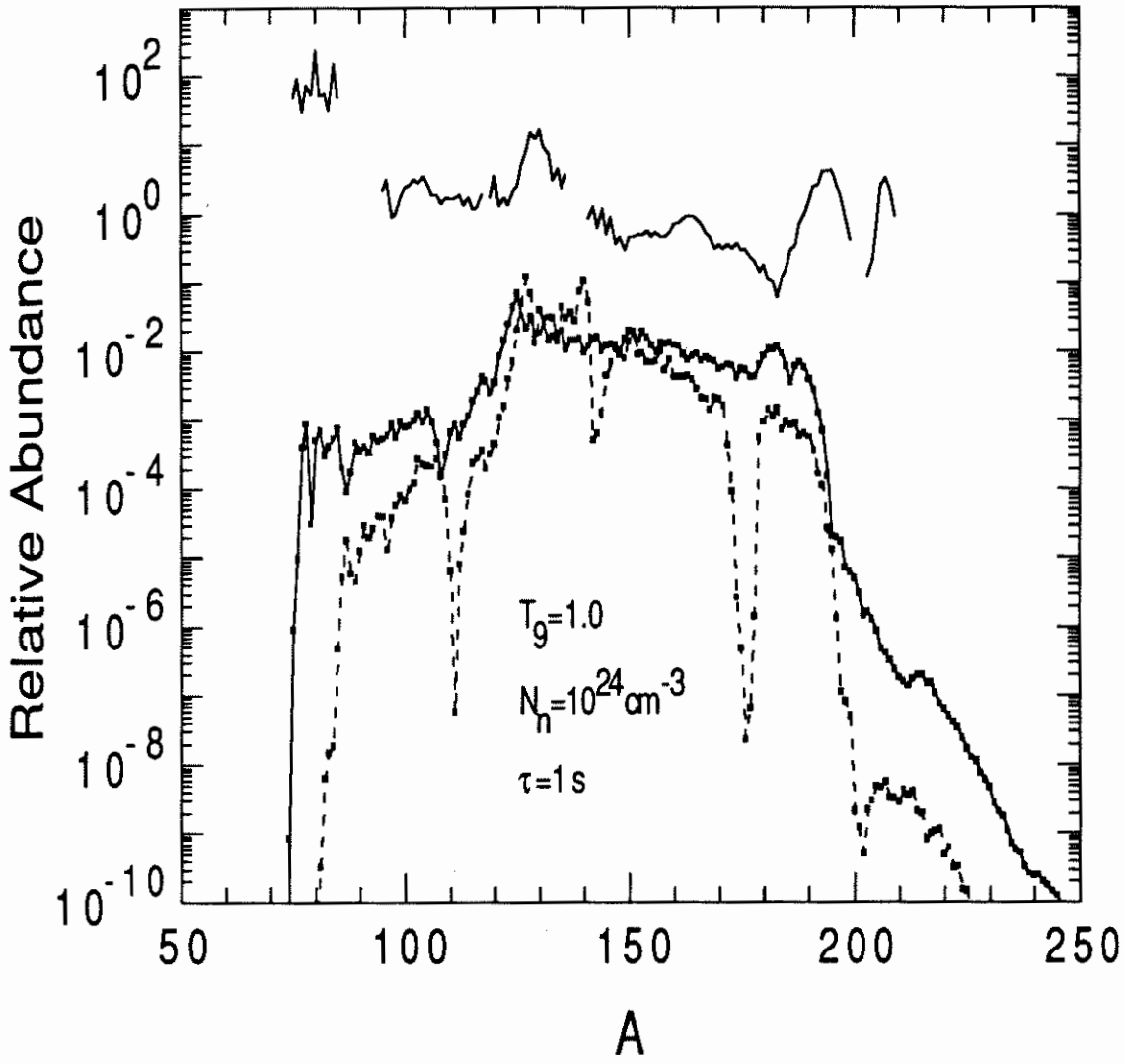

Figure 11. r-process yield curves for the set of physical parameters $T_9 = 1$, $N_n = 10^{24}\,\mathrm{cm}^{-3}$ and $\tau = 1\,\mathrm{s}$ obtained in the framework of the canonical model. The full curve has been obtained making use of the DM mass predictions, while the dashed curve corresponds to the use of the ETFSI masses. Both yields have been obtained with the initial composition N(^{56}Fe)=1, where N is a normalized abundance. The top curve corresponds to the observed solar system r-process abundances from Anders and Grevesse (1989) with an arbitary normalization.

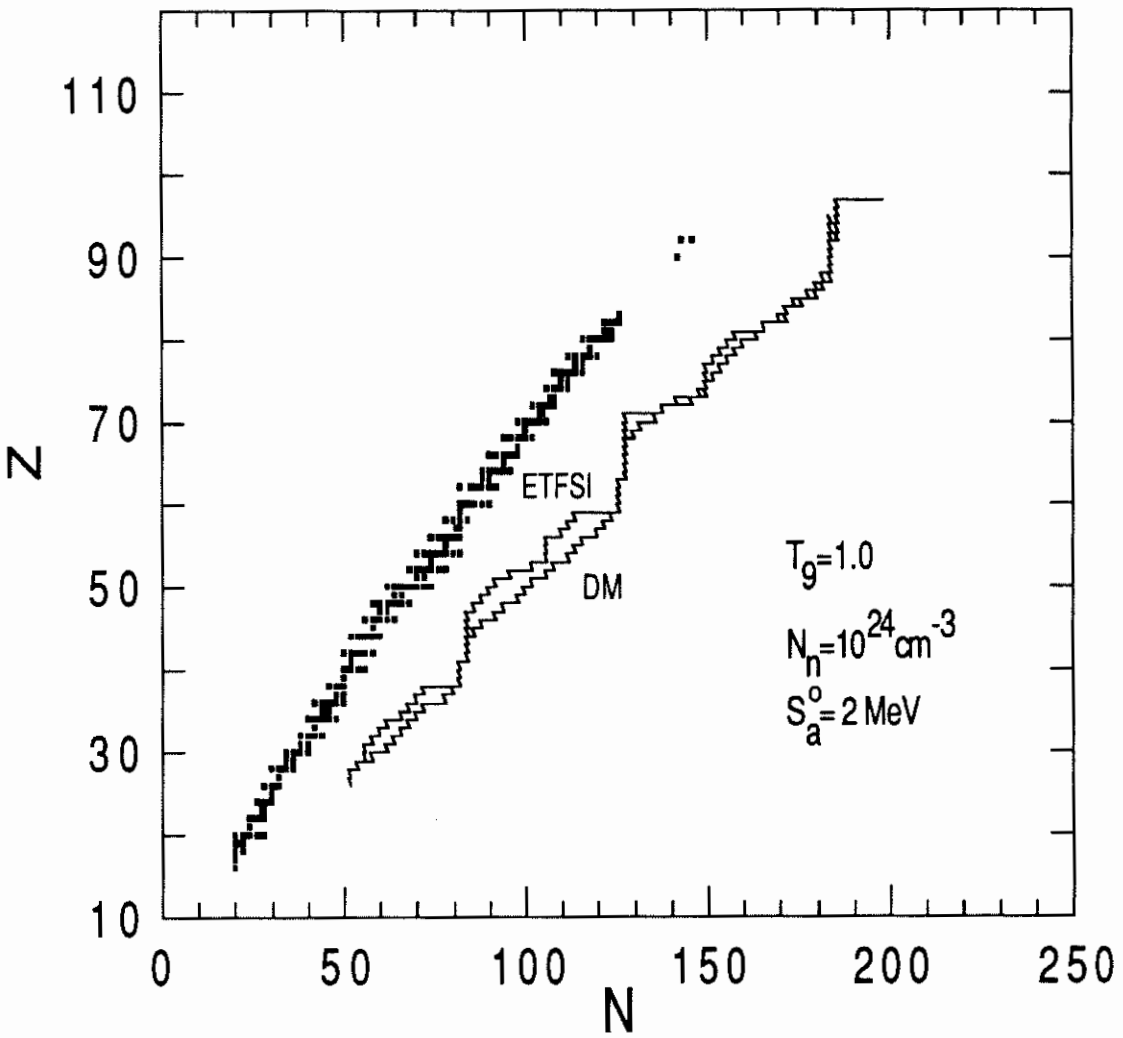

Figure 12. r-process paths corresponding to the set of physical parameters $T_9 = 1$, $N_n = 10^{24}\,\mathrm{cm}^{-3}$, i.e. $S_a^0 = 2\,\mathrm{MeV}$ and obtained with the two mass formulae considered. Black squares correspond to stable nuclei. The closest path to the valley of stability corresponds to the r-process path when use is made of the ETFSI mass table while the r-process path corresponding to the DM mass model drives the nuclear matter to a more neutron-rich region. Both paths are identical at neutron shell closures.

of the odd-even-averaged neutron separation energy $S_a(Z,A)$ within a Z-chain. An example is displayed in Fig. 13 for the three isotopic chains corresponding to Z=52, Z=62 and Z=73. In the ETFSI case, by the large shell correction, the neutron magic numbers tend to *attract* strongly the waiting points. As observed in Fig. 13, the slope of S_a as a function of the neutron number tends to decrease before reaching the magic numbers when a very sharp fall-off begins to appear. This characteristic of the ETFSI S_a-curves just before reaching the shell closures is responsible for the important underproduction of the elements around A=110 and A=175 (see Fig. 11), which corresponds to the two plateaus of Fig. 12 at Z=38 and Z=59, respectively.

In addition, a strong shell effect also implies that if the waiting point is located at a neutron magic number, the surrounding isotopes might not be produced, as predicted by Saha equation (5) (or (11)). An example can be found in the ETFSI abundance distribution around A=189. The two waiting points (Z,A)=(62,188) and (63,191) will not *feed* the A=189 element during the neutron irradiation because of the sharp shell contribution at N=126 which strongly centres the abundance distribution on the waiting points. Such a depletion is, however, not visible on the abundance curve (Fig. 11) because of the abundance redistribution by β-delayed neutron emission after freezing out.

The different treatment of deformation by the two mass models also plays an important role in the depletion of certain nuclei. In particular, the abundance gap around A=145 (Fig. 11) is clearly due to an important variation of the nuclear deformation when one passes from the Z=51 isotopic chain to the Z=52 one. The emergence of a nuclear deformation increases the S_a-value as can be observed for different isotopes of $_{52}$Te, $_{62}$Sm and $_{73}$Ta in Fig. 13 and therefore reduces the slope of the S_a-curve as predicted by expression (14) (B_s is indeed equal to unity for spherical nuclei and is greater than 1 for deformed nuclear shapes). The ETFSI model allows all kinds of axially symmetric deformations, as the DM approach considers small ellipsoidal deformations only. The

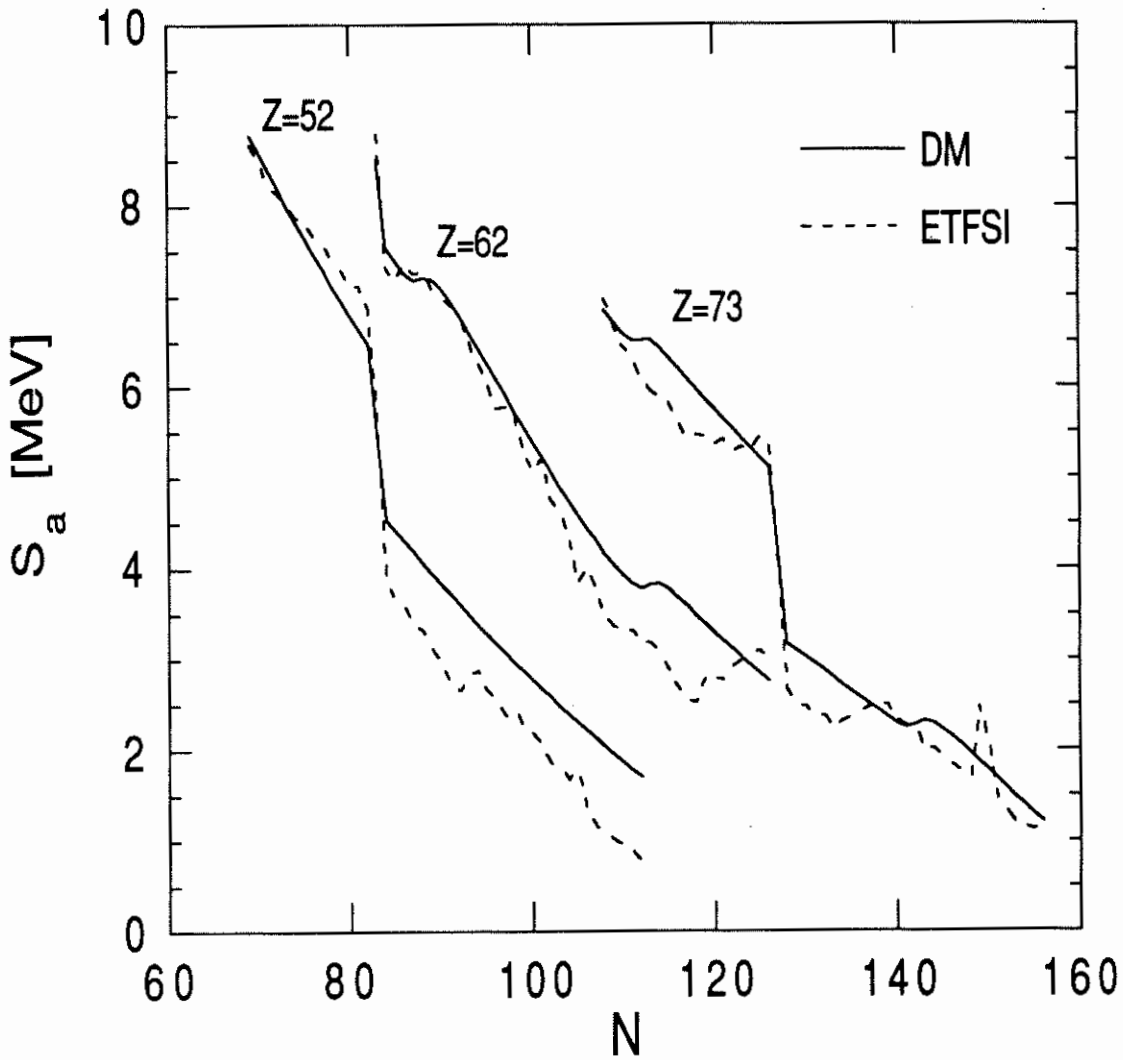

Figure 13. Odd-even-averaged neutron separation energy $S_a(Z,A)$ as a function of the neutron number N and within three isotopic chains Z=52, Z=62 and Z=73. The full curves corresponding to the DM prediction are compared with the ETFSI prediction given by the dashed lines.

deformation in the DM case is therefore a much slower varying function, so that the S_a-curve does not encounter fast variations due to the emergence of a new nuclear shape. For that reason, the DM abundance curve does not present the same strong discontinuities resulting from deformation effects as the ETFSI curve does around A=145 for example.

When higher S_a^0 values are considered, the r-process paths move back further from the neutron drip line. Effects bred of the strong ETFSI shell correction, relative to the DM prediction, remain and still lead to significantly sharper as well as slightly wider abundance peaks, shifted to higher A-values. Effects produced by rapidly varying ETFSI deformations are more cumbersome and cannot be predicted so easily for other astrophysical environments—i.e. characterized by a different set of astrophysical conditions—since they depend on the precise region encountered by the r-process flow.

Differences in the β-decay rates calculated with different nuclear models also have important effects on the abundance curves. As indicated by Fig. 10, the ETFSI half-lives tend to be shorter than their DM prediction by a factor less than 10. Yet the ETFSI r-process path is usually located closer to the valley of stability because of the steeper slope and stronger shell effects of its mass parabola, so that the waiting points are more stable against β-decay than their DM homologues. These two effects tend to compensate each other. For each isotopic chain, we can define the effective timescale against β-decay by

$$\tau_\beta(Z) = \frac{1}{\sum_A P(Z,A)\lambda_\beta^{Z,A}} \tag{19}$$

where $P(Z,A)$ are the relative isotopic abundances normalized in a given Z-chain as given by expression (6) and $\lambda_\beta^{Z,A}$ the β-decay rate of the nucleus (Z,A). Figure 14 displays the quantity $\tau_\beta(Z)$ for the physical conditions of Figs. 11–12. Even if, for each nucleus (Z,A) the ETFSI prediction of the β-decay rates are generally larger than the DM approximation, Fig. 14 clearly shows that the fact that the ETFSI path is translated to less neutron-rich regions is predominant.

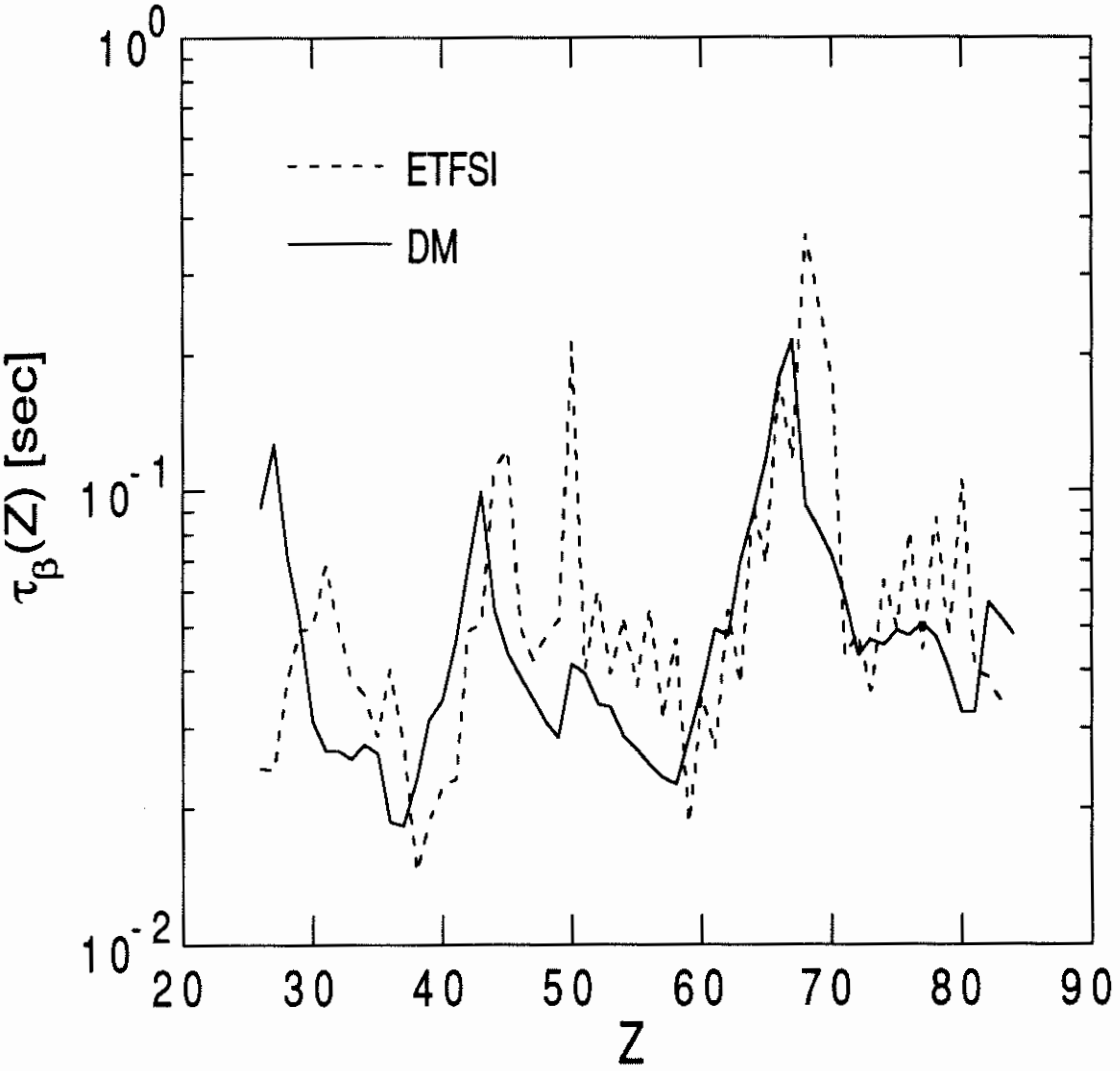

Figure 14. Effective timescales against β-decay for all isotopic chains, as defined by expression (19), for the physical parameters $T_9 = 1$, $N_n = 10^{24}\,\mathrm{cm}^{-3}$ and for the two mass models considered: DM (full line) and ETFSI (dashed line). The Z-values for which $\tau_\beta(Z)$ is maximum correspond to the bottlenecks leading to the abundance peaks of Fig. 11. The values of $\tau_\beta(Z)$ must be compared to the timescale of the r-process equal to $\tau = 1\,\mathrm{s}$ in the case of the Fig. 11.

For most of the isotopic chains, we are left with

$$\tau_\beta^{ETFSI}(Z) > \tau_\beta^{DM}(Z)$$

This is, however, not always true, especially for the iron-group nuclei. The main consequence of the large DM value for $\tau_\beta(27)$ ($\tau_\beta(27) \approx 10^{-1}$s which should be compared to the r-process timescale $\tau = 1$ s) is that it delays the synthesis of heavier elements. The ETFSI depletion of elements with $A < 100$ appears to be much more important than in the DM case and, as seen in Fig. 11, more material is driven to the first peak at $Z = 43$. This characteristic is due to the fact that contrary to what happens at the other neutron magic numbers, there corresponds at N=50 a DM shell correction which is relatively important in comparison with the ETFSI shell correction. This strong DM shell effect compensates for the slowly decreasing DM symmetry term (see expression (10)) so that the waiting points corresponding to the iron-group elements are quite similar for the two mass formulae. Yet the DM half-lives are predicted to be larger than the ETFSI estimation. Consequently, the ETFSI model predicts a much faster depletion of the seed nuclei, as observed on the abundance curve (Fig. 11).

As already stressed, the ETFSI abundance peaks are shifted to a higher Z-(and thus A-) value relative to the corresponding DM peaks. Consequently, the ETFSI β-decay half-lives at the neutron shell closures N=82 and N=126 (i.e. Z=45 and Z=68, respectively, in the case considered) are larger than their DM homologues since they concern nuclei closer to the stability valley. The resulting abundance peaks will, therefore, be higher than the DM peaks, at least if the β-decay timescales at the accumulation points remain of the same order as the neutron irradiation timescale τ. This is illustrated in Fig. 11 where the first ETFSI abundance peak at A=126 (i.e. N=82) is significantly higher.

However, the emergence of a second bottleneck at Z=50 hinders material to be driven to higher Z-value and this only in the ETFSI case. Once again the strong shell contribution to the

ETFSI masses is held responsible for such an increase of $\tau_\beta(Z)$ at Z=50. The passage by the Z=50 isotopic chain significantly slows down the ETFSI flow, a feature that the DM model does not disclose. This characteristic explains the appearance of a second ETFSI abundance peak at A=140 as well as the non-significant production of the heavier elements. A timescale larger than τ = 1 s is, indeed, required to synthesize the $A \gtrsim 150$ nuclei and in particular to obtain an important accumulation of material at the A=182 peak.

When r-process paths are considered for larger S_a^0, the Z=50 ETFSI abundance peak tends to feed lower A-elements, i.e. to widen and strengthen the N=82 peak. As a matter of fact, for a large range of astrophysical parameters corresponding to 3 MeV $\leq S_a^0 \leq$ 6 MeV, the Z=50 waiting point corresponds to the N=82 isotope. From the point of view of timescale, the Z=50 bottleneck remains of great importance since it significantly slows down the progression of the ETFSI flow. The synthesis of the $A \gtrsim 150$ elements is consequently affected and requires a much longer neutron irradiation.

In summary, the calculation performed with the astrophysical conditions (T_9 = 1, N_n = 10^{24} cm^{-3} and τ = 1 s) enables us to predict to some extent the effect of the adopted nuclear mass model on the r-nuclei abundance distribution, in the framework of the canonical model. Two main quantities related to the nuclear mass formula appear to have a decisive influence on the yield curve: the shell effect and the contribution of the symmetry terms. A large shell correction as well as a large symmetry term tend to move the r-process path closer to the valley of stability. This shift has two main consequences on the abundance pattern. On the one hand its shifts the abundance peaks to higher A-value—the peaks can also be expected to become slightly wider at their top and much sharper on the edges—while, on the other hand, it significantly increases the time required to overcome the bottlenecks at the shell closures and therefore delays the synthesis of the post-peak elements. The treatment of deformation is also of importance since it clearly

modifies the r-process path and can accidently lead to a significant underproduction of certain specific elements.

Two other characteristic sets of physical parameters, ($T_9 = 1.5$, $N_n = 10^{24}\,\mathrm{cm}^{-3}$, $\tau = 10\,\mathrm{s}$) and ($T_9 = 3$, $N_n = 10^{30}\,\mathrm{cm}^{-3}$, $\tau = 4\,\mathrm{s}$) have been studied in detail. The resulting abundance distributions are displayed in Figs. 15 and 16, respectively for the two nuclear models considered. These particular conditions, constraining the r-process paths to a region closer to the valley of stability ($S_a^0 \simeq 3\,\mathrm{MeV}$) are neither more nor less justified from an astrophysical point of view. Yet the latter parameter set is of interest since it has been previously considered (Kodoma and Takahashi, 1975) to reproduce the solar abundance distribution of r-nuclei, by making use of the Myers and Swiatecki (1966) droplet model mass formula. While for these particular conditions the DM abundance curve of Fig. 16 appears to reproduce fairly well the position of the observed abundance peaks, an agreement between the location of the ETFSI and observed peaks can hardly be claimed. Figs. 15 and 16 clearly show the same characteristic features as Fig. 11. In particular, the important shift of the first abundance peak can be seen. It should be noted that such modifications in the abundance distributions, as discussed previously are far from being of no consequence from the astrophysical point of view. A shift in calculated abundance curves, especially for the most abundant nuclei, can drastically affect the comparison with the observed data. Alternatively, fits to the observed abundances will constraint the parameter set in a domain which might strongly differ from one nuclear model to the other. For example, it appears that the ETFSI S_a^0-value which would reproduce the DM abundance distribution might be smaller than the DM S_a^0-value by as much as 1 MeV. If a similar temperature T_9 is considered, then the appropriate N_n values given by expression (12) differ by $\left(\frac{5}{T_9}\right)$ orders of magnitude depending on the adopted mass model, which may be hard to reconcile with astrophysically realistic estimates for N_n.

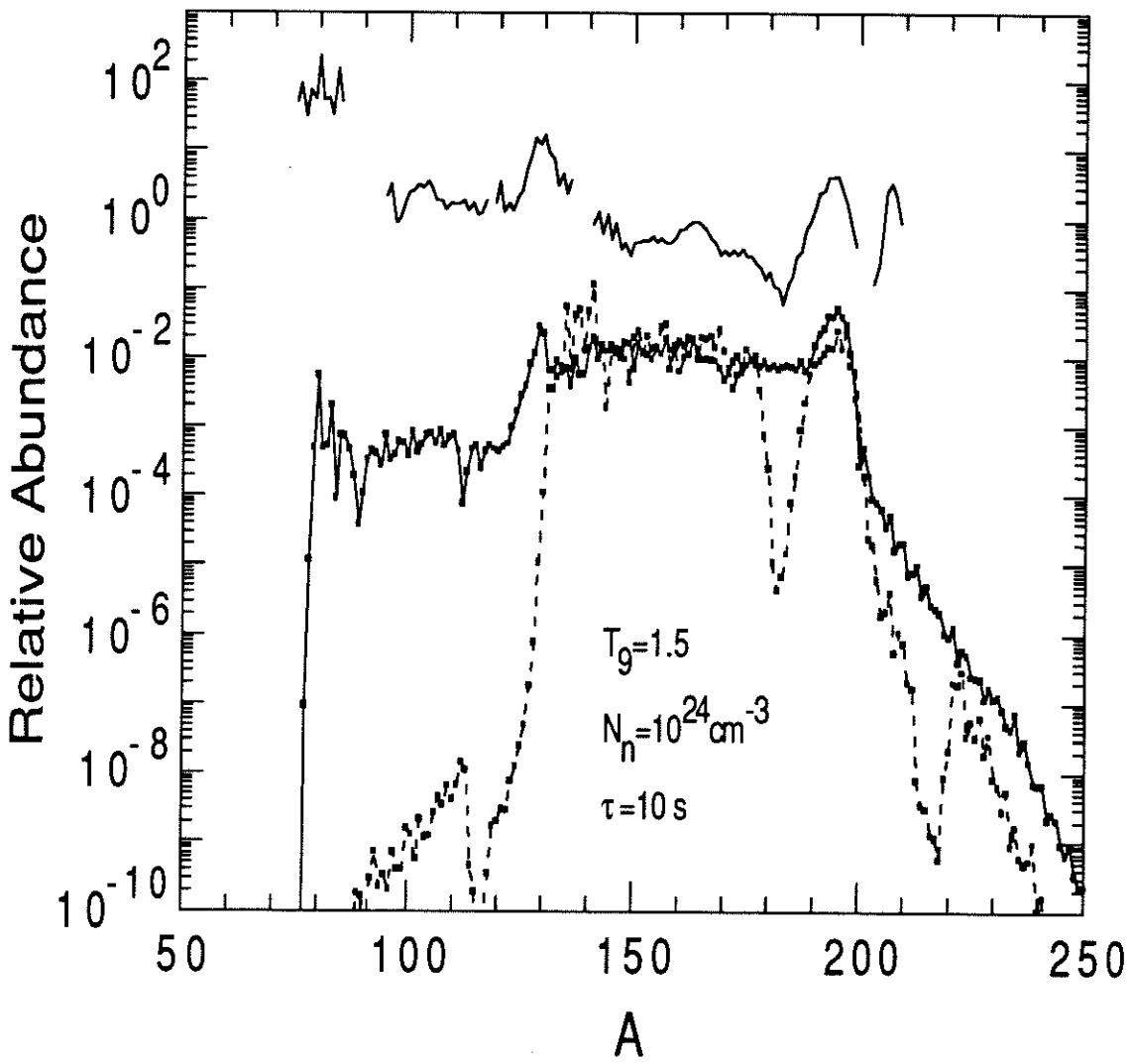

Figure 15. Same as Fig. 11 for the set of physical parameters $T_9 = 1.5$, $N_n = 10^{24}\,\mathrm{cm}^{-3}$ (i.e. $S_a^0 = 3.1\,\mathrm{MeV}$) and $\tau = 10\,\mathrm{s}$.

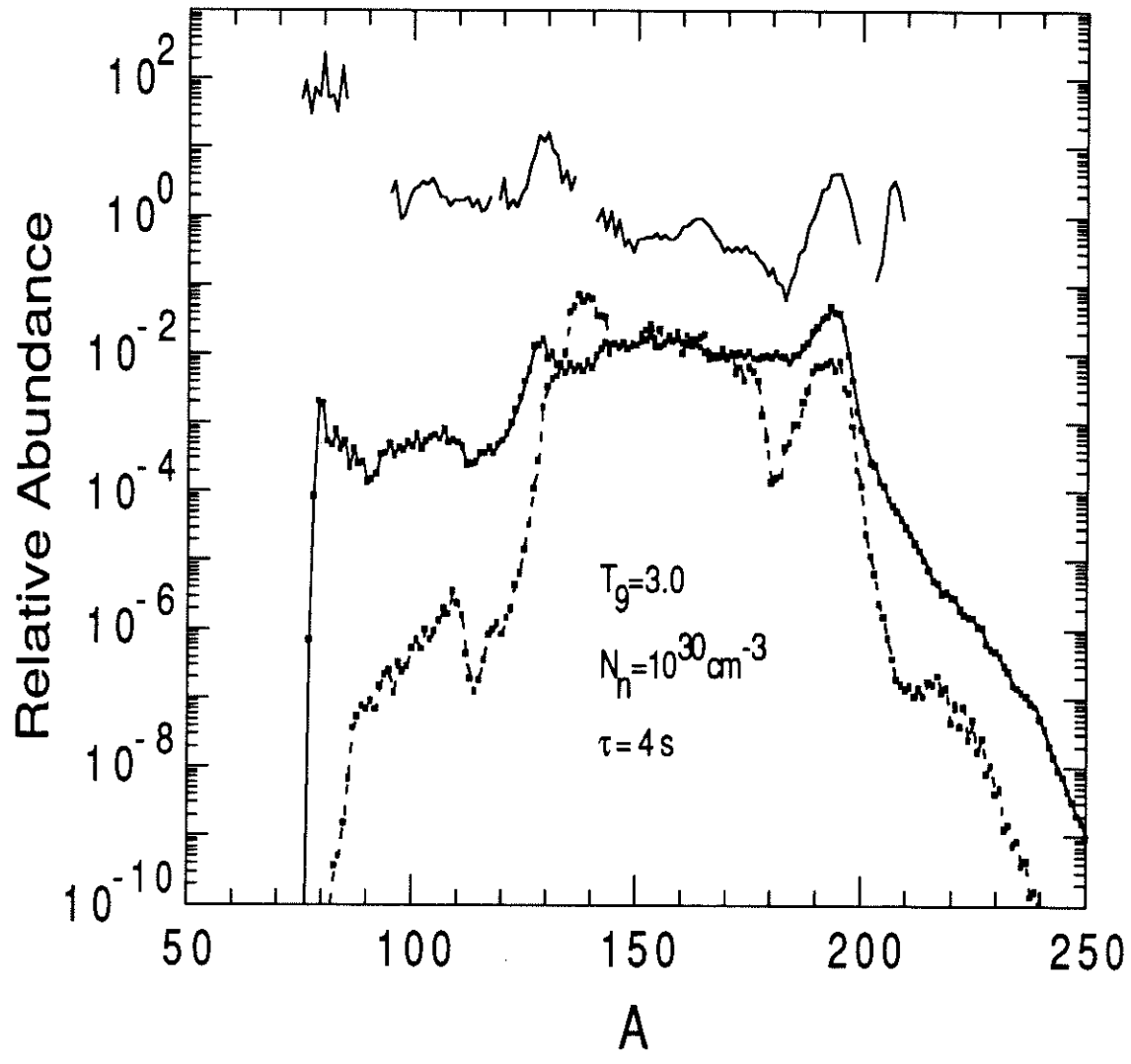

Figure 16. Same as Fig. 11 for the set of physical parameters $T_9 = 3$, $N_n = 10^{30}\,\mathrm{cm}^{-3}$ (i.e. $S_a^0 = 2.9\,\mathrm{MeV}$) and $\tau = 4\,\mathrm{s}$.

I.4 Conclusion

This study of the r-process in the framework of the canonical model shows how important the influence of the adopted nuclear mass model on the abundance distribution can be. The use of two different mass formulae leads to significantly different predictions of the abundance curves. Moreover, it appears very dangerous to draw conclusions from such r-process calculations about the astrophysical conditions appropriate for explaining the observed solar system abundance distribution. It should be stressed that our purpose has not been to judge the quality of the nuclear mass models, but rather to assess their impact on the prediction of the r-abundance curves. Yet it can be concluded that previous r-process calculations using a droplet-type mass formula are of doubtful reliability. The use of two different droplet formulae leads to mass predictions which are so different in the very neutron-rich region that drastic discrepancies between the r-abundance distributions are obtained. As regards the microscopic ETFSI mass table, even if it seems to be more reliable than the classical droplet-type formulae, it is not free of uncertainties when applied to r-process calculations. In particular, the ETFSI prediction of neutron separation energies, as well as Q_β-values, requires further improvements, mainly because of the too strong pairing force adopted (as emphasized by Pearson et al. (1991)). The uncertainties related to these quantities strongly affect the r-abundance predictions. It would be of particular interest to compare the r-abundance distribution obtained with the ETFSI mass table with that obtained with the most recent and sophisticated version of the macroscopic-microscopic approach, namely the finite range droplet model of Möller et al. (1988). Unfortunately, this last mass table is not available yet for the whole neutron-rich region, so this discussion will have to be postponed to a later study.

In conclusion, the remaining uncertainties in the prediction of nuclear masses call for improvements of the theoretical models as well as for new experimental data. It should be stressed that the choice among available nuclear models can only be restricted through constraints coming from

new measurements in the very neutron-rich region. The new experimental techniques devoted to the study of exotic nuclei will certainly play a decisive role in testing the predictive power of the nuclear models.

Part II

Nuclear Level Density Calculation

II.1 Introduction

II.1.1 The nuclear level density in the r-process calculations

As already emphasized in Part I, some nuclear properties like neutron capture cross-sections, β half-lives,... are of fundamental importance in r-process calculations. As soon as the often unrealistic assumption of an (n,γ)-(γ,n) equilibrium is removed, a detailed knowledge of these nuclear properties, and in particular of the neutron capture cross-sections, is required. For the vast majority of nuclei along the r-process path no experimental information is available. Therefore, to determine the neutron cross-sections use is generally made of the Hauser-Feshbach statistical model, at least for atomic numbers $A \gtrsim 20$, where in most cases a high density of excited states in the compound nucleus at the bombarding energy assures the validity of the model. This model assumes that for each angular momentum of the projectile, there exists a state in the compound nucleus at the bombarding energy with appropriate spin and parity (i.e. a high level density has to be provided). The cross-section for the reaction $i^\mu(j,k)l^\nu$ from the target state i^μ to the excited state l^ν of the final nucleus with centre of mass energy E_{ij} and reduced mass μ_{ij} is then given by (e.g. Holmes et al., 1976)

$$\sigma_{ij}^{\mu\nu}(E_{ij}) = \frac{\pi\hbar^2}{2\mu_{ij}E_{ij}} \sum_{J,\pi} \varpi(J) \frac{T_j^\mu(E,J,\pi,E_i^\mu,J_i^\mu,\pi_i^\mu) T_k^\nu(E,J,\pi,E_l^\nu,J_l^\nu,\pi_l^\nu)}{T_{tot}(E,J,\pi)} \qquad (1)$$

where J denotes the spin, E the excitation energy and π the parity of excited states in the compound nucleus (no subscripts), in the target nucleus (subscript i) or the final nucleus (subscript l) and $\varpi(J) = \frac{2J+1}{(2J_i^\mu+1)(2J_j+1)}$ is the spin degeneracy factor.

The important ingredients for such calculations are the particle transmission coefficients and the γ-transmission coefficients T, depending upon whether j and k denote neutrons, protons, alphas or photons. While experiments measure $\sum_\nu \sigma_{jk}^{0\nu}(E_{ij})$ summed over all excited states of the final nucleus with the target in the ground state, target states μ in an astrophysical plasma at temperature T are thermally populated, so that the astrophysical cross-section σ_{jk}^* is given by

$$\sigma_{jk}^*(E_{ij}) = \frac{\sum_\mu (2J_i^\mu + 1)\, \mathrm{e}^{-\frac{E_i^\mu}{k\mathrm{T}}} \sum_\nu \sigma_{jk}^{\mu\nu}(E_{ij})}{\sum_\mu (2J_i^\mu + 1)\, \mathrm{e}^{-\frac{E_i^\mu}{k\mathrm{T}}}} \tag{2}$$

Such a summation leads to the use of the total transmission coefficients

$$T_k(E, J, \pi) = \sum_{\nu=0}^{\omega} T_k^\nu(E, J, \pi, E_l^\nu, J_l^\nu, \pi_l^\nu) + \int_{E_l^\omega}^{E-S_l} \sum_{J_l, \pi_l} T_k^\nu(E, J, \pi, E_l, J_l, \pi_l) \rho(E_l, J_l, \pi_l) dE_l \tag{3}$$

where S_l is the channel separation energy and the summation over excited states above the highest experimentally known state ω is changed to an integration over the level density ρ.

The quality of the theoretically predicted cross-sections is, therefore, determined both by the validity of the statistical model assumption and by the accuracy of the predicted transmission coefficients and level densities.

As regards the reliability of the statistical model to evaluate the cross-sections, it has to be stressed that in many cases of neutron capture along the r-process path, the applicability of statistical model calculations remains somewhat doubtful. Use of the statistical model restricts consideration to cases for which direct reactions or other non-compound nuclear processes are negligible. Such an approximation is generally assumed to be valid if no neutron energies larger than about 10 MeV are considered. This range includes almost all energies of astrophysical interest (10 MeV corresponds to a temperature in excess of approximately 10^{11}K). However, as already demonstrated by Mathews et al. (1983), some nuclei of great importance for the r-process nucleosynthesis (those at shell closures N=82 and N=126—see Part I) disclose, during the neutron

irradiation, a situation which is not observed in the nuclear physics of nuclei near the valley of β-stability, i.e. neutron capture by nuclei with closed neutron shells and small (1–3 MeV) neutron binding energies. An example can be found in chapter I.3, where in the case of a low equi-averaged-neutron-separation-energy S_a^0, the r-process extends to regions close to the neutron drip line before reaching the magic neutron bottlenecks. For example in the special case studied previously, for a temperature $T_9 = 1$ and a neutron density of $10^{24}\mathrm{cm}^{-3}$, $^{185}_{59}\mathrm{Pr}_{126}$ appeared to be an important waiting point for the structure of the final abundance peak at $A \approx 185$. Yet the drip line is situated at the isotope ^{186}Pr. In this situation, the level density may be so low that there might be no compound nuclear states available for the incident neutron. Neutron capture may then be expected to occur predominantly via direct electromagnetic transitions to a bound final state rather than through a compound nuclear intermediary. The direct radiative capture contribution should, therefore, be included in the total neutron capture cross-section since, as shown by Mathews et al. (1983), it can rapidly become comparable to, or even greater than, the statistical component when magic nuclei close to the neutron drip line are considered. However, the lack of currently available models has meant that this contribution has been neglected in all nucleosynthesis studies.

Moreover, when use is made of the compound statistical model in order to evaluate the total neutron capture cross-section, the reliability of the result is still subject to the requirement of a high level density in the compound nucleus at the interaction energy of interest. This implies that a minimum number of resonances must occur in the range of effective energies contributing to the reaction. A rough estimate of this requirement is that $\rho\Delta E \geq 10$ where ρ is the total level density in the compound nucleus at the excitation energy of interest and ΔE is the range of energies contributing to the reaction rate. In astrophysical sites in which the temperature exceeds 10 keV, this restriction limits consideration to nuclei with $A > 70$, even if some anomalous cases near closed shells still give rise to problems, as discussed previously.

It has been shown (e.g. Thielemann et al., 1986) that the reliability of the simple Hauser-Feshbach calculation is rather high. Many statistical model calculations for astrophysical purposes have been performed previously (Truran, 1972; Arnould, 1972; Holmes et al., 1976; Woosley et al., 1987). However, these calculations still suffer from large uncertainties mainly associated with the level density prediction. As shown by expression (3), the theoretical neutron capture cross-section depends sensitively on the accuracy of the predicted transmission coefficients and level densities. The determination of the particle- and γ-transmission coefficients has been described in the above mentioned references and will not be discussed in the present work.

One aim of this work is to improve the level density prediction which remains the weakest point in the current procedures used in the evaluation of cross-sections as required in an r-process calculation. The fundamental importance of the nuclear level density is not just restricted to the statistical estimate of the neutron capture cross-sections. Apart from our practical needs, the theoretical study of the nuclear level density also provides a fundamental insight into an important average property of nuclei and how it is affected by the microscopic, i.e. shell-related, aspects of nucleonic motion. (for a review, see Ericson, 1960).

II.1.2 The nuclear level density models

Since Bethe's pioneering work (Bethe, 1936) many studies have been devoted to the evaluation of the nuclear level density. The so-called partition function method is by far the most widely used technique for calculating level densities, particularly in view of its ability to provide simple analytical formulae. In the simplest form of the analytical approximation, the level density is evaluated for a gas of non-interacting fermions confined to the nuclear volume and having equally spaced energy levels. This model corresponds to the zeroth order approximation of a Fermi gas model and has the great advantage of offering a simple analytical expression for the nuclear level density. Although the equidistant model expressions have been widely used because of their simplicity, the

physical model on which they are based is fairly unrealistic. In an attempt to improve or even to achieve the agreement with experimental data, various phenomenological modifications to the original formulation have been suggested, in particular to allow for shell, pairing and deformation effects. This led first, to the constant temperature formula, then to the popular shifted Fermi gas model and later to the back-shifted Fermi gas model (Gilbert and Cameron, 1965; Huizenga and Moretto, 1972). However, drastic approximations are usually made in deriving such level density formulae and often their shortcomings in matching experimentally known data are overcome by empirical parameter adjustments. In some cases, it appears that it is not possible to reconcile theory and experiment even with phenomenological corrections. In such conditions, the question of the reliability of these methods is bound to arise when dealing with nuclei far from the stability line. It is our opinion that all analytical procedures proposed so far, are rather untrustworthy and should be greatly improved before being applied to the experimentally unknown region of the nuclear chart.

Several of the approximations used to obtain level density expressions in an analytical form can be avoided by quantitatively taking into account the discrete structure of the single-particle spectra associated with realistic average potentials. This approach describes in a natural way, the adopted shell structure of the nucleus and can take pairing effects into account more properly. Although calculations performed in this framework have achieved some success in reproducing experimental data, they are not free from difficulties and uncertainties. First, they require detailed shell model calculations for all nuclei, resulting in a lengthy computational exercise. Although this computational work is not a practical constraint—it can be done rapidly and there are numerous single-particle level schemes currently available in the literature—this has so far been the main reason for neglecting this approach. Nevertheless, even if this numerical approach of the statistical model represents an exact result, relative to the approximated analytical formulae, it strongly

depends on the choice of the adopted potential. As described in Chapter II.2, the crucial quantity on which the calculated level density depends is the single-particle level density in the vicinity of the Fermi energy. This is, however, not a quantity which is reliably adjusted in any shell model calculation. A normalization procedure is required to ensure the consistency between the shell-independent part of the calculated level density and its shell-dependent part. In the absence of such a normalization, the calculated level densities from different single-particle level schemes are expected to be significantly different (Behkami and Huizenga, 1973; Døssing and Jensen, 1974). Moreover, these calculations of level densities are carried out in the independent particle model approximation. Level density calculations performed with an effective potential generated by two body interactions show a significantly different energy dependence to those obtained in the independent particle approximation (French and Ratcliff, 1971; Arnould and Tondeur, 1981).

Very long and cumbersome calculations are also required in the combinatorial model of the level density discussed by Hillman and Grover (1969) and Ford (1978). French and Ratcliff (1971) developed the method of spectral distributions in which the lowest moments of the eigenvalue distribution are calculated from averages and moments of the appropriate operators. This method has the advantage of being able to include sophisticated residual interactions, but remains limited to low excitation energies and low mass nuclei. As for the combinatorial method, the spectral distribution method is of no practical use for astrophysical applications, because of the enormous computer time required. Indeed, one of the major problems encountered in nuclear astrophysics is to find some sort of compromise between the requirements of accuracy and of usability, the latter being of particular significance in problems implying the simultaneous theoretical evaluation of a great number of unmeasured nuclear reaction cross-sections, sometimes thousands of them, as is the case in r-process nucleosynthesis calculations. However, we should stress at this point, that such models remain of great value when highly reliable results are required and more particularly

to nucleocosmochronological calculations (Arnould and Takahashi, 1990).

The remaining problems encountered by the numerical approximations of the statistical model and the inadequacy of the combinatorial and spectral distribution methods to satisfy astrophysical requirements are such that an improvement in the analytical approximation to the statistical model is necessary. As a matter of fact, most statistical models of nuclear reactions make use of the back-shifted Fermi gas formula to describe the nuclear level density. However, this treatment remains phenomenological and is far from being reliable especially when experimentally unknown nuclei are considered. Even for known nuclei, the requirement of fitting experimental data, mainly the s-neutron resonance spacings at an excitation energy close to the neutron separation energy, does not at all ensure the correct energy dependence of the predicted level density. This situation results essentially from the improper treatment of the energy dependence of the shell and pairing corrections.

In order to introduce the shell effect on the nuclear level density in a non-phenomenological way, we have started by removing the equidistant spacing approximation and by substituting more realistic shell model approximations for it. Even in the continuous single-particle spectrum approximation, it is difficult to keep in an analytical form the exact characteristics of the single-particle level density, if known, because of the numerous integrations needed to evaluate the thermodynamical quantities. Therefore, we have developed new methods in order to ensure a description of the shell effect on the thermodynamic quantities that is as exhaustive as possible. These calculations for the total level density will be developed in Chapter II.2 after a description of the semi-classical approximation to the single-particle level density. As shown by expression (3), the quantity of importance in the statistical model of nuclear reactions corresponds to the spin- and parity-dependent level density. Since the angular momentum plays an essential role, in particular, in the analysis of the compound nuclear reactions and in the comparison of theoretical level

densities with experimental data, the density of nuclear levels with a given value of the angular momentum must be determined in an accurate way. In Chapter II.3, a generalization of the previous results will, therefore, be presented to take the spin dependence of the nuclear level density into account. For both, the total as well as the spin-dependent level densities, the results will be compared with the exact numerical evaluation, based on a discrete single-particle level scheme derived from a Woods-Saxon potential.

To introduce the pairing correlation, analytical expressions for the nuclear level density will be derived from the BCS formulation. It is shown in Chapter II.4 how in a very simple and accurate way the pairing interaction can be introduced into the previously derived formulae, without making new assumptions at the expense of the shell structure description. For such a purpose, a new model of the average neutron and proton pairing gaps taking the shell structure into account is proposed.

The resulting level density formula, as well as the semi-classical approximation to the level density parameters, will be compared to experimental data in Chapter II.5. To prove the reliability of the adopted semi-classical shell description, a new ground-state shell correction energy will be formulated and fitted to experimental masses. Similarly, a new analytical expression for the pairing gap will be given and fitted to reproduce the experimental odd-even mass differences. Finally, the comparison of our theoretical level density formula with experimental data, mainly the s-neutron resonance spacings, will be discussed.

II.2 The total nuclear level density and the shell effect

II.2.1 The statistical description of the nucleus

Let us consider a system of A non-interacting fermions with total energy E. The particles occupy the single particle states ε_s of an average potential. In the independent-particle approximation, we can write

$$A = \sum_s n_s \tag{4}$$

$$E = \sum_s \varepsilon_s n_s \tag{5}$$

where n_s are the occupation numbers of the single particle states s, i.e. 0 or 1 for a system of fermions.

Because of the additive nature of these relations, it is convenient to introduce the grand partition function containing all the statistical properties of the system:

$$\begin{aligned} Z(\alpha,\beta) = e^{\Omega(\alpha,\beta)} &= \sum_{A',E'} \exp(\alpha A' - \beta E') \\ &= \sum_{A'} \int \rho(A',E')\exp(\alpha A' - \beta E')dE' \end{aligned} \tag{6}$$

where the sum over E' has been replaced by an integral, allowing for the introduction of the continuous weighting function $\rho(A',E')$, identified with the level density of the system. As described by expression (6), $\rho(A',E')$ is the inverse Laplace transform of the partition function $Z(\alpha,\beta)$:

$$\rho(A,E) = \left(\frac{1}{2\pi i}\right)^2 \int\int_{-i\infty}^{+i\infty} Z(\alpha,\beta)\exp(-\alpha A + \beta E)d\alpha d\beta \tag{7}$$

This integration can be performed approximately by the method of steepest descent (Bohr and Mottelson, 1969). The integrand being a rapidly varying function of α and β, the main contribution

to the integral comes from a small region around the saddle point (α_0,β_0), where the integrand is stationary and defined by the relations

$$A = +\frac{\partial\Omega(\alpha,\beta)}{\partial\alpha}\bigg|_{\alpha_0,\beta_0} \tag{8}$$

$$E = -\frac{\partial\Omega(\alpha,\beta)}{\partial\beta}\bigg|_{\alpha_0,\beta_0} \tag{9}$$

The level density is then given by

$$\rho(A,E) = \frac{e^{S(\alpha_0,\beta_0)}}{2\pi\sqrt{D}} \tag{10}$$

where

$$S(\alpha_0,\beta_0) = \Omega(\alpha_0,\beta_0) - \alpha_0 N + \beta_0 E \tag{11}$$

is known to represent the nuclear entropy of the system. The independent variables α_0 and β_0 are also related to the familiar thermodynamical variables T and μ_0 by the relations $\beta_0 = 1/T$ and $\alpha_0 = \beta_0\mu_0$, where T is the thermodynamic temperature and μ_o the chemical potential.

The factor D corresponds to the 2×2 determinant of the second derivatives of Ω with respect to the Lagrange multipliers α_0 and β_0

$$D = \left|\begin{array}{cc} \dfrac{\partial^2\Omega}{\partial\alpha^2} & \dfrac{\partial^2\Omega}{\partial\alpha\partial\beta} \\ \dfrac{\partial^2\Omega}{\partial\beta\partial\alpha} & \dfrac{\partial^2\Omega}{\partial\beta^2} \end{array}\right|_{\alpha=\alpha_0,\beta=\beta_0} \tag{12}$$

Thus, the level density can be obtained if the function Ω is known as a function of β and μ (or α). Combining expressions (4), (5) and (6), we get

$$\Omega(\mu,\beta) = \sum_s \ln\left[1 + e^{\beta(\mu - \varepsilon_s)}\right] \tag{13}$$

The above formulation of the level density problem can easily be generalized for two components, protons and neutrons, in nuclei by introducing the Lagrange multipliers α_n and α_p to be determined by specifying the number of neutrons, protons and the energy of the nucleus. Since the proton

and neutron contributions to the thermodynamic quantities are additive, we will just refer for the corresponding equations, to reviews such as Gilbert and Cameron (1965) or Huizenga and Moretto (1972).

In this statistical approach of nuclear level density, nuclear structure enters only through the single-particle level states ε_s. They are distributed according to a distribution function g(ε) which can be written in terms of δ-functions as

$$g(\varepsilon) = \sum_s \delta(\varepsilon - \varepsilon_s) \tag{14}$$

The introduction of the distribution function $g(\varepsilon)$ enables us to rewrite the saddle point equations (8) and (9) as well as the entropy expression (10) in a way more suitable for describing degenerate systems (Ericson, 1958):

$$A = \int_0^\infty g(\varepsilon) \frac{1}{1 + \mathrm{e}^{-\beta_0(\mu_0 - \varepsilon)}} d\varepsilon \tag{15}$$

$$U = -\frac{\partial}{\partial \beta_0} \int_0^\infty [g(\mu_0 - \varepsilon) + g(\mu_0 + \varepsilon)] \ln\left(1 + \mathrm{e}^{-\beta_0 \varepsilon}\right) d\varepsilon \tag{16a}$$

$$= -\int_{\varepsilon_F}^{\mu_o} g(\varepsilon)\,(\mu_0 - \varepsilon)\, d\varepsilon + \int_0^\infty [g(\mu_0 - \varepsilon) + g(\mu_0 + \varepsilon)] \frac{\varepsilon}{1 + \mathrm{e}^{\beta_0 \varepsilon}} d\varepsilon \tag{16b}$$

$$S = \left(1 - \beta_0 \frac{\partial}{\partial \beta_0}\right) \int_0^\infty [g(\mu_0 - \varepsilon) + g(\mu_0 + \varepsilon)] \ln\left(1 + \mathrm{e}^{-\beta_0 \varepsilon}\right) d\varepsilon \tag{17a}$$

$$= \int_0^\infty [g(\mu_0 - \varepsilon) + g(\mu_0 + \varepsilon)] \left[\ln\left(1 + \mathrm{e}^{-\beta_0 \varepsilon}\right) + \frac{\beta_0 \varepsilon}{1 + \mathrm{e}^{\beta_0 \varepsilon}}\right] d\varepsilon \tag{17b}$$

where $U = E - E_g$ defines the excitation energy of the system. Introducing the Fermi energy ε_F, we can express the total number of particles A and the total ground state energy E_g as

$$\begin{aligned} A &= \int_0^{\varepsilon_F} g(\varepsilon)\, d\varepsilon \\ E_g &= \int_0^{\varepsilon_F} \varepsilon\, g(\varepsilon)\, d\varepsilon \end{aligned} \tag{18}$$

The energy scale used here is such that $\varepsilon_s \geq 0$ for all states s so that $g(\varepsilon) = 0$ for $\varepsilon < 0$. These expressions have been written in a form which particularly stresses the properties of a degenerate system of independent Fermions, namely to be completely specified by the excitation energy U and

by the distribution function $g(\varepsilon)$ in a close energy interval (of width $\sim 1/\beta_0$) around the chemical potential. (The chemical potential usually does not deviate appreciably from the Fermi energy, at least at low temperatures).

This very interesting property originally gave rise to the analytical approximation of the nuclear level density. An analytical expression for the total level density can be derived if $g(\varepsilon)$ as given by expression (14) is replaced by a mathematically more suitable function, i.e. a continuous function. This continuous-spectrum approximation is well adapted for treating degenerate systems, but it is not very suitable for investigating the limitations on the system due to the finiteness of the number of particles. For example, expressions (15) and (18) require the complete knowledge of the distribution function on the whole energy range $[0, \varepsilon_F]$ and will, consequently, be described by the continuous-spectrum approximation in a relatively poor way. Although the level density of the system can now be described without making use of the expressions (15) and (18), they come into play when level densities need to be expressed as a function of the particle number A (instead of the Fermi energy).

The above formulation originally led to the very simple model, in which the one-Fermion levels are assumed to be equally spaced and non-degenerate. This model corresponds to the zeroth order approximation of a Fermi gas model as introduced by Bethe in 1936. In this equidistant spacing approximation a remarkably simple expression for the level density can be obtained. However, this widely used model gives relatively crude results, especially at low excitation energy and for systems which have anomalies in the spacing near the Fermi energy, as can be expected from a more realistic system of nucleons.

It has long been recognized that odd-even and shell effects in actual nuclei give level densities which are very different from the predictions of the simple Bethe formula. In order to partially remove some discrepancies, many phenomenological modifications of the original formula have been

suggested. In particular, to account for the odd-even effects, a pairing energy has been subtracted from the excitation energy, leading to the shifted Fermi gas model (Newton, 1956). To include shell effects, the constant temperature formula has been proposed. Later a composite level density using the constant temperature model at low energy and a back-shifted Fermi gas model (which in contrast to the shifted Fermi gas model treats the energy shift as a free parameter to account for both shell and pairing effects) at higher energies appeared to be successful in reproducing the neutron resonance data (Gilbert and Cameron, 1965). Improvements of the Fermi gas formula have been attempted by introducing into the above expressions more realistic single-particle level densities, i.e. by removing the equidistant spacing approximation (Ericson, 1956; Kataria et al., 1978; Jensen and Sandberg, 1978). However, they reduced the shell effect in the distribution function to a simple periodic function, corresponding to the first term of a Fourier expansion. Such a procedure remains obscure in many respects. The adopted single-particle level density is purely phenomenological and, therefore, cannot be related to physical quantities or even be justified on grounds of nuclear properties. Moreover, in order to carry out integrations (16) and (17) with these more complex sets of single particle levels, use is made of methods, as developed by Bloch (1954), which in our opinion are not adequate to describe the temperature dependence of the shell contribution to thermodynamic quantities. These methods are based on a power series expansion of the single-particle level density, and have the disadvantage of smoothing out the rapidly varying behaviour of the oscillating contribution and reducing the effects of shell structure into a simple constant energy shift.

Therefore, we have undertaken the removal of the discrepancies related to this phenomenological treatment of the single-particle level density and the improvement of the methods to deal with these more complex functions. It should be pointed out that the adopted point of view is significantly different from the one generally adopted in previous studies. The idea is to describe

accurately the single-particle level density and to deduce the thermodynamic quantities without adversely affecting the characteristics of the adopted single-particle level density. Such an approach requires the single-particle level density to be expressed in both a realistic and a suitable way. A compromise between these two requirements can be found for an infinite square well potential, as shown in Section II.2.2. Integrations (16) and (17) can then be conducted following some assumptions and the thermodynamic quantities can be determined (Section II.2.3). A final comparison with the exact numerical evaluation derived from a Woods-Saxon type single-particle scheme emphasizes the predictive power of this approach (Section II.2.4).

II.2.2 The semi-classical approximation to the single-particle level density

The semi-classical methods constitute one of the three classes of approximation (with the perturbation techniques and the variational methods) commonly used in quantum mechanics. In this particular approximation, the behaviour of wave functions, energy levels, phase shifts, etc. are studied and analytically described in the limiting case where Planck's constant $\hbar$ is small in comparison with the action functions occurring in the corresponding classical problem. Therefore, the quantum-mechanical quantities are expressed in a power series in $\hbar$ whose first terms are the values of the quantities according to classical mechanics. However, the resulting formulae are often analytically quite complicated, but they have the great merit of describing almost all the physics, and as a numerical approximation they are often surprisingly accurate (for a review, see Berry and Mount, 1972).

In the semi-classical approximation, the density of eigenvalues is not evaluated by direct counting of eigenstates, but through the construction of the Green function for the equation studied. The distribution of eigenfrequencies can be expressed (Gutzwiller, 1967) by

$$\begin{aligned} g(\varepsilon) &= \sum_n \delta(\varepsilon - \varepsilon_n) \\ &= -\frac{1}{\pi} Im \int G(\mathbf{r}', \mathbf{r}, \varepsilon) \Big|_{\mathbf{r}' \to \mathbf{r}} d\mathbf{r} \end{aligned} \tag{19}$$

where $G(\mathbf{r}', \mathbf{r}, \varepsilon)$ is the energy-dependent Green function of the problem and ε_n the eigenvalues. The above approach can lead to an analytical expression of the single-particle level density, if the Schrödinger equation of the independent particle model is considered. Using a time-independent Green function method involving a multiple expansion, Balian and Bloch (1970) expressed the distribution of eigenvalues of the wave function in terms of power expansion in $kV^{1/3}$ (where $k = \sqrt{\frac{2m}{\hbar^2}\varepsilon}$ is the wave number and V the cavity volume) in the case of the wave equation with generalized Neumann-Dirichlet boundary conditions.

In the same manner, Balian and Bloch (1972) used the semi-classical methods to give the first consistent theoretical explanation of the concentrations of levels in regularly distributed bunches. Based on the quasi-classical solution of the problem of the distribution of eigenfrequencies in a cavity of arbitrary form, they applied their theory to an infinite spherical potential. The first results for the wave equation, based on the concept of multiple reflection for the Green's function of a problem with reflecting walls, were then extended to the general case of the Schrödinger equation (Balian and Bloch, 1974; Strutinsky and Magner, 1976). The general quasi-classical solution of the problem was obtained in the framework of the stationary phase method, from the Feynman path integral for the propagator, from which the Green function is obtained by a simple Fourier transformation.

The main conclusion of the above studies is that the level bunching in the single-particle spectra is a result of a specific quantization of the single-particle motion along the stationary classical orbits in the closed volume of the many-dimensional potential well. This result can be understood through the density expression as described by equation (19). Since $g(\varepsilon)$ depends on $G(\mathbf{r}', \mathbf{r}, \varepsilon)$ when $\mathbf{r}' \rightarrow \mathbf{r}$, the semi-classical density of states depends only on the classical paths which start and end at the same point $\mathbf{r}$. There are two types of paths :

(a) paths of zero length corresponding to $\mathbf{r}' \equiv \mathbf{r}$. This non-trivial case leads to the Thomas-Fermi formula i.e. the smooth contribution $\tilde{g}(\varepsilon)$ to the total single-particle level density. It corresponds to the first term of a formal series expansion of $g(\varepsilon)$ in powers of $\hbar$.

(b) looped paths which involve an excursion away from the point $\mathbf{r}$ before returning. These paths give rise to the oscillatory contribution $g_{osc}(\varepsilon)$ to the single-particle level density. It can be shown that the main contribution to the looped paths is obtained when the system has the same momenta, as well as the same coordinates at both ends of its trajectory. This is the condition of periodic motion. All other kinds of non-closed looping paths give negligible

contribution to the integration (19) because of destructive interferences. On the other hand, each periodic orbit contributes an infinite number of terms to $g_{osc}(\varepsilon)$, corresponding to returns to $\mathbf{r}$ after different numbers of traversal (in both directions). It is the interference between the waves making these successive circuits that gives rise to sets of quantized energy levels. In turn, the level bunching in the single-particle spectra (i.e. the shell structure) is a result of this specific quantization. It can be interpreted as being a generalization to the case of many-dimensional periodic motion of the familiar Bohr-Sommerfeld one-dimensional quantization rule. In the many-dimensional case the level density is quantized in a manner analogous to the Bohr-Sommerfeld rule with the action integral evaluated for periodic paths in the potential well.

In the general iterative expansion for the single-particle Green's function, the Thomas-Fermi contribution G_0, corresponding to the shortest classical paths between the point $\mathbf{r}$ and $\mathbf{r}'$, must be the principal term of the iterative series in the classical limit. However, the terms of the series associated with more complicated paths, with one or more reflection points, contain a contribution of at least the same order in $\hbar$ as G_0. For a Hamiltonian of high symmetry, this contribution to the Green's function may even be of lower order in $\hbar$ than the Thomas-Fermi component.

The eigenvalue density finally takes the form (Balian and Bloch, 1974)

$$\begin{aligned} g(\varepsilon) &= \tilde{g}(\varepsilon) + g_{osc}(\varepsilon) \\ &= \tilde{g}(\varepsilon) + \frac{1}{\pi\hbar^2} \sum_{\alpha} ImA_{\alpha} \exp(i\frac{S_{\alpha}}{\hbar}) \end{aligned} \tag{20}$$

where the summation in the oscillating function $g_{osc}(\varepsilon)$ is carried over all closed periodic trajectories α; S_{α} is the stationary value of the action along the closed path and A_{α} the corresponding amplitude.

(i) the smooth contribution to the single-particle level density

The semi-classical approach is well suited to study the smooth contribution $\tilde{g}(\varepsilon)$ to the total

density. As a matter of fact, the smooth (or macroscopic) behaviour of the density depends only upon integrated local geometric properties of the boundary surface: the volume V, the surface S, the integral of the main curvature C, etc. Expressed as a power series in $kV^{1/3}$, the two leading terms, known as the volume and surface terms, correspond to the bulk variation of the level density and are, therefore, of fundamental importance when the continuous-spectrum approximation is used. The smooth contribution to the single-particle level density has been the subject of many controversies (Kataria and Ramamurthy, 1980; Töke and Swiatecki, 1981; Ramamurthy et al., 1983; Handloser and Stocker, 1985). More particularly the sign of the surface term, as well as its relative contribution, remain entirely unknown.

In the case of a Woods-Saxon potential of volume V, surface area S, depth V_0 and diffuseness a, an analytical expression $\tilde{g}(\varepsilon)$ can be derived (see Appendix A) and is given by:

$$\begin{aligned}\tilde{g}(\varepsilon) &= \tilde{g}_V(\varepsilon) + \tilde{g}_S(\varepsilon) \\ &= \frac{D}{4\pi^2}\frac{2m^*}{\hbar^2}\left[\sqrt{\frac{2m^*}{\hbar^2}\varepsilon}\,V + \left(\delta_{WS}(\varepsilon) - \frac{\pi}{4}\right)S + \cdots\right]\end{aligned} \tag{21}$$

where m^* is the effective nucleonic mass and D is the degeneracy factor taking the spin ($D = 2$) or the spin and isospin ($D = 4$) degeneracy into account. The phase shift $\delta_{WS}(\varepsilon)$ is a more or less complicated function of ε, a and V_0

$$\delta_{WS}(\varepsilon) = \tan^{-1}\sqrt{\frac{\varepsilon}{V_0 - \varepsilon}} - \sum_{n=1}^{\infty}\tan^{-1}\frac{2k_0 a\sqrt{\varepsilon}}{n} + 2\sum_{n=1}^{\infty}\tan^{-1}\frac{k_0 a\sqrt{\varepsilon}}{n + k_0 a\sqrt{V_0 - \varepsilon}} \tag{22}$$

with $k_0 = \sqrt{\frac{2m^*}{\hbar^2}}$

As shown in Fig. A1 (see Appendix A), the surface contribution can be reduced to a monotonic increasing function of the energy ε, almost independent of the diffuseness parameter a (because of the small range of values considered) and slightly varying with the potential depth V_0. It is worth noting that the Woods-Saxon shape of the potential well influences the single-particle level density only through the surface correction and that the volume term remains identical to the one derived for an infinite square well potential.

As shown by expressions (16) and (17), the statistical approach requires the knowledge of $\tilde{g}(\varepsilon)$ for all energies $\varepsilon > 0$. This raises the question of the role of the unbound levels for the state density of a nucleus. The Woods-Saxon potential, as a finite depth well, has no bound levels above the particle binding energies. Although the main contribution to the thermodynamic quantities comes from a narrow energy range around the Fermi energy, the influence of the unbound levels on the nuclear level density remains uncertain, especially for nuclei with low nucleonic binding energy. In the level density of a compound nucleus, the phase space at high single-particle energies inside the nucleus is involved. For a thermally equilibrated nucleus to exist, the particles with energies higher than the binding energy also have to be considered as being confined to the volume of the nucleus by interactions with the other nucleons. The concept of the compound nucleus holds only as long as the probability for the nucleon's leaving the nucleus as a free particle is much smaller than the probability of its staying inside the nucleus. Schmidt et al. (1982) show that the single-particle level density in the continuum increases in a similar manner to that in an infinite box, so that we can also expect expression (21) to describe, in a fairly reliable way, the behaviour of $g(\varepsilon)$ in the continuum. It can be seen in Fig. A3 (see Appendix A) that expression (21) reproduces fairly well the exact Woods-Saxon result, even at high energies where the unbound levels appear.

(ii) the oscillating contribution to the single-particle level density

In contrast to the smooth gross behaviour of the level density, shell effects appear as oscillations in the eigenvalue density, which depend in a complicated way on the shape of the boundary surface as a whole. Therefore, the semi-classical approach can be expected to give rise to complicated expressions of the oscillation correction $g_{osc}(\varepsilon)$, in the case of realistic potential, like the Woods-Saxon potential, even for spherical nuclei. Such a description of the shell structure is not suitable for determining the thermodynamic quantities involved in the statistical model of nuclear level densities and fails to give an accurate quantitative estimation of the subsequent shell effect.

However, the special case of the infinite square well potential represents a compromise between a realistic description of the nuclear shell structure and the ease with which it can be expressed analytically, as required in the framework of the statistical model. In this case, the Schrödinger equation is reduced to the wave equation, the quasi-classical solutions of which are now well known (see Appendix A). In particular, the periodic orbits are given by simple polygons (Fig. A4), each of them giving rise to a non-negligible contribution to the oscillating level density

$$\begin{aligned} g_{osc}(\varepsilon) &= \sum_{t=1}^{\infty} \sum_{p=2t}^{\infty} g_0(p,t,\varepsilon) \\ &= \sum_{p>2t} g_1(p,t)\varepsilon^{1/4} \sin\left[g_2(p,t)\varepsilon^{1/2} + K(p,t)\right] + \sum_{p=2t} g_1(p,t) \sin\left[g_2(p,t)\varepsilon^{1/2}\right] \end{aligned} \tag{23}$$

where the two integers (p,t) characterize the periodic orbits, as shown in Fig. A4. Full details about the amplitudes $g_1(p,t)$, frequencies $g_2(p,t)$ and phases $K(p,t)$ can be found in Appendix A. It is the constructive interferences between the different polygonal contributions that produce the gross oscillations around the bunching of eigenvalues. As can be seen in Fig. A5 (see Appendix A), the semi-classical approximation (23), instead of predicting positions of specific eigenvalues, now determines the distribution of maxima of the level density.

It could be argued that the description of the two single-particle level density contributions derived from two different potential models (the Woods-Saxon for the smooth part and the infinite square well for the oscillating correction) do not constitute a consistent approach. Yet it should be remembered that this choice is a consequence of the compromise between a realistic description of the single-particle spectrum and the usability of such a description for our purposes. Moreover, the above treatment has the advantage of being based on physical grounds and provides a much clearer understanding of the effect of the nucleonic motions on the total state density. A general parametrization of the final nuclear level density can be considered reliable, not only if it gives good fit to experimental data, but also if it is supported by a sound theoretical base, in contrast to purely empirical formulations. This statement is of particular importance when extrapolations

from experimentally known domains are concerned. It will be shown (see Chapter II.5) how from such simple models, a more realistic description of the nuclear shell structure (especially taking the spin-orbit potential, i.e. the exact magic numbers into account) can be derived.

II.2.3 Determination of the thermodynamic quantities

In order to extract analytical expressions for the entropy S and the excitation energy U, as well as to maintain the physical features of the single-particle level density, we have chosen to carry out the integrals (16a) and (17a) by approximating the integrand functions instead of expanding the single-particle level density in a power series, as has been done previously. It is shown in Fig. 1 that the universal function

$$y(x) = \frac{1}{\ln 2} \ln\left(1 + \mathrm{e}^{-x}\right) \tag{24}$$

can be well reproduced in the domain $x \geq 0$ by the mathematically more suitable function

$$y_a(x) = \mathrm{e}^{-x/\sigma_a} \tag{25}$$

where $\sigma_a = \frac{\pi^2}{12 \ln 2}$ has been determined to obtain the same area between the curve and the axis, i.e. such that the leading terms of S and U are evaluated exactly. However, the derivative of $y(x)$ is slightly underestimated by the derivative of $y_a(x)$ in the vicinity of $x = 0$, so that some discrepancies can be expected if the quantities calculated with the above approximation mainly depend on the derivative of $y(x)$ around $x = 0$.

If we assume that, in the range of temperatures of interest in nuclear reaction analysis, the effect of the weak temperature dependence of the chemical potential μ_0 on the calculation of the entropy and excitation energy is negligible, μ_0 can be treated as energy-independent in expressions (16) and (17). The lengthy but straightforward integrations, under the assumption $T \ll \mu_0$ then lead to the following analytical expressions

$$\begin{aligned} S = {} & 2\alpha\tilde{g}(\mu_0)T + \sum_{p>2t} 2\alpha\ g_1\mu_0^{1/4} \sin(g_2\mu_0^{1/2} + K)\ T\ \frac{1}{(1+\gamma_2^2T^2)^2} \\ & + \sum_{p>2t} 2\alpha\ \frac{\sigma_a}{\mu_0\gamma_2}\ g_1\mu_0^{1/4} \cos(g_2\mu_0^{1/2} + K)\ T\ \frac{\gamma_2^2T^2}{(1+\gamma_2^2T^2)^3} \\ & + \sum_{p=2t} 2\alpha\ g_1 \sin(g_2\mu_0^{1/2} + K)\ T\ \frac{1}{(1+\gamma_2^2T^2)^2} \end{aligned} \tag{26}$$

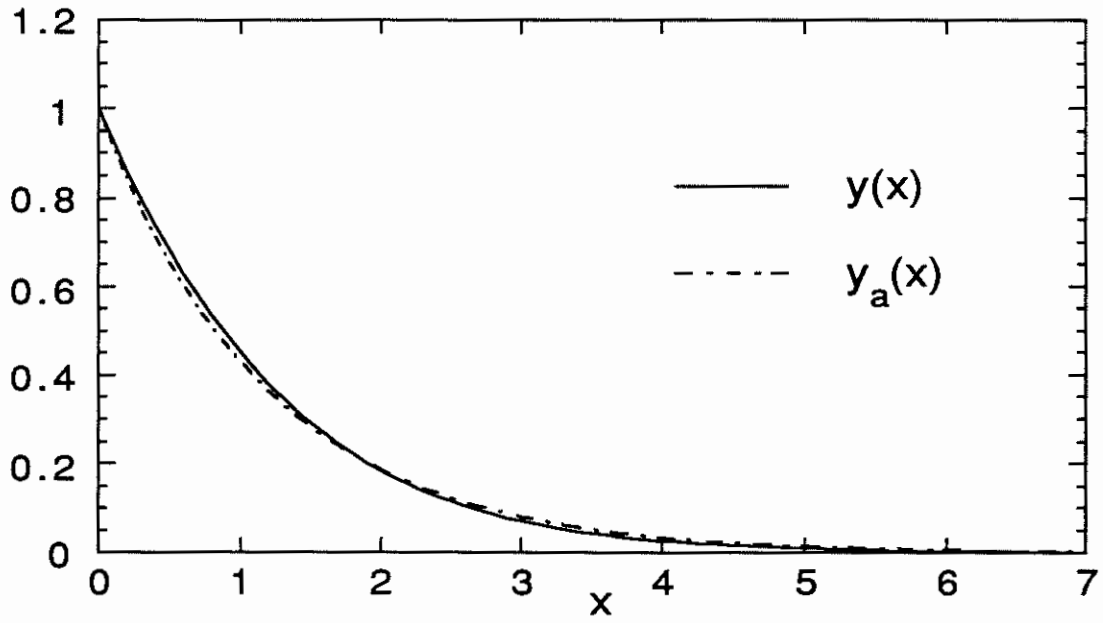

Figure 1. Comparison of the function $y(x)$ defined by expression (24) in the text with the approximate function $y_a(x)$ given by expression (25).

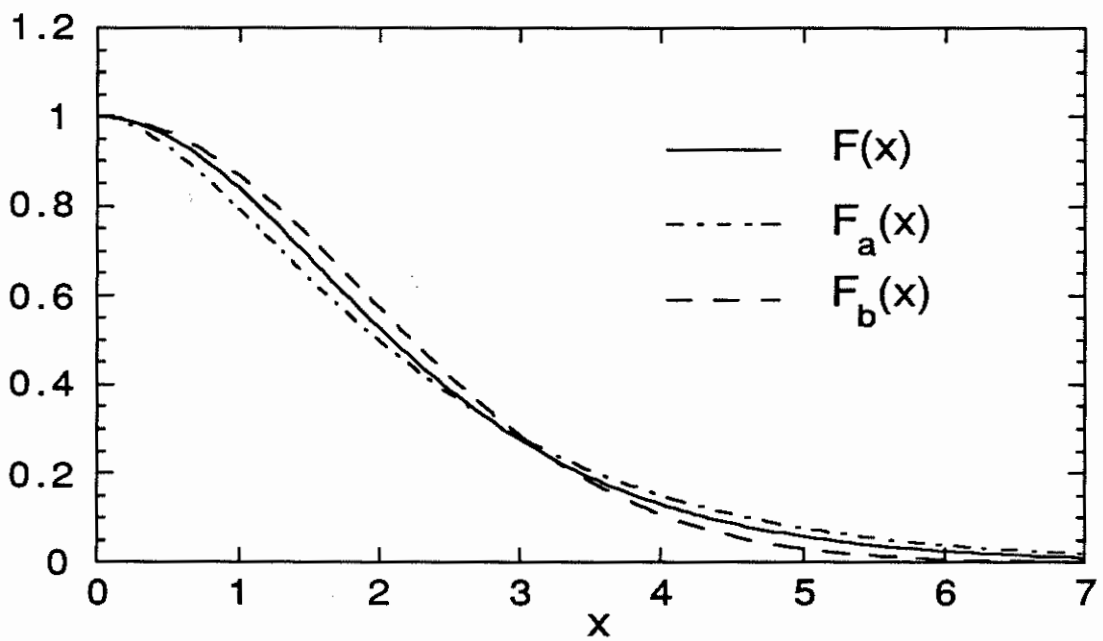

Figure 2. Comparison of the function $F(x)$ given by expression (35) with the two approximations $F_a(x)$ and $F_b(x)$ defined, respectively, by expressions (36) and (37) in the text.

$$U = \alpha\tilde{g}(\mu_0)T^2 + \sum_{p>2t} \alpha\ g_1\mu_0^{1/4} \sin(g_2\mu_0^{1/2} + K)\ T^2\ \frac{1-\gamma_2^2T^2}{(1+\gamma_2^2T^2)^2}$$
$$+ \sum_{p>2t} \alpha\ \frac{\sigma_a}{2\mu_0\gamma_2}\ g_1\mu_0^{1/4} \cos(g_2\mu_0^{1/2} + K)\ T^2\ \frac{(3-\gamma_2^2T^2)\gamma_2^2T^2}{(1+\gamma_2^2T^2)^3} \qquad (27)$$
$$+ \sum_{p=2t} \alpha\ g_1 \sin(g_2\mu_0^{1/2} + K)\ T^2\ \frac{1-\gamma_2^2T^2}{(1+\gamma_2^2T^2)^2}$$

where $\alpha = 2\sigma_a \ln 2 = \frac{\pi^2}{6}$ and $\gamma_2 = \frac{1}{2}g_2\frac{\sigma_a}{\mu_0^{1/2}}$, which is temperature-independent.

These analytical expressions show the characteristic features of the equidistant spacing model, namely

$$S \sim \frac{\pi^2}{3}g(\mu_0)T \qquad (28a)$$

$$U \sim \frac{\pi^2}{6}g(\mu_0)T^2 \qquad (28b)$$

However, the introduction of an oscillation contribution to the single-particle level density leads directly to a shell correction to the entropy, and to the excitation energy, which is far from being negligible at low temperatures. Moreover, these formulae agree with the commonly accepted idea that the shell effect disappears at high excitation energies. Within the limit of high temperature we can write

$$S \sim \frac{\pi^2}{3}\tilde{g}(\mu_0)T \qquad (29a)$$

$$U \sim \frac{\pi^2}{6}\tilde{g}(\mu_0)T^2 - \delta W \qquad (29b)$$

where the quantity

$$\delta W = \delta W_1 + \delta W_2$$
$$= \frac{\pi^2}{6}\sum_{p\geq 2t}\frac{1}{\gamma_2^2}\ g_0(p,t,\mu_0) + \frac{\pi^2}{6}\sum_{p>2t}\frac{\sigma_a}{2\mu_0\gamma_2}\ \frac{1}{\gamma_2^2}\ g_0(p,t,\mu_0)\cot(g_2\mu_0^{1/2} + K) \qquad (30)$$

turns out to be the difference between the excitation energy of an equivalent Fermi gas nucleus (i.e. without shell effects) and that of the actual nucleus in the asymptotic limit of high temperatures. Therefore, the quantity δW can be associated with the ground state shell correction energy. Yet

it should be noticed that the calculation of the excitation energy for high temperature raises some problems, since it strongly depends on the variation of the function y around the Fermi energy, i.e. on the derivative of $y(x)$ around $x = 0$. A more accurate evaluation shows that expression (30) overestimates the shell correction by a factor of $\pi^2/(6\sigma_a^2) \sim 1.18$. This problem is of no consequence as long as δW is considered as a parameter. However, if δW is extracted from another expression than approximation (30), this correction factor has to be considered in the evaluation of the entropy and excitation energy.

On the other hand, if we assume that the parameter γ_2 is almost independent of the orbit type, we can approach S and U by the expressions

$$S = 2\,\tilde{a}\,T + 2\,\gamma^2\delta W_1\,\frac{1}{(1+\gamma^2T^2)^2}\,T + 2\,\gamma^2\delta W_2\,\frac{2\gamma^2T^2}{(1+\gamma^2T^2)^3}\,T \tag{31}$$

$$U = \tilde{a}\,T^2 + \gamma^2\delta W_1\,\frac{1-\gamma^2T^2}{(1+\gamma^2T^2)^2}\,T^2 + \gamma^2\delta W_2\,\frac{(3-\gamma^2T^2)\gamma^2T^2}{(1+\gamma^2T^2)^3}\,T^2 \tag{32}$$

with $\tilde{a} = \frac{\pi^2}{6}\tilde{g}(\mu_0)$. This approximation can be made, since the main contribution to the summation in expressions (26) and (27) comes from the first band (t=1) of polygons, which are characterized by a fairly constant value of γ_2, defined as γ (see Appendix A). The $t > 1$ bands can be omitted since their amplitude values g_1 will be smaller and their frequency g_2 will be larger, leading to a much weaker contribution in expressions (26) and (27). Moreover, it will be demonstrated (see Section II.5.1) that a more realistic description of the shell effects, based on the semi-classical approximation (30), leads to the consideration of a fairly constant frequency $\bar{g}_2$, independent of the contributing orbit type, so that the assumption of the constancy of γ over the different contributing orbits appears to be confirmed.

To describe the shell effects on the entropy, it is convenient to introduce in the usual way the temperature-dependent level density parameter

$$\begin{aligned} a(T) &= S(T)/2T \\ &= \tilde{a}\left[1 + \frac{\delta W_1}{\tilde{a}/\gamma^2}\,\frac{1}{(1+\gamma^2T^2)^2} + \frac{\delta W_2}{\tilde{a}/\gamma^2}\,\frac{2\gamma^2T^2}{(1+\gamma^2T^2)^3}\right] \end{aligned} \tag{33}$$

Expression (33) shows how the shell correction affects the smooth value of the level density parameter $\tilde{a}$ at low temperatures. Depending on the sign of the ground state shell correction energies, $a(T)$ will either be larger or smaller than its asymptotic value $\tilde{a}$. Before estimating the quantitative influence of the shell term on the total entropy, it should be recalled that the state density (10) is an exponential function of the $a(T)$-parameter, so that a small modification of a can lead to a drastic effect on the nuclear level density. This property of the state density lies behind the great difficulties associated with the derivation of a reliable expression for the level density. If the state density depends mainly on the single-particle level density evaluated at the Fermi energy, it also requires a very accurate knowledge of that quantity. As a result studies have so far failed to relate the a-parameter to an analytical approximation of $g(\mu_0)$.

The critical temperature at which the shell effects disappear is

$$T_{sh} = \frac{1}{\gamma} \sim \frac{\hbar}{\bar{\tau}_{orb}} \tag{34}$$

where $\bar{\tau}_{orb}$ corresponds to the mean period of revolution of the particle along the orbits (p,t). This result agrees closely with the evaluation of T_{sh} by Strutinsky and Magner (1976). For $T > T_{sh}$, the oscillating component of the entropy rapidly vanishes according to equation (31).

In order to test the validity of the approximations used to derive the T-dependence of the oscillating contribution to the entropy, we have re-evaluated $S(T)$ making use of an alternative approximating function in expression (16b). In this new approximation the universal even function

$$\begin{aligned} F(x) &= y(x) - x\frac{dy(x)}{dx} \\ &= \frac{1}{\ln 2}\left[\ln\left(1+\mathrm{e}^{-x}\right) + \frac{x}{1+\mathrm{e}^{x}}\right] \end{aligned} \tag{35}$$

is replaced no longer by

$$\begin{aligned} F_a(x) &= y_a(x) - xy_a'(x) \\ &= \mathrm{e}^{-x/\sigma_a}\left(1+\frac{x}{\sigma_a}\right) \end{aligned} \tag{36}$$

as previously but by a simple Gaussian function

$$F_b(x) = \mathrm{e}^{-(x/\omega)^2} \tag{37}$$

where $\omega = \frac{\pi^2}{3\sqrt{\pi}\ln 2}$ has been determined in a similar way to σ_a. These curves, displayed in Fig. 2, show the interesting feature of being the upper or lower bounds (depending on the x-domain) to the exact function $F(x)$. the function $F_a(x)$ has the disadvantage of underestimating $F(x)$ for low x-values ($x \lesssim 3$), so that a slight underestimate of $S(T)$ can be expected at low temperatures. If $F_b(x)$ is used to evaluate the entropy, an upper bound of $S(T)$ in the corresponding temperature range can be obtained . Similarly a lower bound of $S(T)$ at high temperatures can also be estimated.

Integration (17b) has been carried out and related to the first expression of $S(T)$ as given by equation (26), by introducing the same parameters and in particular the same definition of the ground state shell correction energies (30). Assuming, as previously, that the parameter γ_2 remains approximately constant (and equal to γ) along the different contributing orbits, we are led to the new analytical expression

$$S = 2\,\tilde{a}\,T + 2\,\gamma^2\delta W_1\,T\,\mathrm{e}^{-\frac{4}{\pi}\gamma^2T^2} + 2\,\gamma^2\delta W_2\,T\,\frac{4}{\pi}\,\gamma^2T^2\,\mathrm{e}^{-\frac{4}{\pi}\gamma^2T^2} \tag{38}$$

As expected, the smooth contribution to the entropy is identical in both evaluations. It corresponds to the zeroth order term which only depends on the total area of the integrand curve. To compare the shell term in expression (31) and (38), the shell damping functions, defined by

$$s_1^{(a)}(\tau) = \frac{1}{(1+\tau^2)^2} \qquad s_1^{(b)}(\tau) = \mathrm{e}^{-\frac{4}{\pi}\tau^2} \tag{39}$$

$$s_2^{(a)}(\tau) = \frac{2\tau^2}{(1+\tau^2)^3} \qquad s_2^{(b)}(\tau) = \frac{4}{\pi}\,\tau^2\,\mathrm{e}^{-\frac{4}{\pi}\tau^2} \tag{40}$$

(with $\tau = \gamma T$) are shown in Fig. 3. The main oscillating contribution clearly appears to be due to the δW_1 term and to disappear quickly at temperatures $T > T_{sh}$ (i.e. $\tau > 1$). This second approximation (38) allows us to be quite confident about the accuracy of the proposed oscillating

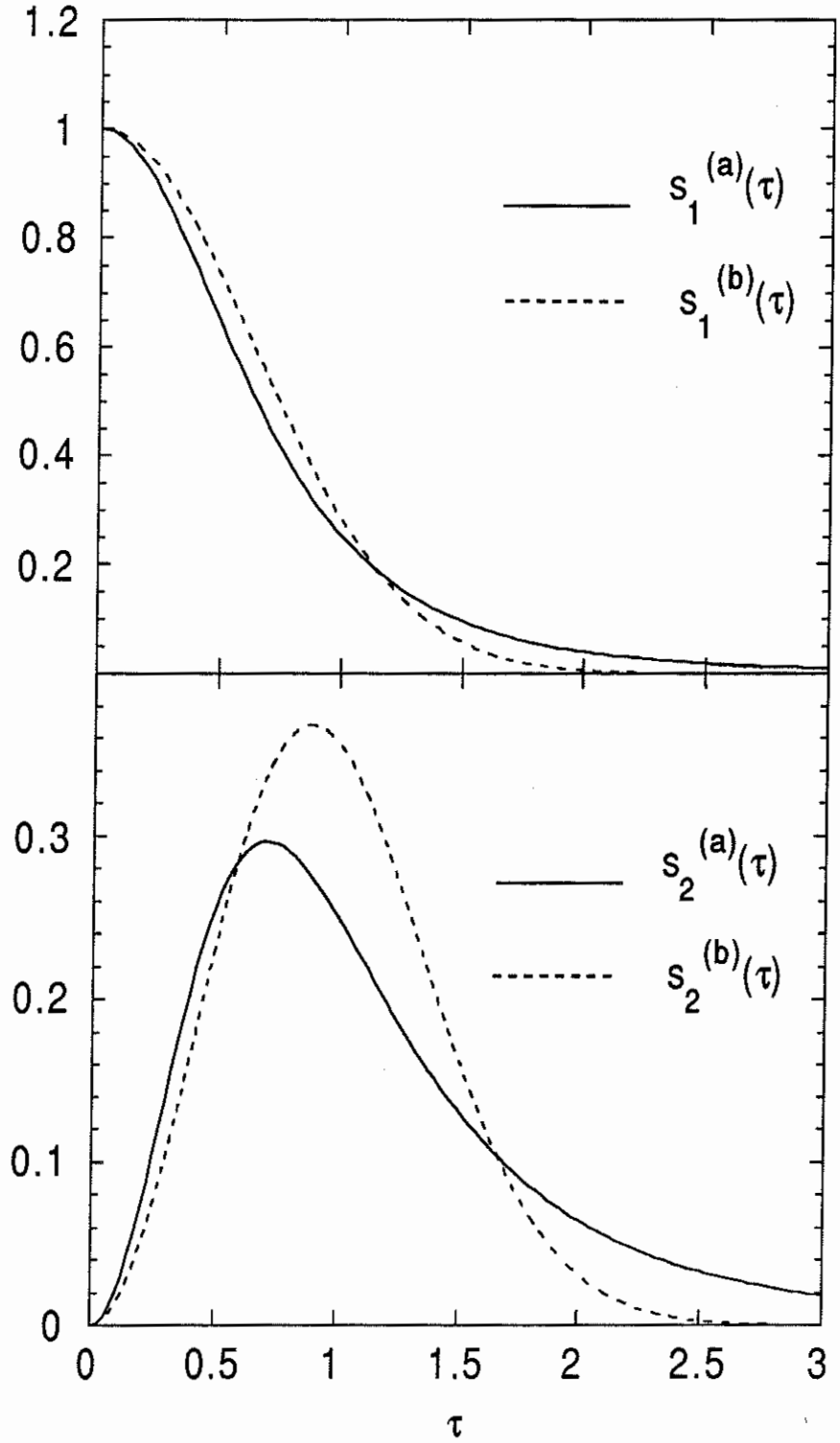

Figure 3. Comparison of the shell damping functions obtained with the approximate functions $F_a(x)$ and $F_b(x)$. The upper part corresponds to the shell damping functions in the δW_1 contribution to the entropy and the lower part to the functions in the δW_2 contribution. The curves are plotted as a function of the reduced temperature $\tau = \gamma T$.

contribution to $S(T)$, since the exact damping function $s_1(\tau)$ ($s_2(\tau)$) is now known to lie between the two approximations $s_1^{(a)}$ and $s_1^{(b)}$ ($s_2^{(a)}$ and $s_2^{(b)}$) and is, therefore, believed to be reproduced within a few percent by both approximations. Moreover, the error associated with this uncertainty on the damping function remains much smaller than that involved in the determination of the energies δW_1 and δW_2 (see Section II.5.1). We have chosen the first approximation to describe the $s_i(\tau)$ functions (i=1,2). This approximation has the advantage of making it easier to determine the relation $U(T)$ as given by expression (32). Also its asymptotic behaviour at high temperatures is more reliable because of the identical x-dependence of the two functions $F(x)$ and $F_a(x)$ for high x-values, while the more rapidly decreasing function $F_b(x) \propto \mathrm{e}^{-x^2}$ leads to a too fast cancellation of the shell effects at high temperatures.

The quantitative influence of the shell term on the total entropy will obviously depend upon the magnitude of the energies δW_1 and δW_2. The total ground-state shell correction energy δW is defined as the sum of these two terms (positive or negative), as given by expression (30). It can be proved that δW can be obtained by different, but essentially equivalent ways. In particular, Das Gupta and Rhadakant (1974) have already emphasized that any pair of variables can be used to estimate δW. We have verified this statement by calculating the ground state shell correction energy through

$$\delta W = \int_0^\infty \left[S(T) - \tilde{S}(T) \right] dT \tag{41}$$

where $\tilde{S}(T)$ is the asymptotic expression of the total entropy $S(T)$ for very high temperatures, where the shell structure of the single-particle spectrum is vanishing. Another equivalent representation of the shell energy correction can be found in the expression (Brack et al., 1972)

$$\delta W = \int_0^{\mu_0} (\varepsilon - \mu_0)\, g_{osc}(\varepsilon)\, d\varepsilon \tag{42}$$

which leads this time to a δW_2 contribution larger by a factor of 4, relative to expressions (30) and (41). Expression (42) also confirms the overestimate of expression (30) by the factor of $\pi^2/(6\sigma_a^2)$.

It can be seen from expression (30) that the amplitude of the δW_2 energy is smaller than δW_1 by a factor of $\frac{2\mu_0\gamma_2}{\sigma_a} = g_2\mu_0^{1/2}$, which could justify the total neglect of the δW_2 terms in expressions (31) and (32). However, its magnitude relative to the δW_1 contribution, as given by equation (30), may have been underestimated. The technique used for the evaluation of δW_2 approximates the function $y(x)$ by a simpler exponential function $y_a(x)$. It can be proved that such an approximation leads to an underestimation of the second order terms. In this case, the δW_2 contribution may be more important than suggested by expression (30) and as confirmed by expression (42). Moreover, at high temperatures ($T \gtrsim T_{sh}$), the s_2 damping function becomes relatively more important than the s_1 function. Therefore, we have not neglected *a priori* the δW_2 contribution.

If we introduce the T-dependent shell correction energy of the nucleus, $\delta E(T)$, expression (27) gives

$$\delta E(T) = \delta W_1 \left[1 + \frac{1-\gamma^2T^2}{(1+\gamma^2T^2)^2}\,\gamma^2T^2\right] + \delta W_2 \left[1 + \frac{3-\gamma^2T^2}{(1+\gamma^2T^2)^3}\left(\gamma^2T^2\right)^2\right] \qquad (43)$$

It is of interest to see that the shell correction $\delta E(T)$ tends to disappear at high temperatures, but not in a monotonic way. At low temperatures, $\delta E(T)/\delta W_1$ increases with T before vanishing completely at very high temperatures (see Fig. 4). For closed-shell configuration (corresponding to a strongly negative value for δW), an even higher stability (i.e. a decrease of $\delta E(T)$ or an increase of $\delta E(T)/\delta W_1$) might be found at a low temperatures. As already pointed out by Bohr and Mottelson (1975), this initial decrease of $\delta E(T)$ as a function of T, reflects the reduced single-particle level density in the neighbourhood of the Fermi energy for the closed-shell configuration. For a given temperature , the excitation energy is proportional to the number of elementary excitations with energies of order T (Ericson, 1960), so that the total energy $E(T) = \tilde{E}(T) + \delta E(T)$ increases less rapidly with temperature than does the smooth contribution $\tilde{E}$ ($\propto T^2$).

Another interesting feature corresponds to the case $\beta = \delta W_2/\delta W_1 < -1/2$, where a shell-reversal effect appears at high temperatures, before the shell energy vanishes completely (see Fig.

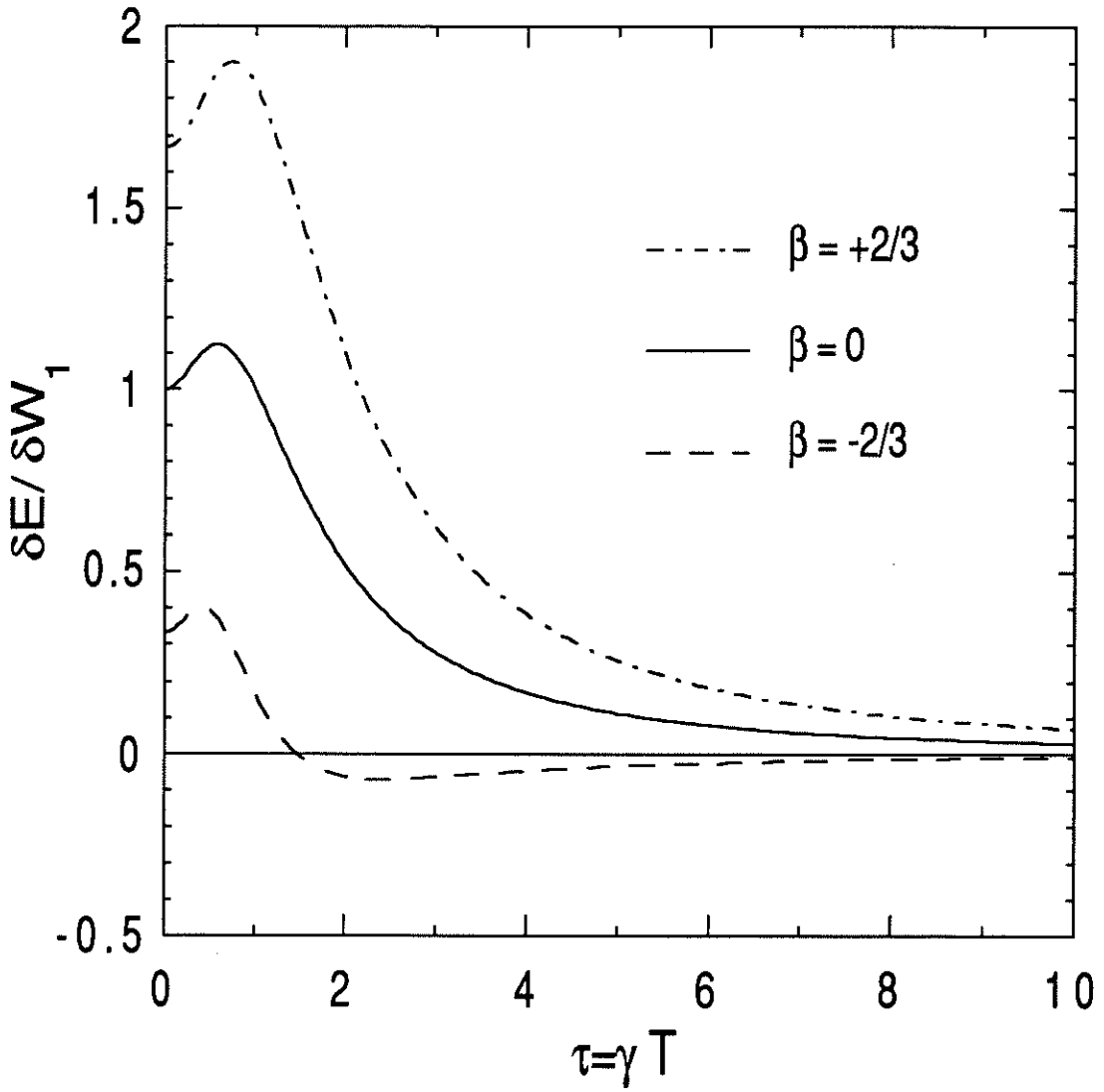

Figure 4. Total shell correction energy of the nucleus δE relative to the ground-state shell energy δW_1 as a function of the reduced temperature $\tau = \gamma T$. The shell energies have been displayed for three values of the ratio $\beta = \delta W_2/\delta W_1$.

4). This case is of particular interest for strongly positive values of δW_1. In fact, the shell damping shape of expression (43) is qualitatively quite similar to the empirical function introduced by Myers and Swiatecki (1967) in their liquid drop model of nuclear masses used to describe the way the ground-state shell energy fades away for increasing deformations. In both cases, before being annihilated, the shell effect gets reversed (a low single-particle level density at the Fermi energy becomes important). However, if the deformation acts mainly as a "debuncher" of levels, as described by Nilsson level diagram, the temperature effect reflects the sensitivity of the particles to existing gaps during the excitation process. Yet such behaviour depends on the relative magnitudes and signs of δW_1 and δW_2 and remains to be confirmed by quantitative results (see Chapter II.5).

Amongst the numerous theoretical works on nuclear level density, only two analytical models have accounted for such energy-dependent shell effects on the thermodynamic quantities. Both of them relate the shell effects on the level densities to the ground-state shell correction energy δW. The first work (Ignatyuk et al., 1975) corresponds to a purely empirical evaluation of the energy dependence of the level density parameter a, by simple comparison with calculations using more realistic single-particle states. Despite offering a very simple expression, this procedure suffers from many uncertainties and its empirical character makes it highly unreliable. The lack of experimental data over a large energy range means that a reliable phenomenological evaluation of the parameters is not possible. Moreover, the estimation of the critical energy at which shell effects disappear remains highly cumbersome and the universality of the shell damping function doubtful.

The model of Kataria et al. (1978) uses a phenomenological Fourier expansion to describe the shell fluctuations of the single-particle level density. The neglect of high harmonics terms finally reduces the oscillating contribution $g_{osc}(\varepsilon)$ to a simple sine function with a constant amplitude. However, such an assumption has not been justified except through comparisons with numerical

shell model calculations. Once again the fundamental frequency of oscillation in $g_{osc}(\varepsilon)$, which defines the critical temperature, cannot be related to known physical quantities. Nevertheless, the $a(T)$-parameter of Kataria et al., even if based on a totally different description of the single-particle state density, shows a behaviour as a function of the temperature very similar to the first two terms of our evaluation (33). The δW_2-contribution to the entropy is completely absent in the model of Kataria et al. since this model neglects the ε-dependence of the amplitude of $g_{osc}(\varepsilon)$ responsible for the δW_2 terms.

Calculation of the Determinant factor

Since the main part of the variation of the level density with energy and with irregularities in the distribution function is due to the change in the entropy S which enters exponentially, the uncertainty related to determinant factor evaluation (12) has only a small effect on the final level density. Shell effects, as expressed by correction (23) to the single-particle state density, can be introduced in expression (12) in the same manner as that developed for the calculation of the thermodynamic quantities. However, we have chosen to restrict ourselves to the main contribution given by the smooth part, because of the insignificant contribution resulting from the shell effects.

In this case, the determinant factor can be expressed accurately by the simple formula

$$D(T) = \frac{12}{\pi^2}\ \tilde{a}^2\ T^4 \tag{44}$$

where $\tilde{a} = \frac{\pi^2}{6}\tilde{g}(\mu_0)$, as previously.

II.2.4 Comparison with numerical shell model calculations

In order to test our analytical expressions for $U(T)$, $a(T)$, $S(T)$ and $D(T)$, we have performed a numerical evaluation of these quantities, making use of a realistic Woods-Saxon single-particle scheme. Such a calculation has the advantage of retaining the discrete nature of the single-particle spectra associated with realistic average potentials. Therefore, the shell effects are automatically taken into account. The computation of the nuclear level density by this technique remains one of the most reliable evaluations (despite the remaining inherent problems which are discussed in Section II.1.2) and so it has been used as a reference since it corresponds to the exact result that the analytical approximation tries to reproduce. As a matter of fact, the analytical approach is based on exactly the same statistical model as the numerical calculations. The only differences are to be found in the treatment of the single-particle level density which can be taken either as the discrete level scheme in an average potential well or as a continuous function of the energy. However, it should be added that in the numerical calculation the chemical potential is not considered as temperature-independent, but is instead extracted by solving equation (8). Yet the assumption made in the analytical approach is fairly good even if few shell effects can be expected at low temperatures and if at high temperatures the chemical potential is known to decrease linearly with the excitation energy (e.g. Moretto, 1972a).

The single-particle spectrum required for the numerical level density calculation is derived from the eigenstates of a Woods-Saxon potential. Let us, however, emphasize some points of special relevance or importance which have been adopted in order to enable a meaningful comparison of the analytical and numerical calculations:

(i) All nuclei are assumed to be spherically symmetric

(ii) The usual spin-orbit term has been added to the Woods-Saxon potential in order to describe the shell structure realistically. In the proton case, the Coulomb repulsion has been introduced

in the classical electrostatic way (e.g. Bohr and Mottelson, 1969)

(iii) No momentum or energy dependence of the potential has been considered, so that the effective mass is equal to the nucleonic mass. Calculations with $m^* < m$ yield a smaller single-particle level density around the Fermi energy. Consequently, the gaps which correspond to magic numbers in the single-particle spectra are larger than when $m^* = m$, leading to an overestimation of the shell effects when m^* is much smaller than m. A good evaluation of the shell effects can be obtained only when m^* is not too different from m.

Calculations have been performed for neutrons and protons separately because of the introduction of the Coulomb and asymmetry potentials. The parametrization of the potential can be found in Hodgson (1990) where the parameters have been taken as:

$U_u = 52.3 \pm 34.6(N-Z)/A$ MeV	central potential
$U_s = 8.3$ MeV	spin-orbit potential
a = 0.67 fm	diffuseness parameter
$r_0 = 1.26$ fm	nuclear radius parameter

where the upper sign in the central potential corresponds to the protons and the lower to the neutrons. However, it should be noted that since no comparison with experimental data is attempted at this stage, the quantitative values of the potential parameters adopted are of no importance. Yet, in order to estimate the relative effect of the shell correction, we have tried to make use of a realistic Woods-Saxon potential.

As soon as the discrete single-particle level spectrum is known, all the statistical quantities related to the level density can be evaluated numerically. Figures (5)–(10) compare the quantities $U(T)$, $a(T)$, $S(T)$ and $D(T)$ as obtained with the Woods-Saxon single-particle level scheme (W-S) with expressions (32), (33), (31) and (44) derived by means of the semi-classical approximation (SCA) to the single-particle level density. A separate comparison has been made for both the

^{120}Sn: neutrons

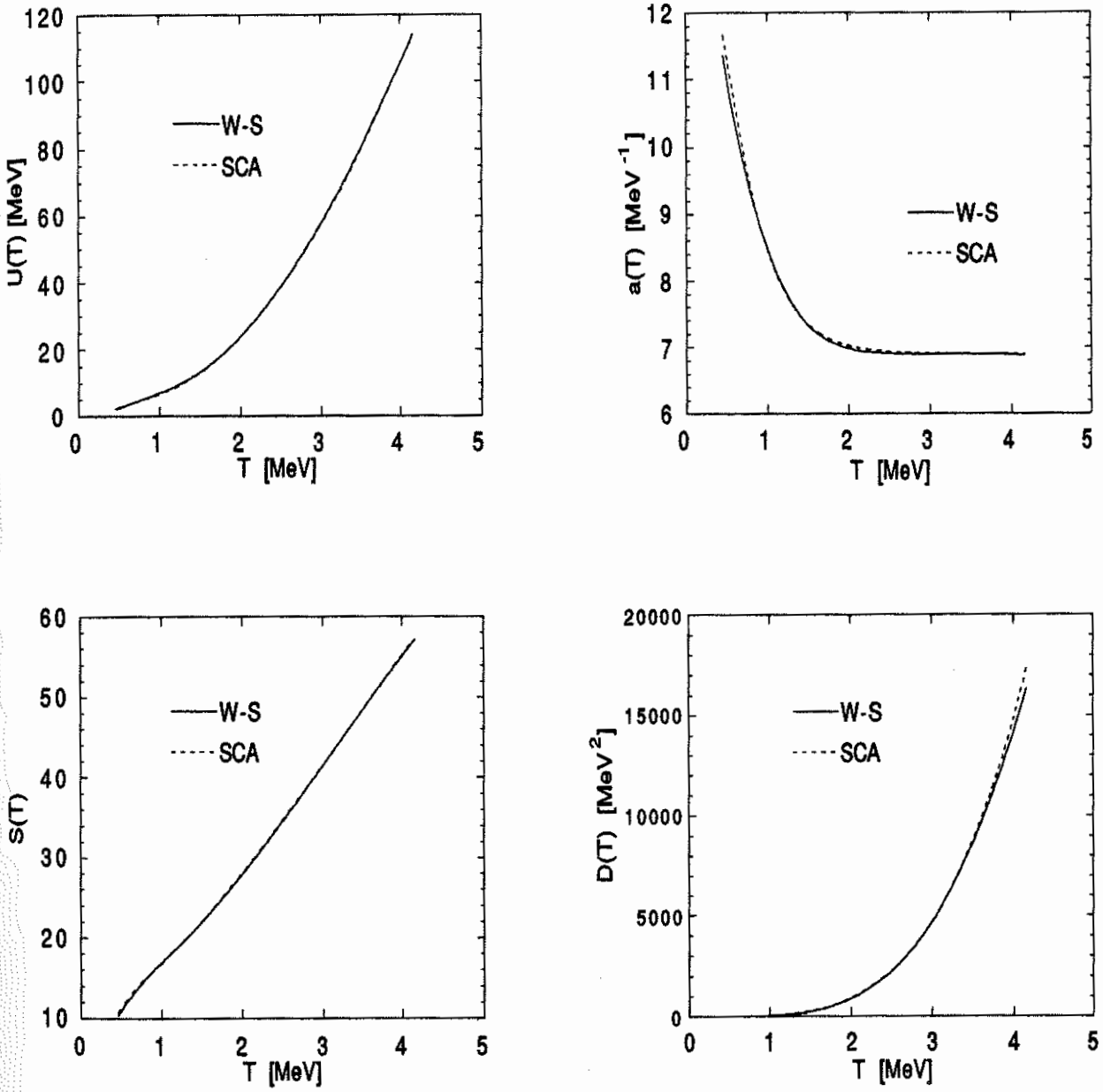

Figure 5. Temperature dependence of the statistical quantities for the neutron system of ^{120}Sn, namely the excitation energy U, the level density parameter $a = S/2T$, the entropy S and the determinant D. The full lines (W-S) correspond to the numerical shell model calculation based on a Woods-Saxon single-particle level scheme, while the dashed line (SCA) have been obtained with the analytical formulae based on the semi-classical approximation to the single-particle level density.

^{120}Sn: protons

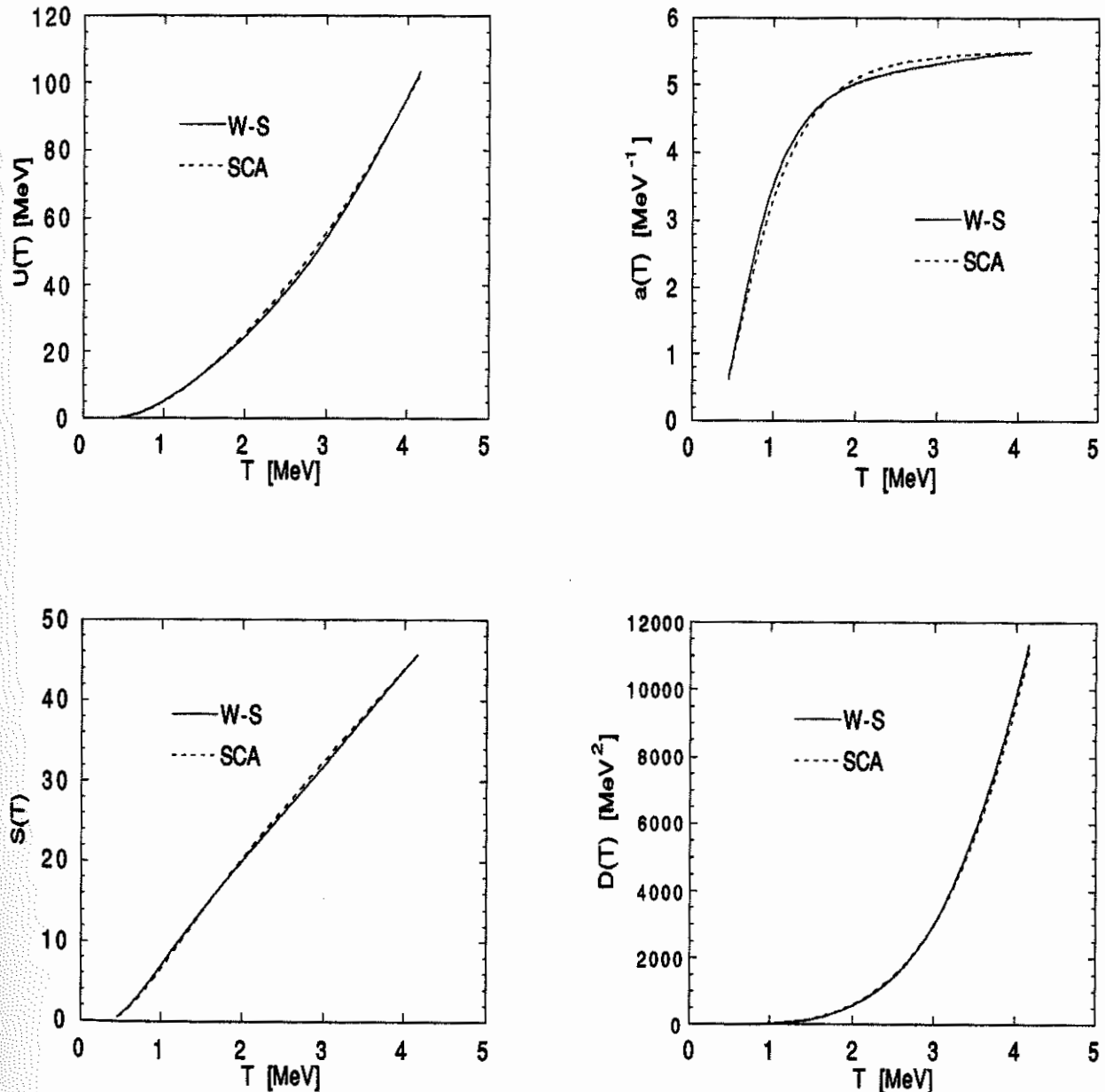

Figure 6. Same as Fig. 5 for the proton system of ^{120}Sn.

^{162}Dy: neutrons

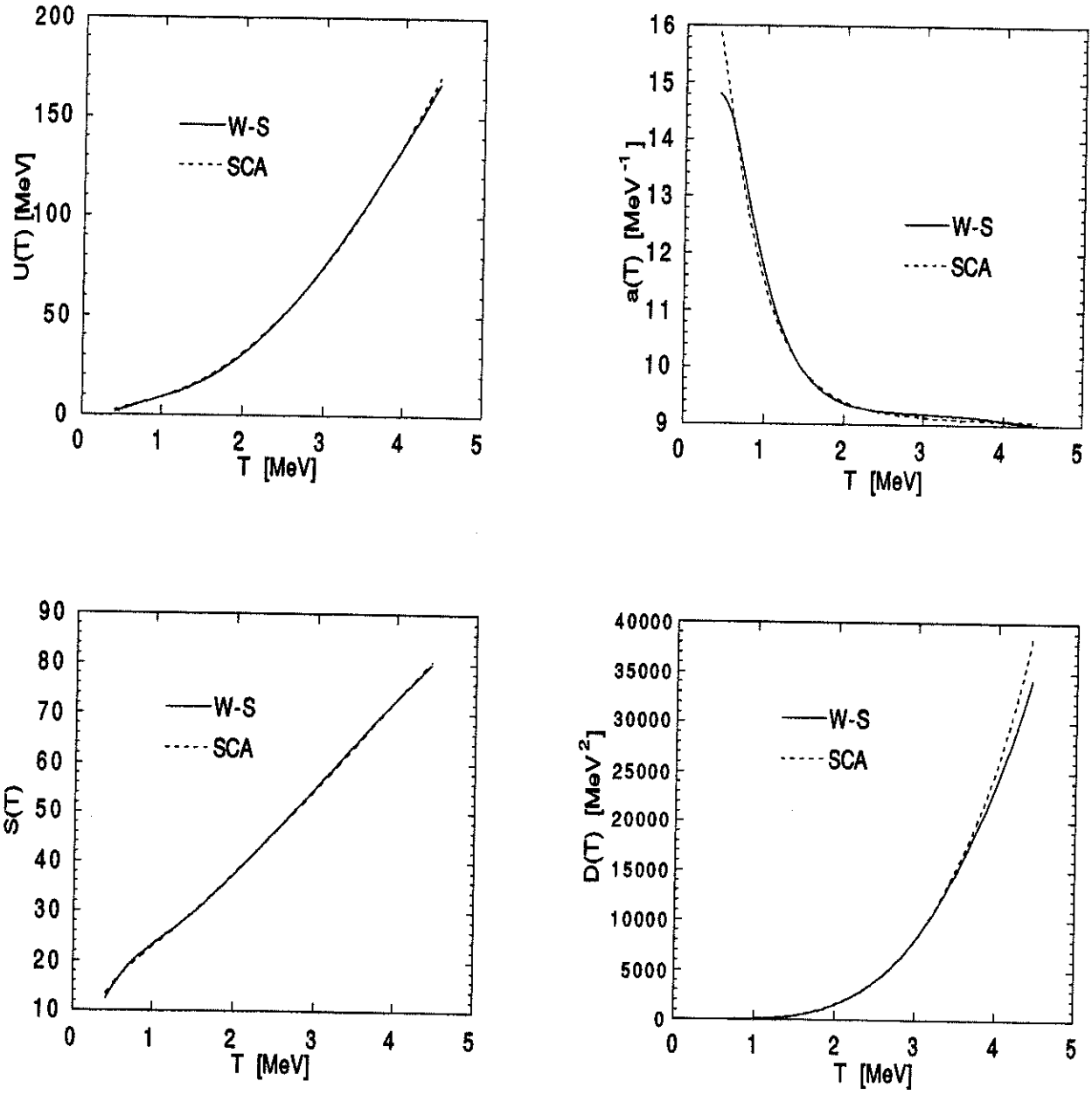

Figure 7. Same as Fig. 5 for the neutron system of ^{162}Dy.

^{162}Dy: protons

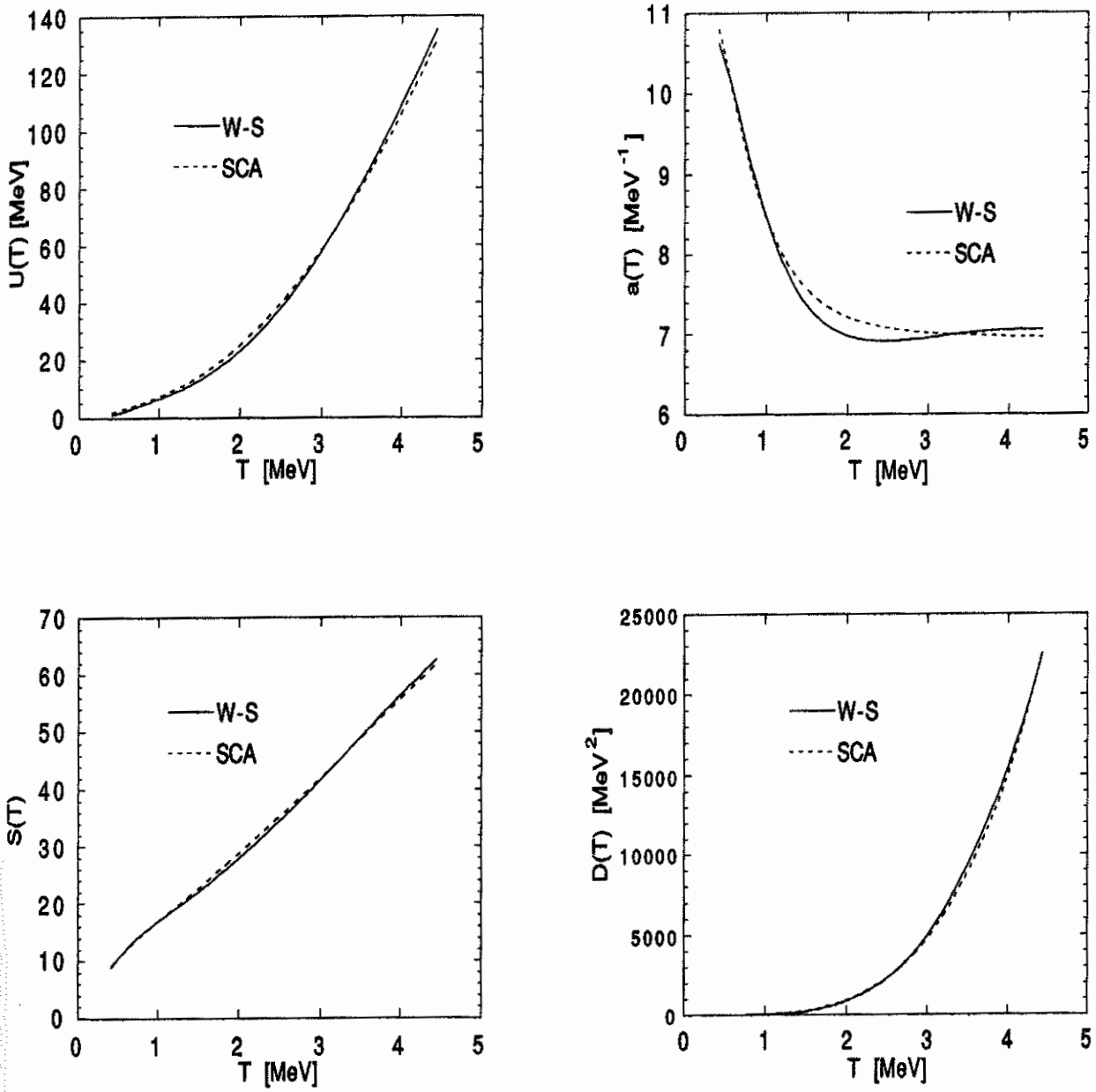

Figure 8. Same as Fig. 5 for the proton system of ^{162}Dy.

^{208}Pb: neutrons

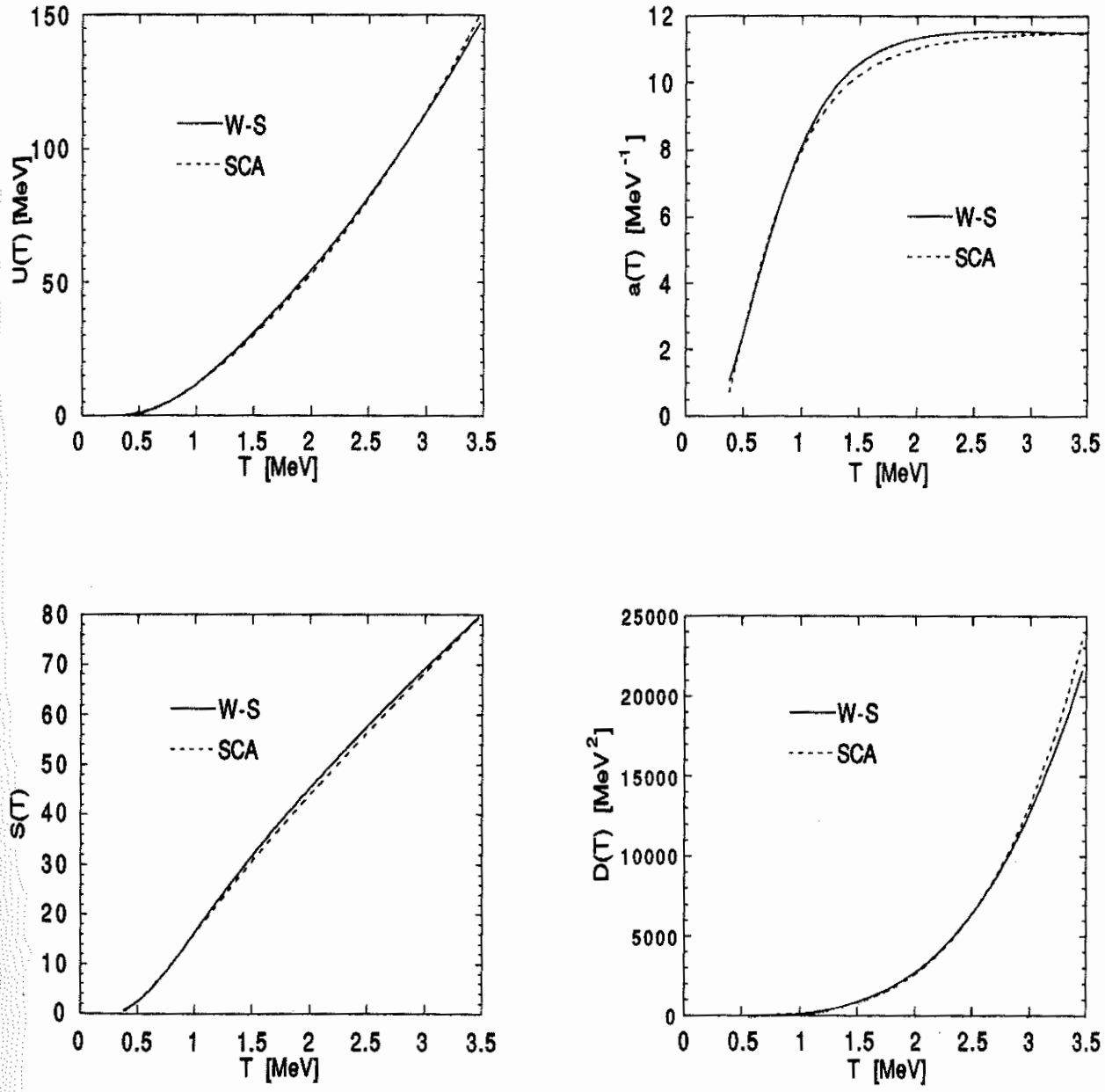

Figure 9. Same as Fig. 5 for the neutron system of ^{208}Pb.

^{208}Pb: protons

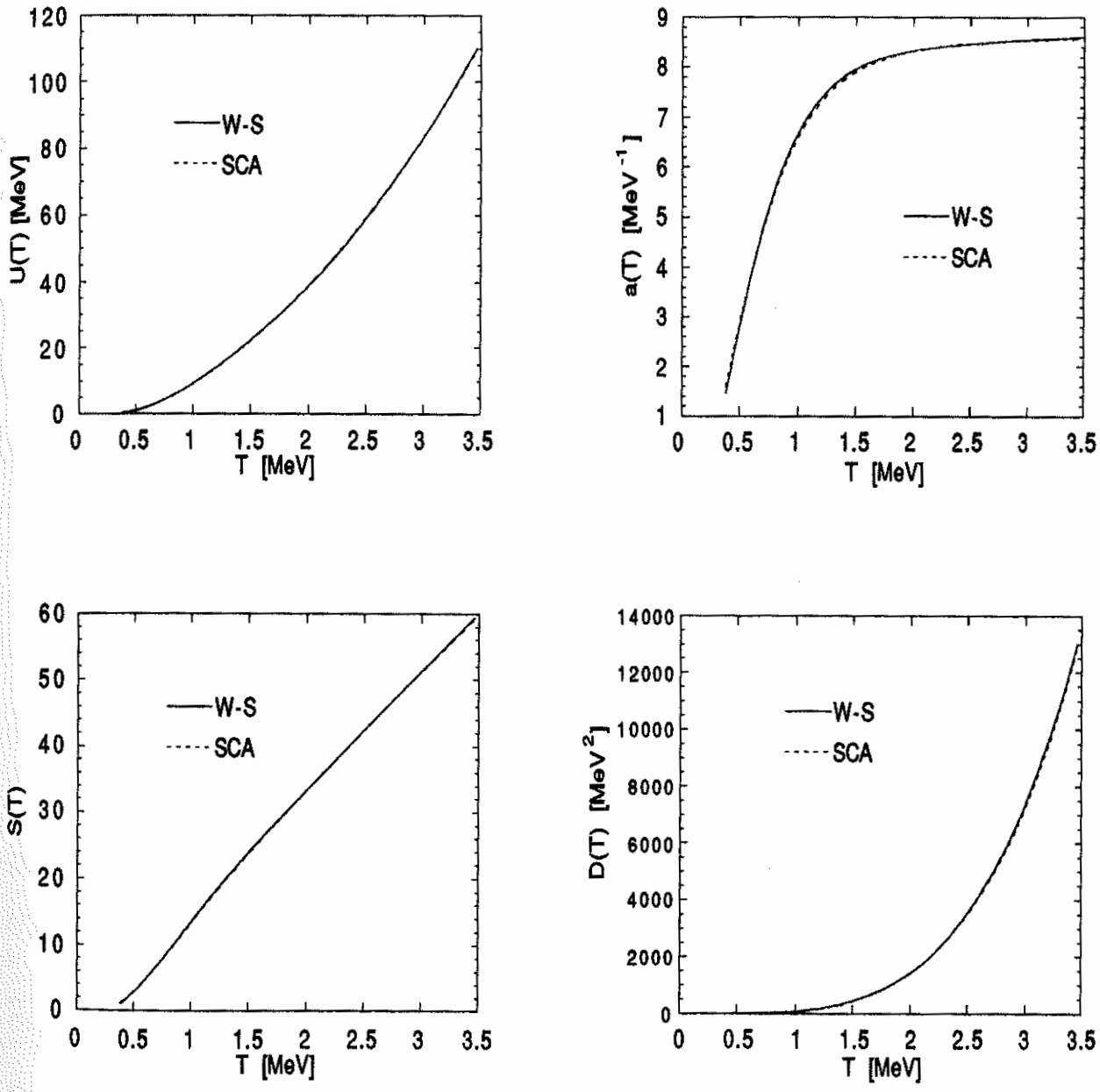

Figure 10. Same as Fig. 5 for the proton system of ^{208}Pb.

neutron and proton systems of three nuclei: a double magic nucleus (^{208}Pb), a double open-shell nucleus (^{162}Dy) and ^{120}Sn characterized by a proton-closed shell and a neutron-open shell.

The analytical evaluation depends on 4 parameters: the asymptotic $\tilde{a}$ parameter, the shell damping temperature $T_{sh} = 1/\gamma$ and the two contributions to the ground state shell correction energy δW_1 and δW_2. These parameters have been determined for each nucleus (and each nucleonic system) to give the best fit to the numerical evaluation and are given in Table 1. Yet it should be stressed that different sets of parameters could lead to the same quality of fit.

Table 1.

Nuclear level density parameters corresponding to the numerical calculation

		$\tilde{a}$ (MeV^{-1})	γ (MeV^{-1})	δW_1 (MeV)	δW_2 (MeV)
$^{120}_{50}Sn_{70}$	neut.	6.9	0.77	11.6	-6.7
	prot.	5.5	0.80	-10.1	1.0
$^{166}_{66}Dy_{96}$	neut.	9.1	0.81	14.0	-5.0
	prot.	7.0	0.85	7.0	-1.0
$^{208}_{82}Pb_{208}$	neut.	11.6	1.00	-14.0	0
	prot.	8.6	1.10	-8.0	0

It is of great interest to estimate the accuracy of the semi-classical approximation in the prediction of these parameters.

(i) semi-classical prediction of the macroscopic quantities

Concerning the smooth $\tilde{a}$ parameter, a direct quantitative evaluation is possible thanks to the analytical approximation given in Appendix A. In the case of a Woods-Saxon potential, $\tilde{a}$ can be approximated by the relation:

$$\tilde{a} = \frac{\pi^2}{6}\,\frac{D}{4\pi^2}\,\frac{2m}{\hbar^2}\Big[k_F V + (\alpha_S V_0 - \beta_S B + \gamma_S)S\Big] \qquad (45)$$

where $D = 2$ is the spin degeneracy factor, $k_F = \sqrt{\frac{2m}{\hbar^2}\varepsilon_F}$ is the Fermi momentum, $V = \frac{4}{3}\pi R^3$ is the potential volume and $S = 4\pi R$ its surface area. The surface parameters α_S, β_S and γ_S are given in Appendix A for a diffuseness parameter a=0.67 fm and within a range of value of the potential depth V_0 and of the last nucleonic separation energy $B = V_0 - \varepsilon_F$.

To relate $\tilde{a}$ to the numerical prediction, we have parametrized expression (45) as a function of the single-particle potential radius $R = r_0 A^{1/3}$. The value of r_0, a and V_0 have been extracted directly from the numerical calculation (the Coulomb effect has been reduced to a simple decrease of the potential depth equal to $1.7\, Z/A^{1/3}$). The Fermi energy (or equivalently the binding energy B) differs from the Fermi energy resulting from the shell model calculation and must be related to the distribution function $\tilde{g}(\varepsilon)$ on condition that the number of particles (protons or neutrons) is conserved:

$$N \text{ (or } Z) = \int_0^{\varepsilon_F} \tilde{g}(\varepsilon)\, d\varepsilon \tag{46}$$

The numerical calculation of $\tilde{a}_{ws} = \lim_{T\to\infty} a(T)$ is compared with the semi-classical prediction $\tilde{a}_{sca}$ in Table 2 for the three studied nuclei. Table 2 also displays the equivalent reduced radius r_0^{eq} required to fit the numerical value $\tilde{a}_{ws}$.

Table 2.

Semi-classical prediction of $\tilde{a}$ for a Woods-Saxon potential

		ε_F (MeV)	V_0 (MeV)	$\tilde{a}_V$ (MeV^{-1})	$\tilde{a}_S$ (MeV^{-1})	$\tilde{a}_{sca}$ (MeV^{-1})	r_0^{eq} (fm)	$\tilde{a}_{ws}$ (MeV^{-1})
$^{120}_{50}Sn_{70}$	neut.	40.6	46.5	5.7	1.0	6.7	1.28	6.9
	prot.	34.2	40.6	5.2	0.6	5.8	1.24	5.5
$^{162}_{66}Dy_{96}$	neut.	40.9	45.9	7.7	1.2	8.9	1.27	9.1
	prot.	32.5	37.9	6.8	0.8	7.4	1.23	7.0
$^{208}_{82}Pb_{208}$	neut.	40.6	45.0	9.8	1.5	11.3	1.27	11.5
	prot.	31.0	35.8	8.5	1.0	9.5	1.22	8.6

Table 2 shows that in general the $\tilde{a}$ formula (45) is in close agreement with the numerical model, even if the uncertainty on r_0 remains one of the weakest points of the semi-classical approach. However, the discrepancies between $\tilde{a}_{ws}$ and $\tilde{a}_{sca}$ can be explained.

In the neutron case, the semi-classical approximation leads clearly to an underestimation of $\tilde{a}$ and therefore requires a higher radius parameter (r_0^{eq}) to fit the numerical calculation. This neutron skin effect can partly be attributed to the total neglect of the curvature term in the series expansion (45) as well as the approximate character of the adopted surface term. Another uncertain parameter is the last neutron separation energy or equivalently the Fermi energy. We have adopted the Fermi energy as given by expression (46), and not the shell model Fermi energy, which is known to lie somewhere between the last filled level and the first unfilled level. Even if small compared, with their absolute values, the difference between the two energies modifies significantly the prediction of $\tilde{a}$. A higher ε_F value tends to increase the volume term as well as the surface term (through a decrease of B) in a non-negligible way. On the other hand, the discrepancy between the shell model calculation and its semi-classical approximation cannot be associated with the spin-orbit term. The spin-orbit potential mainly modifies the oscillating contribution to the a-parameter, so that the smooth value $\tilde{a}$ remains quite insensitive to the amplitude of the spin-orbit correction.

Concerning the proton system, the semi-classical approximation clearly overestimates the $\tilde{a}$-parameter (see Table 2). The Coulomb contribution to the total potential can be held responsible for such an effect. The radial shape of the Coulomb repulsion is very different from the Woods-Saxon form. It tends to reduce not only the well depth, but also the potential radius. Therefore, the equivalent proton potential will be characterized by a parameter r_0^{eq} smaller than the 1.26 fm which corresponds to a pure central potential.

Although the equivalent reduced radius differs from its exact value by only a few percent, it should be remembered that r_0 is by far the most sensitive parameter on which the level density

parameter $\tilde{a}$ depends. It occurs in the third power of the volume term. Therefore, the uncertainty of its exact value casts doubt upon the applicability of an analytical formula, such as expression (45). A correct choice of r_0 is much more important for level density than specific shapes of potential. Unfortunately, this problem is inherent to all models of nuclear level density calculations. How ever realistic the one-body single-particle potential might be, it cannot be expected to give a correct estimate of level densities unless the radius parameter of the potential has been chosen carefully.

Table 2 also points out the relative contribution of the volume ($\tilde{a}_V$) and surface ($\tilde{a}_S$) terms. The surface contribution, in the order of 10% of the total $\tilde{a}$-value, appears to be much less important than suggested by Reisdorf and Töke (1981). This is partly due to the introduction of the diffuseness in the potential shape, which tends to decrease the phase shift significantly (see Appendix A). Therefore, this evaluation does not support (at least for the adopted values of the Woods-Saxon potential parameters) the empirical introduction of a surface contribution $\tilde{a}_S$, which would account for a half of the so-called experimental level density parameter, as suggested by Töke and Swiatecki (1981) and Reisdorf and Töke (1981).

The analysis of the single-particle level density in a Woods-Saxon potential well shows that there is a complicated interplay of various effects arising from the finite depth of the nuclear potential, the nucleonic separation energy and the finite diffuseness of the nuclear surface. Therefore, it seems hazardous to derive a universal A-dependent (where A is the atomic mass number) expression for the nuclear level density parameter $\tilde{a}$ which would not take these numerous corrections into account. This is of particular importance when extrapolation far away from the experimentally known region is concerned.

(ii) semi-classical prediction of the oscillating contribution

In order to achieve the best fit to the numerical evaluation, the shell parameters γ, δW_1 and δW_2 have been adjusted (see Table 1) regardless of their semi-classical prediction. It should be

remembered that the shell description corresponds to an infinite square well potential, which differs significantly from the adopted potential in the numerical calculation. In particular, the inclusion of a spin-orbit term modifies the level bunching drastically. However, it is of interest to see (Figs. (5)–(10)) how well the fits can be made within reasonable values of the parameters.

The shell damping parameter γ appears to be an increasing function of the number of particles as predicted by the semi-classical expression

$$\gamma = \frac{1}{2}\,\bar{g}_2\,\frac{\sigma_a}{\varepsilon_F^{1/2}} \;\propto\; R \;\propto\; A^{1/3} \tag{47}$$

where $\bar{g}_2$ denotes an average value of the frequency $g_2(p,t)$ for the contributing polygons. Since the proton Fermi energy is lower than the neutron Fermi energy, a higher value of γ for the proton system can be justified (see Table 1).

It is of interest to point out the relatively slow disappearance of the shell effect. Temperatures around 2 MeV must be obtained in order to neglect safely the shell contribution. At these temperatures, the corresponding excitation energies of the nucleus are by far higher than the energies for which experimental data are available.

Figures (5)–(10) demonstrate the tremendous influence of shell effects on the level density at low temperatures and emphasize the need to remove the equidistant spacing assumption of the Fermi gas model. For example, in the extreme case of the double magic nucleus ^{208}Pb, errors of several orders of magnitude in the final nuclear level density at low temperatures can be made, if all shell corrections are neglected. In the context of the statistical model of nuclear reactions this is of particular importance, since level densities are required mainly at very low excitation energy ($U < S_l$ where S_l is the channel separation energy—see Section I.1.1).

It should be observed that in the case of open-shell nuclei ($\delta W > 0$), the amplitude of the shell effect is greatly reduced by the appearance of deformation. Deformation tends to decrease the magnitude of the energies δW_1 and δW_2 and consequently the shell contribution to the *a*-

parameter at low energy. Nevertheless, the example of ^{162}Dy, treated as a spherical nucleus, shows that the adopted description of the shell structure is well suited for open-shell as well as closed-shell nuclei, even if a more realistic description must obviously includes the deformation effects. In the case of the nucleus ^{120}Sn, the two shell effects (of opposite sign) resulting from the two nucleonic contributions tend to cancel each other out, so that the total shell effect on the nucleus as a whole is greatly reduced.

Another interesting feature concerns the role of the δW_2 contribution, which in certain cases (for example for ^{162}Dy) is far from being negligible and makes possible a significant improvement of the fit. The main difficulty related to the shell correction in the analytical approach remains in the prediction of the ground state shell correction energy $\delta W = \delta W_1 + \delta W_2$ and consequently in the two separate contributions. This problem is identical to the one encountered in the prediction of nuclear masses. Unfortunately, no semi-classical expression of this quantity has so far been obtained (the classical shell correction of Myers and Swiatecki (1966) is of a more phenomenological type), so that it should still be considered as an artificial quantity without absolute definition. In nuclear mass models, the shell correction energy is linked to the macroscopic part through fits to experimental masses only. Consequently, different mass formulae exhibit shell corrections which are themselves significantly different. Therefore, it would be inconsistent to extract the δW quantity from any arbitrary mass formula in order to describe the shell corrections to the thermodynamic quantities. In addition, even if δW is known, splitting it into the two contributions δW_1 and δW_2 still remains to be done.

Expression (30) corresponds to the first semi-classical approximation of the shell correction energy, although it is limited to the simple case of an infinite square well potential. We postpone the discussion of the predictability of the semi-classical expression (30) to Section II.5.1, where a direct comparison with experimental masses will be carried out and will prove the remarkable

predictive power of this expression.

In summary, it can be seen that the statistical quantities of relevance in the nuclear level density calculations can be fairly well described by the analytical expressions derived in Section II.2.3. The analytical approximation appears to reproduce accurately the numerical calculations by means of 4 parameters. Providing the 4 parameters can be determined, this new formulation is expected to be much more powerful than the numerical evaluation based on the a discrete single-particle level scheme. Not only has it the advantage of offering a realistic and manageable prescription for the excitation-energy dependence of the shell effects on the level densities, but it also avoids most of the problems related to the numerical calculations (see Section II.1.2). However, the determination of the level density parameters in not free from uncertainties, especially because of the lack of reliable experimental information, as will be discussed in Chapter II.5.

II.3 The spin-dependent level density and the shell effect

II.3.1 The statistical model and the approximation of small M

In addition to N, Z and the total energy E, there is at least one other good quantum number for the nucleus: the total angular momentum J. It is, however, well known that it is much simpler to deal with the total magnetic quantum number M, since it is just the sum of the single-particle magnetic quantum numbers. The J-dependence of the level density can later on be obtained in a simple way from its M-dependence. In this case, a nuclear level is defined by the 4 constants:

$$\begin{aligned} N &= \sum_s n_{ns} \\ Z &= \sum_s n_{ps} \\ E &= \sum_s (n_{ns}\varepsilon_{ns} + n_{ps}\varepsilon_{ps}) \\ M &= \sum_s (n_{ns}m_{ns} + n_{ps}m_{ps}) \end{aligned} \tag{48}$$

where n_{ns} (n_{ps}), ε_{ns} (ε_{ps}) and m_{ns} (m_{ps}) are the occupation numbers, energies and magnetic quantum numbers of the neutrons (protons) single-particle states, respectively. The same technique as that used in Section II.2.1 can be applied to the system (48) to deduce the nuclear level density:

$$\rho(E,N,Z,M) = \frac{\mathrm{e}^S}{(2\pi)^2\sqrt{D}} \tag{49}$$

with the extended definitions of S and D obtained from the grand partition function Ω:

- $S = \Omega - \alpha_n N - \alpha_p Z - \gamma M + \beta E$
- D is the 4×4 determinant of second derivatives of Ω with respect to the Lagrange multipliers.
- the saddle points are defined by the relations:

$$\begin{aligned} \frac{\partial\Omega}{\partial\alpha_n} &= N & \frac{\partial\Omega}{\partial\gamma} &= M \\ \frac{\partial\Omega}{\partial\alpha_p} &= Z & \frac{\partial\Omega}{\partial\beta} &= -E \end{aligned} \tag{50}$$

In turn, the J dependence is obtained using the relation (Bethe, 1936):

$$\rho(E,N,Z,J) = \rho(E,Z,N,M=J) - \rho(E,Z,N,M=J+1) \tag{51}$$

In order to simplify the previous equations, we will consider in the subsequent sections only one type of particle (the neutrons for example). Since the proton and neutron contributions to the thermodynamic quantities are additive, the results can be directly extended to a system composed of two non-interacting types of Fermions.

As in the continuous spectrum approximation developed in Section II.2.1, it is convenient to introduce the single-particle state density $g(\varepsilon,m)$, a function this time of both the energy ε and the projection m of the angular momentum on the symmetry axis z. The *state* density $g(\varepsilon,m)$ can be related to the previous single-particle *level* density $g(\varepsilon)$ by the normalization

$$\int g(\varepsilon,m)\, dm = g(\varepsilon) \tag{52}$$

where the integral is carried out over the whole m-space. Having defined $g(\varepsilon,m)$, the thermodynamic quantities can now be determined by the statistical expressions (Huizenga and Moretto, 1972)

$$\Omega = \int_0^{\infty}\int_{-\infty}^{+\infty} g(\varepsilon,m)\, \ln\left(1+\mathrm{e}^{(\alpha+\gamma m-\beta\varepsilon)}\right) dm\, d\varepsilon \tag{53a}$$

$$S = \int_0^{\infty}\int_{-\infty}^{+\infty} g(\varepsilon,m)\left[\ln\left(1+\mathrm{e}^{(\alpha+\gamma m-\beta\varepsilon)}\right) - \frac{\alpha+\gamma m-\beta\varepsilon}{1+\mathrm{e}^{-(\alpha+\gamma m-\beta\varepsilon)}}\right] dm\, d\varepsilon \tag{53b}$$

and the saddle point equations (50) can be rewritten as:

$$N = \int_0^{\infty}\int_{-\infty}^{+\infty} g(\varepsilon,m)\, \frac{1}{1+\mathrm{e}^{-(\alpha+\gamma m-\beta\varepsilon)}}\, dm\, d\varepsilon \tag{54}$$

$$M = \int_0^{\infty}\int_{-\infty}^{+\infty} g(\varepsilon,m)\, \frac{m}{1+\mathrm{e}^{-(\alpha+\gamma m-\beta\varepsilon)}}\, dm\, d\varepsilon \tag{55}$$

$$E = \int_0^{\infty}\int_{-\infty}^{+\infty} g(\varepsilon,m)\, \frac{\varepsilon}{1+\mathrm{e}^{-(\alpha+\gamma m-\beta\varepsilon)}}\, dm\, d\varepsilon \tag{56}$$

where no assumption concerning the form of the distribution function $g(\varepsilon,m)$ has been made.

The approximation of small angular momenta

Except for extremely large values of M, the parameter γ is sufficiently small so that it is a good approximation to expand the expression in powers of γ, keeping only the terms up to γ^2. Such an approximation is known to be good till fairly high values of M, which are found only in reactions with heavy ions (Ignatyuk, 1985). In such conditions, since there is an equal probability for finding a $+m$ and a $-m$ states at any energy ε, $g(\varepsilon, m) = g(\varepsilon, -m)$ and the average value of m is obviously zero

$$< m >= \int_0^{\infty} \int_{-\infty}^{+\infty} g(\varepsilon, m)\ dm\ d\varepsilon = 0 \tag{57}$$

so that only even powers of γ contribute to the series. This property results directly from time reversal symmetry or invariance of the one-particle potential with respect to a rotation of π about an axis perpendicular to the symmetry axis.

The thermodynamic quantities of interest in the framework of the analytical approach can consequently be reduced to

$$\Omega \simeq \Omega_0 + \frac{1}{2}\ \gamma^2 \sigma^2 \tag{58}$$

$$E \simeq E_0 + \frac{1}{2}\ \frac{1}{\beta}\ \gamma^2 \sigma'^2 \tag{59}$$

$$M \simeq \gamma \sigma^2 \tag{60}$$

$$S \simeq S_0 + \frac{1}{2}\ \gamma^2 (\sigma''^2 - \sigma^2) \tag{61}$$

where the subscript (0) refers to the spin-independent quantity as calculated in Section II.2.1, i.e. corresponding to a zero γ value. We have introduced the parameter σ^2, classically referred to as the spin cut-off parameter, and two new spin parameters σ'^2 and σ''^2 defined by

$$\sigma^2 = \int_0^{\infty} m^2(\varepsilon)\ \frac{e^{-\beta(\mu - \varepsilon)}}{\left[1 + e^{-\beta(\mu - \varepsilon)}\right]^2}\ d\varepsilon \tag{62}$$

$$\sigma'^2 = -\int_0^{\infty} m^2(\varepsilon)\ \beta\varepsilon\ \frac{e^{-\beta(\mu - \varepsilon)}\left[1 - e^{-\beta(\mu - \varepsilon)}\right]}{\left[1 + e^{-\beta(\mu - \varepsilon)}\right]^3}\ d\varepsilon \tag{63}$$

$$\sigma''^2 = \int_0^\infty m^2(\varepsilon)\ \beta(\mu - \varepsilon)\ \frac{e^{-\beta(\mu-\varepsilon)}\left[1 - e^{-\beta(\mu-\varepsilon)}\right]}{\left[1 + e^{-\beta(\mu-\varepsilon)}\right]^3}\ d\varepsilon \tag{64}$$

In turn, we define the energy-dependent variance of the m-distribution

$$m^2(\varepsilon) = \int_{-\infty}^{+\infty} g(\varepsilon, m)\ m^2\ dm \tag{65}$$

As in Chapter II.2, the effect of the weak temperature dependence of the chemical potential will be ignored here. It can be shown that in the same approximation relation (54)—which corresponds to the conservation of the particle number—can be rewritten as $N \simeq N_0$, so that the chemical potential μ will be treated as energy- and angular-momentum-independent.

Similarly, in the approximation of small M, the determinant factor must be written as

$$D = D_0\ \sigma^2 \tag{66}$$

where D_0 is the 2×2 determinant given by expression (44).

The equidistant model and the approximation of the Gaussian distribution

Expressions (58)–(66) have been derived in a very general way making use of the small angular momenta approximation only and without any restriction on the shape of the distribution function $g(\varepsilon, m)$. It should, however, be mentioned that these relations have never been analytically studied except in the equidistant-model approximation. In this case, the single-particle level density $g(\varepsilon, m)$ is assumed to be energy-independent and equal to its value at the Fermi energy. Relations (58)–(66) are consequently greatly simplified, since $m^2(\varepsilon)$ has now become an energy-independent parameter. The following equalities are then obtained

$$\begin{aligned} \sigma^2 = \sigma'^2 = \sigma''^2 &= \frac{1}{\beta}\int_{-\infty}^{+\infty} g(\varepsilon_F, m)\ m^2\ dm \\ &= \frac{1}{\beta}\ m^2(\varepsilon_F) \end{aligned} \tag{67}$$

so that the introduction of the angular momentum quantum number can be summarized by the classical excitation-energy-dependent relation

$$S(U, N, M) = S(U, N, M = 0) - \frac{M^2}{2\sigma^2} \tag{68}$$

which if introduced in the level density expression (49), justifies the usual assumption that the nucleus spin projections on the quantization axis have a Gaussian distribution with an average value of zero and a mean square deviation σ^2 as given by expression (67). In such conditions, the M-dependent level density reduces to

$$\rho(E,N,M) = \frac{\rho(E,N)}{\sqrt{2\pi\sigma^2}}\ \mathrm{e}^{-M^2/2\sigma^2} \tag{69}$$

Such an expression can also be deduced from more physical arguments. Since there is an equality in the average occupation number $\bar{n}_s$ for the $+m$ and $-m$ states, the average value of the projection of the total angular momentum $< M >$ which is obtained by summing all the projections m for every state multiplied by its probability of occupation $\bar{n}$, must be zero. Therefore, if all occupation numbers have their exact average values, the system would have a zero total angular momentum. The occurrence of other angular momenta is consequently ascribed to fluctuations of the occupation numbers away from their average values.

The probability ν_s that a Fermion in state s does not have the average occupation number $\bar{n}_s$ is given by (Ericson, 1960)

$$\nu_s = \bar{n}_s(1-\bar{n}_s) = \frac{\mathrm{e}^{-\beta(\mu-\varepsilon_s)}}{\left[1+\mathrm{e}^{-\beta(\mu-\varepsilon_s)}\right]^2} \tag{70}$$

Therefore, the resulting average value of m^2

$$< m^2 >= \int_0^{\infty}\int_{-\infty}^{+\infty} g(\varepsilon,m)\ m^2\ dm\ d\varepsilon \tag{71}$$

will differ from zero and give rise to a non-zero M value. The projection of the angular momentum M on the z-axis of the system is the sum of the projections of the ν excited particles. These projections can have both different signs and different values. If we apply the idea of random coupling to this system, so that the distribution of M can be regarded as the result of the random values of the projections of the ν excited particles and holes with the conditions

$$< m >= 0 \qquad \text{and} \qquad < m^2 > \neq 0\,,$$

the central limit theorem of statistics then implies that the distribution of M-values for large ν asymptotically becomes a Gaussian with a mean square deviation

$$\sigma^2 = \nu < m^2 >= \sum_s m_s^2 \frac{e^{-\beta(\mu - \varepsilon_s)}}{\left[1 + e^{-\beta(\mu - \varepsilon_s)}\right]^2} \tag{72}$$

identical to expression (62) and leading to the density of states (69).

This derivation of the nuclear state density emphasizes that expression (69) is only an asymptotic form valid for large ν. Therefore, this approximation might face some problems at low excitation energies where the number of excited particles is small. Moreover, the Gaussian form will not be adequate for very large values of M. Because a finite number of particles cannot couple to give arbitrarily large spin, the distribution function is then exactly zero. Yet it is surprising to know that in the statistical approach use is almost never made of a different form than the Gaussian distribution. In the analytical, as well as in the numerical approach, the spin distribution is always assumed to be given by relation (69). The exact statistical formulation of the spin-dependent level density (expressions (53)–(56)) leads to calculations which are in general rather complicated especially if the pairing interaction is included by means of the classical BCS approximation (see Chapter II.4). Even the approximate expressions (58)–(61) based on the series expansion in powers of γ have never been used previously. However, despite its simplicity, the Gaussian approximation can give rise to significant discrepancies since its only parameter σ^2 is never taken as a free parameter. Comparisons with experimental data always assume the *a priori* knowledge of the cut-off parameter, so that a spurious choice of σ^2 can, for obvious reasons, not lead to reliable predictions for the a-parameter. Therefore, it is our opinion that the spin distribution should be studied in a much more careful way than it has been in the past. It should be recalled that the angular momentum plays an essential role, in particular in the analysis of experimental neutron resonance data.

As in Chapter II.2, we have tried to remove the equidistant spacing approximation, which

might by its unrealistic character lead to significant discrepancies. All analytical formulae for the spin-dependent level density have so far been derived under the assumption of a constant single-particle state density. Such an approach neglects, not only the significant effects of the shell structure, but also the contribution of the first order term in $g(\varepsilon, m)$ which appears to affect the equidistant model results significantly (see Section II.3.3). In order to improve the analytical approximation, the knowledge of the single-particle state density $g(\varepsilon, m)$ is required. We show in Section II.3.2 (and Appendix B) how the semi-classical theory described in Appendix A can be generalized to the case with fixed projection m. In particular, for our purposes the special case of an infinite square well potential will be studied, since it is able to provide a suitable analytical expression for $g(\varepsilon, m)$. As emphasized by expressions (62)–(65), all the information concerning the m-distribution is contained in the energy-dependent variance $m^2(\varepsilon)$, which will consequently be estimated with great care.

When the m^2-distribution is known, a direct evaluation of the thermodynamic quantities and more particularly of the spin cut-off parameters is possible (Section II.3.3). To do so, new methods will once again be developed in order to retain the exact nature of the shell effect and to relate the spin-dependent terms to already calculated quantities, such as the entropy or the a-parameter. Our new formulation of the spin cut-off parameters is finally compared with the numerical predictions based on a Woods-Saxon single-particle scheme (Section II.3.4).

II.3.2 The m-distribution of the single-particle state density

(i) the single-particle state density with fixed angular momentum projection

As in Section II.2.2, the semi-classical methods can be used to extract the distribution of single-particle states $g(\varepsilon, m)$ with fixed angular momentum projection m. The quasi-classical theory, as developed in Appendix A, does not make any restriction on the quantity m and can be generalized to the case with fixed m. If axially symmetric potentials are considered, the corresponding Green function $G(\mathbf{r}', \mathbf{r}, \varepsilon)$ (see equation $(A1)$) depends on the difference of the angular coordinates $\psi = \varphi' - \varphi$ (where φ corresponds to the angular coordinate in a cylindrical frame with z as the symmetry axis). A simple Fourier transformation of the Green function with respect to the variable ψ leads to the m-dependent Green function, which in turn, if introduced in expression $(A1)$, enables an evaluation of the state density $g(\varepsilon, m)$ (see Appendix B)

Making use of a semi-classical approximation for the quantity G, the state density $g(\varepsilon, m)$ can be expressed in the form

$$g(\varepsilon, m) = \tilde{g}(\varepsilon, m) + g_{osc}(\varepsilon, m) \tag{73}$$

where $\tilde{g}(\varepsilon, m)$ is the smooth part of the state density, known as the Thomas-Fermi term. The oscillating component $g_{osc}(\varepsilon, m)$ is related to the gross shell effects (Magner et al., 1978) which appear in the semi-classical approach to be associated with the quasi-classical quantization of motion in the potential well along the multidimensional periodic orbits.

We will restrict ourselves here to spin-independent central potential only. In this case, the projections along the z-axis m_l and m_s of the orbital momentum and of the spin of the nucleons are independent. Because of the straightforward treatment of the spin distribution (see sub-section *(ii)*), we will consider here the orbital contribution only.

In the special case of an infinite square well potential, expression (73) can be reduced to a

very simple analytical formula, as discussed in detail in Appendix B:

$$\tilde{g}(\varepsilon, m_l) = \frac{D}{4\pi\varepsilon}\left[-(m_l+\frac{1}{2})\sqrt{\frac{\varepsilon}{\varepsilon_0}+\frac{1}{4}-(m_l+\frac{1}{2})^2}+(\frac{\varepsilon}{\varepsilon_0}+\frac{1}{4})\cos^{-1}\frac{m_l+1/2}{\sqrt{\frac{\varepsilon}{\varepsilon_0}+1/4}}\right] \tag{74}$$

$$g_{osc}(\varepsilon, m_l) = \frac{1}{2\iota}\left(\frac{\varepsilon_0}{\varepsilon}\right)^{1/2} g_{osc}(\varepsilon) \tag{75}$$

where we have defined the centrifugal energy ε_0 by

$$\varepsilon_0 = \frac{\hbar^2}{2mR^2} \tag{76}$$

with R as the radius of the potential well.

The function $g_{osc}(\varepsilon)$ corresponds to the oscillating contribution to the single-particle level density as derived in Chapter II.2 (equation (23)). The constant ι ($\simeq 0.6$ for the infinite square well) is an average value of the orbital angular momentum, expressed in terms of the ratio $(\varepsilon/\varepsilon_0)^{1/2}$, over the contributing orbits:

$$\bar{l} = \iota\left(\frac{\varepsilon}{\varepsilon_0}\right)^{1/2} \tag{77}$$

The smooth contribution $\tilde{g}(\varepsilon, m_l)$ is defined for positive value of $m_l < m_l^*$, where m_l^* corresponds to the turning point in the m-space given by $\varepsilon = \varepsilon_0\, m_l^*(m_l^*+1)$. Similarly, the oscillating component $g_{osc}(\varepsilon, m_l)$ appears to differ from the known function $g_{osc}(\varepsilon)$ by the factor of $\frac{1}{2\bar{l}}$, at least for not too large m values. Expression (75) has, indeed, been derived under the assumption $|m| < l_{min} \lesssim \bar{l}$ (see Appendix B).

(ii) Energy-dependent variance of the m-distribution

In the case of a spin-independent potential, we can write the energy-dependent variance of the m-distribution as

$$m^2(\varepsilon) = m_l^2(\varepsilon) + m_s^2(\varepsilon) \tag{78}$$

Since $m_s = \pm\frac{1}{2}$, the spin projection contribution can be calculated directly by

$$\begin{aligned} m_s^2(\varepsilon) &= \int g(\varepsilon, m_s)\; m_s^2\; dm_s \\ &= \frac{1}{4}\; g(\varepsilon) \end{aligned} \tag{79}$$

from the definition of the single-particle level density $g(\varepsilon)$.

In the heavy nuclei, the contribution of the spin is small compared with the orbital term, since large orbital momenta occur near the top of the Fermi distribution. Moreover, $m_s^2(\varepsilon)$ corresponds to a correction to $m^2(\varepsilon)$ in the order of the curvature term, so that in practice its contribution can be neglected.

Concerning the orbital contribution, with the knowledge of the single-particle state density $g(\varepsilon, m_l)$ we can know evaluate the second moment of the m-distribution by

$$m_l^2(\varepsilon) = \tilde{m}_l^2(\varepsilon) + m_{l,osc}^2(\varepsilon) \tag{80}$$

$$= \int \tilde{g}(\varepsilon, m_l)\; m_l^2\; dm_l + \int g_{osc}(\varepsilon, m_l)\; m_l^2\; dm_l \tag{81}$$

Integration of the smooth contribution using expression (74) leads to

$$\begin{aligned} \tilde{m}_l^2(\varepsilon) &= 2\int_0^{m_l^*} \tilde{g}(\varepsilon, m_l)\; m_l^2\; dm_l \\ &= \left(\frac{\varepsilon}{\varepsilon_0}\right) \frac{D}{4\pi^2}\frac{1}{\varepsilon_0}\left[\frac{2}{15}\frac{4\pi}{3}\left(\frac{\varepsilon}{\varepsilon_0}\right)^{1/2} - \frac{\pi}{4}\cos^{-1}\frac{1}{2\sqrt{\dfrac{\varepsilon}{\varepsilon_0}+1/4}} + \cdots\right] \qquad (82) \\ &= \left(\frac{\varepsilon}{\varepsilon_0}\right)\left[\frac{2}{15}\;\tilde{g}_V(\varepsilon) + \frac{1}{8}\;\tilde{g}_S(\varepsilon) + \;\cdots\right] \qquad (83) \\ &\simeq \frac{2}{15}\left(\frac{\varepsilon}{\varepsilon_0}\right)\tilde{g}(\varepsilon) \qquad (84) \end{aligned}$$

where we have introduced the volume and surface contributions of the single-particle level density in the case of an infinite well, as derived in Appendix B (see expression ($B18$)). Although expression (83) has been obtained in the special case of the infinite square well potential, we can expect it to be reliable for more general models. As already emphasized, in a Woods-Saxon type potential the

volume term is identical to the one corresponding to the infinite well. Since the surface term leads to a small correction (at least in the vicinity of the Fermi energy), we can hope that expression (83) should yield good results if applied to a Woods-Saxon potential.

In order to test the validity of expression (83), we can compare it to the exact quantity

$$m^2_{ws}(\varepsilon) = \sum_{\nu} m^2_{\nu}\ \delta(\varepsilon - \varepsilon_{\nu}) \tag{85}$$

where the summation is carried over the single-particle state ν of a Woods-Saxon potential.

For a more understandable comparison, we have however evaluated the integrated value of $\tilde{m}^2$ with respect to the energy ε:

$$\mathcal{M}^2(\varepsilon) = \int_0^{\varepsilon} \tilde{m}^2(\varepsilon)\ d\varepsilon \tag{86}$$

Figure 11 displays the exact $\mathcal{M}^2(\varepsilon)$ function obtained from a Woods-Saxon single-particle level scheme for the 126 neutrons of ^{208}Pb (see Section II.2.4 for the potential parameters). Superimposed is the smooth function as obtained from expression (86) and (83) where use is made of the semi-classical approximation of the Woods-Saxon single-particle level density (see Appendix A). We have, however, introduced a scaling factor $\kappa = 0.7$ to obtain the semi-classical curve of Fig. 11. The origin of the semi-classical overestimate is mainly due to the fact that the state density $g(\varepsilon, m)$ has been derived for an infinite square well and not for a Woods-Saxon potential. A similar scaling factor should be introduced in the semi-classical approximation of the level density $g(\varepsilon)$ if the surface term was neglected. The very approximate treatment of the surface contribution can be held responsible for this discrepancy.

Figure 11 is of particular interest since it shows that the quantity $m^2(\varepsilon)$ is far from being energy-independent as assumed in the equidistant spacing model. A linear fit to $\mathcal{M}^2(\varepsilon)$ would lead to a really poor approximation of the Woods-Saxon curve. This statement is of particular importance when application to the thermodynamic quantity is concerned (see Section II.3.3).

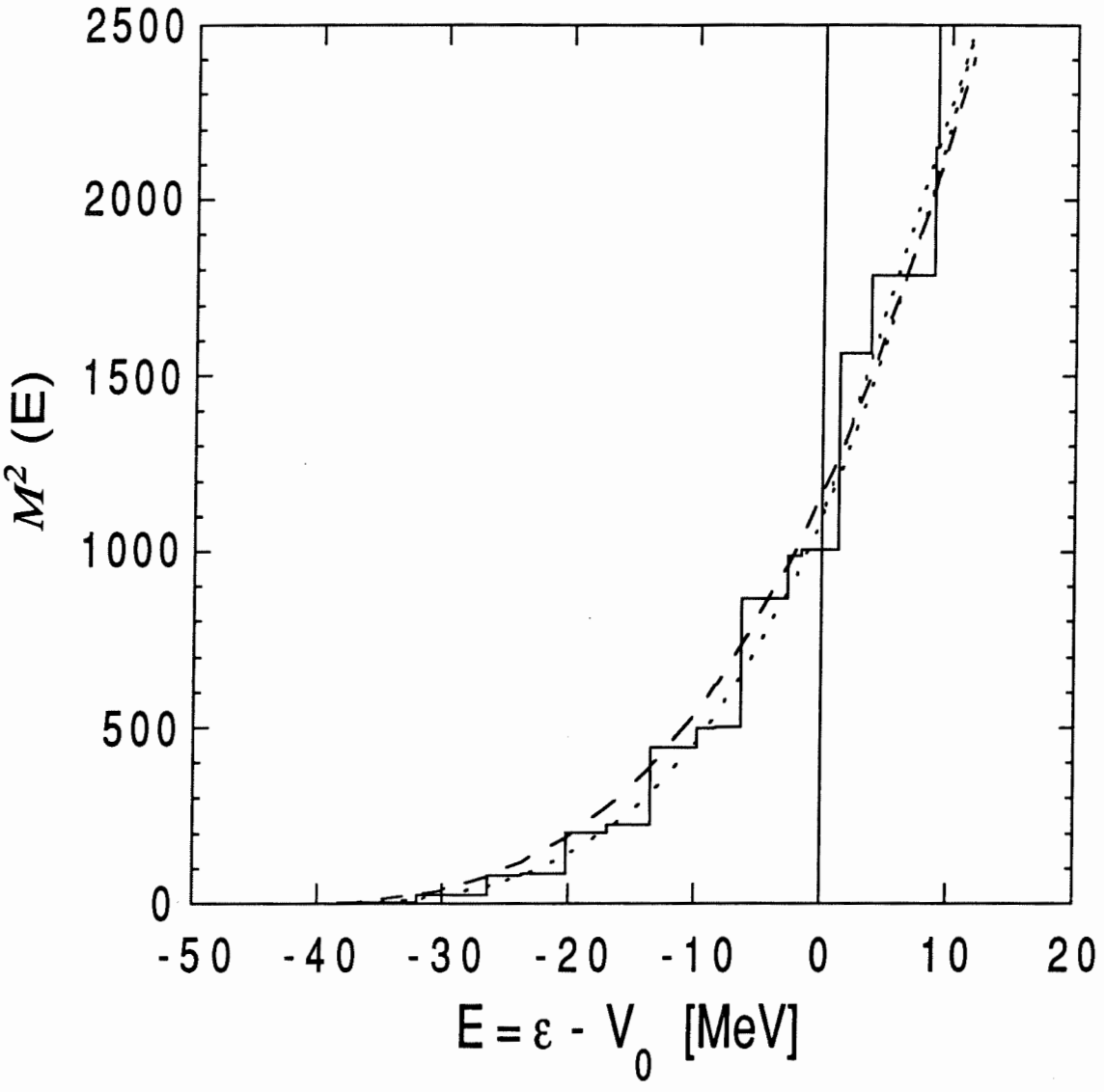

Figure 11. Integrated variance $\mathcal{M}^2(\varepsilon)$ of the m-distribution in a Woods-Saxon potential for the neutron sytem of ^{208}Pb as a function of the single-particle energy $E = \varepsilon - V_0$, where $V_0 = 45\,\mathrm{MeV}$ is the potential depth. The dashed line corresponds to the semi-classical prediction taking the volume and surface terms into account. The dotted curve has been obtained with the ansatz (87) with $n = 2.5$: $m^2(\varepsilon) = 0.063\,\varepsilon^{2.5}$.

Moreover, the predicted $\varepsilon^{3/2}$ dependence of $\tilde{m}^2(\varepsilon)$ appears to reproduce fairly well the gross behaviour of the Woods-Saxon estimate, at least if the surface correction, as derived in Appendix A for a Woods-Saxon potential, is included. It should, however, be noted that if the surface contribution is neglected, the $\varepsilon^{3/2}$ dependence of $\tilde{m}^2(\varepsilon)$ becomes too weak. In this case, it can be shown (see Fig. 11) that a very good fit to $\mathcal{M}^2(\varepsilon)$ can be obtained if use is made of the approximation

$$\tilde{m}^2(\varepsilon) \sim \varepsilon^n \qquad \text{with} \quad 1.5 \lesssim n \lesssim 3 \tag{87}$$

which includes the volume as well as the surface contributions. Expression (87) often constitutes a reliable ansatz to the semi-classical approximation (83) derived for a Woods-Saxon potential because of the very uncertain surface contribution. If the volume term only is considered and since to first approximation $\tilde{m}^2(\varepsilon) \sim \varepsilon\, g(\varepsilon)$, it can be seen that the case $n = 1.5$ corresponds to the infinite square well potential while the case $n = 3$ would describe the case of an harmonic oscillator. Since the smooth single-particle level density in a Woods-Saxon potential is known to lie between the density in an infinite box and an harmonic oscillator (Schmidt et al., 1982), we can have some confidence in expression (87). The coefficient n mainly reflects the influence of the surface contribution (negative at low energies and positive at energies slightly higher than the Fermi energy), so that a higher n value can be expected for lighter nuclei (their surface correction being relatively more important).

As regards the oscillating contribution to the variance in the case of an infinite square well, a similar calculation can be performed which finally leads to

$$\begin{aligned} m^2_{l,osc}(\varepsilon) &= 2 \int_0^{\bar{l}} g_{osc}(\varepsilon, m_l)\; m_l^2 \; dm_l \\ &= \frac{1}{3}\, \bar{l}^2 \; g_{osc}(\varepsilon) \end{aligned} \tag{88}$$

Since $\frac{\bar{l}^2}{3} \sim \frac{2}{15}\frac{\varepsilon}{\varepsilon_0}$, we can approximate the total energy-dependent variance of an infinite square well by its semi-classical expression

$$m^2(\varepsilon) \simeq m_l^2(\varepsilon) = \frac{2}{15}\, \frac{\varepsilon}{\varepsilon_0}\, g(\varepsilon) \tag{89}$$

As mentioned above, this result can be generalized to the more realistic case of a Woods-Saxon potential by introducing the simple scaling factor κ and by associating the single-particle level density with its corresponding semi-classical expression (or by the ansatz $g(\varepsilon) \sim \varepsilon^{n-1}$ if the volume and surface contributions are enclosed in one single term). The energy-dependent variance can finally be expressed by

$$m^2(\varepsilon) = \kappa \, \frac{2}{15} \, \frac{\varepsilon}{\varepsilon_0} \, g(\varepsilon) \tag{90}$$

II.3.3 Determination of the spin parameters

(i) Evaluation of the spin cut-off parameter σ^2

The main parameter which is believed to influence the spin distribution of the nuclear level density is known as the spin cut-off parameter σ^2 and is given in the continuous spectrum approximation by expression (62). Now that an analytical expression for the energy-dependent variance $m^2(\varepsilon)$ has been derived, integration (62) can be carried out. Such a calculation could be performed by expanding the $m^2(\varepsilon)$ in a power series around the Fermi energy and integrating the different terms. Yet this procedure is strictly equivalent to the equidistant spacing approach if the leading term only is retained and has the disadvantage of neglecting the rapidly varying behaviour of the oscillating contribution as well as the energy dependence of the smooth term.

We have therefore tried to carry out integration (62) in a different way, which does not affect the analytical form of the $m^2(\varepsilon)$ function. The technique adopted is based on replacing the universal integrand function

$$h(x) = 4\,\frac{\mathrm{e}^{-x}}{\left(1+\mathrm{e}^{-x}\right)^2} = \mathrm{sech}^2 x/2 \tag{91}$$

by the already known function

$$F(\sigma_a x) = \frac{1}{\ln 2}\left[\ln\left(1+\mathrm{e}^{-\sigma_a x}\right) + \frac{\sigma_a x}{1+\mathrm{e}^{\sigma_a x}}\right] \tag{92}$$

where $\sigma_a = \frac{\pi^2}{12\ln 2}$. As can be seen in Fig. 12, $F(\sigma_a x)$ is a surprisingly good approximation to $h(x)$. This substitution can, therefore, be made with total confidence. In addition, the evaluation of σ^2 can now be directly related to the calculations performed in Chapter II.2 and more precisely to already calculated quantities, such as the entropy S or the a-parameter. Expression (62) can be rewritten as

$$\sigma^2 = \kappa\,\frac{2}{15}\,\frac{1}{4\ln 2}\int_0^\infty \frac{\varepsilon}{\varepsilon_0}\,g(\varepsilon)\,\left[\ln\left(1+\mathrm{e}^{-\beta'(\mu-\varepsilon)}\right) + \frac{\beta'(\mu-\varepsilon)}{1+\mathrm{e}^{\beta'(\mu-\varepsilon)}}\right] d\varepsilon \tag{93}$$

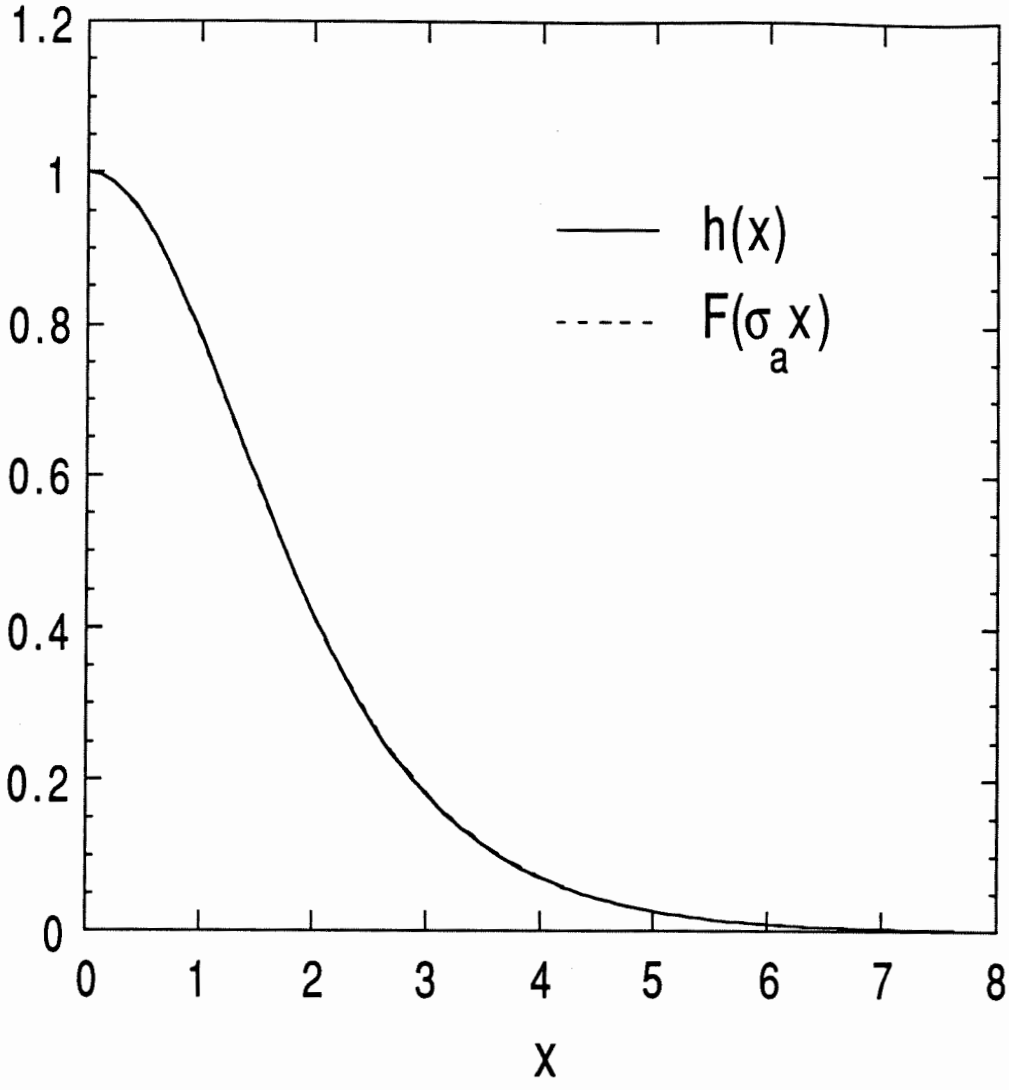

Figure 12. Comparison of the function $h(x)$ with the function $F(\sigma_a x)$, as defined in the text. The two functions are so similar that they cannot be distinguished on the figure.

where $\beta' = \sigma_a \beta$. Integration (93) can be carried out in the same manner as integration (17a) which led to the determination of the entropy $S(T)$. We finally find

$$\sigma^2(T) = a_\sigma(T)\, T \tag{94}$$

$$= \kappa \frac{2}{15} \frac{1}{4 \ln 2} \frac{\mu_0}{\varepsilon_0} S(T/\sigma_a) \tag{95}$$

$$= \kappa \frac{2}{15} \frac{6}{\pi^2} \frac{\mu_0}{\varepsilon_0} a(T/\sigma_a)\, T \tag{96}$$

where $S(T)$ and $a(T)$ are the T-dependent entropy (31) and level density parameter (33), respectively. We introduce, at this point, a new T-dependent parameter a_σ which in the limit of high temperatures (i.e. after the washing-out of shell effects) can be related to the quasi-classical approximation to the moment of inertia. The moment of inertia $\mathcal{I}_{rig}$ around an axis of the nucleus considered as a rigid body can be expressed as (Bloch, 1954)

$$\frac{\mathcal{I}_{rig}}{\hbar^2} = \tilde{a}_\sigma = \kappa \frac{2}{15} \frac{6}{\pi^2} \frac{\mu_0}{\varepsilon_0} \tilde{a} \tag{97}$$

Expression (96) is of particular interest because it constitutes the first proof of the usually adopted empirical relation between the spin cut-off parameter and the entropy (e.g. Kataria et al., 1978; Vonach et al., 1988)

$$\sigma^2(T) = \frac{\mathcal{I}_{rig}}{\hbar^2} \frac{a(T)}{\tilde{a}}\, T \tag{98}$$

which is identical to expression (96) if the a-parameter is calculated at the temperature T/σ_a instead of T. Such a difference, even if small ($\sigma_a \simeq 1.19$), can have a non-negligible influence on the T-dependence of $\sigma^2(T)$. The excitation energy is a quadratic function of the temperature, so that the critical energy at which shell effects disappear can be shifted to a relatively higher value.

The amplitude of the shell corrections to the spin cut-off parameter appears to be as important as the one characterizing the a-parameter. Numerical calculations including realistic single-particle level density have confirmed the influence of shell structure on the spin cut-off parameter (e.g. Ignatyuk and Stavinskii, 1970). As shown in Section II.2.4, these shell effects are often far from

being negligible and might significantly affect the spin distribution of the total level density though the influence of the spin cut-off parameter on the nuclear level density is not as drastic as the one due to an entropy change. Some previous fits to experimental data based on the Back-Shifted Fermi Gas model (e.g. Dilg et al., 1973) have shown that a decrease of the spin cut-off parameter by a factor of 2 modifies the prediction of the a-parameter by 10 to 20%. However, this result is model-dependent and does not take into account the possible unreliability of the Fermi Gas model for describing the spin distribution. In particular, the parameters σ'^2 and σ''^2 need to be evaluated carefully and their influence to be estimated before drawing conclusions about the total spin distribution. The introduction of these two new parameters not only modifies the value of the effective spin cut-off parameter, but also questions seriously the generally accepted idea that the spin cut-off parameter includes all information concerning the spin distribution.

(ii) Evaluation of the parameters σ'^2 and σ''^2

While in the constant spacing model, the parameters σ'^2 and σ''^2 reduce to the same value as the spin cut-off parameter, now that the variance $m^2(\varepsilon)$ is considered as energy dependent, differences can be expected. As a matter of fact, a simple integration by parts of expressions (63) and (64) leads to

$$\sigma'^2 = \int_0^\infty \left[m^2(\varepsilon) + \varepsilon \, \frac{\mathrm{d}m^2(\varepsilon)}{\mathrm{d}\varepsilon} \right] \frac{\mathrm{e}^{-\beta(\mu-\varepsilon)}}{\left[1+\mathrm{e}^{-\beta(\mu-\varepsilon)}\right]^2} \, d\varepsilon \tag{99}$$

$$\sigma''^2 = \int_0^\infty \left[m^2(\varepsilon) - (\mu-\varepsilon) \, \frac{\mathrm{d}m^2(\varepsilon)}{\mathrm{d}\varepsilon} \right] \frac{\mathrm{e}^{-\beta(\mu-\varepsilon)}}{\left[1+\mathrm{e}^{-\beta(\mu-\varepsilon)}\right]^2} \, d\varepsilon \tag{100}$$

The first term in both integrals corresponds to the already calculated σ^2 contribution and leads to the equidistant model prediction which neglects the $\frac{\mathrm{d}m^2(\varepsilon)}{\mathrm{d}\varepsilon}$ contribution to the integrals and assumes that m^2 remains constant. However, the semi-classical approximation, as derived in the previous section, predicts a strong energy dependence of $m^2(\varepsilon)$, so that the second term in

expression (99) can give rise to a contribution even larger than the first term. If we use the analytical approximation (90) to $m^2(\varepsilon)$, integrating (99) and (100) gives

$$\sigma'^2 = \tilde{a}_\sigma T\Big[\,(n+1) + f(\delta W_1, \delta W_2, \gamma, T)\,\Big] \tag{101}$$

$$\sigma''^2 = \tilde{a}_\sigma T\left[1 + \frac{\gamma^2 \delta W_1}{\tilde{a}} \frac{1}{\left(1+\dfrac{\gamma^2 T^2}{\sigma_a^2}\right)^2} + 2\frac{\gamma^2}{\tilde{a}}(\delta W_2 - 2\,\delta W_1)\frac{\gamma^2 T^2/\sigma_a^2}{\left(1+\dfrac{\gamma^2 T^2}{\sigma_a^2}\right)^3}\right] \tag{102}$$

$$= \sigma^2(T) - \tilde{a}_\sigma T \frac{4\gamma^2 \delta W_1}{\tilde{a}} \frac{\gamma^2 T^2/\sigma_a^2}{\left(1+\dfrac{\gamma^2 T^2}{\sigma_a^2}\right)^3} \tag{103}$$

where $1.5 \lesssim n \lesssim 3$. Expressions (102) and (103) have been obtained similarly to σ^2. The function $f(\delta W_1, \delta W_2, \gamma, T)$ describes the shell correction to σ'^2 which can hardly be estimated by the same technique (see below). At high temperatures, the function f however vanishes.

(iii) Discussion

Before discussing the physical meaning of these numerous parameters, let us relate them first to the better known thermodynamic quantities. If we introduce the relation $\gamma = M/\sigma^2$ into the expressions of the energy (59) and the entropy (61), we find

$$U = U_0 + \frac{1}{2}\,\frac{M^2}{a_\sigma(T)}\,\frac{\sigma'^2}{\sigma^2} \tag{104}$$

$$S = S_0 + \frac{1}{2}\,\frac{M^2}{\sigma^2}\left(\frac{\sigma''^2}{\sigma^2} - 1\right) \tag{105}$$

where the excitation energy U is derived from the total energy E by subtracting the ground state energy of the zero spin nucleus. The quantity $E_{rot} = \frac{1}{2}\frac{M^2}{a_\sigma}\frac{\sigma'^2}{\sigma^2}$ is commonly associated with the rotational energy. It corresponds to the energy that is expected to go into rotational motion and has consequently become unavailable for the random or thermodynamic excitation of the system. At zero temperature, E_{rot} describes the so-called yrast line corresponding to the lowest energy for each angular momentum. All the excitation energy is rotational energy and used to generate

angular momentum. The level density along this line is known to be much lower than the level density of the zero spin nucleus at the corresponding energy because the rotational energy does not contribute to what is usually called the intrinsic level density. Since the nucleus is "cold" in the yrast region, a high degree of order is expected and therefore shell effects play an important role.

These new expressions for $U(T)$ and $S(T)$ differ from the ones generally adopted in the analytical as well as numerical approaches in many respects. In the statistical model, $U(T)$ and $S(T)$ are usually approximated by

$$U = U_0 + \frac{1}{2}\,\frac{M^2}{a_\sigma} \tag{106}$$

$$S = S_0 \tag{107}$$

Moreover, in the analytical approach, a_σ is generally taken as temperature-independent and equal to its asymptotic value $\tilde{a}_\sigma$. Therefore, it appears that in addition to the T-dependence introduced in the expressions of U and S in order to describe the shell structure of the nucleus, two new correction factors affect the spin-dependent quantities.

Let us discuss separately the smooth contribution (i.e. the asymptotic behaviour) and the oscillating correction to the different parameters.

At the limit of high temperatures, the shell correction terms vanish and the excitation energy (104) and entropy (105) have the asymptotic behaviour

$$U = U_0 + \frac{1}{2}\,\frac{M^2}{\mathcal{I}_{eff}/\hbar^2} \tag{108}$$

$$S = S_0 \tag{109}$$

where the effective moment of inertia is now given by

$$\frac{\mathcal{I}_{eff}}{\hbar^2} = \frac{1}{n+1}\,\frac{\mathcal{I}_{rig}}{\hbar^2} = \frac{1}{n+1}\,\tilde{a}_\sigma \tag{110}$$

If the entropy is not affected asymptotically, as predicted by the classical expression (107), the rotational energy appears to be increased by a factor of $(n+1)$ relative to expression (106). Since $(n+1)$ is predicted to lie between $2.5 \lesssim (n+1) \lesssim 4$, this result is of great importance and is in total disagreement with the generally adopted expression (106). On the other hand, it agrees well with the generally accepted fact that the experimental moments of inertia are a factor of 2 to 3 smaller than their rigid body values (e.g. Ring and Schuck, 1980). Yet it should be noted that expression (110) does not question the rigid body value, but rather its classical relation to the rotational energy. Such a decrease in the effective moment of inertia by a factor of $(n+1)$ is directly due to the energy dependence of the variance $\tilde{m}^2(\varepsilon)$ and consequently of the state density $g(\varepsilon, m)$. In contrast to the spin cut-off parameter, the parameter σ'^2 does not depend on the local mean square value of the level spins close to the Fermi energy, but on the difference between its value above and below the Fermi surface. At higher excitation energies single-particle levels with higher spin are found, or equivalently 'particle' type excitons carry more angular momentum than 'hole' type excitons. This explains the increase of $\tilde{m}^2(\varepsilon)$ with the energy and consequently the important effect of its derivative in the evaluation of σ'^2.

Although the discrepancies between the experimental moments of inertia and their rigid body values are generally ascribed to the pairing correlation (see Chapter II.4), we see that even without the pairing interaction, the semi-classical approximation developed in this section suggests an effective moment of inertia much smaller than the rigid body value.

As regards the shell effects on the spin parameters, they appear to be basically identical to those affecting the entropy. In particular, the rotational energy becomes T-dependent. Yet the shell effects on the spin distribution of the nuclear level density disappear more slowly than they do in the energy distribution, i.e. in the spin-independent quantities. The critical temperature for the spin cut-off parameter is given by $T_\sigma = \frac{\sigma_a}{\gamma}$ which is to be compared with $T_{sh} = \frac{1}{\gamma}$ characterizing the

disappearance of the shell structure in the entropy S_0 or excitation energy U_0. This feature can be explained in the following way: the effects associated with the shell structure of the single-particle levels vanish when the nucleons are so distributed in the one-particle levels that the equivalent average distribution of levels can be assimilated to an equidistant spacing distribution. The excited single-particles responsible for the bulk configuration are then spread in an energy range wide enough to mask the shell structure. When a given M-value is imposed on the system, a new constraint on the configuration of excited particles appears, since the occupied states must now also fulfill the condition $M = \sum_\nu n_\nu m_\nu$. A higher energy must therefore be reached in order to populate levels not only uniformly distributed, but such that $\sum n_\nu m_\nu$ is equal to the given M-value. In the approximation of small M, the factor σ_a of the critical temperature appears to be a universal constant.

Expression (104) also suggests that the energy E_{rot} used to generate a certain M projection is more important if the degree of order is high. For a stable spherical nucleus (characterized by $\delta W < 0$), $a_\sigma(T)$ is an increasing function of the temperature so that E_{rot} decreases when the temperature increases (for a given M). The increasing temperature tends to break the nuclear order and to enable an easier rotation of the nucleus.

However, some uncertainties remain concerning the influence of the T-dependent factor σ'^2/σ^2. Unlike all quantities derived so far, the parameter σ'^2 does not depend only on the single-particle level density in the vicinity of the Fermi energy. The integrand function in expression (63) of σ'^2 turns out to be identically zero at the Fermi energy, positive above it and negative below so that σ'^2 depends on the difference of the quantity $\varepsilon\, m^2(\varepsilon)$ above and below the Fermi surface. Moreover, the calculation of σ'^2 requires the knowledge of the kinetic energy distribution of the nucleons, while in all the other quantities the kinetic energy always enters the calculations relative to the Fermi energy. It has been stressed in Section II.2.1 that the continuous-spectrum approximation is not

well adapted for describing this kind of quantity. In particular, the crude oscillatory contribution to the single-particle state density becomes quickly unreliable when energy levels away from the Fermi energy are considered. Other models, such as Strutinsky type calculations, might be more suited to evaluate σ'^2 in the same manner as they can fairly well reproduce the shell correction energy.

On the contrary, the evaluation of the parameter σ''^2 is much more reliable. This quantity is of particular interest since in contrast to the currently used models, it shows that the entropy might be directly affected by the introduction of the new quantum number M. The spin distribution as described by the Gaussian approximation (69) results from the rotational correction to the excitation energy only. However, according to expression (105), the shell structure also gives rise to a "rotational" entropy, which vanishes at high temperatures, but which might affect the amplitude of the total entropy at low energy.

In summary, the semi-classical approach, as developed in this chapter, leads to significantly different expressions of the spin parameters to those obtained with the equidistant-model approximation. Not only have the shell effects been introduced consistently in the rotational energy but it now appears that two major corrections concerning the amplitude of the rotational energy and of the rotational entropy might strongly affect the classical Gaussian approximation. An estimation of the corresponding effective spin cut-off parameter can be obtained by substituting the temperature as given by expression (104) into the entropy (105), so that the entropy is now expressed as a function of the intrinsic excitation energy U (see e.g. Gilbert and Cameron, 1965). Under the approximation of small M, the spin-dependent level density can be expressed to first approximation (essentially for excitation energies much larger than the rotational energy) as

$$\rho(U,N,J) = \frac{\rho(U,N)}{\sigma\sqrt{2\pi}} \; \frac{2J+1}{2\,\sigma_{eff}^2} \; \mathrm{e}^{-\frac{(J+1/2)^2}{2\,\sigma_{eff}^2}} \tag{111}$$

The effective spin cut-off parameter is given by

$$\frac{1}{\sigma_{eff}^2} = \frac{1}{\sigma^2}\left[\frac{\sigma'^2}{\sigma^2} - \left(\frac{\sigma''^2}{\sigma^2} - 1\right)\right] \tag{112}$$

and is expected to exhibit important shell effects resulting from the fluctuations in the m- and ε-distribution of the single-particle levels. In addition, at high temperatures, a reduction by the factor $(n+1)$ of the effective moment of inertia relative to the classical spin cut-off parameter is predicted.

In order to test the validity of the numerous assumptions made in the semi-classical approach, a comparison with numerical calculations remains to be done.

II.3.4 Comparison with numerical shell model calculations

Since the numerical approach of the statistical model making use of a realistic Woods-Saxon single-particle level scheme must be regarded as the exact result that our analytical approximation is trying to reproduce, we have compared our analytical results concerning the spin parameters with the numerical predictions. To perform such calculations, the same single-particle spectrum as the one adopted in Section II.2.4 has been used. Moreover, we have considered here the neutron and proton configurations of the same nuclei (^{120}Sn, ^{162}Dy and ^{208}Pb) and use the same parameters $\tilde{a}$, γ, δW_1 and δW_2 to describe the spin-independent quantities (see Table 1).

The spin cut-off parameter $a_\sigma = \sigma^2/T$ and the corrective factor $\left(\sigma''^2/\sigma^2 - 1\right)$, as derived from the semi-classical approach, are displayed in Figs. (13)–(18) as a function of the temperature, and compared with their numerical evaluation obtained with the Woods-Saxon single-particle level scheme.

Let us estimate the accuracy of the analytical approach, for the macroscopic contribution as well as for the oscillating contribution to the spin parameters.

(i) semi-classical prediction of the macroscopic contribution

Figs (13)–(18) have been plotted by identifying the smooth asymptotic value of the spin parameters with the value resulting from the numerical calculation. Using such a procedure is equivalent to treating the parameters κ and κ'' defined by

$$\kappa = \frac{\tilde{a}_\sigma}{\frac{2}{15}\frac{6}{\pi^2}\frac{\mu_0}{\varepsilon_0}\tilde{a}} \tag{113}$$

$$\kappa'' = \lim_{T\to 0} \frac{\sigma''^2(T)}{\sigma^2(T)} \tag{114}$$

as free parameters. The parameter κ already introduced in Section II.3.2 corresponds to the correction to the macroscopic quantity $\tilde{a}_\sigma$ when the semi-classical approximation to the infinite

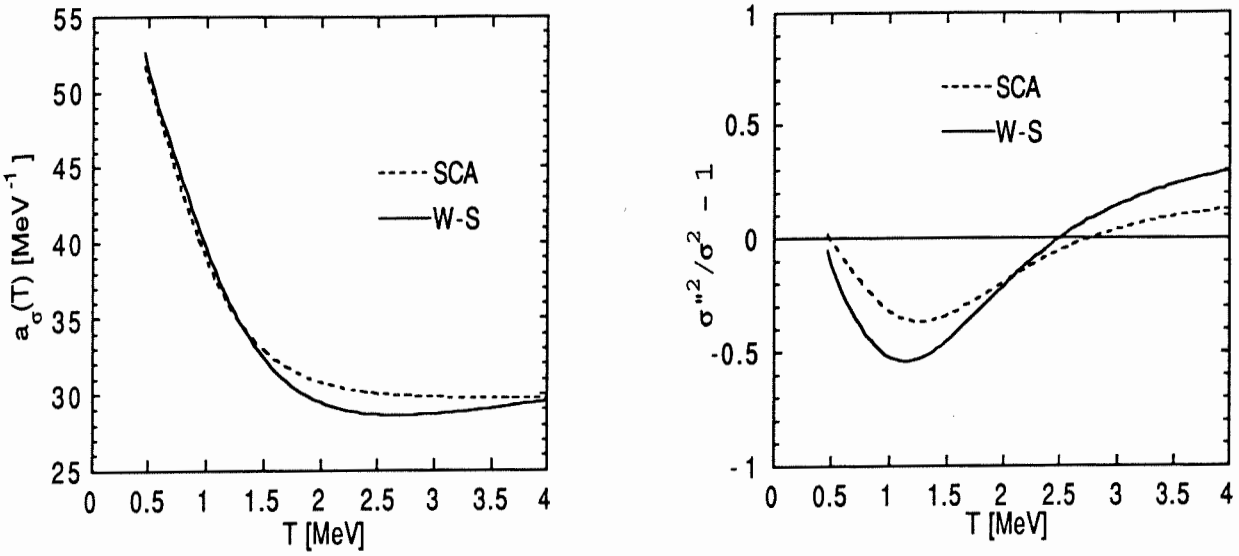

Figure 13. Spin parameters for the neutron system of ^{120}Sn as a function of the temperature. The left part displays the T-dependence of the parameter a_σ (or equivalently, the moment of inertia), while the right part shows the correction factor $(\sigma''^2/\sigma^2 - 1)$ affecting the entropy. The full lines have been obtained with the numerical model based on a Woods-Saxon single-particle level scheme (W-S). The dashed line correspond to the analytical approximation obtained with the semi-classical approximation (SCA) to the single-particle level density.

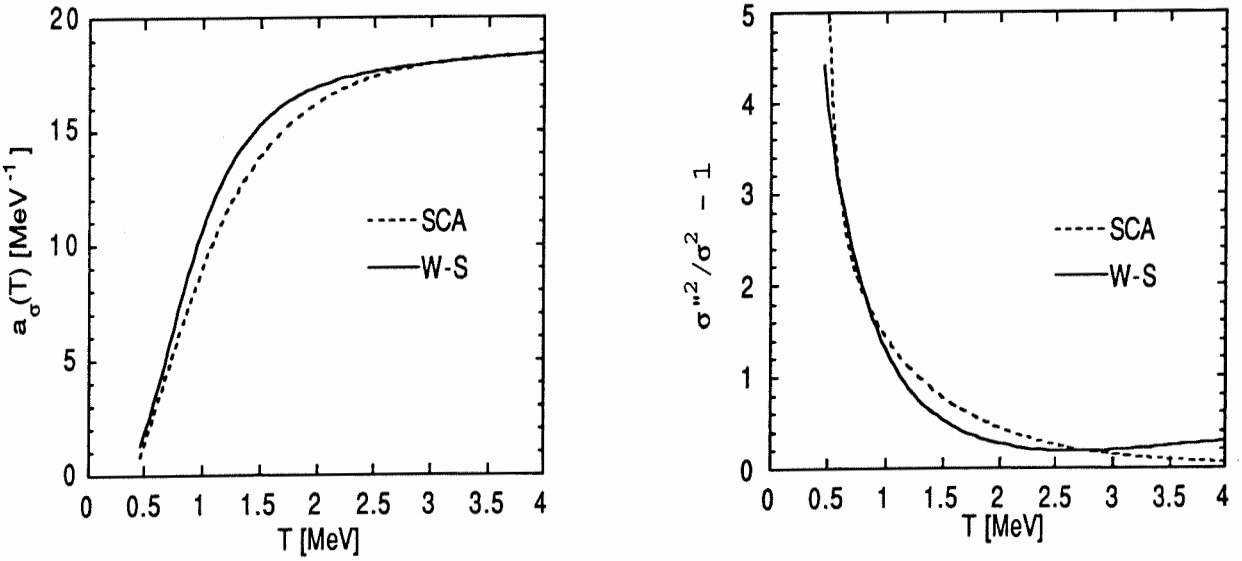

Figure 14. Same as Fig. 13 for the proton system of ^{120}Sn.

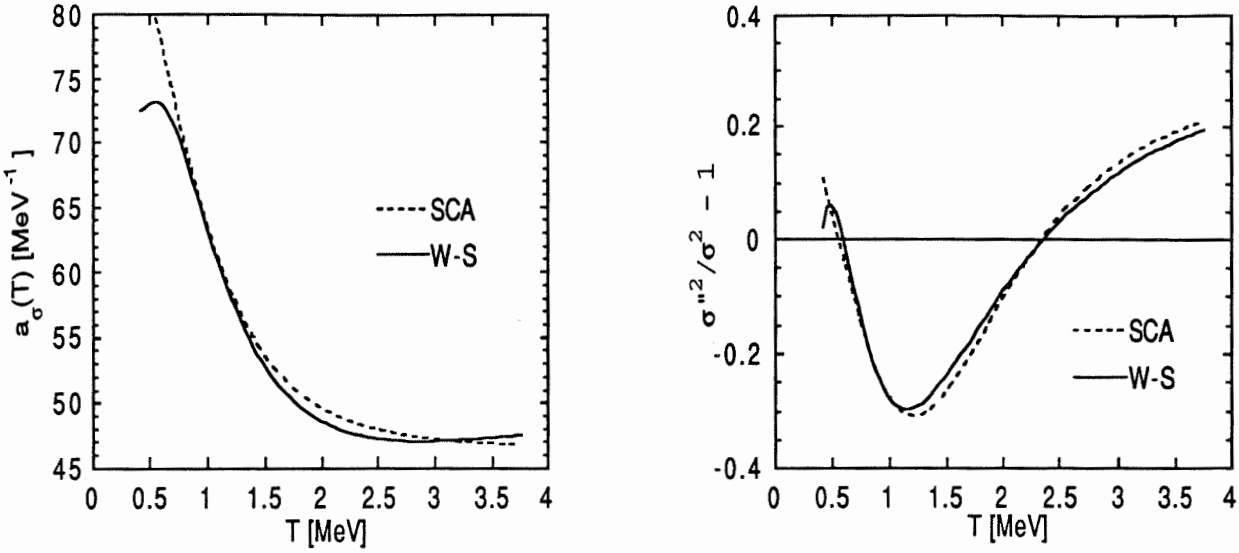

Figure 15. Same as Fig. 13 for the neutron system of ^{162}Dy.

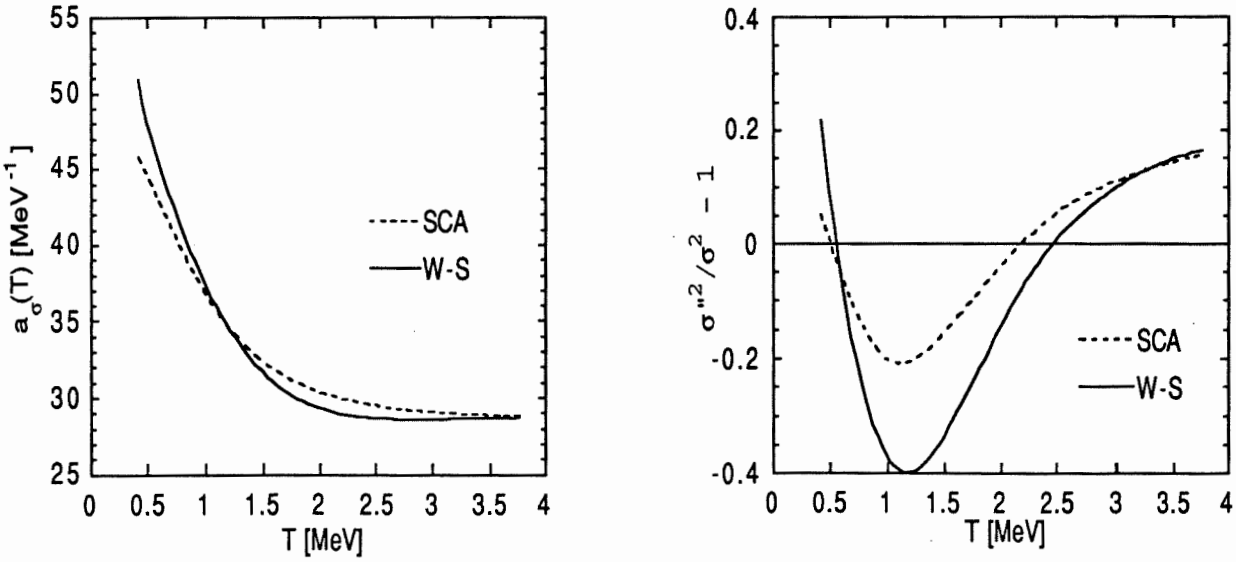

Figure 16. Same as Fig. 13 for the proton system of ^{162}Dy.

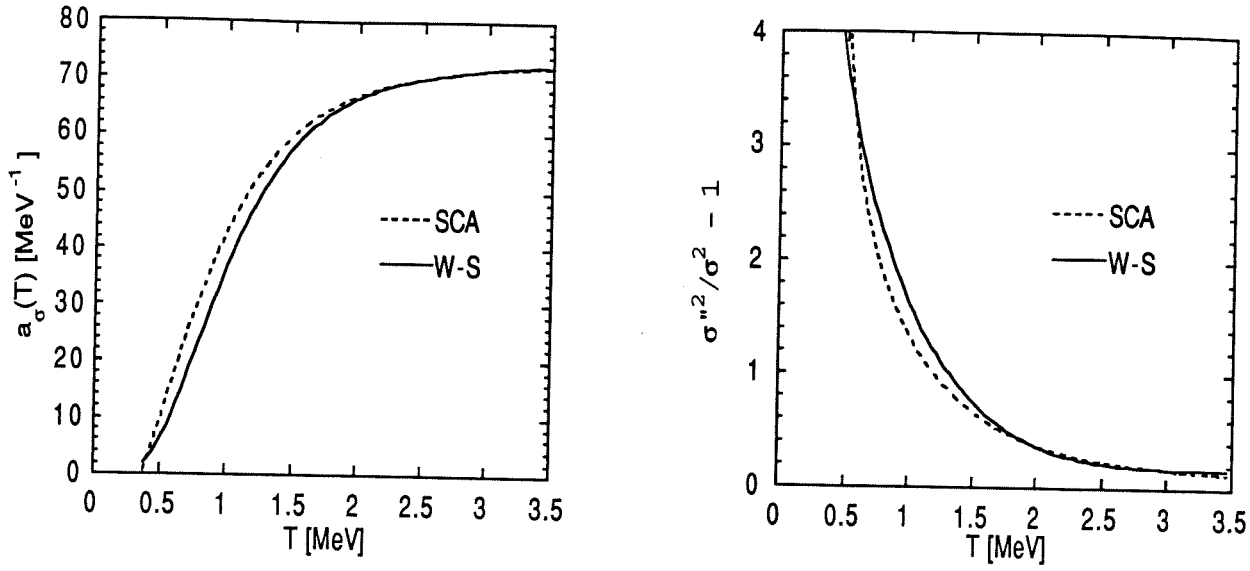

Figure 17. Same as Fig. 13 for the neutron system of ^{208}Pb.

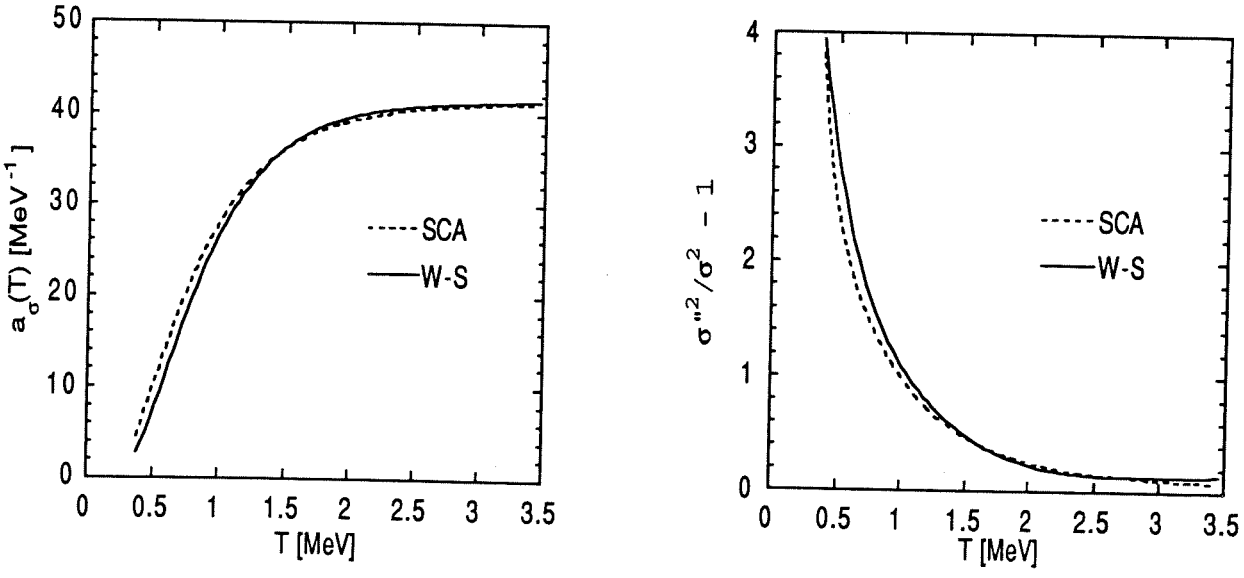

Figure 18. Same as Fig. 13 for the proton system of ^{208}Pb.

square well is extended to the more realistic case of a Woods-Saxon potential. The predictive power of the semi-classical approach can be tested by evaluating $\tilde{a}_\sigma = \kappa \frac{2}{15} \frac{6}{\pi^2} \frac{\mu_0}{\varepsilon_0} \tilde{a}$ using the parameters of Table 2. The corrective factors κ required to reproduce the Woods-Saxon value $\tilde{a}_\sigma$ are displayed in Table 3 for each nucleus. As can be seen, the value of κ remains fairly constant and equal to the empirical value of 0.7, already introduced in Section II.3.2 to fit the variance $m^2(\varepsilon)$ to its discrete value in the Woods-Saxon potential. The constancy of the parameter κ proves that the semi-classical prediction is surprisingly good. A way of renormalizing the macroscopic value $\tilde{a}_\sigma$ consists in replacing the chemical potential (assumed to be equal to the Fermi energy and therefore energy-independent) by its expression as a function of the particle number. If the same approximation for the single-particle level density is used, the parameter κ disappears, and we are left with the classical expression for the rigid-body value of the moment of inertia

$$\frac{\mathcal{I}_{rig}}{\hbar^2} = \tilde{a}_\sigma = \frac{2}{5} \frac{\mathrm{m}R^2}{\hbar^2} N \tag{115}$$

This well-known formula has the advantage of being independent of the empirical parameter κ and reproduces relatively well the value predicted by the numerical model, as shown in Table 3. The small discrepancies between $\frac{\mathcal{I}_{rig}}{\hbar^2}$ and $\tilde{a}_\sigma$ can be explained by the uncertain value of the reduced radius r_0 (see Table 2), as well as by the different energy dependences in the expressions of the single-particle level density and of the energy-dependent variance. However, it is of interest to see how the uncertainty inherent in the amplitude of the single-particle level density can be eliminated by substituting the chemical potential by the particle number. We will come back to this problem in Chapter II.5.

The second parameter κ'' has been introduced to account for the small correction to σ''^2 resulting from the second order terms in expression (100) and which apparently (see Table 3) lead to a small contribution to the asymptotic value of σ''^2. The value of κ'' remains, however, close to the predicted value of unity. Our confidence in the semi-classical prediction is consequently

increased.

Table 3.

Smooth spin parameters reproducing the numerical evaluation:

$\tilde{a}_\sigma$ (97), $\frac{\mathcal{I}_{rig}}{\hbar^2}$ (115) and the parameters κ (113), κ'' (114), $n+1$ (110)

		$\tilde{a}_\sigma$ (MeV^{-1})	$\frac{\mathcal{I}_{rig}}{\hbar^2}$ (MeV^{-1})	κ	κ''	$n+1$
$^{120}_{50}\mathrm{Sn}_{70}$	neut.	29.8	26.9	0.68	1.20	4.2
	prot.	18.6	18.1	0.68	1.10	3.8
$^{166}_{66}\mathrm{Dy}_{96}$	neut.	47.0	44.1	0.67	1.29	4.0
	prot.	28.8	28.6	0.72	1.23	3.4
$^{208}_{82}\mathrm{Pb}_{208}$	neut.	72.0	68.9	0.70	1.08	3.8
	prot.	41.5	41.3	0.74	1.05	3.2

Also given in Table 3, is the value of the factor $n+1$. If the shell effects on the spin parameter σ'^2 remain obscure in the analytical approach, the asymptotic value of the ratio σ'^2/σ^2 is well determined. The numerical model gives for $n+1$ the average value of 3.5 which is in close agreement with the semi-classical prediction. Yet some variations around this average value can be observed, and, more particularly, it appears that lower values can be ascribed to the proton systems. Such a result can be related to the role played by the Coulomb repulsion which tends to reduce the effective potential radius (see Section II.2.4), and consequently the energy dependence of the single-particle state density. It must, however, be stressed that in the numerical approach, the evaluation of the factor $n+1$ still suffers from some uncertainties owing to the inaccurate knowledge of the kinetic energy, or equivalently of the potential depth (especially for the proton potential). The uncertainty on the factor $n+1$, associated with this inaccuracy, has been estimated to be of the order of 20%. Yet the numerical model clearly confirms the possible increase of the classical rotational energy

(i.e. a reduction of the effective moment of inertia relative to its rigid body value) by a factor of 2 to 4.

(ii) semi-classical prediction of the oscillating contribution

As regards the oscillating contribution to the spin parameters, the agreement of the analytical results with the Woods-Saxon predictions are rather good, even if more significant discrepancies appear in comparison with Figs. (5)–(10) corresponding to the spin-independent quantities for the same nuclei. It should, however, be stressed that the shell parameters γ, δW_1 and δW_2 have been determined to reproduce the spin-independent thermodynamic quantities and that more assumptions have been made to extract the spin parameters. In particular, the shell correction to the single-particle state density has been described in a relatively crude way.

Despite the numerous approximations, the analytical shell corrections to the spin parameters reproduce the numerical calculations relatively well. To emphasize the non-negligible effects of the shell structure, it should be recalled that in the uniform model the parameter a_σ is taken as T-independent and equal to the rigid body value of the moment of inertia. Such an approximation is obviously unrealistic for a nucleus like ^{208}Pb which exhibits a very strong shell structure. In that case, the shell corrections lead at low temperatures to a reduction of σ^2 by a factor of 5 to 10 relative to the usually adopted value (i.e. the smooth asymptotic value $\tilde{a}_\sigma$)—see Figs. (17)–(18).

The shift of the critical temperature to a larger value ($T_\sigma = \sigma_a T_{sh}$) also appears to be confirmed by the numerical calculations. To emphasize that feature, we have displayed in Fig. 19 the ratios $a_\sigma(T)/a(T/\sigma_a)$ calculated in the numerical approach for the two nucleonic systems of ^{208}Pb. As can be observed, this ratio remains fairly constant and does not exhibit a strong shell effect (the T-dependence at very low temperatures is partially due to the T-dependence of the chemical potential which is taken into account in the numerical calculations). On the contrary, the ratio $a_\sigma(T)/a(T)$, also shown in Fig. 19, has at low temperatures a much more variable behaviour with respect to

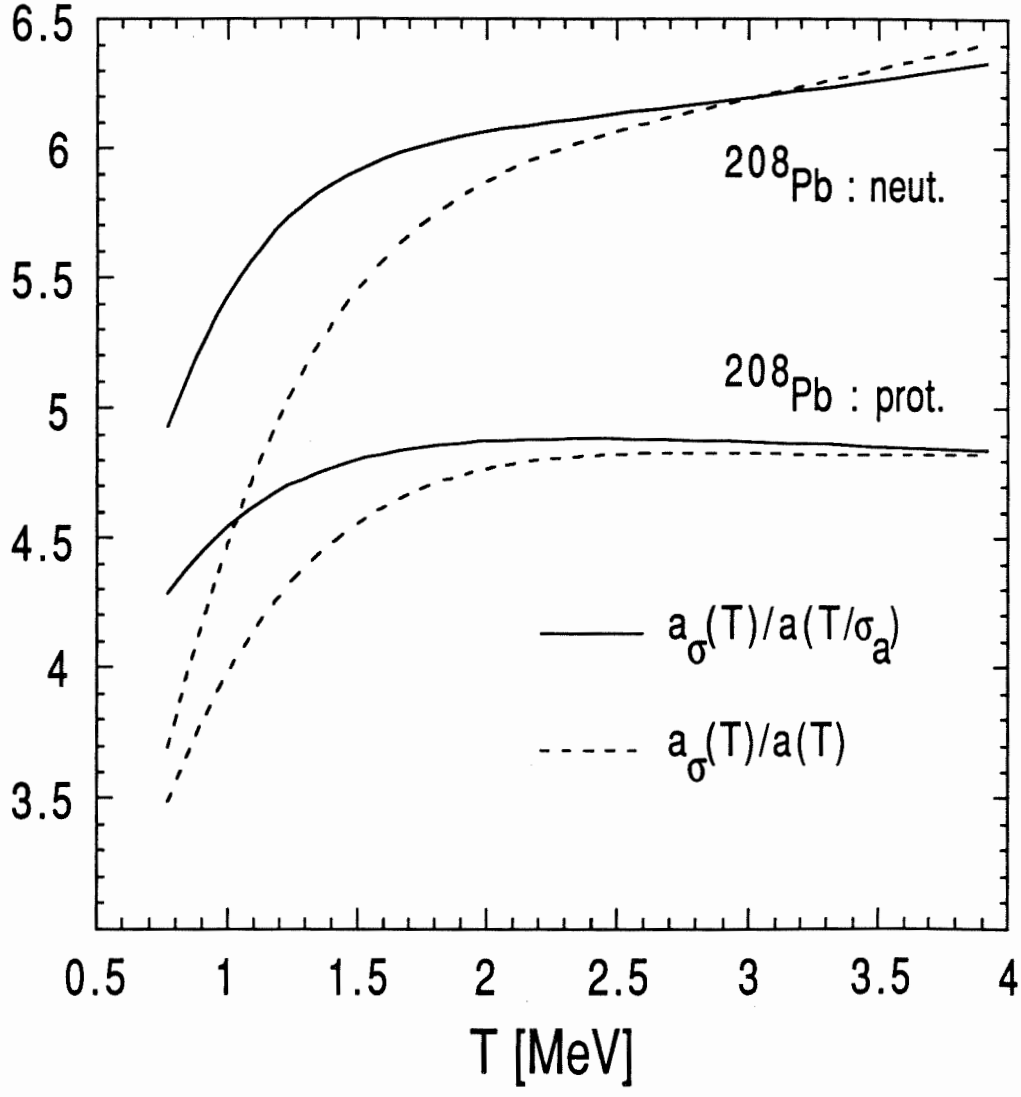

Figure 19. Comparison of the T-dependent ratio $a_\sigma(T)/a(T/\sigma_a)$ with the ratio $a_\sigma(T)/a(T)$, for the two nucleonic systems of ^{208}Pb.

the temperature. The comparison of these two ratios favours the introduction of the factor σ_a in the shell damping function of the spin parameters, even if the predicted value might have been slightly underestimated.

Another non-negligible modification brought to the spin distribution can be found in the correction factor $\left(\sigma''^2/\sigma^2 - 1\right)$, i.e to a possible non-zero rotational entropy. Such a correction has always been neglected so far since asymptotically it is supposed to vanish totally. However, Figs. (13)–(18) show that at low temperatures its effect can be remarkably important. The semi-classical approximation appears to be surprisingly good if we remember that it essentially depends on the second order terms of the shell corrections to the single-particle level density.

We have finally estimated the total correction factor f_c defined from relation (112) by

$$f_c = \frac{\sigma^2}{\sigma^2_{eff}} = \frac{\sigma'^2}{\sigma^2} - \left(\frac{\sigma''^2}{\sigma^2} - 1\right) \tag{116}$$

The factor f_c takes the shell effects as well as the correction factors introduced in the rotational energy and entropy into account. It remains, however, uncertain because of the difficulties associated with the evaluation of the spin parameter σ'^2, as mentioned above. We have estimated its amplitude by means of the Woods-Saxon single-particle level scheme, for the neutron systems of the three nuclei studied (see Fig. 20). It is unexpected to see that the total reduction factor f_c can be so important, although at very low temperatures the use of expression (116) is known not to apply (expression (116) can be used only if the excitation energy is much higher than the rotational energy). If in the limit of high temperatures, we find the average value of 3.5, it appears that at low temperatures shell effects can lead to a considerable increase of f_c. This behaviour is mainly due to the large amplitude of the spin parameter σ'^2 which can exhibit at low temperatures a very strong shell effect resulting from fluctuations in the m-distribution of the single-particle levels around the Fermi energy. It has been emphasized that σ'^2 essentially depends on the difference between the mean square deviation m^2 (weighted by the kinetic energy) above and below the Fermi surface. In

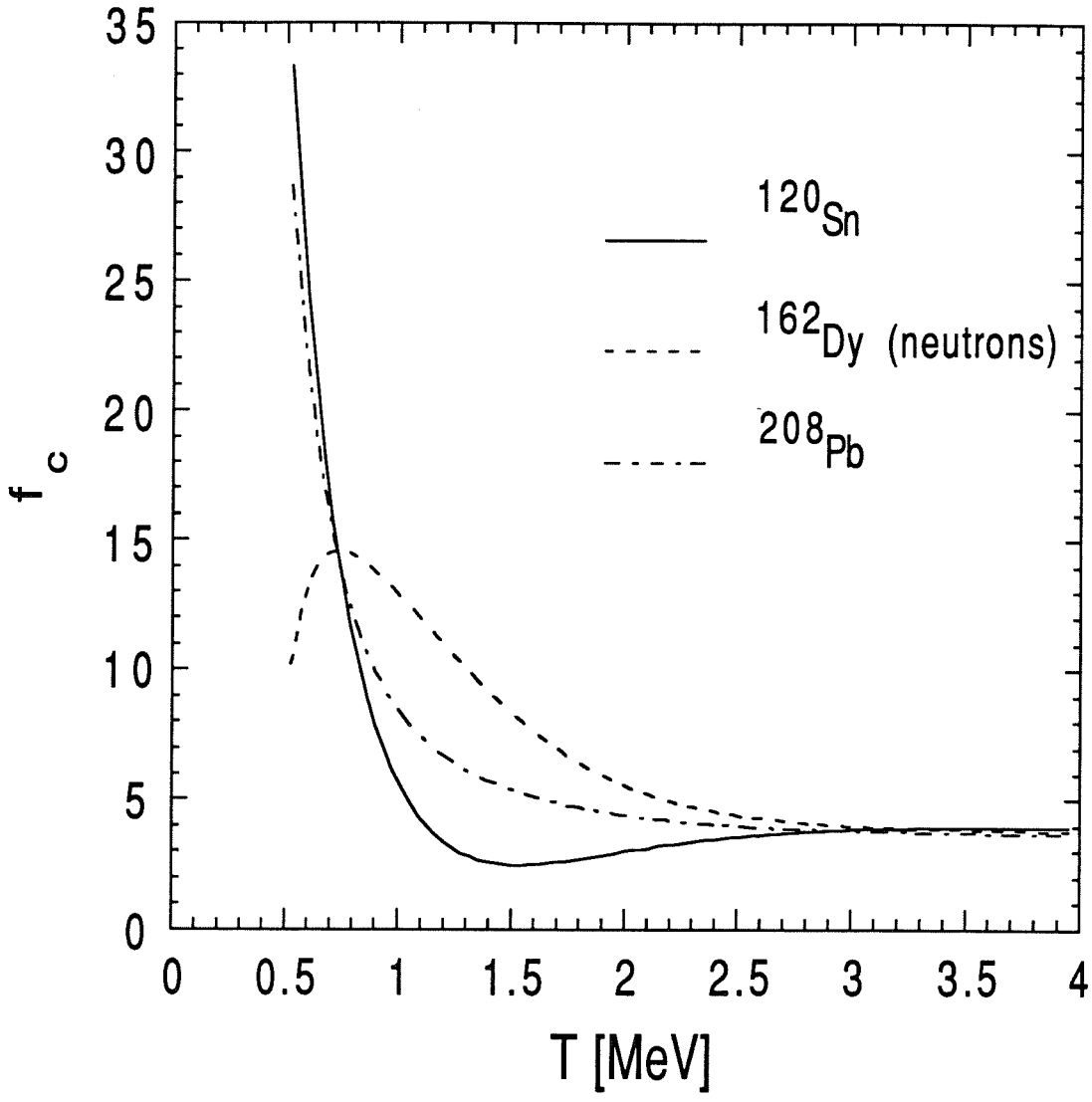

Figure 20. Correction factor f_c to the spin cut-off parameter as a function of the temperature T for the neutron system of the three nuclei ^{120}Sn, ^{162}Dy and ^{208}Pb. The curves have been obtained using the Woods-Saxon single-particle level scheme.

the case of ^{120}Sn for example the neutron Fermi energy lies below the $1h_{11/2}$ level and above the $3s_{1/2}$ and $2d_{3/2}$ levels, so that the quantity εm^2 is much higher above than below the Fermi energy and consequently the factor f_c is expected to be relatively important, as confirmed by Fig. 20. On the contrary, the ^{162}Dy neutrons in the levels $3p_{3/2}$ $1i_{13/2}$ above the Fermi energy do not carry much more angular momentum than the holes in the levels $2f_{7/2}$ $1h_{9/2}$ below the Fermi energy, even if their kinetic energies are also higher. A less important shell effect will consequently affect the quantity f_c in this case.

In summary, it appears that the corrective factor f_c is subject to the oscillatory structure characterizing the energetic distribution of the single-particle levels as well as to the one found in the angular momentum distribution of the levels. These two effects can lead to an effective spin cut-off parameter significantly lower (3 to 5 times at high temperatures but in some cases 10 to 20 times at low temperatures) than the usually adopted value. For light nuclei ($N, Z \lesssim 50$), we can expect the amplitude of the factor f_c to be reduced because of the absence of levels with high angular momenta. However, the determination of f_c remains very uncertain at low temperatures because of its strong sensitivity to the location of the Fermi level. Different single-particle level schemes, especially if obtained with a different spin-orbit potential, would inevitably be characterized by differences in their m-distributions around the Fermi surface and consequently lead to a different behaviour of f_c as a function of the temperature, even if at high temperatures the same behaviour can globally be expected.

As already stressed, the reduction of the spin cut-off parameter does not have as significant an impact on the final nuclear level density as the one resulting from an entropy change. Expression (111) shows the slow varying behaviour of the spin-dependent level density with the effective moment of inertia. Yet a decrease of the spin cut-off parameter is far from being of no consequence and can, in particular, strongly modify the quantitative evaluation of the a-parameter which repro-

duces the experimental neutron spacing data. The so-called experimental a-parameter is generally deduced from the Back-Shifted Fermi gas formula assuming that the spin cut-off parameter is given by the rigid body value of the moment of inertia. A decrease in the effective moment of inertia will consequently lead to a decrease in the "experimental" a-parameter.

The reduction of the effective spin cut-off parameter relative to the usually adopted value remains to be confirmed. Originally, Newton (1956) and Cameron (1958) noticed that the moment of inertia could be reduced well below its rigid body value and used a factor f_c equal to 8 and 33, respectively, to fit the experimental data available at that time. Later analysis (Facchini and Saeta Menichella, 1968; Moretto et al., 1970) of the shell model prediction for the average value $< m_j^2 >$ suggested an increase in the moment of inertia by the factor of 1.5. More recent experimental studies on light nuclei ($20 \lesssim A \lesssim 40$) are however in favour of the classical Gaussian approximation without a reduction in the moment of inertia (Beckerman, 1977). Yet the experimental determination of the spin cut-off value remains very difficult. The most direct method of obtaining σ_{eff}^2 is by counting the number of known levels with various spins. Attempts have been made (von Egidy, 1986, 1988) to extract this value near the ground state by fitting the theoretical spin distribution (111) to the experimental spin distribution. However, very large error bars remain and this method is still unable to predict the energy dependence of the spin cut-off parameter. Therefore, it is our opinion that the determination of the spin parameters remains very uncertain and requires drastic improvements.

We would like to stress again that we do not question the value of the spin cut-off parameters. As shown on Table 3, our analytical prediction of the shell-independent moment of inertia agrees closely with the generally adopted rigid body value. The significant difference is associated with the so-called rotational energy which could be according to expression (104) strongly increased. If the associated shell effects remain obscure, the increase of the rotational energy by a factor of 3 to 5

is confirmed by the shell model calculations. This result should, however, be investigated in much more detail. Combinatorial calculations of the spin distribution could constitute an interesting tool for evaluating the effective spin cut-off parameter. These calculations are under study.

II.4 The superconductivity effects in nuclear level densities

II.4.1 The statistical model and the BCS approximation

The nucleus has been treated so far as an assembly of non-interacting nucleons confined to the nuclear volume by an average potential. This treatment corresponds to the first approximation to the behaviour of a system of particles interacting via two-body forces. However, a realistic description of the statistical nuclear properties should include the correlations amongst the motions of the particles which inevitably arise from the short range components of the two-body forces. It is well know that the pairing interaction is the most important residual interaction and that it was originally introduced to explain certain characteristic properties of low-lying excited nuclear states. The pairing forces also account for the known differences in the level density between even, odd-mass and doubly odd nuclei and are known to affect strongly the spin dependence of the level density. Since the wave functions of two nucleons in the same degenerate orbit have a large overlap, an additional energy is required to break a pair of nucleons before exciting the two nucleons into unpaired orbits. In the analytical approach, this effect is generally accounted for, in a phenomenological way, by subtracting a pairing energy from the excitation energy. Since these odd-even effects are also found in nuclear masses and nucleon binding energies, the pairing energy has been associated with the one derived from a semi-empirical mass formula. However, this phenomenological correction is known to be fairly unrealistic at low energy and to describe poorly the correlation effects occurring in the low-lying states. More secure techniques have, therefore, been adopted to take the pairing effects on the statistical nuclear properties into account. In particular, the microscopic BCS theory (Bardeen, Cooper and Schriffer, 1957) has been applied to the problem of the nuclear level density and has considerably helped to improve the comparison

with experimental data (Sano and Yamasaki, 1963; Decowski et al., 1968; Moretto, 1972). Most of the experimental data on level densities (mainly the neutron resonance spacings and the cumulative number of known levels) concern the very low energy region (0–10 MeV), so that it can be expected that the correlation effects in these low-lying states strongly affect the statistical properties of the nucleus. Consequently, when comparison with experimental data is made, it is of great importance to include the residual interactions in the description of the level density.

In the BCS theory of superconductivity, the Fermion system can be described in terms of the classical BCS Hamiltonian which can be expressed in its second quantization form as

$$H = \sum_k \varepsilon_k (b^+_{k+} b_{k+} + b^+_{k-} b_{k-}) - G \sum_{k,k'} b^+_{k'+} b^+_{k'-} b_{k-} b_{k+} \tag{117}$$

where $b^+_{k\pm}$ and $b_{k\pm}$ are creation and annihilation operators of the particles with opposite spin projections, respectively, and ε_k is the energy of the k^{th} doubly-degenerate single-particle level of a nucleon in the nuclear potential. The pairing interaction is characterized by the pairing strength G which is generally supposed to be independent of k and k', if they lie between given values, and to vanish outside this k-range.

Such an Hamiltonian can be approximately diagonalized by means of a linear quasi-particle transformation. In such a description, the excitations are considered to be independent Fermions whose energy is given by

$$E_k = \sqrt{(\varepsilon_k - \mu)^2 + \Delta^2} \tag{118}$$

where μ is the chemical potential and the quantity Δ or gap parameter is a measure of the pairing correlation. The sum of states of the Fermions system follows

$$Z = \mathrm{Tr}\ \mathrm{e}^{-\beta H_0} \tag{119}$$

with

$$H_0 = \sum_k (\varepsilon_k - \mu - E_k) + \frac{\Delta^2}{G} + \sum_{k,s} E_k \alpha^+_{ks} \alpha_{ks} \tag{120}$$

In this last expression, the second summation is carried over both negative and positive values of the spin projection s, and α^{+}_{ks} and α_{ks} denote the creation and annihilation operators, respectively, of the quasi-particle in the ks state. The logarithm of the grand partition function can finally be expressed as

$$\Omega = -\beta \sum_{k} (\varepsilon_k - \mu - E_k) + 2 \sum_{k} \ln \left(1 + \mathrm{e}^{-\beta E_k}\right) - \beta \frac{\Delta^2}{G} \tag{121}$$

The energy gap Δ is related to the Lagrange multipliers $\beta = 1/T$ and μ by the so-called gap equation

$$\frac{2}{G} = \sum_{k} \frac{1}{E_k} \tanh \frac{1}{2} \beta E_k \tag{122}$$

The first integrals of motion as well as the entropy of the system can then be derived from Ω:

$$N = \sum_{k} \left[1 - \frac{\varepsilon_k - \mu}{E_k} \tanh \frac{1}{2} \beta E_k\right] \tag{123}$$

$$E = \sum_{k} \varepsilon_k \left[1 - \frac{\varepsilon_k - \mu}{E_k} \tanh \frac{1}{2} \beta E_k\right] - \frac{\Delta^2}{G} \tag{124}$$

$$S = 2 \sum_{k} \left[\ln \left(1 + \mathrm{e}^{-\beta E_k}\right) + \frac{\beta E_k}{1 + \mathrm{e}^{\beta E_k}}\right] \tag{125}$$

where the summations are over doubly degenerate orbitals k. The pairing correlations are mainly described by the gap parameter Δ. It can be seen that for $\Delta \equiv 0$, expressions (123)–(125) reduce to the respective expressions derived in Chapter II.2 in the uncorrelated conditions. The gap parameter Δ given by the gap equation (122) decreases with increasing temperature and vanishes at a critical temperature T_{cr}. Above this temperature, the pairing correlations disappear and the system can be described in its so-called normal phase where the only recollection of the pairing interaction is a shift of the effective ground state. It is to this energy shift that the phenomenological correction to the excitation energy—as introduced in the classical analytical models of the nuclear level density—corresponds. However, below the critical temperature, the nucleus is in the superconducting phase and the pairing effects on the thermodynamic quantities appear to be much more complex.

To complete the formalism, the second derivatives of the grand partition function Ω, with respect to the Lagrange multipliers, are to be calculated to evaluate the level density denominator. Such quantities appear to be rather complicated (see for example, Moretto, 1972), since they also depend on the derivatives of the pairing gap Δ with respect to the Lagrange multipliers. However, it can be seen (e.g. Ignatyuk, 1985) that in the superfluid model, the pairing effects do not drastically affect the T-dependence of the determinant factor. In such conditions, and taking into account the minor role played by the determinant factor on the total level density, we have assumed that, in the scope of the present work, the determinant could be approximated by its expression (66) in the normal as well as in the superconducting phases.

Since the pairing interaction is assumed to occur between identical nucleons only, the above expressions can easily be generalized for a two-component system. The behaviour of a paired system characterized by a fixed angular momentum can also be described in the same formalism (Sano and Wakai, 1972; Moretto, 1972, 1974). In such models, the BCS parameters, and in particular the energy gap, are functions of both the excitation energy and the angular momentum. Unfortunately those models lead to formulae which are in general very complicated, even numerically unless numerous, and rather crude approximations, are introduced. For this reason, the spin-dependent level density is generally estimated from the total level density using the classical assumption that the nucleus spin projections on the quantization axis have a Gaussian distribution with an average value of zero and a mean square deviation σ given in the BCS approximation by

$$\sigma^2 = \frac{1}{2}\sum_k m_k^2 \operatorname{sech}^2 \frac{1}{2}\beta E_k \tag{126}$$

However, it has been shown in Chapter II.3, that the Gaussian approximation is valid only if many nucleons are excited, which is not the case for relatively low excitation energies and more particularly, in the superconducting phase. In the same respect, the Gaussian approximation predicts a finite level density for any J value, whereas the coupling of a finite number of nucleons

with finite spin must lead to a level density of zero for angular momenta above some maximum value (the Yrast level).

Such shortcomings could be avoided by using, in particular, a BCS Hamiltonian in which the angular momentum is described by means of the Lagrange multiplier approach and where no approximation, except the approximation of small M, is made. If only low spin values are considered, the rotational corrections to the thermodynamic quantities are small enough to allow an approach to be used, similar to the one adopted in Chapter II.3. As long as the Lagrange multiplier γ, corresponding to the spin projection M is small, it is a good approximation to expand the thermodynamic quantities in power of γ. Under these conditions, the cut-off parameter (126) appears to play the same role as it did in absence of pairing interaction. It can be shown that the saddle point equations and the entropy can be expressed as

$$E \simeq E_0 + \frac{1}{2} f_\sigma \frac{M^2}{\sigma^2/T} \tag{127}$$

$$M \simeq \gamma\, \sigma^2 \tag{128}$$

$$S \simeq S_0 \tag{129}$$

where the subscript (0) denotes here the spin-independent quantities obtained by including the pairing interaction. Although the rotational entropy has been neglected, the correction to the rotational energy has been considered and is included in the factor f_σ. If in the normal phase the factor f_σ is given by the ratio σ'^2/σ^2 (see expression (104)), more complicated expressions should be used to describe it in the superconducting phase. However, the evaluation of f_σ will not be discussed here, since it already remains highly problematic for the simple case of a non-interacting system of Fermions.

It should be remembered that the thermodynamic functions, as given by (127)–(129), remain inadequate to describe effects associated with large angular momenta or with the correlation between the pairing interaction and the rotational motion. In particular, the pairing gap Δ is known

to be a decreasing function of the spin J because of its strong coupling to the rotational motion. For sufficiently large J, angular momentum tends to destroy pairing. Consequently, the critical temperature corresponding to the disappearance of the energy gap is also a function of the angular momentum. These high spin phenomena will not be studied in the present work.

As in the Fermi gas model, analytical expressions for the nuclear level density have been derived from the BCS formulation, but at the expense of numerous approximations, and in particular by treating the shell effects in a rather crude way. The derivation of the thermodynamic functions in an analytical form is so complicated that comparisons with numerical shell model calculations are usually used to construct a pairing correction empirically. In particular, the latest widely-used analytical form of the pairing correction has been obtained "after several guesses and subsequent comparison with model results" (Jensen and Sandberg, 1978). Therefore, it is clear that none of the currently available analytical formulae can be regarded as treating the pairing effect realistically. Such shortcomings can have significant consequences for the description of level densities, mainly at low energy. In particular, it will be shown in Section II.4.3, that the critical energy at which the normal phase follows the superconducting phase is around 8 MeV and consequently that an important amount of experimental data should be analyzed in the superfluid model. Therefore, we have tried to improve the analytical description of the superconductivity effects in the nuclear level density. Since all the information about the pairing interaction is contained in the gap parameter Δ, Section II.4.2 will be devoted to a careful study of the gap equation. More specifically, an accurate estimation of the ground-state energy gap, taking the shell effects into account, will be performed before solving the gap equation for all temperatures $T \leq T_{cr}$. New analytical expressions for the gap parameter $\Delta(T)$ will be derived. We will then show in Section II.4.3 how the pairing effect can be introduced in the thermodynamic functions as well as in the spin cut-off parameter in a very simple and accurate way without adversely affecting the quantities calculated

for the non-interacting Fermions system (and which already include the shell effects). Since the superconductivity theory formalism describes the behaviour of pairs of particles, the calculations will be first performed for doubly even nuclei. A generalization to odd-mass and doubly odd nuclei will follow. We will finally compare in Section II.4.4 our analytical formula with shell model calculations including the BCS approximation to the pairing interaction.

II.4.2 The gap equation

Before estimating the gap parameter, it should be stressed that the gap equation, as given by expression (122), has been derived under the classical assumption that the pairing strength G is a constant within an energy interval $2\varepsilon_\Lambda$ around the Fermi energy and equal to zero otherwise. A more general description of the pairing interaction can be found by considering a gap matrix $G_{kk'}$, the elements of which can be calculated for a given pairing interaction, such as a δ-interaction or a finite range Gaussian interaction. Although the diagonal matrix elements for realistic forces are systematically larger than the non-diagonal ones and, consequently, the configuration mixing is weaker than in the constant-G model, the constant-G approximation is known to give fairly good results, provided that the correct prescription to estimate the effective pairing strength is used (Moretto and Kataria, 1974; Tondeur, 1979). Moreover, it has been shown (Ignatyuk, 1985) that the principal characteristics of the thermodynamic quantities in the superconducting phase do not depend on the assumptions made regarding the form of the matrix elements of the interaction. The change in its functional dependence, in the energy representation, essentially leads to a renormalization of the constants determining the interrelationship between the critical temperature and the correlation characteristics of the ground-state of the system. Comparisons of nuclear level density calculations making use of different pairing models (the constant-G approximation and the pairing matrix approach on grounds of a δ-interaction model) have confirmed the weak influence of the adopted model on the thermodynamic functions (Arnould and Tondeur, 1981). For these reasons, we have adopted in the present work the constant-G approximation to describe the pairing interaction. In addition, it will be seen that this widely used model allows us to express the different thermodynamic quantities of relevance in the nuclear level density calculations in a very simple analytical way.

(i) The ground-state energy gap and the critical temperature

At zero temperature, the gap equation (122) can be written as

$$\frac{2}{G} = \sum_k \frac{1}{\sqrt{\varepsilon_k - \mu)^2 + \Delta_0^2}} \tag{130}$$

The main contributions to the sum (130) come from the states in the vicinity of the Fermi level. In the constant pairing force approximation, the pairing force is assumed to be non-negligible only in a certain energy range $2\varepsilon_\Lambda$ (commonly referred to as the Λ-shell and ε_Λ as the energy cut-off) around the Fermi energy.† The sum occurring in equation (130) must be restricted to a finite energy interval, since the contribution of distant levels would diverge logarithmically. This divergence results from the assumption of a sharply local pair field and would be removed by taking the finite range of the effective interactions into account. Therefore, the energy cut-off is directly related to the prescription used for the constant G-value. In spite of the simplifying assumptions made in the constant pairing force model, the gap equation can only be solved numerically. However, an approximate solution can be obtained in the continuous spectrum approximation: if the average single-particle level spacing is much smaller than the energy gap Δ_0, the summation (130) can be approximately replaced by an integration over the energy interval $[\mu - \varepsilon_\Lambda, \mu + \varepsilon_\Lambda]$. Assuming that the level density of the paired nucleons $\rho(\varepsilon)$ is constant within the Λ-shell, the ground-state energy gap can finally be expressed (e.g. Ring and Schuck, 1980) as

$$\Delta_0 = \frac{\varepsilon_\Lambda}{\sinh \frac{1}{\rho_0 G}} \tag{131}$$

where ρ_0 corresponds to the density of doubly-degenerate single-particle levels at the Fermi energy and can be related to the better known single-particle level density by $\rho_0 = \frac{1}{2} g(\mu)$ or to the a-parameter (which is known to be an expression of the single-particle level density at the Fermi

† It is of interest to note that the restriction of the pairing to the vicinity of the Fermi level is also the reason for treating the neutrons and protons separately (at least for heavy nuclei). For heavy nuclei, the neutron excess is important enough to prevent the neutron and proton levels close to the Fermi energy to overlap, so that the neutron-proton correlation is generally neglected.

energy) by $\rho_0 \sim \frac{3}{\pi^2} a$. This last relation is correct when it concerns the gross behaviour of the quantities considered. However, it is of great importance to stress that if shell corrections to the a-parameter are taken into account, this last relation holds only if the quantities ρ_0 and a (as given by expression (33)) correspond to the same definition, i.e. to the same averaged value, of the single-particle level density at the Fermi energy. On the one hand, the a-parameter has been derived by averaging the single-particle level density around the Fermi energy with the weight-function $F(\varepsilon/T)$. The larger the temperature, the wider the energy range contributing to the averaging, and consequently the less significant the shell effects become. The oscillating contribution to the level density progressively dies away when larger temperatures are considered. This effect is reflected in the T-dependence of the a-parameter.

On the other hand, the density distribution $\rho(\varepsilon)$ in expression (130) is averaged around the Fermi energy by the slowly decreasing function $W_0(\varepsilon, \Delta_0) = \frac{1}{\sqrt{\varepsilon^2+\Delta_0^2}}$. In this case, the width of the weight-function W_0 is a function of the gap parameter Δ_0 instead of the temperature. The shell contribution to the quantity ρ_0 can consequently be related to the shell correction to the a-parameter, provided both weight-functions, $F(\beta\varepsilon)$ and $W_0(\varepsilon, \Delta_0)$, have the same width. If we define an equivalent temperature T_{Δ_0} such that this condition is fulfilled (it can be shown that $T_{\Delta_0} \simeq \frac{\sqrt{3}}{\sigma_a}\Delta_0$), we can write

$$\rho_0 = \frac{1}{2}\, g(\mu) = \frac{1}{2}\frac{6}{\pi^2}\, a(T = T_{\Delta_0}) \tag{132}$$

$$\simeq \frac{3}{\pi^2}\left[\tilde{a} + \frac{\gamma^2 \delta W_1}{(1+\gamma^2 T_{\Delta_0}^2)^2}\right] \tag{133}$$

Since T_{Δ_0} is proportional to the gap Δ_0, introducing (133) in expression (131) leads to an implicit equation to be solved to determine the gap parameter. However, the factor $\gamma^2 T_{\Delta_0}^2$ is small and could be replaced to a good approximation by its smooth contribution only, so that further simplifications can be made. Such calculations will be developed in Section II.5.1 when dealing with comparison to experimental pairing energies.

Despite the numerous approximations made, it appears that the semi-classical approach developed in Chapter II.2 enables us to introduce the shell effects in the gap equation in a very simple way. This new approximation to the gap parameter is of great interest since it is well known that the experimental pairing energies show significant local variations correlated with the shell structure. Many studies have been devoted to the prediction of the pairing energies and attempts have been made to derive analytical formulae to reproduce the experimental data (Nemirovsky and Adamchuk, 1962; Kennedy, 1966; Zeldes et al., 1967; Madland and Nix, 1988). Although shell effects are known to play an important role, none of the previous studies have been able to take the shell corrections into account analytically. Despite the oversimplified treatment of the shell corrections, we will show (see Section II.5.1) that expressions (131) and (133) can significantly improve the fit to experimental pairing gaps compared with the above-mentioned studies. As regards the nuclear level density, the introduction of shell effects in the pairing gap is of great importance. The thermodynamic quantities appear to be highly sensitive to the adopted value of the pairing gap Δ_0 at low energy, so that an accurate knowledge of Δ_0 is strongly desired for reliable prediction of the level density. In most of the level density models which do not solve the BCS equations completely, use is made of a smooth, analytical approximation to Δ_0. This procedure is fairly unrealistic when nuclei with a number of nucleons close to a magic number ($\Delta_0 = 0$ for a magic number) are considered. The shell correction to the pairing energy also plays an important role in droplet-type nuclear mass models (Möller et al., 1988), so that expression (131) using the shell correction (133) can be expected to improve the description of the pairing energy contributing to the total nuclear mass.

The critical temperature at which the pairing correlation disappears—i.e. such that $\Delta(T_{cr}) = 0$—can be extracted in the same way, making use of the same approximations. Basically, it can be related to the ground-state energy gap by the BCS formula

$$\frac{2\,\Delta_0}{T_{cr}} = 3.50 \tag{134}$$

However, some deviations from the above classical formula as a result of the shell structure of the nucleus can be expected. The critical temperature is proportional to the single-particle density averaged around the Fermi energy by the weight-function $W_c(\varepsilon, T_{cr}) = \frac{2T_{cr}}{\varepsilon} \tanh \frac{\varepsilon}{2T_{cr}}$. The shell effects on both the gap parameter Δ_0 and the critical energy T_{cr} would be identical, provided that the two weight-functions W_0 and W_c have accurately the same width. Since grossly, Δ_0 is related to T_{cr} by expression (134), it can be shown that the function W_0 is more centred on the Fermi energy than the function W_c. Consequently, shell effects are more significant on Δ_0 than they are on T_{cr} and the ratio Δ_0/T_{cr} can be expected to deviate from the classical BCS value of 1.75 in correlation with the shell structure of the nucleus. Yet for the sake of simplicity, we will neglect the shell effects on the ratio Δ_0/T_{cr} and consider expression (134) only.

(ii) The temperature-dependent gap parameter

If above the critical temperature the gap energy is identically zero, to find the gap parameter $\Delta(T)$ at any temperature $T \leq T_{cr}$, the gap equation (122) must be solved. In the continuous spectrum approximation, the reduced gap $\delta(T) = \Delta(T)/\Delta_0$ is known to be a universal function of the reduced temperature $\tau = T/T_{cr}$ (Rickayzen, 1965). However, no solutions of the T-dependent gap equation have been derived in an analytical form so far, even if rather crude approximations to the dependence $\Delta(T)$ have been proposed in the vicinity of the critical temperature or in the region of low temperatures $T << \Delta$ (e.g. Ignatyuk, 1985). For that reason, the gap equation is generally solved numerically.

Since the temperature dependence of the gap parameter is of fundamental importance to describe the nuclear statistical properties in the superconducting phase, we have reinvestigated the gap equation in the continuous spectrum approximation. To simplify the gap equation, we have

made use of the approximation

$$\frac{1}{E}\tanh\frac{E}{2T} \simeq \frac{1}{\sqrt{E^2+p^2}} \tag{135}$$

where the quasi-particle energy E is given by expression (118). Such an approximation is fairly good if the temperature-dependent parameter p is chosen such that the exact function is reproduced correctly in the region where it gives rise to its maximum contribution to the gap equation, i.e. in the vicinity of Fermi energy. Therefore, the parameter p can be derived from the condition that both functions are identical at the energy $E = \Delta(T)$:

$$p^2 = \frac{\Delta^2}{\sinh^2\dfrac{\Delta}{2T}} \tag{136}$$

The approximations corresponding to $p = 0$ or $p = 1$ that would come more naturally to mind differ significantly from that adopted here. As a matter of fact, no good results can be expected if the exact function (135) is not correctly fitted at the Fermi energy.

If we introduce the approximate function in the gap equation, we are left with an expression similar to equation (130). A simple integration leads in the continuous spectrum approximation to the relation

$$\Delta^2 + p^2 = \Delta_0^2 \tag{137}$$

to which correspond the boundary conditions

$$\begin{aligned} p^2(T=0) &= 0 \\ p^2(T=T_{cr}) &= \Delta_0^2 \end{aligned} \tag{138}$$

and, in the given model, the critical temperature is related to the ground-state gap parameter by the expression

$$T_{cr} = \frac{1}{2}\Delta_0 \tag{139}$$

To satisfy the conditions (136)–(139), the reduced gap parameter $\delta(T)$ can be determined for each reduced temperature τ by the implicit relation

$$\frac{\delta^2}{\sinh^2\dfrac{\delta}{\tau}} = 1 - \delta^2 \tag{140}$$

or equivalently

$$\frac{\tau}{2} \ln \frac{1+\delta}{1-\delta} = \delta \tag{141}$$

This implicit equation has been solved for all temperatures τ in the range $0 < \tau < 1$ and is compared in Fig. 21 to the exact universal solution obtained numerically (Mühlschegel, 1959). Expressions (140) or (141) appear to reproduce the exact solution within less than 0.2% over all the temperature range. Even if expressions (140) or (141) lead to remarkably good results, it is still necessary to make a numerical evaluation of the temperature dependence of $\delta(T)$. A simplification of these implicit equations can be found if use is made of the approximation

$$\tau = \frac{2\delta}{\ln\left(\frac{1+\delta}{1-\delta}\right)} \simeq (1-\delta^2)^{1/m} \tag{142}$$

where m is determined to fit τ in relation (142).

Finally we can express the temperature dependence of the gap parameter by the very simple approximation

$$\Delta(T) = \Delta_0 \left[1 - \left(\frac{T}{T_{cr}}\right)^m\right]^{1/2} \tag{143}$$

Since $\delta(\tau)$ is a universal function, the parameter m can be determined univoquely without regard of the different quantities such as ε_Λ, G or ρ_0. An excellent agreement between expression (143) and the exact function (see Fig. 21) is found for the value $m = 3.23$ which makes it possible to approximate $\Delta(T)/\Delta_0$ in the whole superconducting phase within 2%. It should be stressed at this point that the very simple approximation (143) corresponds to the first analytical approximation which is able to reproduce the T-dependence of the gap parameter in the whole superconducting phase ($0 \leq T \leq T_{cr}$). Moreover, this approximation is so good that it can be applied to nuclear level density calculations with great confidence.

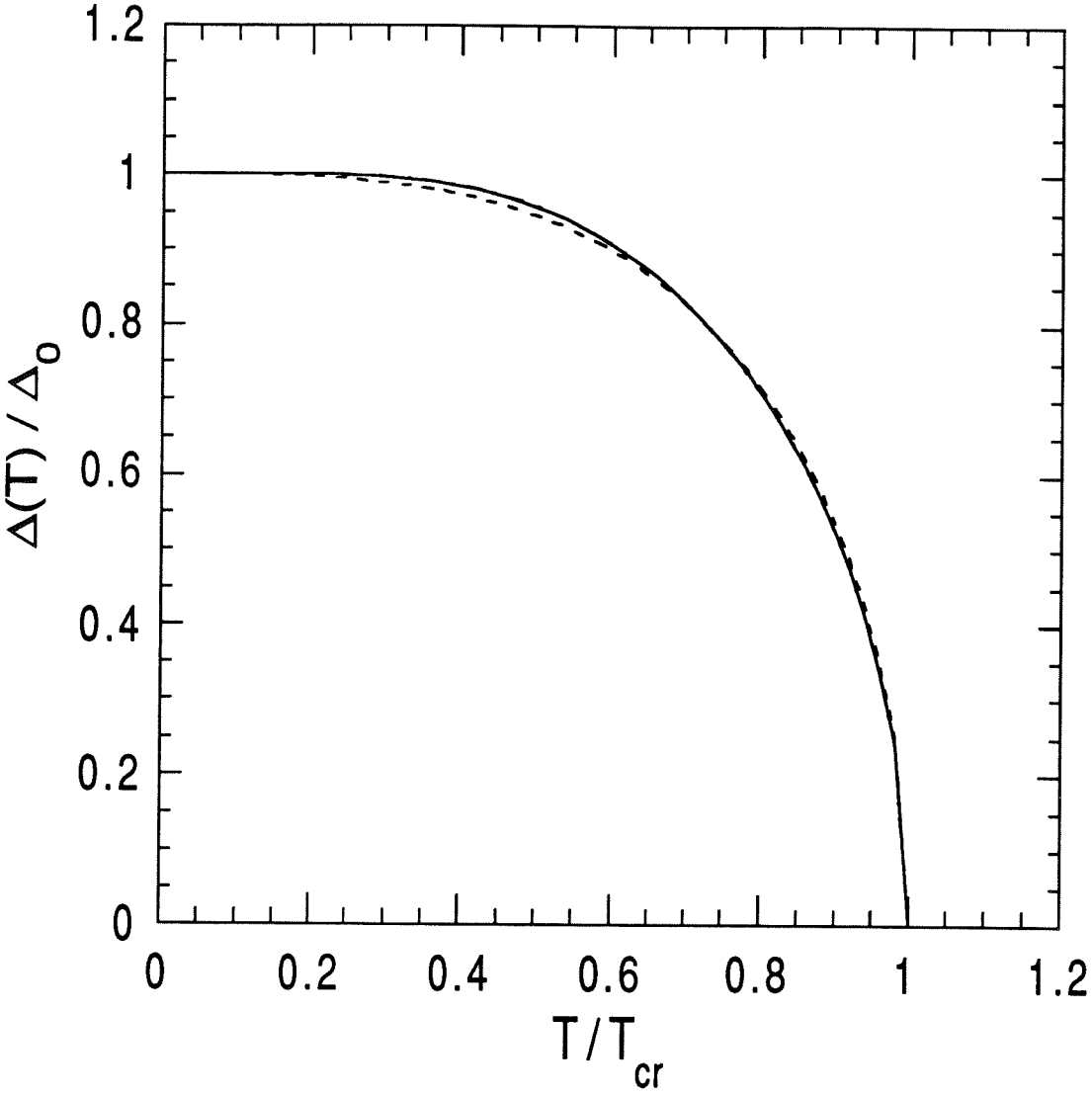

Figure 21. Ratio $\Delta(T)/\Delta_0$ as a function of the reduced temperature T/T_{cr}. The full curve corresponds to the exact numerical evaluation (Mühlschlegel, 1959) and is compared with the approximations (141) (dotted line) and (143) (dashed line). The approximation (141) is so good that the dotted line cannot be distinguished from the full curve.

II.4.3 Determination of the thermodynamic quantities

It has been shown in Section II.4.1 that the effects of the pairing interaction on the statistical properties of the nucleus can be considered in a fairly simple way by means of the BCS theory. The problem reduces to the use of the BCS quasi-particles as the basic non-interacting Fermions. Since in the BCS theory of superconductivity concerns systems of pairs of particles, the thermodynamic quantities calculated in the next section will refer to doubly even nuclei. The generalization to the case of odd-mass and doubly odd nuclei will be discussed in part B of this section.

A1. Evaluation of the entropy

In the statistical model of nuclear level density, the entropy (125) of the system at a temperature T can be expressed as

$$S(T) = 2 \ln 2 \sum_k F(E_k/T) \tag{144}$$

where the function $F(x)$ has already been defined in Section II.2.3 (see expression (35)) and the quasi-particle energy E_k is given by (118). An interesting property of the function F is emphasized by its Gaussian-like shape (see Fig. 2) and can mathematically be expressed by the relation

$$F(\sqrt{x^2 + y^2}) \simeq F(x/\omega_F)\, F(y) \tag{145}$$

Had the function $F(x)$ been a Gaussian, it would have been trivial to prove the above equality. Since this is not the case, a correction factor ω_F to the width of the function F must be introduced. The factor ω_F can be determined in order for the left and right terms of expression (145) to cover the same area with respect to the x-axis. This condition leads to the relation

$$\omega_F(y) = \frac{\int_0^\infty F(\sqrt{x^2 + y^2})dx}{F(y) \int_0^\infty F(x)dx} \tag{146}$$

$$= \frac{6 \ln 2}{\pi^2} \frac{1}{F(y)} \int_0^\infty F(\sqrt{x^2 + y^2})dx \tag{147}$$

This dependence of the width ω_F with variations of the y variable is shown in Fig. 22. Also displayed in Fig. 22 is an arbitrary approximation to expression (147) in the analytical form:

$$\omega_F(y) \simeq 1 + u_1 y \left(1 - \mathrm{e}^{-u_2 y}\right) \tag{148}$$

where a fit to the numerical evaluation leads to the choice of the constants $u_1 \simeq 0.083$ and $u_2 \simeq 0.5$.

The function $F(\sqrt{x^2 + y^2})$ and its approximation (145) are shown in Fig. 23 for 4 values of y, namely y =1, 2, 3 and 4. As can be observed, the approximation is remarkably good over the whole range considered. For $y = 0$, the approximation is obviously exact, while for increasing value of y, the approximation tends to become slightly less accurate, even if it remains highly reliable. However, the absolute amplitude of the function decreases exponentially with y, so that the small discrepancies arising when very high y-values are considered ($y \geq 10$), are of no consequence for our practical use. If we make use of these approximations in the entropy expression (144), we can write, in a trivial way:

$$S(T) = 2 \ln 2 \sum_k F\left[\tfrac{1}{T}\sqrt{(\varepsilon_k - \mu)^2 + \Delta^2}\right] \tag{149}$$

$$\simeq 2 \ln 2 \; F(\Delta/T) \sum_k F\left[\tfrac{1}{\omega_F T}(\varepsilon_k - \mu)\right] \tag{150}$$

$$\simeq F(\Delta/T) \; S_0(\omega_F T) \tag{151}$$

where S_0 is the entropy of the non-interacting Fermions system ($\Delta \equiv 0$) as derived in Section II.2.3, and $\omega_F = \omega_F(\Delta/T)$ is a function of the pairing gap given by expressions (147) or (148) with $y = \Delta/T$.

Expression (151) shows that the pairing interaction can easily be introduced in the entropy expression. It is of great interest to point out that this formula has been derived independently of the model adopted to describe the non-interacting system. Therefore, any analytical expression for the entropy S_0 can be substituted in expression (151). Moreover, a high degree of accuracy can be expected since the approximations made are very reliable.

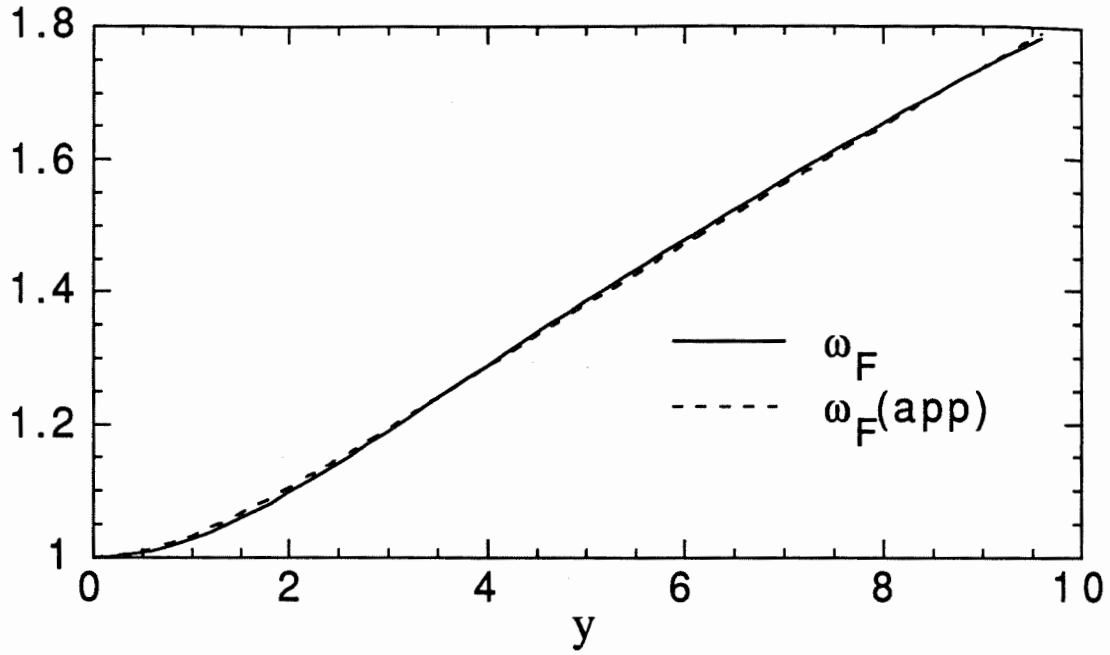

Figure 22. Correction $\omega_F(y)$ to the width of the F-function as given by expression (147) (full line) and by the analytical approximation (148) (dashed line).

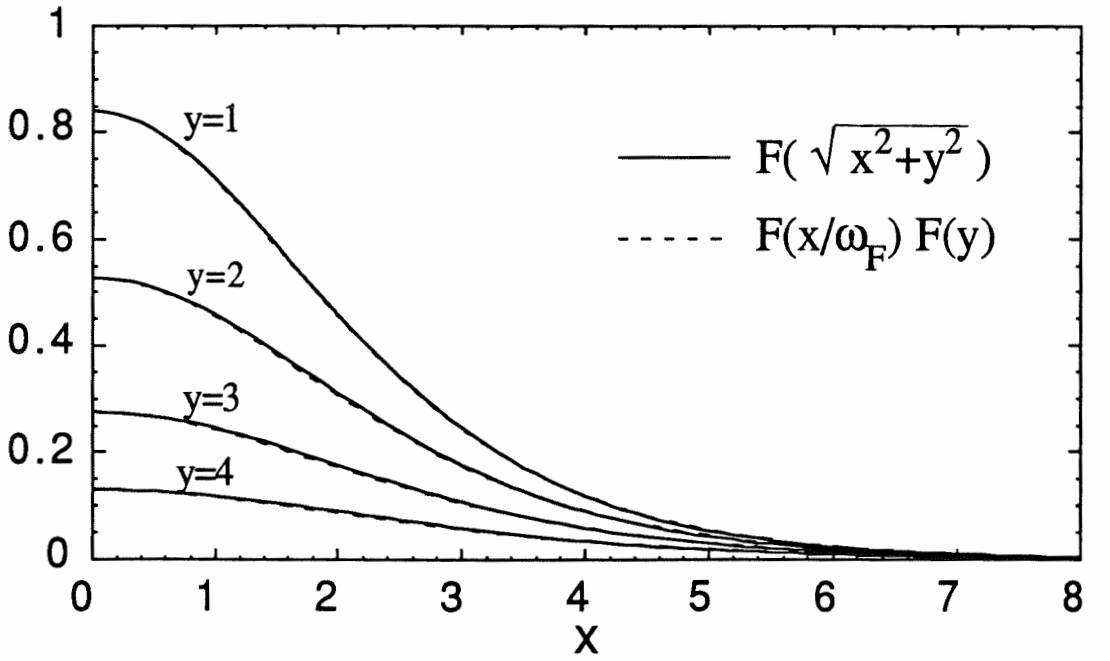

Figure 23. Comparison of the function $F(\sqrt{x^2+y^2})$ (full line) with the approximation $F(x/\omega_F)F(y)$ (dashed line) as a function of x and for 4 values of the parameter y. The approximation is so good that the curves can hardly be distinguished

As described by expression (151), the effects of the pairing forces on the entropy of the system appear to affect its amplitude as well as its temperature scaling relative to the non-interacting system. For temperatures $T \geq T_{cr}$, $\Delta = 0$ and thus, $F(\Delta/T_{cr}) = 1$ and $\omega_F = 1$, so that the normal regime is reestablished in its exact form. For decreasing temperatures, the energy gap $\Delta(T)$ increases and greatly reduces the entropy amplitude by the factor $F(\Delta/T)$, always lower than unity as could have been predicted from the second principle of thermodynamics. For temperatures $T \ll \Delta$, the function F vanishes exponentially, and with it the entropy.

A second pairing effect can be found in the ω_F-factor. At a temperature $T \leq T_{cr}$, the entropy of the paired system is related to the entropy of the non-interacting system evaluated at a higher temperature $\omega_F T \geq T$. However, the equivalent temperature of the non-interacting system in a state characterized by the same entropy as the paired system is globally lower (because of the predominant reduction of the amplitude by the factor F). This modification of the temperature scale shows that the emergence of a pairing force tends slightly to broaden the single-particle energy interval contributing to the statistical properties of the system. As a matter of fact, for $\Delta \neq 0$, the entropy depends on the single-particle energy distribution in an interval of width $\sim \omega_F T$ around the Fermi energy (which should be compared to the interval of width $\sim T$ in absence of pairing interaction). This temperature scaling factor has a non-negligible influence on the entropy S_0 at low temperatures, especially when the nucleus reveals important shell effects. Such an effect remains, however, minor in comparison with the amplitude reduction resulting from the F-factor.

A2. Evaluation of the excitation energy

Compared with the entropy evaluation, the determination of the excitation energy in the superconducting phase is rather complicated and requires a careful study. The excitation energy can be derived from the total energy of the system by subtracting the ground-state energy (corresponding

to $T = 0$) and can be expressed by the relation

$$U = \sum_k \varepsilon_k(\varepsilon_k - \mu)\left[\frac{1}{E_k^0} - \frac{1}{E_k}\tanh\frac{E_k}{2T}\right] + \frac{\Delta_0^2 - \Delta^2}{G} \tag{152}$$

where the quasi-particle excitation energy E_k is given by (118) and at zero temperature by

$$E_k^0 = \sqrt{(\varepsilon_k - \mu)^2 + \Delta_0^2} \tag{153}$$

It is of importance to recall here that the summation (152) is carried over the energy interval $|\varepsilon_k - \mu| \leq \varepsilon_\Lambda$ and runs only over half the configuration space. Each index k corresponds to the state $\{k, \bar{k}\}$ where $\bar{k}$ is the conjugate state of k, connected to k by the operation of time reversal.

To simplify expression (152), use is made of the traditional assumption

$$\Delta \leq \Delta_0 \ll \varepsilon_\Lambda \tag{154}$$

and of the continuous spectrum approximation, in which the level density available to the paired nucleons $\rho(\varepsilon) = \frac{1}{2}g(\varepsilon)$ is assumed to remain constant. Under these conditions, expression (152) can be reduced to

$$U(T) \simeq \frac{1}{2}T\,S(T) + \frac{1}{2}\rho_0\Delta_0^2\left(1 - \frac{\Delta^2}{\Delta_0^2}\right) \tag{155}$$

and using the approximation (151) to the entropy of the interacting Fermion system, we finally obtain

$$U(T) \simeq \frac{1}{\omega_F}F(\Delta/T)\,U_0(\omega_F T) + \frac{1}{2}\rho_0\left(\Delta_0^2 - \Delta^2\right) \tag{156}$$

where $U_0(T)$ is the excitation energy of the non-interacting Fermion system as given in Section II.2.3. As can be seen, the expression of the effective excitation energy obtained on the basis of the BCS model differs considerably from the simple description derived from the Fermi gas model. Above the critical temperature, $\Delta = 0$ and the classical BCS approximation to the excitation energy in the normal phase is obtained (e.g. Sano and Yamasaki, 1963)

$$U_N(T) = U_0(T) + \frac{1}{4}g_0\Delta_0^2 \tag{157}$$

$$= U_0(T) + \frac{3}{2\pi^2}\tilde{a}\Delta_0^2 \tag{158}$$

where g_0 is the single-particle level density at the Fermi energy averaged, this time, on an energy interval large enough (of the order of ε_Λ) to assume that the oscillating contribution to g_0 is negligible (see Section II.4.2). The pairing correlations in the normal phase are consequently reduced to a simple energy shift equal to $E_p = \frac{3}{2\pi^2}\tilde{a}\Delta_0^2$, which reflects the lowering of the ground-state energy resulting from the pairing interaction. On the one hand, it appears that the phenomenological energy shift adopted in the classical analytical models of nuclear level densities is also predicted by the BCS theory, at least for temperatures $T > T_{cr}$. On the other hand, the phenomenological energy shift generally used differs significantly from the BCS energy E_p. The analytical models generally assume that the ground-states of the even and odd mass nuclei are shifted by an amount similar to the corresponding odd-even shift in the semi-empirical formula. Following this approach, the energy correction is linear in Δ_0, rather than quadratic as suggested by expression (158).

The transition energy U_{cr}, corresponding to the critical energy T_{cr}, is given by

$$U_{cr} = U_0(T_{cr}) + \frac{3}{2\pi^2}\tilde{a}\Delta_0^2 \tag{159}$$

Expression (159) is of particular interest because it enables us to estimate to first approximation the critical energy by the relation

$$U_{cr} = \tilde{a}T_{cr}^2 + \frac{3}{2\pi^2}\tilde{a}\Delta_0^2 \tag{160}$$

If we use the BCS formula $\Delta_0 = 1.75\,T_{cr}$, the empirical level density parameter $a \simeq A/8$ and the empirical gap parameter $\Delta_0 = \frac{12}{\sqrt{A}}$MeV, we find a critical energy equal to 8.5 MeV, which appears to be close to the neutron separation energy S_n. Therefore, it is of importance to note that comparisons of theoretical level densities with experimental data, such as the neutron resonance spacings or the cumulative number of observed low-lying levels, should be made in the superfluid model and not in the oversimplified shifted Fermi gas approach. As shown by expression (156), the pairing effects on the excitation energy in the superconducting phase cannot be reduced to a

simple energy shift. Similar characteristics to those already discussed for the entropy expression (151) can be found in the energy relation (156) for temperatures $T \leq T_{cr}$.

A3. Evaluation of the spin cut-off parameter

Adopting a method very similar to the one used to derive the effect of pairing interaction on the entropy, we can rewrite the spin cut-off parameter (126) as

$$\sigma^2(T) = \frac{1}{2} \sum_k m_k^2 \, h(E_k/T) \tag{161}$$

where the function $h(x)$ has been defined in Section II.3.3 (see expression (91)). It has also been shown (see expression (92)) that an excellent approximation to this function could be found in the relation $h(x) \simeq F(\sigma_a x)$. We can consequently generalize the results obtained for the function $F(x)$ to the function $h(x)$:

$$h(\sqrt{x^2 + y^2}) \simeq h(x/\omega_h) \, h(y) \tag{162}$$

where, similarly to expressions (145)–(148), we define the width ω_h by

$$\omega_h(y) = \frac{\displaystyle\int_0^\infty h(\sqrt{x^2 + y^2})dx}{h(y) \displaystyle\int_0^\infty h(x)dx} \tag{163}$$

$$= \frac{1}{2h(y)} \int_0^\infty h(\sqrt{x^2 + y^2})dx \tag{164}$$

The function ω_h is displayed in Fig. 24. A fit to expression (164) can be found in the analytical expression

$$\omega_h(y) \simeq 1 + v_1 y \left(1 - \mathrm{e}^{-v_2 y}\right) \tag{165}$$

with the numerical constants $v_1 \simeq 0.11$ and $v_2 \simeq 0.5$ (see Fig. 24). The function $h(\sqrt{x^2 + y^2})$ and its approximation (162) are shown in Fig. 25 for the 4 values of y: y =1, 2, 3 and 4. As can be seen, the approximation is also remarkably good in the whole range considered.

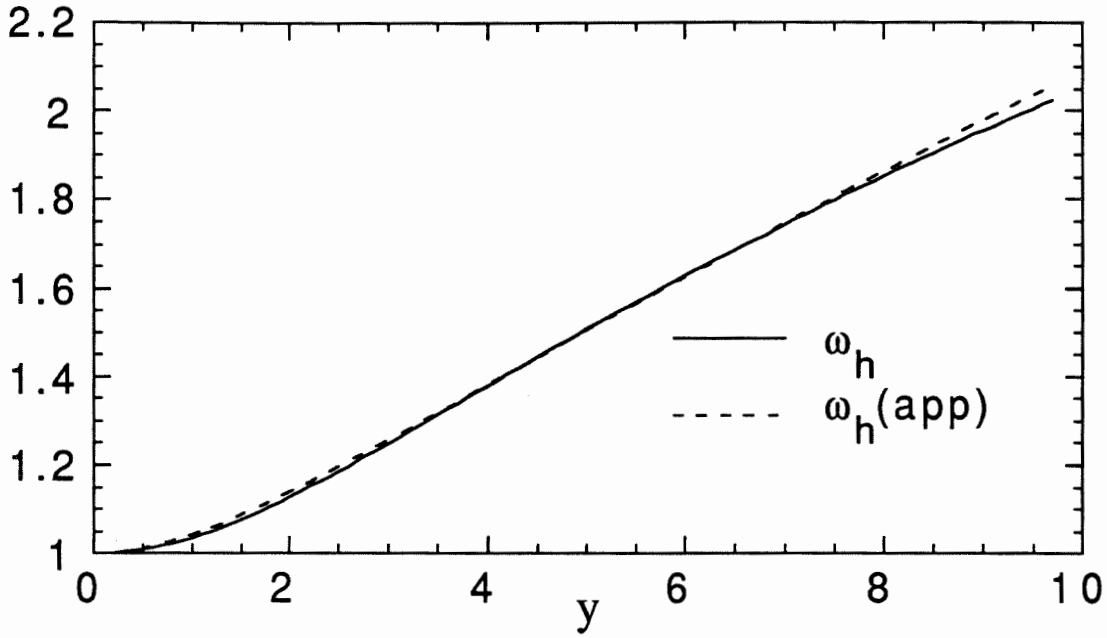

Figure 24. Correction $\omega_h(y)$ to the width of the h-function as given by expression (164) (full line) and by the analytical approximation (165) (dashed line).

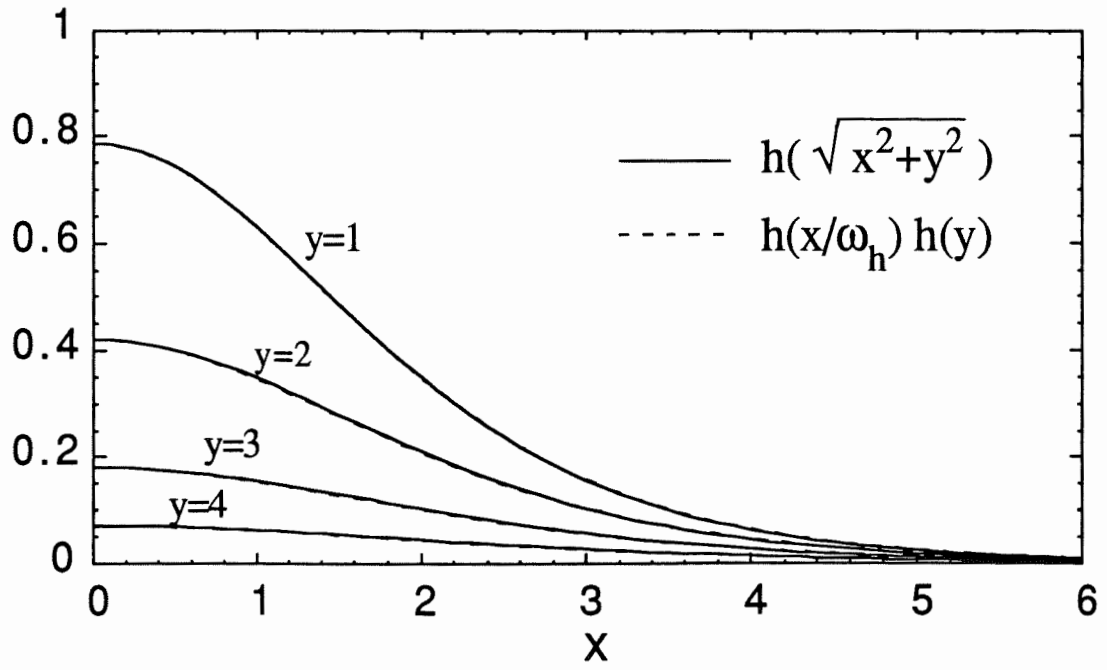

Figure 25. Comparison of the function $h(\sqrt{x^2+y^2})$ (full line) with the approximation $h(x/\omega_h)h(y)$ (dashed line) as a function of x and for 4 values of the parameter y.

The spin cut-off parameter can finally be written as

$$\sigma^2(T) = \frac{1}{2} \sum_k m_k^2 \; h\left[\tfrac{1}{T}\sqrt{(\varepsilon_k - \mu)^2 + \Delta^2}\right] \tag{166}$$

$$\simeq \frac{1}{2}\, h\,(\Delta/T) \sum_k m_k^2 \; h\left[\tfrac{1}{\omega_h T}(\varepsilon_k - \mu)\right] \tag{167}$$

$$\simeq h(\Delta/T)\; \sigma_0^2(\omega_h T) \tag{168}$$

where $\sigma_0^2(T)$ is the spin cut-off parameter of the non-interacting Fermions system. In particular, in the normal phase, $\Delta = 0$ and thus $h = 1$ and $\omega_h = 1$, so that the pairing effects fade away and the normal regime as derived in Chapter II.3 is recovered. For temperatures $T < T_{cr}$, the spin cut-off parameter and consequently the moment of inertia $\frac{\mathcal{I}}{\hbar^2} = \frac{1}{T}\sigma^2$ appear to be greatly reduced by the pair correlations. The higher the pairing gap Δ, the smaller σ^2 becomes. As already emphasized, the fact that the moments of inertia are found to be appreciably smaller than their rigid body values is generally attributed to pair correlations. In the model developed here, the reduction factor resulting from the pairing correlations is given by $h(\Delta/T)$ which tends exponentially to zero when the temperature vanishes. The strong dependence of the moment of inertia on the pair correlation parameter Δ emphasizes the significant coupling between Δ and the rotational motion.

B. Generalization to odd-mass and doubly odd nuclei

The calculations performed in the preceding section concerns the evaluation of the thermodynamic quantities of even-even nuclei only. When dealing with odd-mass and doubly odd nuclei, the so-called blocking effect has to be taken into account. Following the Pauli principle, the unpaired particle blocks the level it occupies and prevents the level from participating in the scattering process of nucleons caused by the pairing correlations. As in the case of an even nucleon number, blocking is completely ignored in all nuclear excited states. It is generally assumed that the odd nucleon does not significantly affect the parameters of the nucleus above the ground-state (it gets "lost" among other excited nucleons).

Yet blocking cannot be neglected in the description of the ground-state of an odd-nucleon system. In fact, the ground-state of a nucleus with the odd neutron (or proton) in a state k' (or k''), which can be assumed to be the level just above the Fermi energy, corresponds to a good approximation to the state of the neighbouring doubly-even nucleus with the excitation $E_{0k'}$ (or $E_{0k''}$) defined by the excitation energy of the quasi-particle

$$E_{0k'} = \sqrt{(\varepsilon_{k'} - \mu)^2 + \Delta_0^2} \tag{169}$$

According to the above model, the level density of an odd-N (or Z) or odd-odd nucleus at an excitation energy U is equal to the level density of the neighbouring even-even nucleus calculated at the energy $U + E_{0k'}$ (or $U + E_{0k''}$) and $U + E_{0k'} + E_{0k''}$, respectively. Such a simple procedure has been shown to reproduce satisfactorily the results derived from more sophisticated models including the blocking effects (Kennedy, 1966; Bekhami and Huizenga, 1973). In addition, we will assume that $E_{0k'} \simeq \Delta_0$. Such an approximation is known to be fairly good for nuclei far away from closed shells.

II.4.4 Comparison with numerical shell model calculations

To test the validity and the accuracy of our analytical approximation to the BCS equations, we have performed shell model calculations using the single-particle levels as already introduced in Sections II.2.4 and II.3.4. The pairing interaction has been included in the framework of the constant-G model where the prescription of Tondeur (1978) has been considered. The pairing strengths for neutrons and protons are given by the smooth empirical expressions

$$G_n = 2.25/N^{0.7}, \qquad G_p = 2.00/Z^{0.7} \tag{170}$$

The contributing levels to the BCS equations include all bound single-particle levels and bound states up to the energy $2\hbar\omega_0 \simeq 82\,A^{-1/3}\,\mathrm{MeV}$. The quantitative values adopted for the pairing strength and energy cut-off are of no importance at this stage, since no attempt is made to compare our results to experimental data. However, we have preferred to make use of an already-tested prescription to estimate the relative effect of the pairing interaction on the thermodynamic functions. The above description has been used by Tondeur (1978) to reproduce the experimental odd-even mass differences and by Arnould and Tondeur (1981) to evaluate the pairing effects on nuclear level densities. Moreover, this choice in adopting a smooth empirical expression for G enables us to take the non-negligible shell effects in the gap parameter into account. This treatment of the pairing interaction is known to be more realistic than the one making use of a smooth ground-state gap parameter.

Numerical calculations have been performed for the same nuclei, but since no superconducting phase exists for magic numbers, only the results for the three systems of particles with non-magic numbers have been displayed, i.e. the proton and neutron configurations of ^{162}Dy and the neutron system of ^{120}Sn. The analytical thermodynamic quantities $U(T)$, $a(T)$, $S(T)$, and $a_\sigma(T)$ are shown as a function of the temperature in Figs. (26)–(28) and compared with the numerical

^{120}Sn: neutrons

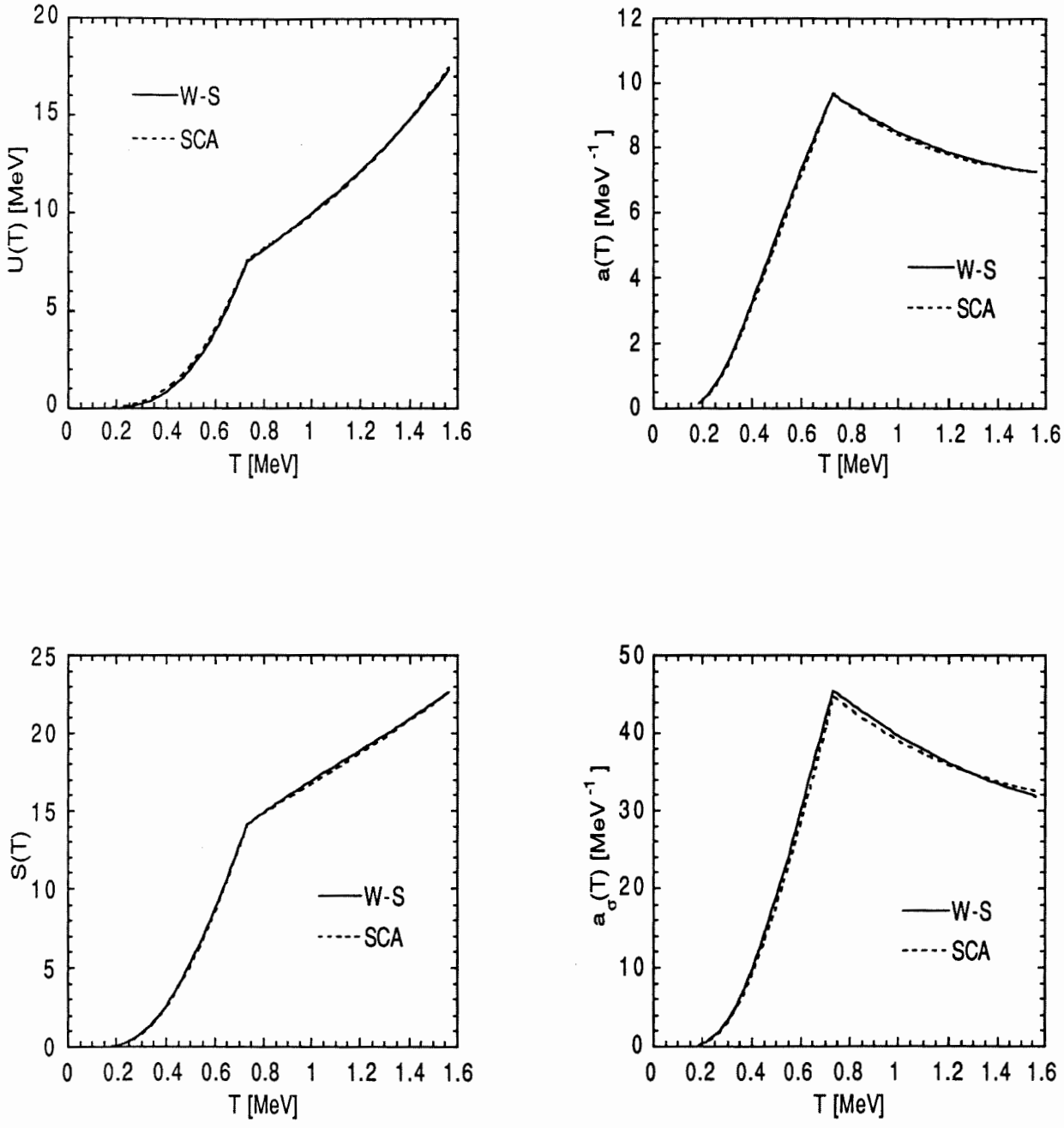

Figure 26. T-dependence of the thermodynamic quantities $U(T)$, $a(T)$, $S(T)$ and $a_\sigma(T)$ for the neutron system of ^{120}Sn. The full lines correspond to the numerical shell model calculation (W-S), while the dashed lines have been obtained with the analytical approximation (SCA). At low temperature ($T < T_{cr}$), the system is in the superconducting phase leading to an important reduction of the different quantities.

^{162}Dy: neutrons

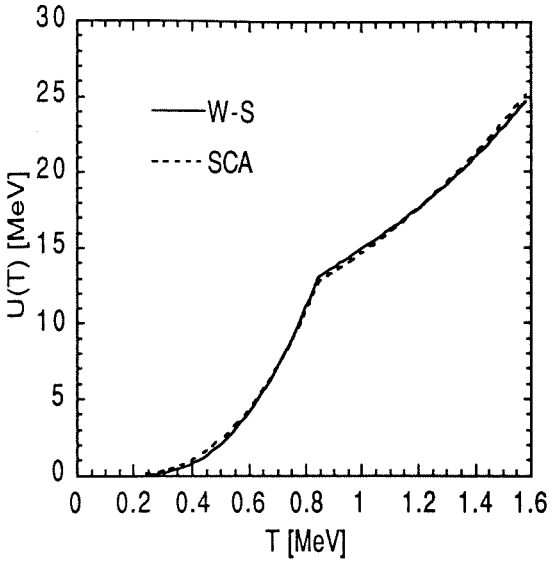

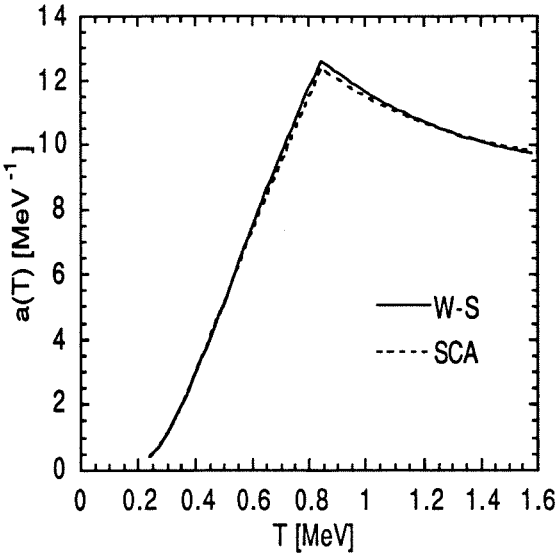

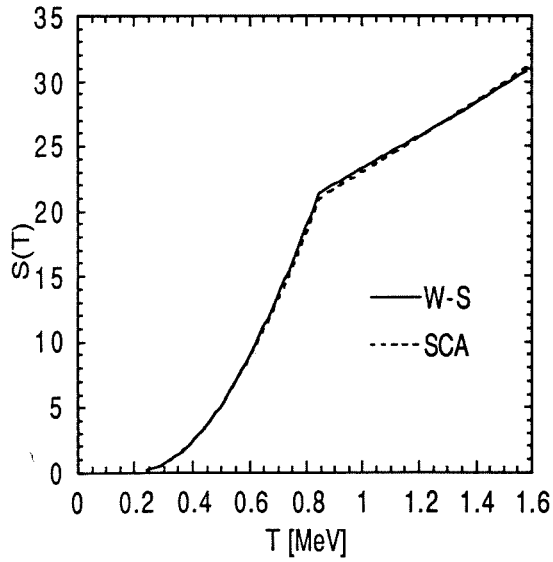

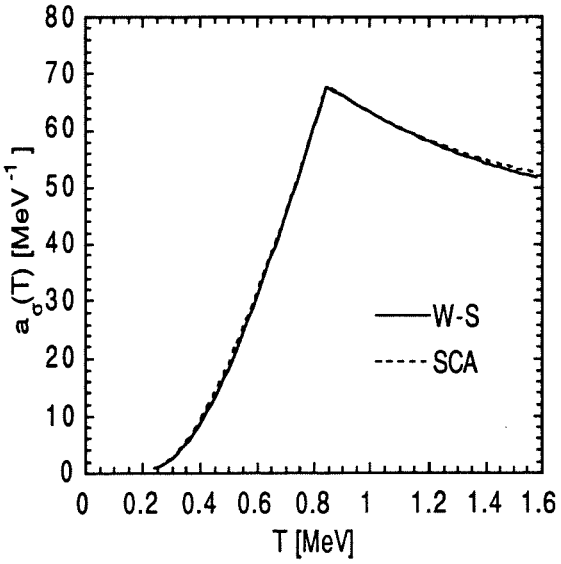

Figure 27. Same as Fig. 26 for the neutron system of ^{162}Dy.

^{162}Dy: protons

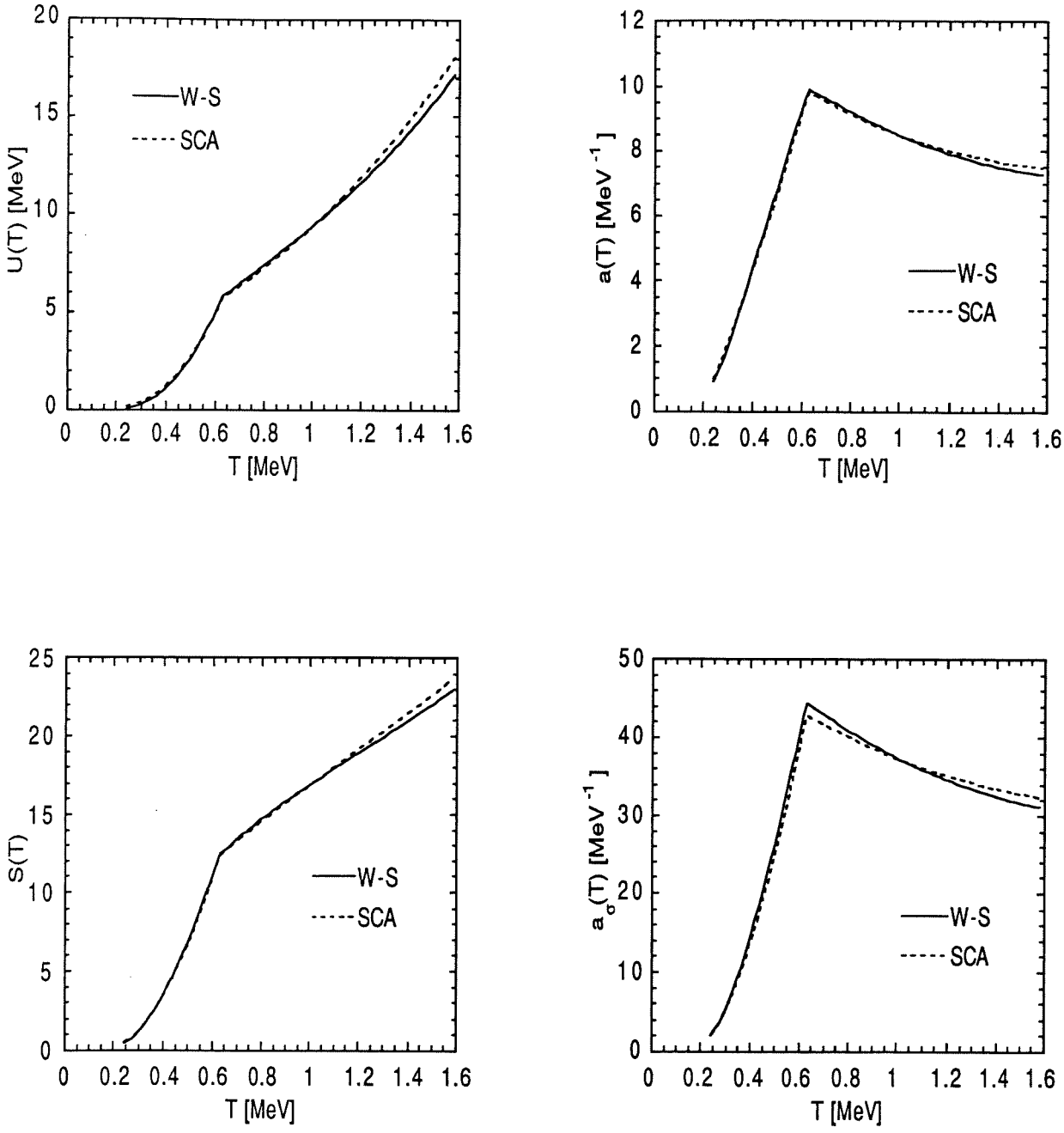

Figure 28. Same as Fig. 26 for the proton system of ^{162}Dy.

evaluation obtained with the use of the Woods-Saxon single-particle level schemes. As can be observed, the agreement in both phases—the superconducting phase for $T < T_{cr}$ and the normal phase for $T > T_{cr}$ —is remarkably good. The analytical curves have been obtained making use of expressions (151), (156) and (168) and the temperature dependence of the gap parameter has been taken from the approximate relation (143). As regards the ground-state pairing gap Δ_0, the critical temperature T_{cr} and the ground-state energy shift $E_p = \frac{1}{2}\rho_0\Delta_0^2$, the same values as the ones obtained in the numerical calculation have been adopted. These values are given in Table 4.

Table 4.

Pairing parameters derived from the numerical evaluation

	Δ_0 (MeV)	T_{cr} (MeV)	E_p (MeV)
$^{120}_{50}Sn_{70}$ neut.	1.30	0.73	3.4
$^{166}_{66}Dy_{96}$ neut.	1.45	0.84	5.5
prot.	1.12	0.63	2.2

On the one hand, it can be verified that the ratio of the pairing gap to the critical temperature remains fairly constant and equal to 1.75 as predicted by the BCS formula (134). On the other hand, the pairing energy E_p appears to be twice as important as had been suggested by expression (157). The origin of this discrepancy remains obscure but can mainly be attributed to the specific prescription used for the pairing interaction. In particular, the cut-off energy is relatively large, so that it is a rather poor approximation to assume the single-particle level density constant over the whole Λ-shell. The constant spectrum approximation can consequently not be applied to the above prescription to approximate either the gap equation or the ground-state energy shift E_p. This explains why we have adopted the computed values of these parameters in the comparison of

our analytical formula with the numerical calculations.

As regards the temperature dependence of the thermodynamic functions, it can be seen how accurate the fits to the Woods-Saxon quantities are. Below the phase transition, the uncertainties associated with the shell effects are greatly reduced for two main reasons. First, the effects of the pairing correlations become predominant, so that the reduction factors $F(\Delta/T)$ or $h(\Delta/T)$ mask the effects resulting from the shell structure. Although the shell effects in the three systems studied tend to increase the thermodynamic quantities at low energy (see the corresponding Figs. (5)–(10) without pairing effects), the reduction resulting from the pairing interaction is by far the most dominant. Second, the shell effect at a given temperature is reduced relative to the system without pairing interaction. This feature is reflected by the temperature shifts $\omega_F T$ and $\omega_h T$ in expressions (151), (156) and (168). The increase of the single-particle energy range contributing to the averaging of the thermodynamic quantities partially averages out the discrete nature of the level structure. However, this second effect is relatively minor (if not negligible) in comparison with the important amplitude reduction of the thermodynamic functions.

The approximations made to derive the pairing effects are more accurate than those made to take the shell effects into account. The reliability of the analytical formula is consequently higher with pairing than without it. For that reason, the agreement with the numerical calculations is closer in the superconducting phase than in the normal phase, where the pairing effects vanish. Above the critical temperature, the differences between both calculations are slightly more important. Yet they are identical to those shown in Figs. (5)–(10) (except for the excitation energy curves) since, in the normal phase, the only recollection of the pairing correlations results from the ground-state energy shift.

An interesting feature of the analytical approximation is that all formulae describing the thermodynamic quantities are continuous functions of the temperature and that the discontinuities

observed in the statistical quantities occurring at the phase transition result only from the discontinuity of the gap parameter $\Delta(T)$ at this temperature.

In summary, the introduction of the pairing interaction through the analytical approximation to the BCS equations—as derived in Section II.4.3—appears to be in excellent agreement with the numerical predictions. The analytical approach is not only particularly simple to use, but also very accurate, in both the superconducting and normal phases. Moreover, the pairing correlations strongly affect the thermodynamic quantities and cannot be neglected or even treated in the oversimplified model of an odd-even pairing shift. In particular, the superconducting effects are significant up to rather high excitation energies ($U_{cr} \simeq 8\,\mathrm{MeV}$) and tend to reduce greatly the entropy as well as the moment of inertia.

II.5 Comparison with experimental data

II.5.1 The semi-classical approximation to the level density parameters

The semi-classical approximation to the single-particle level density, as developed in the present work, allows us to construct a new analytical formula of nuclear state densities for spherical nuclei taking the shell and pairing effects into account. Before comparing the level densities predicted by this new theoretical formulation with experimental data, the different parameters appearing in the level density expression have to be estimated. It turns out that the level density depends essentially on 6 quantities:

- the asymptotic $\tilde{a}$-parameter corresponding to the smooth single-particle level density at the Fermi energy
- the shell parameters: γ defining the temperature at which the shell effects disappear and δW_1 and δW_2 corresponding to the two contributions to the ground-state shell correction energy
- the rotational correction factor f_σ taking the possible reduction of the moment of inertia below the rigid body value into account
- the ground-state energy gap Δ_0 (or equivalently the pairing strength G and the energy cut-off ε_Λ).

These 6 quantities, when not fixed by experimental data, must not be considered as free parameters since in the semi-classical approach they are strictly defined and can be related to physical quantities such as the the Fermi energy and the potential properties (radius, depth, surface diffuseness). Yet the semi-classical approximation derived in the present work might not be accurate enough to enable a reliable determination of these parameters since it refers to oversimplified nuclear models such as the infinite square well or the Woods-Saxon potential. These models are known to be rather crude approximations to the behaviour of a nucleonic system interacting via many-body

forces, so that significant discrepancies can be expected when comparing with experimental data. Nevertheless, the semi-classical approach enables a possible parametrization of the above quantities. In particular, it becomes possible to express them as a function of the particle number and to estimate the remaining parameters through fits to experimental data. This possible procedure constitutes one major advantage of the semi-classical approach in comparison with previous empirical approximations. The lack of experimental data on nuclear level densities, especially over a wide energy range, does not make an empirical parametrization of the unknown quantities possible. In addition, a reliable formula with sound theoretical basis is of fundamental importance when extrapolations far away from the known experimental region are concerned. The semi-classical approach appears qualitatively to be an excellent guide in that respect.

The semi-classical expressions for the above parameters—as they have been given in the previous sections—depend on the particle number through the N- (or Z-) dependence of the potential radius R (approximated by $R = r_0 A^{1/3}$) and of the chemical potential (which has been assimilated to the Fermi energy and therefore assumed to be temperature-independent). The knowledge of the Fermi energy expressed as a function of the particle number requires the relation (for the neutron system)

$$N = N(\varepsilon_{F,n}) = \int_0^{\varepsilon_{F,n}} [\tilde{g}_V(\varepsilon) + \tilde{g}_S(\varepsilon)]\, d\varepsilon \tag{171}$$

be inverted (and similarly for the proton system). When only the volume term is considered, the inversion is trivial and constitutes the classical approximation to the Fermi energy. However, the non-negligible surface contribution to integral (171) gives rise to a complicated equation (see Appendix A) which cannot be solved so easily. It has been shown in Fig. *A*1 that the surface term $\tilde{g}(\varepsilon)$ leads to a negative contribution to the total density at low energies which then becomes positive at energies around the Fermi energy. In these conditions, the neglect of the surface term tends to overestimate the single-particle level density, i.e. to underestimate the Fermi energy (see

Fig. *A*3 in Appendix A). A phenomenological way of taking the surface term into account consists in considering the volume term only in which a reduction factor κ is introduced. This technique has already been used in Section II.3.2. It should be stressed that this rather crude approximation to equation (171) corresponds to a compromise between a complicated description of the surface contribution and an inconsistent use of the volume term only. In this approximation we can then expressed the neutron Fermi energy as

$$\varepsilon_{F,n} = \left[\frac{3}{2\kappa}\frac{N}{g_0^V}\right]^{2/3} \tag{172}$$

where the volume constant is expressed by (see Appendix A)

$$g_0^V = \frac{D}{4\pi^2}\left(\frac{2\mathrm{m}}{\hbar^2}\right)^{3/2}\mathrm{V} \tag{173}$$

A similar expression can be obtained for the proton system. The quantity g_0^V is identical for both the neutron and proton systems if the the neutron skin effect is neglected.

Strictly speaking, the factor κ must be considered as N-dependent. Yet we will assume that it remains constant (and roughly equal to 0.7) for all values of N. Although this treatment would require important improvements, it remains more reliable than the ideal degenerate Fermi gas approximation which takes $\kappa = 1$. Expressions (172)–(173) lead (for a radius parameter $r_0 = 1.26\,\mathrm{fm}$ and a constant $\kappa = 0.7$) to a Fermi energy equal to $\varepsilon_{F,q} \simeq 38(1 \pm \frac{2}{3}I)\,\mathrm{MeV}$ in close agreement to the usually accepted value.† The level density parameters can now be evaluated as a function of the particle number on the basis of relation (172).

---

† In this chapter, the index q will be used to denote either the neutron system ($q = n$) or the proton system ($q = p$). Similarly, N_q will stand either for N or Z. To simplify the relations, the different quantities can be expressed as a series expansion of the neutron excess $I = (N - Z)/A$. When expressions differ for the neutron and proton contributions, the upper sign will always refer to neutrons and the lower to protons.

A. Evaluation of the $\tilde{a}$-parameter

The parameter $\tilde{a} = \frac{\pi^2}{6}\tilde{g}(\varepsilon_F)$ is by far the most decisive parameter affecting the nuclear level density (because of the exponential dependence of the level density on the entropy). Therefore, uncertainties in its evaluation have an enormous impact on the prediction of the level density. Unfortunately, it remains very difficult to obtain, in an analytical form, a reliable evaluation of $\tilde{a}$. The oversimplified treatment of the single-particle level density generally leads to unreliable or inaccurate predictions of $\tilde{a}$.

As regards the volume contribution to the $\tilde{a}$-parameter, a straightforward estimation of its amplitude, taking both the neutron and the proton contributions into account, leads to

$$\tilde{a}_V \simeq \alpha A = \frac{\pi^2}{3}\left(\frac{1}{3\kappa\pi^2}\right)^{1/3}\frac{2mr_0^2}{\hbar^2}A \tag{174}$$

In particular, for $\kappa = 0.7$ and $r_0 = 1.4\,\mathrm{fm}$, we find $\alpha = 0.11\,\mathrm{MeV}^{-1}$ which agrees with the empirical value of $0.12\,\mathrm{MeV}^{-1}$ (e.g. Bohr and Mottelson, 1969). The value of $r_0 = 1.4\,\mathrm{fm}$ is somewhat larger than usual in order to account for the larger effective radius of the single-particle potential at the Fermi surface compared with the half-value radius. When the surface contribution is included, the increase of the effective radius is contained in the surface term, so that a lower radius can be considered. Yet the non-negligible surface contribution appeared to be a complicated function of the potential depth, the nucleonic separation energy and the surface diffuseness. Therefore, it seems dangerous to extract a universal A-dependence of the surface contribution. In addition, it has been shown (Section II.2.4 and Appendix A) that not only the amplitude but also the sign of the surface contribution $\tilde{a}_S$ depend drastically on the relative values of the potential depth V_0 and the nucleonic separation energy B. If we use the approximate expression $(A8)$ for the surface contribution and the parameters $(A9)$, derived in the case of a Woods-Saxon potential of surface diffuseness a=0.67 fm, then the sign of $\tilde{a}_S$ is predicted to be

$$\begin{cases} \tilde{a}_S \leq 0 & \text{if} \quad \mathrm{B} \gtrsim 0.2\,V_0 + 3.0\ \mathrm{MeV} \\ \tilde{a}_S \geq 0 & \text{if} \quad \mathrm{B} \lesssim 0.2\,V_0 + 3.0\ \mathrm{MeV} \end{cases} \tag{175}$$

where V_0 is expressed in MeV. The surface term is consequently expected to be mainly positive (if we assume the surface diffuseness not to differ significantly from the average value of 0.67 fm).

The amplitude of the surface contribution remains highly uncertain. However, from ($A8$) we can approximate its functional dependence for the total nucleus by

$$\tilde{a}_S = \beta\, A^{2/3} - \gamma\, Z A^{1/3} \tag{176}$$

where the two parameters β and γ are quadratic functions of the radius r_0. The second term corresponds to the effects of the Coulomb interaction which greatly decreases the potential depth of the proton system. An evaluation of these parameters yields for the parameters of the Woods-Saxon potential of Hodgson (1990): $\beta \simeq 0.07\,\mathrm{MeV}^{-1}$ and $\gamma \simeq 0.0014\,\mathrm{MeV}^{-1}$

The total smooth contribution to the a-parameter can finally be expressed for the total nucleus including the two nucleonic systems as

$$\tilde{a} = \alpha\, A + \beta\, A^{2/3} - \gamma\, Z A^{1/3} \tag{177}$$

The quadratic dependence of the $\tilde{a}$-parameter on the neutron excess I has been neglected because of its very small contribution ($\tilde{a} \propto (1 - \frac{1}{9} I^2)$). Nevertheless, the neutron and proton contributions individually show a strong linear dependence on the neutron excess: $\tilde{a}_{Vq} = \frac{1}{2}\alpha(1 \pm \frac{1}{3} I)A$. If, on the one hand, the nuclear level densities essentially depend on the total value $\tilde{a}_n + \tilde{a}_p$, on the other hand, the treatment of the pairing interaction, as developed in Chapter II.4, requires the knowledge of the two nucleonic contributions separately. In that case, the I-dependence of $\tilde{a}$ cannot be neglected.

It should be stressed that expression (177) is not expected to predict the level density parameter with a high accuracy, because of the numerous approximations made. As already emphasized in Section II.2.4, the $\tilde{a}$-parameter is highly sensitive to a variation of the uncertain potential radius r_0. Yet the parameters α, β and γ appear to depend quadratically on r_0, so that a modification

of its value affects the 3 parameters in the same way. The functional form of the $\tilde{a}$-parameter has been the subject of many controversies in the past and many different formulae have been proposed to reproduce the experimental data. The major uncertainty lies in the determination of the surface term. While Kataria et al. (1978), Kataria and Ramamurthy (1980) or Ramamurthy et al. (1983) required a negative surface contribution to reproduce the experimental data; Töke and Swiatecki (1981), Prakash et al. (1983) or Handloser and Stocker (1985) claimed a high positive theoretical value. Yet it has to be remembered that the so-called experimental a-parameter, as derived by Kataria et al. (1978), is model-dependent and drastically depends on the adopted treatment of the shell and pairing effects as well as the spin dependence. A modification of the spin cut-off parameter, for example, leads to different experimental a-parameters and consequently to different parameter sets in the functional form of $\tilde{a}$. The discrepancies between the theoretical and experimental a-parameter has raised the question that the present models might have been missing some important features, either in the evaluation of the a-parameter (as suggested by Ramamurthy et al., 1983) or more generally in the level densities formulation. The analysis made in the present work clearly emphasizes the possible variation of the amplitude as well as the sign of the surface term from one region of the nuclear chart to another one. Yet the semi-classical approximation to the Woods-Saxon single-particle level density would be in favour of a positive surface term, even if its quantitative contribution appears to be significantly reduced in comparison with the above-mentioned works.

B. Evaluation of the ground-state shell correction energies δW_1 and δW_2

As described in Section II.2.3, the level density at low temperatures ($T < T_{sh}$) is strongly correlated with the shell correction to the ground-state energy. The problems associated with the ground-state shell energy have already been discussed in Part I in the context of the droplet-type mass formulae and are encountered in a similar way when dealing with the shell effects on nuclear level densities.

The main difficulty lies in the proper definition of the shell energy and more generally in the interrelationship between the macroscopic and microscopic quantities, as discussed by Strutinsky (1989). The shell energy, as derived in the literature, must be regarded as a purely artificial quantity which has been introduced to account for the discrepancies obtained when fitting semi-classical approximations to quantum quantities. In particular, in nuclear mass models, the shell corrections to the ground-state energy differ significantly from one mass formula to the other one since they are defined by

$$M_s(Z,A) = M_{exp}(Z,A) - M_{macro}(Z,A) \tag{178}$$

where M_{exp} is the experimental mass defect and M_{macro} the theoretical macroscopic term obtained in the framework of a classical or semi-classical model. Most initial works used the liquid drop model as the macroscopic model (Myers and Swiatecki, 1966, 1967). Later, the addition of new features to the liquid drop model led to the development of the droplet model (Hilf et al., 1976; von Groote et al., 1976) and the finite-range model (Möller et al., 1988). To reproduce experimental masses, all the above models introduce a microscopic correction to account for the non-uniform distribution of single-particle levels in the nucleus. Different methods can be found to estimate the microscopic term, even if basically all the macroscopic-microscopic models use either the phenomenological correction of Myers and Swiatecki (1966) or Strutinsky's method (Strutinsky, 1967). In both cases, the different parameters of the model are estimated from a least-squares adjustment to experimental ground-states masses. Different models lead inevitably to different contributions to the macroscopic and microscopic terms and consequently to different shell correction energies. Even a single mass formula can have two different parameter sets which both fit the experimental masses with the same accuracy, but lead to drastically different shell energies. An example can be found in Part I, with the mass formulae of Hilf et al. (1976) and von Groote et al. (1976).

For these reasons, it seems inconsistent to introduce into the level density expression a shell

correction energy, which has been derived from a given nuclear mass model and linked to an arbitrary macroscopic term. Ideally, for the level density calculations, the only consistent way of using the shell energy extracted from an empirical mass formula, is simultaneously to relate the smooth $\tilde{a}$-parameter to the macroscopic term of the given mass model. Unfortunately, the semi-classical approach does not allow a reliable evaluation of the parameters of the droplet contribution to the nuclear mass. As a matter of fact, the calculation of the ground-state nuclear mass in the semi-classical approach requires an accurate knowledge of the single-particle level density $g(\varepsilon)$ in the whole energy range from the bottom of the potential well up to the Fermi energy. Moreover, the effects of the nuclear two-body forces have to be taken into account in the evaluation of the nuclear potential energy. Therefore, this technique cannot be used to link consistently the $\tilde{a}$-parameter to the macroscopic contribution to the nuclear mass in the same manner as the shell-dependent a-parameter is related to the ground-state shell correction energy.

In addition to the above-mentioned methods, the semi-classical approach developed in Section II.2.3 seems to offer a new way of evaluating the ground-state shell correction energy analytically. It has been shown that the semi-classical approximation to the statistical properties of the nucleus can predict the spherical shell energy δW of a system of nucleons confined in an infinite square well (see expression (30)). Yet the resulting expression is a rather complicated function since it is given by a double infinite sum of oscillating functions. Moreover, expression (30) describes the shell correction energy in the fairly unrealistic case of an infinite square potential and cannot be expected to have any reliable predictive power when dealing with more realistic shell models.

Nevertheless, we have tested the semi-classical approximation to δW by trying to generalize and renormalize its expression to the case of a shell model including a spin-orbit potential. Since the semi-classical expression (30) is far to complicated for practical purposes and especially for a simple parametrization of δW, we have replaced the double infinite summation by a more suitable

phenomenological function. Using the A-dependence of the nuclear radius ($R = r_0 A^{1/3}$) and of the Fermi energy ($\varepsilon_{F,q} \propto \left(\frac{N_q}{A}\right)^{2/3}$), we show in Appendix C that the two contributions to the shell correction energy $\delta W = \delta W_1 + \delta W_2$ can be reduced in the optical diffraction approximation to the simple expressions

$$\delta W_1^q \simeq s_1 N_q^{1/2} \left[1 - \frac{t_1}{1 + r_1 \sin^2\left(\bar{g}_1 N_q^{1/3} + k_1\right)}\right] \tag{179}$$

$$\delta W_2^q \simeq s_2 N_q^{1/6} \left[1 - \frac{t_2}{1 + r_2 \sin^2\left(\bar{g}_2 N_q^{1/3} + k_2\right)}\right] \tag{180}$$

Full details about the calculations and simplifications made to obtain expressions (179)–(180) can be found in Appendix C. An estimation of the above parameters is also given in Appendix C for the simple model of an infinite square well potential. Also discussed in Appendix C are the effects on the shell correction energy resulting from the constructive or destructive interferences in the nucleonic motions.

Approximations (179) and (180) represent fairly good fits to the semi-classical expression (30). Better fits can be obtained (see Appendix C), but at the expense of an increase in the number of parameters. For the sake of simplicity, we have adopted the above expressions to estimate the shell corrections to the ground-state energy. Since they correspond to the simple model of nucleons confined in a spherical infinite well, the different quantities s_i, t_i, r_i, $\bar{g}_i$ and k_i ($i = 1, 2$) will be taken as free parameters in an attempt to describe more realistic shell effects. We can hope that a renormalization of these parameters could reproduce known features of the actual nuclear shell structure, such as the magic numbers.

Ideally, the different parameters defining the energies δW_1 and δW_2 should be determined by fitting expressions (179) and (180) to experimental nuclear masses. However, the nuclear mass models, especially in the droplet approach, still suffer from other uncertainties (such as the deformation effects) which makes an unambiguous extraction of the nuclear shell correction energies

impossible. In particular, the error associated with the predicted nuclear masses remains larger than the amplitude expected for the shell correction δW_2 (see Appendix C). The energy δW_2 corresponds to a correction smaller than typically 0.5 MeV to a total energy of the order of a few hundred MeV. For that reason, we will neglect to a first approximation its contribution to the total nuclear mass. Moreover, since the extraction of the energy δW_2 appears ambiguous—fits to experimental masses still constitute the only method to derive the ground-state shell correction energies—we have provisionally assumed that its contribution to the nuclear level density could also be neglected.

If we assume for simplicity that the neutron and proton contributions to the total shell correction energy are identical, we can finally write the ground-state shell correction energy for spherical nuclei as

$$\delta W_q \simeq \delta W_{1q} = s N_q^{1/2} \left[1 - \frac{t}{1 + r \sin^2 \left(\bar{g} N_q^{1/3} + k \right)} \right] \tag{181}$$

which requires a knowledge of 5 parameters. However, two of them, namely $\bar{g}$ and k, should not be regarded as free parameters, since they are fixed by the requirement of reproducing the magic numbers. As a matter of fact, the main constraint to any shell function is to exhibit minima at the shell closures, i.e. at neutron and proton numbers N_q=2, 8, 14, 28, 50, 82, 126, 184. Because of the approximate and spherical nature of the shell function (181), only the four major magic numbers—N_q=28, 50, 82, 126—are considered here. The shell correction energy (181) exhibits minima at the particle number N_q^*, such that

$$\bar{g} N_q^{*1/3} + k = n\pi \tag{182}$$

where n is an integer. Expression (182) defines the magic numbers. It is of particular interest to see that the four main magic numbers can approximately be obtained with only two parameters $\bar{g}$ and k. We find for the specific values $\bar{g} = 4.74$ and $k = 1.37$, the numbers N_q^*=27.7, 50.1, 82.3, 126.0, which correspond to the magic integers required. Some little deviations around the two

values of $\bar{g}$ and k are allowed as long as the resulting integer minima correspond exactly to the magic numbers. It can also be seen from the simple condition (182) that the two other minima, for the same values of $\bar{g}$ and k as above, are 13.2 and 182.9, which do not greatly differ from the known minima at 14 and 184, respectively.

To a first approximation, the consideration of one single frequency $\bar{g}$ in the oscillating shell function appears to be able to reproduce the four main magic numbers. This result is of great importance since it justifies the assumption made in Section II.2.3 about the constancy of the shell parameter γ. The shell effects on the nuclear level density have been obtained assuming that the main periodic orbits contributing to the single-particle level density were characterized by a fairly constant frequency $g_2 \simeq g$. The fact that the different paths contributing to the shell energy can be reduced to a single orbit with the average frequency $2\bar{g}N_q^{1/3}$ and that the shell correction energy δW depends on the single-particle level density in the same manner as the shell contribution to the level densities, confirms this assumption made. Moreover, the heavy constraint related to the exact matching of the magic numbers leads to a well defined value of $\bar{g}$, so that the approximation made is thought to be fairly good.

We have used expression (181) to generate a new shell correction to the droplet nuclear mass formula. The adopted mass formula consists of the usual terms (e.g. Myers, 1976)

$$M(N,Z) = \tilde{M}(N,Z,\theta) + M_p(N,Z) + M_W(N,Z) + M_s(N,Z,\theta) \tag{183}$$

where θ describes the nuclear deformation dependence of the different mass contributions and $\tilde{M}$, M_p and M_W correspond to the smooth droplet energy, the pairing contribution and the Wigner term, respectively. We have treated these three terms in the classical droplet model formalism (von Groote et al., 1976). However, the shell correction energy M_s is now given by

$$M_s(N,Z,\theta) = \left[\delta W_n(N) + \delta W_p(Z)\right]\left(1 - 2\theta^2\right)\mathrm{e}^{-\theta^2} \tag{184}$$

where the deformation effects have been introduced by the simple procedure of Myers and Swiatecki (1967). Although this treatment of the nuclear deformation remains highly uncertain and might account for other phenomena inherent to the spherical shell function (see Appendix C), it has been successful in reducing the discrepancies between the theoretical and experimental shell correction energies for deformed nuclei.

To the first three contributions to the total mass (183) correspond 10 parameters (if the obscure contribution of the curvature correction and symmetry anharmonicity energy are neglected). Our shell function depends on three parameters, so that the total mass is finally a function of 13 parameters. These 13 parameters have been adjusted in order to reproduce the 1997 masses of nuclei with $25 \leq Z \leq 109$, available in the experimental mass table of Wapstra et al. (1988).† Only the $Z \geq 25$ nuclei have been considered because of the rather poor predictive power of our shell function for very light nuclei. Fits to lower-Z nuclei would require a more accurate approximation to the shell energy. The adjustment of the 13 parameters on some 2000 data constitutes a rather difficult task, so that only a first but promising attempt will be presented here.

For the adjustable parameters of the macroscopic term, we obtained (see von Groote et al. (1976) for the parametrization):

$r_0 = 1.166\,\mathrm{fm}$	Nuclear radius constant
$a_V = 16.20\,\mathrm{MeV}$	Volume energy
$a_S = 20.82\,\mathrm{MeV}$	Surface energy
$J = 38.0\,\mathrm{MeV}$	Symmetry energy
$Q = 17.65\,\mathrm{MeV}$	Effective-surface stiffness
$K = 275.0\,\mathrm{MeV}$	Compressibility
$L = 200.0\,\mathrm{MeV}$	Density symmetry

† The estimated masses of Wapstra et al. (1988) derived from systematic trends have also been included in the fits.

$b_0 = 0.7\,\mathrm{fm}$	Diffuseness width
$a_0/r_0 = 0.5$	Deformation parameter
$W = 29.5\,\mathrm{MeV}$	Wigner constant
$\Delta = 12.0\,\mathrm{MeV}$	Pairing constant

For the shell function (181), we used the parameters

$$s = 0.90\,\mathrm{MeV}$$

$$t = 1.50$$

$$r = 2.00$$

$$\bar{g} = 4.746$$

$$k = 1.373$$

This set of parameters lead to a root mean square (rms) deviation from the 1997 experimental masses of Wapstra et al. (1988) equal to $\left[\sum^{1997}(M_{exp} - M_{cal})^2/1997\right]^{1/2} = 955\,\mathrm{keV}$ and an average deviation (defined as usual by the average difference of the calculated masses M_{cal} and the experimental masses M_{exp}) equal to $-13\,\mathrm{keV}$. The resulting theoretical shell correction energies are displayed in Fig. 29 as a function of the neutron number and compared with the so-called experimental shell energies as defined by expression (178).

This preliminary fit should be regarded as very promising. To describe the shell function, we used the simplest expression, neglecting, in particular, the second order term δW_2 and the difference in the neutron-proton contributions. Many improvements to the shell function can be envisaged to reduce the deviations from the experimental masses. More specifically, a systematic underestimation of the shell energy can be observed in the vicinity of the magic numbers and can be ascribed to the too soft shape of the shell function at the minima i.e. to a too small parameter r. However, the main uncertainties remain related to the deformation dependence of the shell

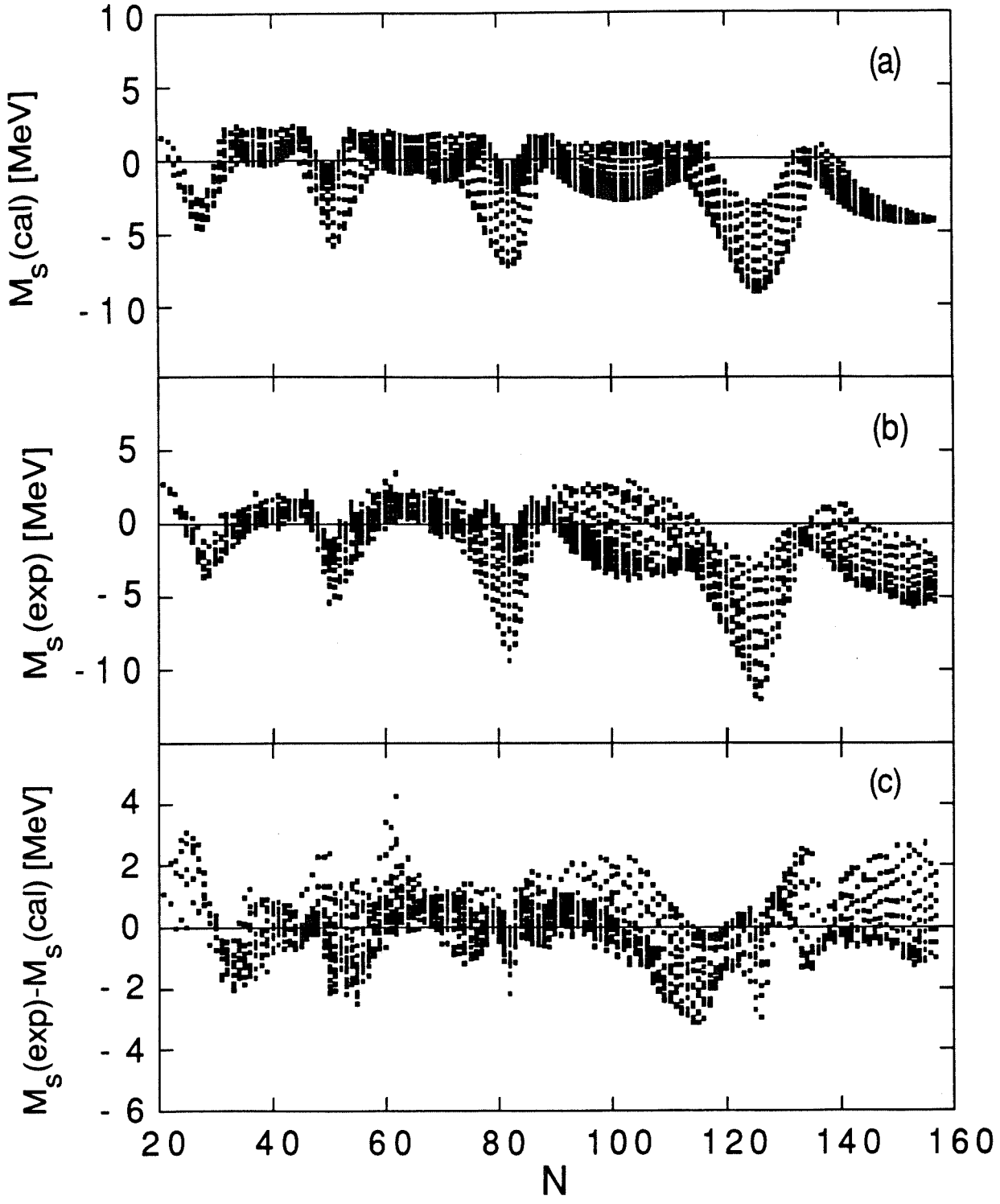

Figure 29.(a) Calculated shell correction energies (184) as a function of the neutron number for known nuclei with $Z \geq 25$. The theoretical shell function corresponds to the parametrized semi-classical approximation to the ground-state shell correction energy (181).
(b) Experimental shell correction energies for the same nuclei obtained by the difference of the experimental masses and the macroscopic droplet masses.
(c) Residual discrepancies between the theoretical and experimental shell correction energies.

correction.

Our new mass formula appears to be relatively good in comparison with previous works. An important decrease in the rms deviation is obtained relative to the original mass formula of Myers and Swiatecki (1966, 1967, 1976) which is around 1.4 MeV. Myers and Swiatecki (1966) derived an expression for the shell correction (depending on three parameters) by considering it to be the result of the bunching of an originally smooth distribution of single-particle levels (an ideal degenerate Fermi gas) into one that consists of groups of levels corresponding to the observed magic numbers. Although this phenomenological procedure led to the first satisfactory description of the shell effects on nuclear masses, it clearly corresponds to an idealistic representation of the bunched levels scheme and remains highly uncertain and arbitrary.

If we compare our new mass formula with the more recent, but also more complicated mass models, our result in view of its high simplicity can be considered very satisfactory. The mass formula of von Groote et al. (1976), discussed in detail in Part I, reproduces the same 1997 experimental masses (with $Z \geq 25$) with an rms deviation of 803 keV and an average deviation of -235 keV. However, it is accompanied by an increase of the number of free parameters, since they used 50 parameters, among which 34 describe the shell functions. Yet their shell correction is basically similar to the shell function of Myers and Swiatecki, in which the contributions of inner shells have been included. As regards the latest macroscopic-microscopic models of Möller and Nix (1988) or Möller et al. (1988), the adjustment of 26 parameters leads to an rms deviation of around 800 keV. However, they use a Strutinsky-type shell correction which remains far from being easily accessible.

It should be stressed that, as far as nuclear mass prediction is concerned, we do not pretend to compete with the most recent and sophisticated mass models. Further investigations and improvements of the shell function (181) would be necessary for reliable nuclear mass predictions.†

† The weakest point in the droplet-type mass formulae concerns the treatment of deformation,

Yet the satisfactory preliminary results obtained with our new shell correction energy in view of its remarkable simplicity make it very promising. These results also emphasize the great predictive power of the semi-classical approach. If our new shell function should be regarded as semi-empirical because of the numerous approximations made to simplify the original semi-classical expression, it has a sound theoretical base compared with the purely phenomenological approach of Myers and Swiatecki. Moreover, the semi-classical approach has the advantage of offering a clear insight into the effects of the nucleonic motions on the nuclear shell structure (see Appendix C).

When dealing with nuclear level densities, the problem associated with the consistency between the shell-independent and shell-dependent terms remains open. It remains inconsistent to make use of any shell correction energy to describe the shell effects on the nuclear level density. However, since no other possibilities are offered so far, we have provisionally assumed that the contribution of the δW_2 energy to the level density expression could be neglected and that the total shell energy δW_1 could be derived from the microscopic term of an arbitrary mass formula. The use of our shell function (181) is expected to lead to unsatisfactory results for level densities of magic nuclei because it tends to underestimate the shell correction energy at shell closures (see Fig. 29). The choice of the shell function of von Groote et al. (1976) also gives rise to problems. In particular, the neutron and proton shell functions are significantly different. The proton shell energy appears to be strongly shifted to positive values: for example, for a symmetric nucleus ($N = Z$), the proton shell energy of von Groote et al. at $Z = 82$ is $-0.5\,\mathrm{MeV}$ while Hilf et al. (1976) predict a value of $-5\,\mathrm{MeV}$. This global positive shift is mainly compensated by a negative shift in the neutron shell energy. If such a difference does not have an important influence on the total ground-state shell correction energy, it may affects the level density prediction which does not depend on the shell energy of the total nucleus as a whole. Therefore, it seems dangerous to use the energies of

---

so that improvement of the shell function requires first a better description of the deformation effects. Such a study is beyond the scope of the present work.

von Groote et al. in nuclear level density calculations. Since the shell function of Hilf et al. does not exhibit such an asymmetry between the neutron and proton energies, we have provisionally adopted their shell corrections to describe the shell effects on the nuclear level density. Yet it should be kept in mind that this arbitrary choice remains inconsistent and that improvements of the shell energy treatment are seriously required.

C. Determination of the shell damping parameter γ

The shell damping parameter γ corresponds to the inverse of the critical temperature at which shell effects disappears. It has been defined for an infinite square potential by

$$\gamma_q = \frac{1}{2}\,\bar{g}_2\,\frac{\sigma_a}{\varepsilon_{F,q}^{1/2}} \tag{185}$$

$$= \bar{g}\,\frac{\sigma_a}{\varepsilon_{F,q}}\,N_q^{1/3} \tag{186}$$

where $\sigma_a = \frac{\pi^2}{12\ln 2} \simeq 1.19$ and $\bar{g}_2$ is an average value of the frequencies g_2 of the different paths contributing to the oscillating a-parameter (see Section II.2.3). In fact, the quantity $\bar{g}_2$ can be related to the frequency $\bar{g}$, defined in the above subsection, by $\bar{g}_2 = 2\bar{g}\,\varepsilon_{F,q}^{-1/2} N_q^{1/3}$. Making use of approximation (172) to the Fermi energy, we can rewrite expression (186) as

$$\gamma_q = \gamma_0 \left(1 \mp \frac{1}{3} I\right) A^{1/3} \tag{187}$$

The quantity γ_0 is independent of the type of nucleons (if the neutron skin effect is not taken into account) and equal to $0.12\,\mathrm{MeV}^{-1}$ for the parameters: $r_0 = 1.26\,\mathrm{fm}$, $\kappa = 0.7$ and $\bar{g} = 4.74$. Yet the uncertainty associated with these parameters might strongly affect the value of γ_0. It can be seen from expression (187) that the parameter γ for protons is expected to be larger than for neutrons, as already shown in Section II.2.4. This nucleonic difference is partially at the origin of the non-dependence of the level density on the total shell correction energy $\delta W = \delta W_n + \delta W_p$, but on its two nucleonic contributions, separately. However, the neutron skin effect tends to reduce the asymmetry between the contribution of the neutron and proton systems.

D. Adopted value for the rotational correction factor f_σ

As far as the spin dependence of the level density is concerned, the main uncertainty clearly lies in the evaluation of the rotational energy. It has been shown that in the approximation of small angular momenta, a global increase of the rotational energy by an average factor of 3.5 was predicted by the semi-classical approximation developed in the present work. In addition, the shell effects appeared to play an important role on the temperature dependence of the parameter f_σ. However, the estimation of the factor f_σ remains highly obscure and is to be confirmed by more detailed calculations, such as combinatorial calculations. At this stage, we have consequently taken f_σ as a free and temperature-independent parameter.

E. Evaluation of the ground-state pairing gap Δ_0

The pairing gap Δ_0 is known to exert a strong influence on nuclear ground-state properties. More particularly, an accurate evaluation of the pairing gap appears to be of fundamental importance when the odd-even effects on nuclear masses as well as on nuclear level densities are to be taken into account. We showed in Section II.4.4 how important the impact of the pairing correlations on the statistical properties of the nucleus can be. For an accurate nuclear mass formula, a careful treatment of the pairing energy—generally assimilated to the pairing gap—is also required. The value of Δ_0 for a given nucleus has been shown to depend upon both the residual pairing interaction and the distribution of single-particle levels near the Fermi energy (see expression (131)). Yet simple analytical expressions are generally adopted to approximate the gross behaviour of the pairing gap throughout the periodic table. In particular, Bohr and Mottelson (1969) introduced the smoothed distribution gap parameter

$$\tilde{\Delta}_{0n} = \tilde{\Delta}_{0p} = \frac{12}{\sqrt{A}} \text{ MeV} \tag{188}$$

to fit experimental odd-even mass differences of nuclei close to the valley of β stability. This widely used formula has then been improved by Vogel et al. (1984) to account for the isospin dependence

of the average pairing gap. More sophisticated is the formula proposed by Madland and Nix (1988) which is based on the BCS approximation (131), applied to a distribution of dense, equally spaced levels. Such a treatment requires the knowledge of the pairing strength G and the energy cut-off ε_Λ. Since the overlap integrals involved in the pairing interactions are inversely proportional to the nuclear volume (Nilsson et al., 1969), the pairing strength G is generally assumed to depend inversely upon the mass number A. The usually adopted functional form of G is expressed by

$$G = \frac{g_o}{A}\left(1 \mp g_1 I + g_2 I^2\right) \tag{189}$$

As regards the energy cut-off, it has to be stressed that in the constant-G model, the energy cut-off is closely related to the adopted value of G, so that it is meaningless not to specify the value of the energy cut-off used, as often happens in the literature. Since to a first approximation the product $\rho_0 G$ in expression (131) is believed to be independent of A, the energy cut-off is sometimes taken to be proportional to $A^{-1/2}$, in order to reproduce the overall dependence of the empirical odd-even mass difference (188) (Nilsson et al., 1969). Another parametrization has been suggested by Madland and Nix (1988): the number of states n_c affected by the interaction is assumed to be proportional to the surface area of the nucleus. Under this condition, the energy cut-off is given by

$$\varepsilon_{\Lambda,q} = \frac{n_c}{2\rho_{0,q}} = k_\Lambda \frac{B_s}{N_q^{1/3}} \tag{190}$$

where B_s is the usual nuclear surface area relative to the spherical shape and k_Λ a free parameter.

It is worthwhile noting at this point that unless the BCS equations are solved numerically, none of the analytical expressions proposed to estimate the pairing gap, takes the shell effects into account. The shell fluctuations of the pairing gaps are always neglected in the analytical approximations, although they are known to be fairly important. We showed in Section II.4.2, that the semi-classical approximation to the single-particle level density can also constitute an interesting tool for determining the shell effects on the pairing gap. Expression (133) can be

simplified by assuming that the equivalent temperature T_{Δ_0} is proportional to the smooth gap parameter (188): $T_{\Delta_0} = c_2\tilde{\Delta}_0$. If we use for the smooth parameter $\tilde{a}_q$ the approximate volume form $\tilde{a}_q = \frac{1}{2}\alpha A(1 \pm \frac{1}{3}I)$, we can write the gap parameter as

$$\Delta_{0,q} = k_\Lambda \frac{B_s}{N_q^{1/3}} \, \mathrm{e}^{-\left[u \pm vI + wI^2\right]} \, f_{osc,q} \tag{191}$$

where we have chosen for the smooth trend of Δ_0 the same parametrization as Madland and Nix (1988):

$$u = \frac{2\pi^2}{3} \, \frac{1}{\alpha g_0} \tag{192}$$

$$v = u \, (g_1 - \frac{1}{3}) \tag{193}$$

$$w = u \left(g_1^2 - \frac{1}{3}g_1 - g_2 + \frac{2}{9}\right) \tag{194}$$

and where the oscillating contribution to the single-particle level density is contained in the factor

$$f_{osc,q} = \frac{1}{1 + \dfrac{\gamma_q^2}{\tilde{a}_q} \dfrac{\delta W_{1q}}{\left[1 + c_2\gamma_q^2\tilde{\Delta}_0^2\right]^2}} \tag{195}$$

If the shell fluctuations are neglected $f_{osc,q} = 1$ and expression (191) reduces to the formulation of Madland and Nix (1988). Expression (191) with the inclusion of the oscillating factor f_{osc} corresponds to the first analytical expression which takes the shell correction to the pairing gap into account. For magic nuclei, the shell correction leads to a lowering of the factor $\rho_0 G$ and consequently of the energy gap. Expressions (191) and (195) raise, once again, the important problem associated with the link between the macroscopic part $\tilde{a}_q$ and the shell energy δW_{1q}. The uncertainties related to the arbitrary choice of the ground-state shell correction energies δW_{1n} and δW_{1p} have important consequences for the calculation of the shell effects on the pairing gap. Each nucleonic contribution clearly depends solely on its respective shell energy, so that both the neutron and proton contributions to δW_1 must be known separately. In particular, the important asymmetries

found in the literature between the proton and neutron contributions have an important impact on expression (191). It should be stressed that we do not imply that the two nucleonic energies must be identical, but that it is very hazardous to extract them from a fitted mass formula. Since the total shell energy, as defined by expression (178), should already be considered as an arbitrary quantity, its division into the two nucleonic contributions becomes even more ambiguous.

The different parameters in expression (191) can be adjusted in order to reproduce the experimental odd-even mass differences. A set of experimental data can be extracted by use of measured ground-state masses in finite-difference equations derived for the pairing gaps from Taylor series expansions of masses in the neighbourhood of the mass of interest. Madland and Nix (1988) introduced the fourth-order even-odd mass differences $\Delta^{(4)}$, defined for the neutron system of an even-even nucleus by

$$\Delta_n^{(4)} = -\frac{1}{8}\Big[M(Z,N+2) - 4\,M(Z,N+1) + 6\,M(Z,N) - 4\,M(Z,N-1) + M(Z,N-2)\Big] \quad (196)$$

where $M(Z,N)$ is the experimental mass of the (Z,N) nucleus. For odd-N and even-Z nuclei, the negative of equation (196) is used. Since for odd-Z nuclei, the residual n–p interaction energy must be included in the expression of the even-odd mass difference, these nuclei will not be considered here. A similar expression to (196) can be obtained for the proton pairing gap.

Expression (196) is based on the assumption that nuclear masses are smooth functions of Z and N except for pairing effects. Yet other physical effects, such as the shell effects, the Wigner energy singular cusp or the granularity of light nuclei, also lead to additional departures from a smooth mass surface. Therefore, to obtain unambiguous experimental information on the pairing gaps, we must exclude the regions of the mass surface where these additional departures from smoothness occur. To do so, we have followed the prescription of Madland and Nix (1988) in order to extract the experimental energy gaps from the nuclear masses of Wapstra et al. (1988). It corresponds for the evaluation of the neutron pairing gap to the omission of the nuclei (Z,N) such

that

- Z, $N-1$, N, $N+1$ equal to one of the magic numbers: 8, 14, 28, 50, 82, 126
- $Z = N-1$, $Z = N$, $Z = N+1$
- $Z + N < 16$

Similar conditions can be obtained for the evaluation of the proton pairing gap. Even so, it is of importance to keep in mind that the pairing gap remains essentially a quantity whose experimental evaluation is far from being well defined. In addition, the odd-even mass differences defined by the above procedure are not strictly identical to the pair correlation constant Δ_0 describing the pairing of nucleons close to the Fermi surface. The pairing energy calculated by equation (196) corresponds to the energy $\sqrt{(\varepsilon_k - \mu)^2 + \Delta_0^2}$, where μ is the chemical potential and ε_k the energy of the last occupied level (see Section II.4.3). However, far away from shell closures, equation (196) is believed to give good results.

Unfortunately, we have just shown that this technique cannot be used to obtain experimental pairing gaps for nuclei near closed shells. Therefore, we are left with the problem that no experimental data are available in the vicinity of shell closures, where the main theoretical corrections have been brought. Yet we have performed a preliminary fit to the experimental pairing gaps, in order to estimate the influence of the shell effects on formula (191). The same nuclei as considered by Madland and Nix (1988) were examined in order to have a direct comparison with their results.

Since the semi-classical shell function derived in sub-section B has the advantage of being identical for neutrons and protons, it has been used to evaluate the factor $f_{osc,q}$. On the one hand, use of an asymmetric shell correction would require a renormalization of the isospin dependence and consequently the adjustment of different parameters k_Λ, u, v, and w for each nucleonic contribution. On the other hand, the weakness of the shell function (181) at magic numbers has no important consequences for the comparison with experimental data since no experimental pairing gaps are

available for these nuclei. It should be added that the adjusted shell energies (181) have been derived for nuclei with $Z \geq 25$ only. Though the experimental pairing gaps also concern nuclei with $18 \leq Z \leq 25$, no large discrepancies are expected because the shell function (181) still reproduces fairly well the experimental shell corrections in this mass region.

If we parametrize the ratio $\gamma_q^2/\tilde{a}_q = c_1(1 \mp I)A^{-1/3}$ (where $c_1 = 2\gamma_0^2/\alpha$), we are left with 6 parameters to fit some 700 experimental gaps. In fact, the parameters k_Λ and u both modulate the amplitude of Δ_0, so that only 5 parameters are effective. The relative surface energy B_s is set to unity, corresponding to a spherical shape. The values of B_s rarely exceeds unity by more than 1% at ground-state deformations for nuclei the pairing gaps of which are known experimentally. The finally adopted parameters are:

$$k_\Lambda = 80.0\,\mathrm{MeV} \qquad w = 4.40$$

$$u = 2.714 \qquad c_1 = 0.277\,\mathrm{MeV}$$

$$v = 0 \qquad c_2\gamma_0^2 = 0.034\,\mathrm{MeV}^{-1}$$

which lead to a root mean square deviation from the 403 experimental neutron pairing gaps equal to 167.4 keV and from the 318 experimental proton pairing gaps equal to 161.0 keV. The rms deviations appear to be reduced by approximately 20 keV compare with the smooth pairing gaps of Madland and Nix (1988). They obtained an rms deviation from the same experimental data of 184.4 keV for the neutron gaps and of 178.0 keV for the proton gaps. This reduction in the rms deviation appears to be fairly small, even if far from being negligible. It should be remembered that the last results of Madland and Nix did not improve significantly the predictions of Vogel et al. (1984) and reduced the rms deviation of Bohr and Mottelson (1969) by approximately the same value of 25keV. The improvements in the agreement between our theoretical prediction and the experimental data are, in fact, important, mainly if we keep in mind that the main corrections brought to the pairing model and concerning the nuclei in the vicinity of a magic number, cannot be tested. Major uncertainties are still related to the derivation of experimental gaps—especially

for magic nuclei—so that the comparison between the theoretical and experimental shell effects on the pairing gaps remains problematic. The theoretical neutron pairing gaps are compared with the experimental data in Fig. 30 (see Fig. 31 for the proton pairing gaps). It can be observed that the global N- or Z-dependence of the experimental pairing gaps as well as the correlation between the shell effects are well reproduced by the analytical approximation. The isospin dependence on the observed odd-even mass differences is also well reproduced by the quadratic dependence adopted. This result is in close agreement with the results of Vogel et al. (1984) and Madland and Nix (1988), even if microscopic calculations of the pairing gaps fitted to the odd-even mass differences show no explicit isospin dependence (Möller and Nix, 1990). It is of interest to see that the introduction of a linear isospin dependence does not significantly improve the agreement when shell effects are introduced in formula (191). This linear contribution appeared to be non-negligible when omitting the shell effects (Madland and Nix, 1988). The isospin dependence of the pairing gaps is of great importance to allow reliable extrapolations to nuclei far removed from the valley of β stability. This concerns the prediction of pairing effects on the nuclear level densities as well as on nuclear masses. Moreover, the introduction of shell effects in the present model highly increases the reliability of the pairing gaps predictions to be extrapolated away from the experimentally known region of the nuclear chart.

If we assume that $\alpha = 0.12\,\mathrm{MeV}^{-1}$ (see Section II.5.3), we can deduce from expressions (192)–(194) the parameters of the pairing interaction

$$G = \frac{20.1}{A}\left(1 \mp \frac{1}{3}I - 1.4\,I^2\right) \quad \mathrm{MeV} \tag{197}$$

$$\varepsilon_{\Lambda,q} = 80\,\frac{B_s}{N_q^{1/3}} \quad \mathrm{MeV} \tag{198}$$

This result is close to the generally adopted value of $g_0 \simeq 20\,\mathrm{MeV}$ derived from microscopic calculations (Nilsson et al., 1969; Ignatyuk, 1985; Pearson et al., 1991). The value of the pairing interaction constant g_0 does not depend heavily upon the prescription used to describe the energy

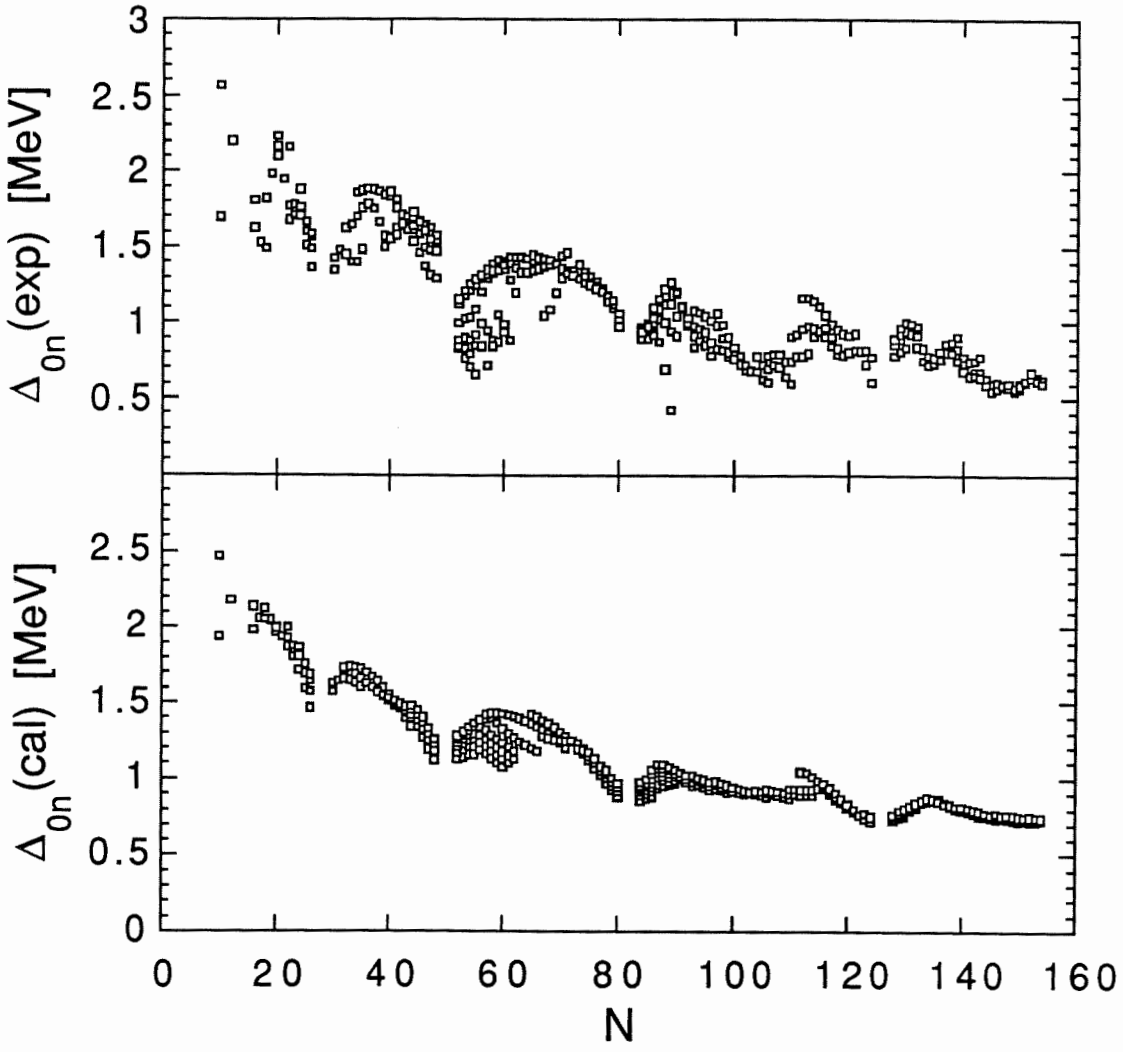

Figure 30. Comparison between experimental (upper part) and calculated (lower part) neutron pairing gaps Δ_{0n}. The theoretical gaps have been calculated with the semi-classical approximation to the single-particle level density. The model parameters are given in the text.

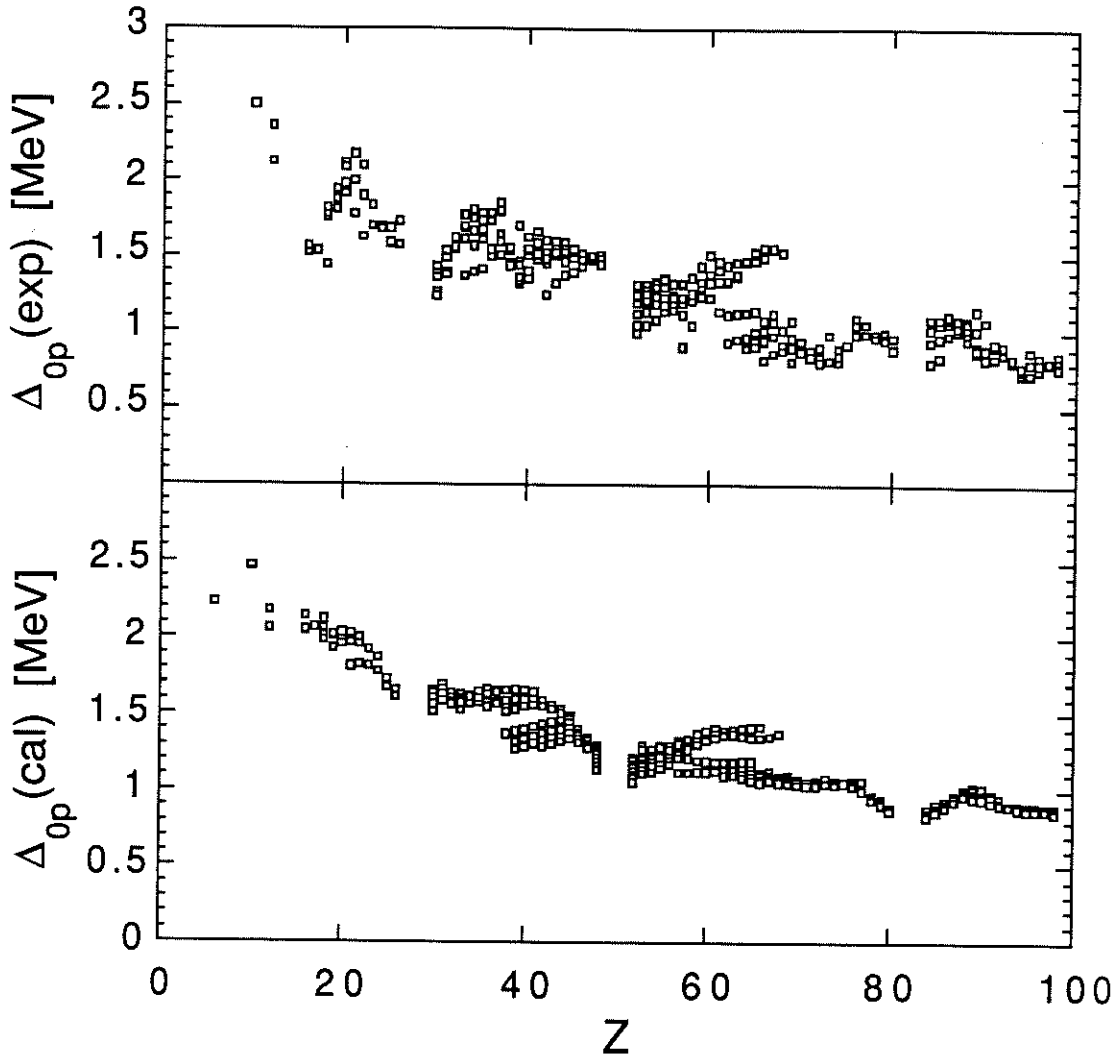

Figure 31. Same as Fig. 30 for the proton pairing gaps Δ_{0p}.

cut-off, so that this comparison is not meaningless. On the contrary, the the pairing gap is not very sensitive to a modification of the energy cut-off. The determination of the energy cut-off remains, therefore, very uncertain. A smaller energy cut-off can be compensated by a greater matrix element G. For example, with a pairing parameter $g_0 = 27\,\mathrm{MeV}$, we find that to the corresponding energy cut-off—i.e. reproducing the experimental odd-even mass differences with a similar accuracy—is reduced by a factor of 2. It should be remembered that in the constant-G model the pairing parameters G and ε_Λ have no unique physical meaning and that the parametrization (197)–(198) is entirely arbitrary.

It can be seen that the semi-classical prediction of the shell parameters c_1 and $c_2\gamma_0^2$ is in close agreement with the above result. Since it has been shown in Section II.4.2 that $c_2 \simeq \frac{\sqrt{3}}{\sigma_a}$, if we use the semi-classical values of $\alpha = 0.12\,\mathrm{MeV}^{-1}$ and $\gamma_0 = 0.12\,\mathrm{MeV}^{-1}$, we find $c_1 = 0.24\,\mathrm{MeV}^{-1}$ and $c_2\gamma_0^2 = 0.031\,\mathrm{MeV}^{-1}$, in good agreement with the adjusted values. However, the use of the shell functions (181) can lead to an overestimate of the pairing gaps at magic numbers.

As regards the condensation energy E_p which determines the reduction in the ground-state energy of the system as a result of the correlation effects, it can be deduced from the gap parameter and the single-particle level density by the relation

$$E_p = c_\Delta\ \tilde{a}\ \Delta_0^2 \tag{199}$$

where we introduce a new parameter c_Δ, theoretically equal to $\frac{3}{2\pi^2}$. However, large deviation from this value can be expected, as already seen in Section II.4.4.

II.5.2 Summary of the parametrized level density formula

The density of levels with spin J at an excitation energy U in a spherical nucleus (Z, A) is given by

$$\rho(U,J) = \rho(U, M = J) - \rho(U, M = J+1) \tag{200}$$

where the M-dependent level density is obtained from the relation

$$\rho(U,M) = \frac{1}{(2\pi)^2\sqrt{D}}\, \mathrm{e}^{S(U,M)} \tag{201}$$

The entropy as a function of the excitation energy can be derived from its temperature dependence, provided that the equation defining the excitation energy as a function of the temperature is solved. Since the function $U(T)$ exhibits a simple monotonic behaviour, the numerical inversion of that relation does not raise any problem. The T-dependent entropy taking the pairing and shell effects into account is given by

$$\begin{aligned} S(T) &= \sum_{q=n,p} S_q(T) \\ &= \sum_{q=n,p} 2F(\Delta_q/T)\; a_q(\omega_{Fq}T)\; \omega_{Fq}T \end{aligned} \tag{202}$$

with

$$a_q(T) = \tilde{a}_q + \frac{\gamma_q^2 \delta W_{1q}}{(1+\gamma_q^2 T^2)^2} \tag{203}$$

$$F(x) = \frac{1}{\ln 2}\left[\ln\left(1+\mathrm{e}^{-x}\right) + \frac{x}{1+\mathrm{e}^{x}}\right] \tag{204}$$

$$\Delta_q(T) = \Delta_{0q}\left[1 - \left(\frac{T}{T_{cr,q}}\right)^m\right]^{1/2} \qquad \text{for } T < T_{cr,q} \tag{205}$$

$$= 0 \qquad \text{for } T \geq T_{cr,q} \tag{206}$$

$$\omega_{Fq}(T) = 1 + u_1 \frac{\Delta_q}{T}\left(1 - \mathrm{e}^{-u_2\Delta_q/T}\right) \tag{207}$$

The excitation energy including the collective rotational motions is given by

$$\begin{aligned} U(T) &= \sum_{q=n,p} \left[U_{iq}(T) + U_{\Delta,q}(T)\right] + E_{rot}(T) \\ &= \sum_{q=n,p} \left[\frac{1}{\omega_{Fq}} F(\Delta_q/T) a_q^u(\omega_{Fq}T)\,(\omega_{Fq}T)^2 + U_{\Delta,q}(T)\right] + E_{rot}(T) \end{aligned} \tag{208}$$

with

$$a_q^u(T) = \tilde{a}_q + \frac{1-\gamma_q^2 T^2}{(1+\gamma_q^2 T^2)^2}\,\gamma_q^2 \delta W_{1q} \tag{209}$$

$$U_{\Delta,q}(T) = c_\Delta \tilde{a}_q \left(\Delta_{0q}^2 - \Delta_q^2\right) \qquad \text{for } N_q \text{ even} \tag{210}$$

$$= c_\Delta \tilde{a}_q \left(\Delta_{0q}^2 - \Delta_q^2\right) - \Delta_{0q} \qquad \text{for } N_q \text{ odd} \tag{211}$$

$$E_{rot}(T) = \frac{1}{2}\, f_\sigma\, \frac{M^2}{\left[\sigma_n^2(T) + \sigma_p^2(T)\right]}\, T \tag{212}$$

$$\sigma_q^2(T) = h(\Delta_q/T)\,\frac{\mathcal{I}_{rig,q}}{\hbar^2}\,\frac{a_q(\omega_{hq}T/\sigma_a)}{\tilde{a}_q}\,\omega_{hq}T \tag{213}$$

$$h(x) = \mathrm{sech}^2 x/2 \tag{214}$$

$$\omega_{hq}(T) = 1 + v_1 \frac{\Delta_q}{T}\left(1 - \mathrm{e}^{-v_2 \Delta_q/T}\right) \tag{215}$$

and the determinant factor is approximated by the expression

$$D(T) = \frac{72}{\pi^4}\,\tilde{a}_n \tilde{a}_p\,(\tilde{a}_n + \tilde{a}_p)\,\left[\sigma_n^2(T) + \sigma_p^2(T)\right]\,T^5 \tag{216}$$

The theoretically known constants are

$$u_1 = 0.083 \qquad u_2 = 0.5$$

$$v_1 = 0.110 \qquad v_2 = 0.5$$

$$m = 3.23 \qquad \sigma_a = \frac{\pi^2}{12 \ln 2}$$

The critical temperature is related to the ground-state pairing gap by the BCS expression

$$T_{cr,q} = \frac{\Delta_{0q}}{1.75} \tag{217}$$

The classical expression for the rigid-body value of the moment of inertia is

$$\frac{\mathcal{I}_{rig,q}}{\hbar^2} = \frac{2}{5}\frac{\mathrm{m}R^2}{\hbar^2} N_q \tag{218}$$

The level density parameters can been expressed, provisionally, by the functionals:

$$\tilde{a}_q = \frac{1}{2}\alpha A\,\left(1 \pm \frac{1}{3} I\right) \tag{219}$$

$$\gamma_q = \gamma_0 A^{1/3}\,\left(1 \mp \frac{1}{3} I\right) \tag{220}$$

while we consider at this stage the parameters α, γ_0, f_σ, c_Δ as free parameters to be adjusted to reproduce experimental data.

The shell correction energies δW_{1q} have been extracted from the mass formula of Hilf et al. (1976) and the ground-state pairing gaps Δ_{0q} from formula (191).

II.5.3 Comparison of the theoretical level density formula with experimental data

In spite of considerable experimental efforts made to derive nuclear level densities, the lack of reliable data—especially over a wide energy range—constitutes the main problem that the nuclear level density theories have to face. Yet a large number of analyses of slow neutron resonances and of cumulative numbers of low energy levels have greatly helped to obtain experimental values of the level density parameters. Other sources of information have also been suggested, such as analyses of spectra of evaporated particles and coherence widths of cross-section fluctuations. However, most of these experimental data are affected by systematic errors resulting from experimental uncertainties as well as the use of approximate theories. For example, it is well known that a large number of levels can be missing in neutron resonance data or in the nuclear spectrum at low energies. It is now also accepted that the only method enabling the determination of level densities at high excitation energies (around 20 MeV)—i.e. the fluctuation width data—cannot give reliable information. It has been shown (e.g. Huizenga et al., 1969) that the spacing of zero spin levels in a compound nucleus can be calculated from differential cross-sections to isolated levels. This method requires an estimate of the energy dependence of the average width Γ which, in turn, can be calculated only if the level density of the compound nucleus is already known. Unfortunately, rather inaccurate approximations to the level density are generally used in the estimation of the experimental data. Moreover, these analyses require the knowledge of the spin cut-off factor of the compound nucleus, the determination of which remains problematic. The sets of optical model parameters used in the evaluation of the particle transmission coefficients are also doubtful (Ivascu et al., 1987). Other methods have been proposed to extract level densities, but they all remain highly uncertain (for a review, see Huizenga and Moretto, 1972). The nuclear reaction theories can also be used to test the predictive power of the nuclear level density formulae. In particular, Avrigeanu and Avrigeanu (1991) stressed the need for realistic nuclear level density

prescriptions for the study of fast-neutron induced reactions. They showed that reaction cross-sections obtained in the framework of the generalized Geometry-Dependent Hybrid (GDH) pre-equilibrium emission model plus Hauser-Feshbach statistical model, are extremely sensitive to the adopted prescription for the level density. This approach requires the knowledge of both the nuclear level densities for the statistical model calculations and the exciton state densities involved in the GDH formalism. These two densities can be derived from one single level density formula, provided that the renormalization factor—defined as the ratio of the two-component level density to the one-component level density—can be calculated (Akkermans and Gruppelaar, 1985). The excitation-energy-dependent level density parameters appear to play a crucial role in the prediction of the reaction cross-sections, so that the large amount of experimental data on fast-neutron induced reaction cross-sections could be used to test the predictive power of the level density formulae. However, this new and promising technique is not free from uncertainties. In particular the renormalization factor remains to be estimated in a consistent way.

For these reasons, we will restrict ourselves essentially to the experimental data concerning the neutron resonance spacings, which correspond to the most extensive and reliable source of information on level densities. If this method limits the evaluation of the level density at one specific energy (equal to the neutron binding energy), it makes possible to investigate the level density in the entire range of A values throughout the whole periodic table. Moreover, the experimental data concern excitation energies at which shell and pairing effects are expected to play an important role. In order to illustrate the energy dependence of the theoretical level density formula, the total level density of ^{60}Co will also be studied and compared to the known experimental data.

(i) The s-neutron resonance spacings

From the resonance pattern obtained in neutron capture reactions at a low energy, it is possible to estimate by direct counting the number of levels of the compound nucleus in a particular neutron

energy interval and at an excitation energy around the neutron binding energy. The neutron resonances mostly result at such low energies from s-waves, so that the spin of the excited levels is either 1/2 if the spin of the target ground state is zero, or $J = J_0 \pm 1/2$ if the spin of the target nucleus is J_0. Similarly, the parity of the excited level corresponds to that of the ground state of the target nucleus. The average resonance spacing $\bar{D}$ is thus given by

$$\frac{2}{\bar{D}_{th}} = \begin{cases} \rho(S_n + \frac{1}{2}\Delta E, J_0 + \frac{1}{2}) + \rho(S_n + \frac{1}{2}\Delta E, J_0 - \frac{1}{2}) & \text{for } J_0 \neq 0 \\ \rho(S_n + \frac{1}{2}\Delta E, \frac{1}{2}) & \text{for } J_0 = 0 \end{cases} \tag{221}$$

where S_n is the neutron separation energy of the compound nucleus and ΔE the upper boundary of the neutron energy interval in which $\bar{D}$ is determined. The factor 2 introduced in the left-hand side of expression (221) results from the classical assumption of the equipartition of both parities.

Level spacing information has been obtained from slow-neutron-resonance data for about 200 nuclei and can be found in several compilations (Baba, 1970; Dilg et al., 1973; Kataria et al., 1978; von Egidy et al., 1988; Vonach et al., 1988). To improve the reliability of the most recent data, mostly extracted from the compilation of neutron resonance data of Mughabghab et al. (1981), statistical techniques have been developed to estimate the fraction of missed levels in an experimental sequence and the contamination of spurious p-wave resonances (Vonach et al., 1988). Yet we have restricted ourselves to the 100 nuclei thought to be spherical and found in Kataria et al. (1978). The introduction of the deformation as a new parameter will be rapidly discussed (see Section II.5.4), but essentially postponed to a later study. The experimental level spacings have been taken from the above compilations. For several cases there is considerable scatter in the available values of $\bar{D}_{exp}$, so that the most recent data have been used in the least square fitting to theory.

Since the reduction of the moment of inertia below the rigid body value remains to be confirmed, we will discuss at this stage two cases only: $f_\sigma = 1$ corresponding to the classical assumption of a rigid body value for the moment of inertia and $f_\sigma = 3.5$ corresponding to the possible

average reduction predicted by the semi-classical approximation developed in Chapter II.3. The parameters α, γ_0 and c_Δ have been adjusted in order to minimize the mean square deviation $\sum_{N_e}(\ln \bar{D}_{th}/\bar{D}_{exp})^2/N_e$ (where N_e is the number of nuclei included in the fittings). The following parameters

for $f_\sigma = 1$: $\alpha = 0.118\,\mathrm{MeV}^{-1}$ $\gamma_0 = 0.34\,\mathrm{MeV}^{-1}$ $c_\Delta = 0.038$

for $f_\sigma = 3.5$: $\alpha = 0.106\,\mathrm{MeV}^{-1}$ $\gamma_0 = 0.34\,\mathrm{MeV}^{-1}$ $c_\Delta = 0.038$

lead identically to a minimum mean square deviation equal to 0.24. The ratios $\bar{D}_{th}/\bar{D}_{exp}$ for the nuclei considered are displayed in Fig.32. All experimental spacings appear to be predicted within a factor of 4 and mostly within a factor of 2. The mean square deviation is also remarkably low in comparison with previous works. The formula of Kataria et al. (1978) including the shell effects, but treating the pairing correlations by a simple energy shift, as prescribed by Gilbert and Cameron (1965), gives a mean square deviation of around 0.4. This difference in the treatment of the pairing interaction has important consequences for the reliability of the formula. It should be recalled that the phenomenological pairing energies introduced by Gilbert and Cameron (1965) have been extracted arbitrarily from the outdated semi-empirical mass formula of Cameron and Elkin (1965) and should consequently be considered greatly unreliable. If we compare our results with microscopic calculations based on the same theoretical models (e.g. Arnould and Tondeur, 1981), it can be seen that the deviations from experimental data are greatly reduced relative to the microscopic results (where deviations up to a factor of 100 are observed). Yet it should be mentioned that these microscopic results are obtained without any fitting to level density data. In that respect, our method has the advantage of enabling a simple fitting while the adjustment of the microscopic parameters on a large body of experimental data remains a difficult task.

Some comments about the values of the adjusted parameters are necessary. As regards the $\tilde{a}$-parameter, it can be seen that the volume contribution is sufficient to describe the global trend of a in the whole periodic table. To study the mass dependence of the $\tilde{a}$ parameter, it is possible

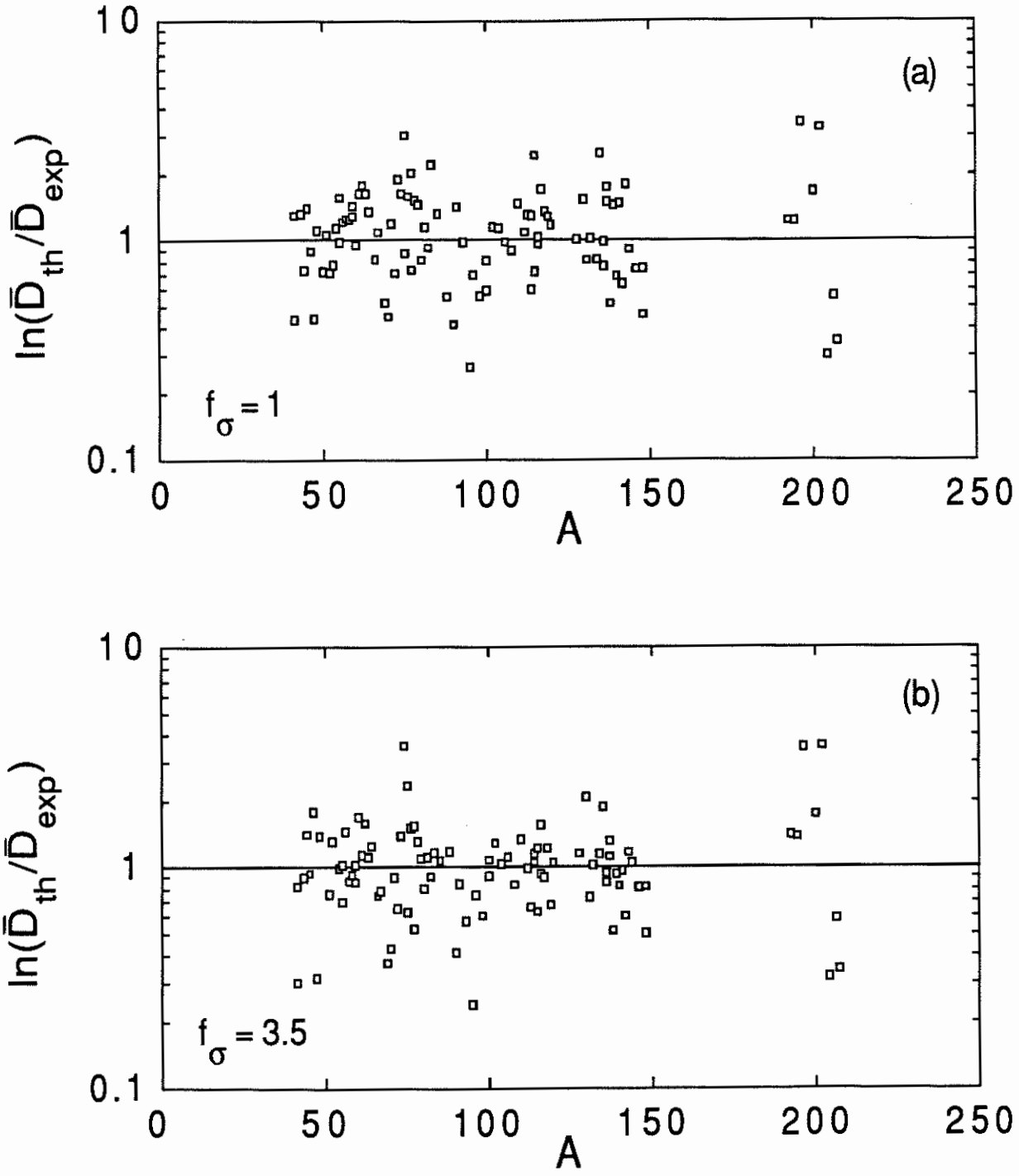

Figure 32. Comparison between theoretical ($\bar{D}_{th}$) and experimental ($\bar{D}_{exp}$) values of the s-neutron resonance spacings at an excitation energy equal to the neutron separation energy. The theroretical predictions have been obtained with the parameter set given in the text and corresponding for (a) to $f_\sigma = 1$ and for (b) to $f_\sigma = 3.5$.

to derive the so-called experimental $\tilde{a}$ parameter for each nucleus, deduced from the experimental spacings by solving equation (221) in which the experimental value $\bar{D}_{exp}$ is substituted in the left-hand side. It is of importance to stress that the resulting $\tilde{a}$-parameters depends not only on the theoretical level density model used, but also on the parameters adopted to solve equation (221). For instance, the experimental $\tilde{a}$ values are drastically different if use is made of the parameter $f_\sigma = 1$ or $f_\sigma = 3.5$. The denomination *experimental* is consequently rather excessive. The so-deduced $\tilde{a}$ parameters corresponding to the parametrization $f_\sigma = 1$, $\gamma_0 = 0.34\,\mathrm{MeV}^{-1}$ and $c_\Delta = 0.038$ are displayed in Fig. 33 and compared with the linear dependence $\tilde{a} = 0.118A\,\mathrm{MeV}^{-1}$. Yet it should be emphasized that neither the experimental data nor the theoretical level density formula are accurate enough to impose heavy constraints on the $\tilde{a}$-parameter. A fit using the same parameter set (corresponding to $f_\sigma = 1$) is obtained with a similar accuracy in the prediction of the experimental data, if we use the formula: $\tilde{a} = (0.11A + 0.09A^{2/3} - 0.0015ZA^{1/3})\,\mathrm{MeV}^{-1}$ (where the A-functional has been derived in Section II.5.1). Therefore, the remaining uncertainties in the evaluation of the experimental $\tilde{a}$-parameter impede the determination of the surface contribution to the $\tilde{a}$-parameter from experimental data. In addition, it can be seen from the adjusted α value that the uncertainty related to the value of the effective moment of inertia affects the prediction of the $\tilde{a}$-parameter by around 10%. This reduction factor is far from being negligible because of the exponential dependence of the nuclear level density on the $\tilde{a}$-parameter.

The shell effects on the level density appear to be fairly well reproduced by our formula over the entire A-range considered. No systematic deviations at shell closures are seen in Fig. 32. However, because of the relatively strong shell effects observed in the experimental level spacings, an important increase of the shell parameter γ_0—by a factor of 3 relative to the semi-classical prediction—has been necessary. Since only one parameter has been used to describe the shell effects on the a-parameter, the value of γ_0 takes over all the inaccuracies associated with our

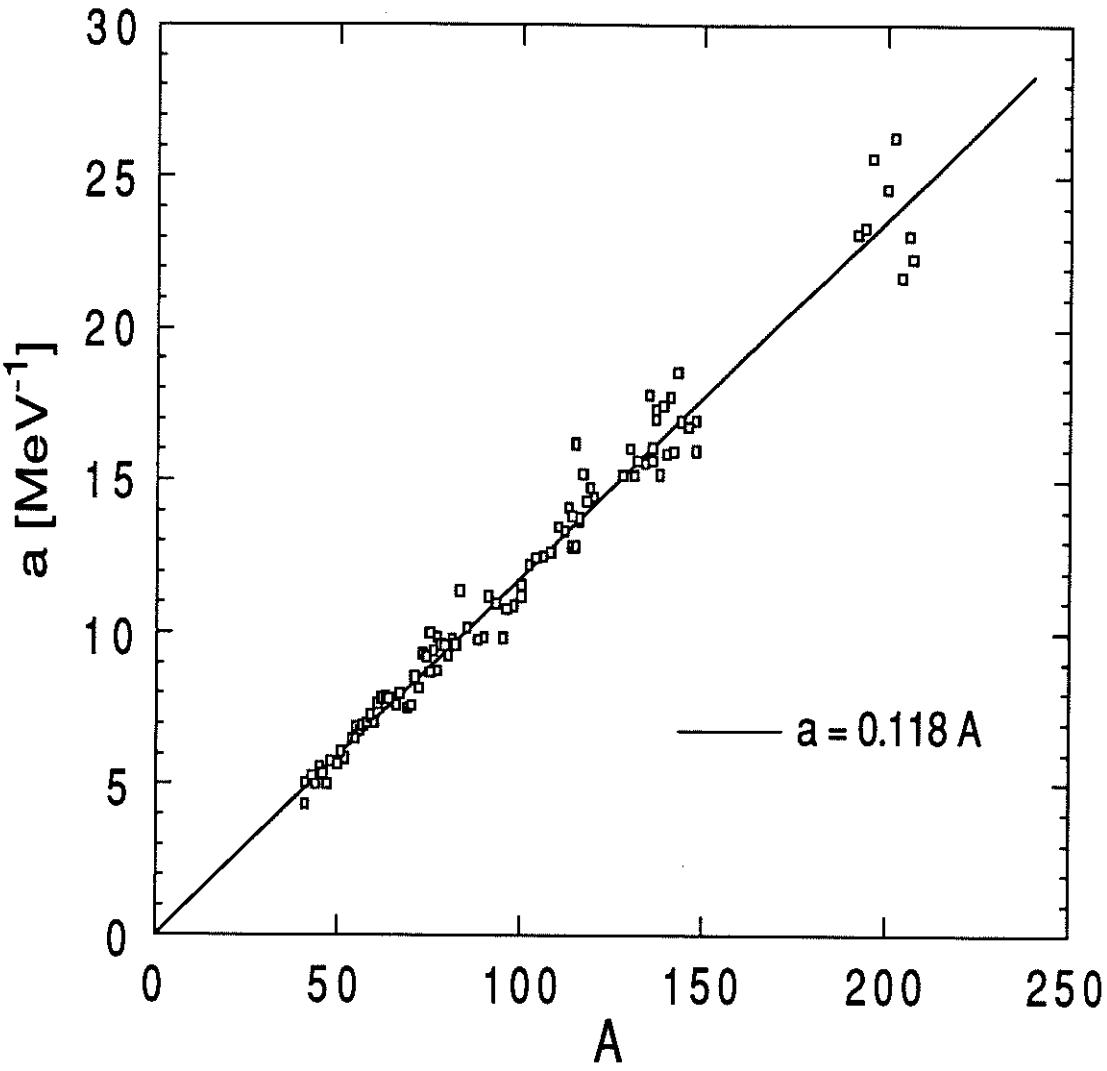

Figure 33. Plot of the a-parameter versus the mass number A for the spherical nuclei considered. The squares correspond to the a-values reproducing the experimental neutron resonance data when use is made of the parameter set $f_\sigma = 1$, $\gamma_0 = 0.34\,\mathrm{MeV}^{-1}$ and $c_\Delta = 0.038$. The straightline corresponds to the linear regression $a = 0.118A\,\mathrm{MeV}^{-1}$.

treatment of the shell structure. In particular, it turns out that the main uncertainties are related to the amplitude of the ground-state shell correction energy. In addition to the problems inherent to the use of a semi-empirical shell correction energy δW_1, as already discussed in detail, two main reasons can explain this underestimation of the semi-classical value of γ_0. First, it has already been mentioned (see Section II.2.3) that the approximations made to derive the temperature-dependent excitation energy lead to an overestimate of the ground-state shell correction energy by a factor of 1.2. In that case, the shell-dependent contribution to the a-parameter is underestimated by the same factor. A comparison with the results of Kataria et al. (1978) even suggests an underestimation of δW_1 by a factor $\pi^2/6$. However, this discrepancy remains to be confirmed. A second problem related to the shell model dependence of the mass correction is bound to arise when dealing with shell corrections. This problem is also at the origin of the well known lead anomaly. The semi-empirical or experimental ground-state shell energy of ^{208}Pb using the droplet model of Hilf et al. (1976) is $\Delta M_{exp} = -11.0\,\mathrm{MeV}$. Yet a Woods-Saxon potential adjusted to fit the experimental positions of the single-particle subshells in lead is known to predict a value of around $-20\,\mathrm{MeV}$ (see for example Table 1 in Section II.2.4). Similarly, the calculation of the mass correction using the experimental single-particle energies leads to a value of around $-21\,\mathrm{MeV}$ (e.g. Brack et al., 1972) exceeding largely the so-called experimental mass. The origin of this discrepancy has been associated with the inaccuracy in the use of an average one-body potential (Brack et al., 1972). Even for the best possible shell-model potential, i.e. the one deviating the least from the actual nuclear field, some differences between the shell model energies and the actual single-particle energies are expected due to non-smooth terms in the real nuclear average potential. Consequently, if the actual single-particle energies were used in the calculations, then the fluctuating part of the average potential energy should be taken into account as well. For that reason, the quality of the shell-model potential is generally judged by its ability to reproduce some important quantities

related to the single-particle state distribution averaged over the essential shell intervals. When dealing with level density calculations, special care should be taken of the definition of the different averaged quantities affecting the level density. In particular, it could seem more consistent to use shell-model potential which can reproduce accurately the positions of the individual single-particle states in real nuclei. In any shell model calculation, the quantity on which the calculated level density crucially depends is the density of single-particle states at the Fermi energy (especially at an excitation energy as low as the neutron separation energy). Under these conditions, it should be required from the shell-model potential to be accurate in reproducing the positions of the individual single-particle states in real nuclei, rather than quantities averaged over larger energy intervals, such as the shell correction energy. This corresponds for the special case of ^{208}Pb to an increase of the shell correction energy by a factor of around 2. If the two mentioned corrections to the amplitude of the shell energy are taken into account by a phenomenological increase of δW_1 by a factor of 2.4, the shell effects in the experimental level spacings can be reproduced with the same accuracy as above with the value of $\gamma_0 = 0.15\,\mathrm{MeV}^{-1}$, in close agreement with the semi-classical prediction. Moreover, the introduction of a new parameter modulating the amplitude of the shell energy is probably more consistent than the use of an overestimated value for γ_0.

As regards our treatment of the pairing correlations, it is of interest to see that with the adopted parameter sets, about 30% of the analysed experimental spacings at the binding energy appear to be in the superconducting phase. Consequently, even at an energy equal to the binding energy, the correlation effects still affects the level density in a more complicated way than predicted by the classical energy shift. The parametrization of our pairing treatment has been exclusively included in the parameter c_Δ. This explains why an important reduction by a factor of 4 relative to the value of $\frac{2}{3\pi^2}$ has been required to reproduce the experimental data. It includes not only the uncertainties related to the fitted values of the pairing gaps, but also the approximation to the

superconducting model as a whole. In particular, the blocking effects have been treated in a rather crude way. Since experimental data mostly concern level densities of odd-mass and doubly odd nuclei, the simple treatment adopted here might affect the accuracy of the theoretical predictions. This large reduction in the energy shift is also at the origin of the relatively low value of the parameter α. if use is made of a larger value of c_Δ, a larger value of α is required to reproduce the experimental data.

(ii) The energy dependence of the level density

A much smaller amount of reliable experimental data is available concerning the energy dependence of the level densities than about the resonance spacings at the neutron separation energy. They are mainly obtained from cross-section fluctuation measurements, and remain very uncertain, as already discussed. However, in the special case of ^{60}Co, the neutron resonance spacings are available at the same time as the fluctuation width data (which are obtained at an energy close to the neutron separation energy: $U < 14\,\mathrm{MeV}$). Since the parametrized Back-Shifted Fermi gas model can be expected to give a reliable estimate of the level density in a close interval around the neutron separation energy, the uncertainties in the extraction of the level densities from the fluctuation width measurements are reduced at the same time. In most of the cases, the two type of experimental data cannot be obtained simultaneously or concern excitation energies significantly different, so that the reliability of the extracted data becomes very doubtful. Fig. 34 shows the experimental level density of ^{60}Co resulting from level countings at energies $U < 2\,\mathrm{MeV}$, neutron resonance spacings at $U = 7.5\,\mathrm{MeV}$ and fluctuation width data at energies $9\,\mathrm{MeV} < U < 14\,\mathrm{MeV}$ (Dilg et al., 1973). Fig. 34 also shows our analytical approximation to the total level density obtained with the parameter set $\alpha = 0.118\,\mathrm{MeV}^{-1}$, $f_\sigma = 1$, $\gamma_0 = 0.34\,\mathrm{MeV}^{-1}$ and $c_\Delta = 0.038$, i.e. the parameters used to reproduce the neutron resonance spacings data. It can be seen that the agreement with the experimental data is fairly good. The values used for the level density

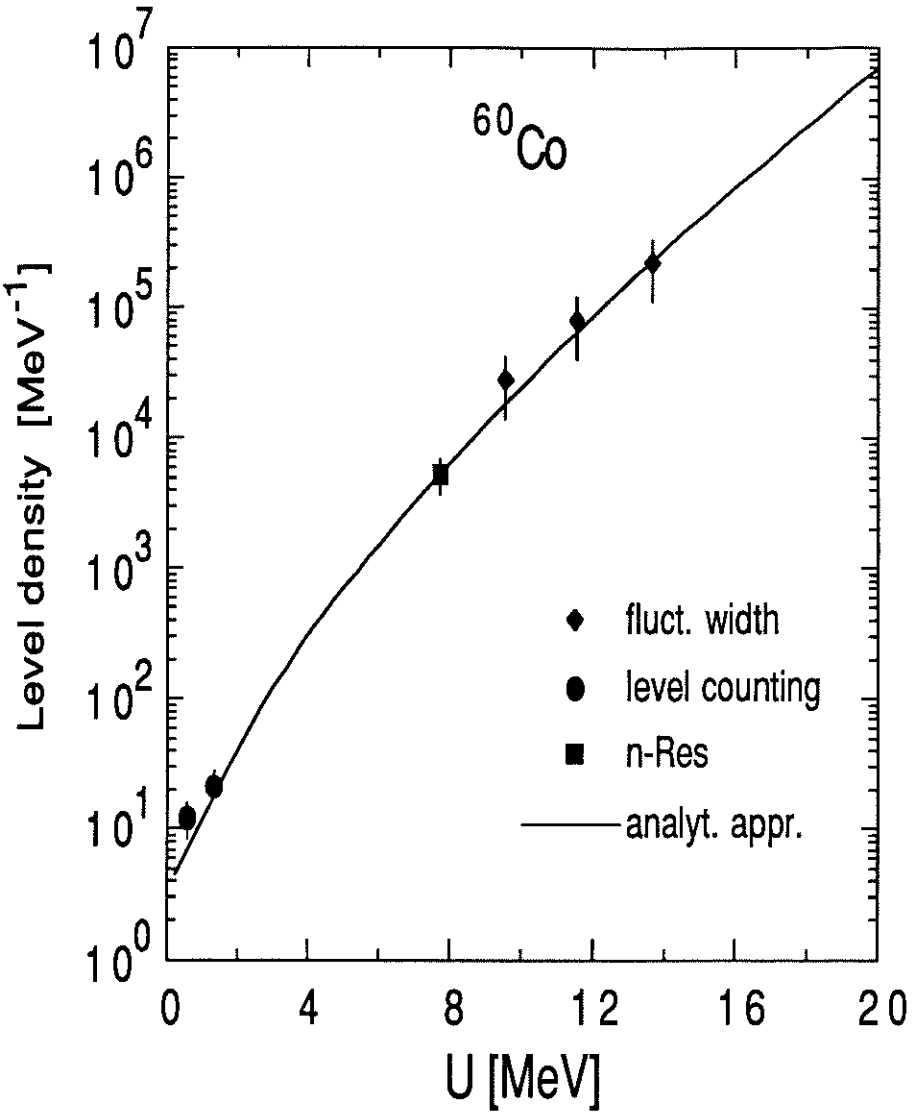

Figure 34. Comparison of the experimental and calculated total level density of ^{60}Co. The experimental data are taken from Dilg et al. (1973). The analytical approximation (full line) to the level density has been obtained with the parameter set: $f_\sigma = 1$, $\alpha = 0.118\,\mathrm{MeV}^{-1}$, $\gamma_0 = 0.34\,\mathrm{MeV}^{-1}$ and $c_\Delta = 0.038$.

parameters lead to $\tilde{a} = 7.08\,\mathrm{MeV}^{-1}$ and a condensation energy equal to $E_p = -2.5\,\mathrm{MeV}$, which are close to the classically adopted values of the Back-Shifted Fermi gas parameters reproducing the level density of ^{60}Co (e.g. Ivascu et al., 1987). Our theoretical formulation predicts a critical energy $U_{cr} = 4\,\mathrm{MeV}$ which can be clearly observed in Fig. 34. The shell effects, resulting from the proton configuration close to a magic number, also affect the total level density at low energies. Both the pairing and shell effects introduced in our formulation greatly reduce the level density at low energies. If at high energies ($U \gtrsim 15\,\mathrm{MeV}$) our analytical model reduces globally to a Back-Shifted Fermi gas formula, the two models lead to significantly different predictions of the level density at low energies.

II.5.4 Conclusion

The level density formula prescribed in the present chapter appears to reproduce the experimental level spacings in a very satisfactory way. By using 3 parameters—characterizing the asymptotic behaviour of the exponential dependence of the level density, and the shell and pairing effects—we are able to predict the experimental data within a factor of 4 in the whole A range throughout the periodic table. Considering the simplicity of the level density formula and its ability to describe the shell and pairing effects, this result should be regarded as much more promising and reliable than both the previous analytical approximations and the lengthy and still problematic microscopic calculations. Yet it is important to stress that the constraints imposed by the comparison with experimental data are not sufficiently strict to limit the possible parameter space of the analytical level density formulae. This problem can result from the theoretical shortcomings of the analytical approximation to the actual level density and/or from the lack of accurate and reliable experimental data. The availability of experimental level densities, essentially over a wide energy range, would be of considerable value in the construction of reliable level density models.

In comparison with previous level density models, our new treatment has the dual advantages of simplicity and reliability. As far as the simplicity is concerned, the use of an analytical formulation to the level density is of particular significance in certain fields of nuclear astrophysics, such as in the r-process calculations, where hundreds of nuclear reaction rates, requiring the knowledge of the level density values, have to be estimated theoretically. The only quantities required for the computation of the level density are the ground-state shell correction energies (and the nuclear deformation when deformed nuclei are considered). It has also been shown that the adopted analytical approximation to the level density is able to reproduce very accurately the numerical BCS calculations based on a discrete single-particle level scheme, and more precisely the corresponding shell and pairing effects. However, for completeness, before applying this new level density

description to the calculation of nuclear reaction cross-sections, two major improvements are required for the analytical approximation. The first improvement concerns the behaviour of the level density for excitation energies approaching zero, while the second goal to reach corresponds to a generalization of the level density formulation for deformed nuclei.

It is well known that for excitation energies $U \lesssim d$ (where d is the average spacing between the one-Fermion levels) the approximation used in the saddle-point method is no longer valid (e.g. Ericson, 1960). Similarly, the temperature concept has little meaning for excitation energies smaller than the single Fermion spacing. This shortcoming, inherent to the saddle-point approximation, is reflected in the divergence of the level density formula at the ground state. Lang and Le Couteur (1954) improved the original formula of Bethe (1936) by introducing a phenomenological correction to the level density denominator which removes the singularity at $U = 0$. More recent corrections (Grossjean and Feldmeier, 1985) have been achieved by subtracting the ground-state contribution before using the saddle-point approximation. This approach, even if more consistent, leads to a more complicated formulation of the level density. Engelbrecht and Engelbrecht (1991) reinvestigated the behaviour of the level density at low temperatures on the basis of the truncated Fermi gas model. In this approach, the finite number of fermions are distributed in a finite number of levels, unlike the Fermi gas model. A simple quadratic form is proposed to approximate the energy dependence of the level density at low energies. Such a treatment can easily be added to our level density formulation by joining smoothly the quadratic form at low energies onto our level density expression. This corrective behaviour of the level density at very low energies can be non-negligible in cross-section calculations when the knowledge of the level density down to the ground state is required.

In the analytical approach developed in the present work, only spherical nuclei have been considered, so that the effects of nuclear deformation have not yet been taken into account ex-

plicitly, except through the ground-state shell correction energy (see Section II.5.1). It is now accepted that deformed nuclei exhibit a larger level density relative to the spherical case because of the appearance of coherent effects of a collective nature. The enhanced nuclear level density for deformed nuclei was originally accounted for by incorporating a constant collective enhancement factor for rotational and vibrational degrees of freedom (Bjørnholm et al., 1974). The excitation-energy dependence of the enhancement factor has also been investigated (Ignatyuk, 1975; Hansen and Jensen, 1983). Another way to account for the deformation effects is to correct the spherical level density parameters by introducing an explicit dependence on the deformation parameter θ (e.g. Kataria, 1985). The deformation degree of freedom is expected to affect mainly the quantities $\tilde{a}$ and δW_1. The ground-state nuclear deformations are generally determined in the macroscopic-microscopic model of nuclear masses, where the droplet surface term as well as the shell correction term depend significantly on the deformation parameter of the nucleus (see Section II.5.1). When the excitation energy increases, the shell effects on the entropy vanish and all the nuclei are expected to acquire a spherical shape. Consequently, the enhancement factor of the level density is believed to result from the deformation effects on both the ground-state shell correction energy and the deformation energy. Since for deformed nuclei the average deformation θ decreases with the increasing excitation energy, the shell correction energy (184) $M_s(N, Z, \theta)$ becomes more and more positive and enhances the nuclear level density. In addition, when the excitation energy increases, the droplet deformation energy follows the decrease of the average deformation, so that more energy becomes available for internal excitations. This second effect, even if less significant, also leads to an increase of the nuclear level density. Kataria (1985) showed that the deformation effects could be taken into account in a relatively simple way by introducing into the spherical level density expression the explicit dependences $\tilde{a}(\theta)$ and $\delta W_1(\theta)$. Such a technique can easily be applied to our formulation of the level density.

However, before generalizing the present formulation of the level density for deformed nuclei and very low energies, it is important to stress that many uncertainties still remain in the description of spherical nuclei. In particular, the problematic spin distribution and the possibility of a significant reduction of the moment of inertia below the rigid body value have to be carefully worked out. The treatment of the shell effects on the level densities as well as on the ground-state masses or the pairing gaps should also be improved. All these nuclear models based on the macroscopic-microscopic approach still suffer from severe uncertainties and inconsistencies in the way they relate the shell-independent and the shell-dependent contributions. For a better understanding of these different phenomena, the semi-classical approximation to the single-particle level density appears to be of great value as a means of exploring the effects due to the nuclear shell structure. In particular, the semi-classical approach provides a fundamental insight into the microscopic, i.e. shell-related, aspects of nucleonic motion, as already emphasized by Strutinsky (1989) for the macroscopic and microscopic aspects in nuclear fission. In the case of the level density calculation (as well as nuclear fission process), the original Fermi gas model corresponds to the macroscopic level of description. By adding shell corrections we move one step down towards the microscopic level—the bridge between the two levels being provided by statistical physics. In this respect, the semi-classical approach enables us to describe the shell structure as a certain macroscopic property of the single-particle phase space, and constitutes a remarkable qualitative as well as quantitative tool for exploring the microscopic aspects of a quantum system.

In spite of the remaining problems, we believe that our method constitutes one of the most reliable evaluations of the level density for nuclei experimentally not well known. We hope in this way to put nuclear reaction cross-section calculations, and consequently r-process calculations, on a more secure basis and to satisfy simultaneously the complementary demands of the nuclear physicists, on one side, and the nuclear astrophysicists, on the other side, which could be summarized,

respectively, by the dictums: *a theory need not be simple, provided it is right* and *a theory need not be right, provided it is simple*.

Appendix A: The energy-dependent single-particle level density

As demonstrated by Berry and Mount (1972) and Strutinsky and Magner (1976), the single-particle level density $g(\varepsilon)$ can be related to the Green's function by the equation

$$g(\varepsilon) = -\frac{1}{\pi} Im \int G(\mathbf{r}', \mathbf{r}, \varepsilon) \Big|_{\mathbf{r}' \to \mathbf{r}} d\mathbf{r} \qquad (A1)$$

Using the quasi-classical approximation to the Green's function G, expressed in terms of classical paths, the level density can then be represented in the form

$$g(\varepsilon) = \tilde{g}(\varepsilon) + g_{osc}(\varepsilon) \qquad (A2)$$

where $\tilde{g}(\varepsilon)$ is the smooth contribution to the total level density and corresponds in equation $(A1)$ to the contribution of the paths of zero length, i.e. the limit of the direct paths as $\mathbf{r}' \to \mathbf{r}$. On the other hand, the looped paths—involving an excursion away from the point $\mathbf{r}$ before returning—give rise to the oscillating contribution $g_{osc}(\varepsilon)$. The semi-classical evaluation of $g(\varepsilon)$ from expression $(A1)$ leads usually to analytically complicated formulae in the case of realistic potentials. However, it is possible to derive in a quite accurate and simple way the smooth contribution to the single-particle level distribution in a Woods-Saxon potential. As regards the oscillating part, we must restrict ourselves to the consideration of more simple nuclear potentials if we want to keep the usability character of the analytical approximation. In the particular case of the infinite square well, it becomes possible to obtain an analytically suitable representation of $g_{osc}(\varepsilon)$. Let us derive the semi-classical approximation to the smooth and oscillating single-particle level density for these two specific models of the average nuclear potential.

A.1 The smooth single-particle level density in a Woods-Saxon potential

It has been shown (Berry and Mount, 1972) that the smooth (or macroscopic) contribution $\tilde{g}$ to the total single-particle level density resulting from the paths of zero length corresponds to the

well-known Thomas-Fermi approximation and can be expressed in a relatively simple way by

$$\tilde{g}(E) = \left(\frac{\mathrm{m}}{2\pi\hbar^2}\right)^{3/2} \frac{2}{\sqrt{\pi}} \int_R [E - V(\mathbf{r})]^{1/2} \mathrm{d}\mathbf{r} \qquad (A3)$$

where E is the absolute energy of the nucleon (of mass m) enclosed in the potential well $V(\mathbf{r})$. The region R includes only the points $\mathbf{r}$ where $E > V(\mathbf{r})$ since in other regions no direct path exists.

When the volume V of the system is sufficiently large for effects associated with the diffuse surface region to be negligible, the density of eigenstates, as given by expression $(A3)$, is known to be quasi-continuous and proportional to V. Some simple cases are the infinite box ($\tilde{g}(\varepsilon) \sim \mathrm{V}\sqrt{\varepsilon}$) or the harmonic oscillator ($\tilde{g}(\varepsilon) \sim \mathrm{V}\varepsilon^2$) if the energy ε is measured from the bottom of the potential well. Yet the smooth single-particle level density in a more realistic potential which includes, for example, the diffuseness of the nuclear density distribution appears to differ significantly from those oversimplified models. A number of attempts have been made in the past to introduce finite size corrections to the Thomas-Fermi relation. Hill and Wheeler (1953) obtained for a system of Fermions confined in a potential well of volume V and surface area S with infinitely repulsive walls:

$$\begin{aligned} \tilde{g}(\varepsilon) &= \tilde{g}_V(\varepsilon) + \tilde{g}_S(\varepsilon) \\ &= \frac{D}{4\pi^2} \frac{2\mathrm{m}}{\hbar^2} \left[k\mathrm{V} - \frac{\pi}{4}\mathrm{S} + \cdots\right] \end{aligned} \qquad (A4)$$

where D is the degeneracy factor taking the spin (D=2) or the spin and isospin (D=4) degeneracy into account and $k = \sqrt{\frac{2\mathrm{m}}{\hbar^2}\varepsilon}$ is the wave number.

The simple model of Hill and Wheeler leads to a negative surface contribution which is in agreement with the concept of infinitely repulsive walls. However, realistic single-particle potentials for nucleons in nuclei differ from the idealized Hill-Wheeler box in two respects: it has a finite depth and a finite surface diffuseness. In addition, the nuclear potential is known to be momentum and energy dependent, so that an exhaustive description of the single-particle level density should also take the non-localicity of single-particle potentials into account.

The distribution of energy eigenstates in a potential box of finite depth has been considered by Balian and Bloch (1970). To take the finite diffuseness of the surface into account, Siemens and Sobiczewski (1972) generalized the Balian and Bloch expression. The density of single-particle states in a thin-skinned potential is finally given by

$$\tilde{g}(\varepsilon) = \frac{D}{4\pi^2}\frac{2\mathrm{m}}{\hbar^2}\left[k\mathrm{V} + (\delta - \frac{\pi}{4})\mathrm{S} + \cdots\right] \qquad (A5)$$

where δ is the phase shift of the wave function in the one-dimensional potential considered. In the particular case of a Woods-Saxon potential, it appears possible to express the phase shift δ by (Flügge, 1971)

$$\delta_{WS} = \tan^{-1}\frac{k}{\kappa} - \sum_{n=1}^{\infty}\tan^{-1}\frac{2k\mathrm{a}}{n} + 2\sum_{n=1}^{\infty}\tan^{-1}\frac{k\mathrm{a}}{n+\kappa\mathrm{a}} \qquad (A6)$$

where a is the thickness of the surface layer and κ is defined by

$$\kappa = \sqrt{\frac{2\mathrm{m}}{\hbar^2}(V_0 - \varepsilon)} \qquad (A7)$$

where V_0 is the depth of the Woods-Saxon potential. It is of interest to see that the Woods-Saxon surface density reduces to the Balian and Bloch expression when a $\rightarrow$ 0 and to Hill and Wheeler formula when a $\rightarrow$ 0 and $\kappa \rightarrow \infty$.

Therefore, for a nuclear potential characterized by a Woods-Saxon profile, the surface correction to the single-particle level density appears to be a rather complicated function of the energy ε, and of the two parameters V_0 and a. The function $\delta_{WS}(\varepsilon) - \frac{\pi}{4}$ is shown in Fig. A1, for a potential depth of 45 MeV and for three values of the diffuseness parameter a. It can be seen that around the Fermi energy (a typical value of the Fermi energy is 38 MeV for such a potential depth), the surface correction $\tilde{g}_S(\varepsilon)$ varies rapidly from negative values to positive values. Consequently, the sign of the surface contribution to the total single-particle level density at the Fermi energy strongly depends on the position of the Fermi energy or more precisely of the nucleonic separation energy $\mathrm{B} = V_0 - \varepsilon_F$. The strong influence of the diffuseness parameter can also be noticed: an

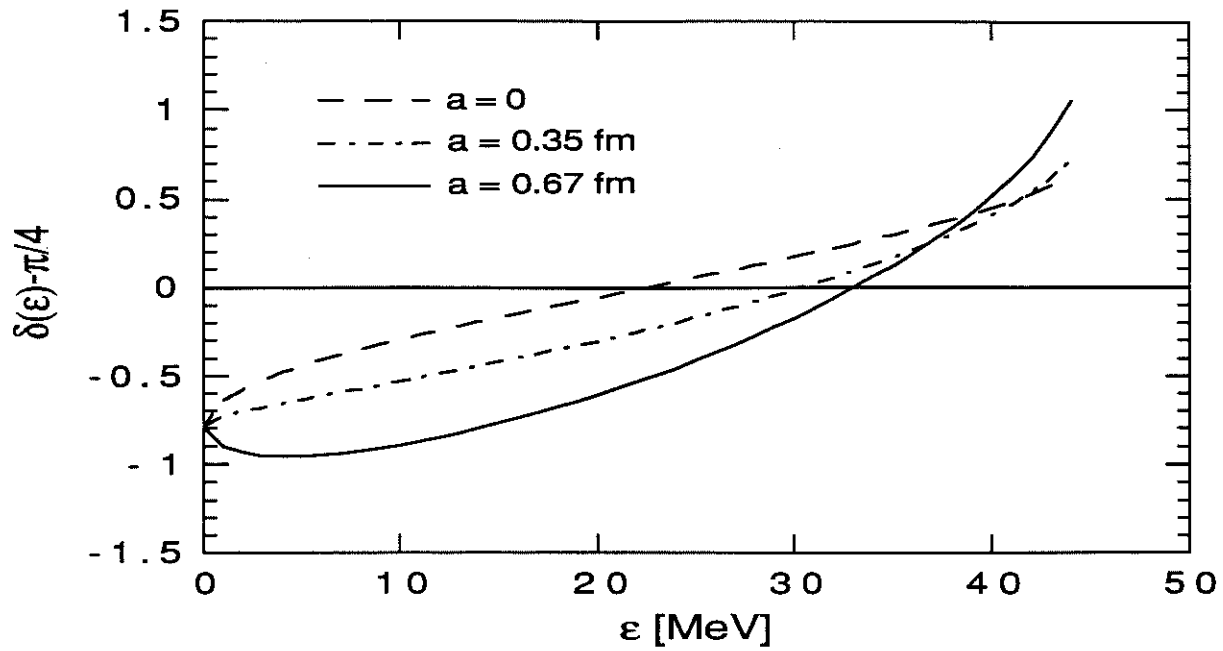

Figure A1. Phase shift $\delta(\varepsilon) - \frac{\pi}{4}$ for a Woods-Saxon potential as a function of the energy ε measured from the bottom of the potential well (equal to $V_0 = 45\,\mathrm{MeV}$). The phase shift is displayed for three values of the surface diffuseness parameter a.

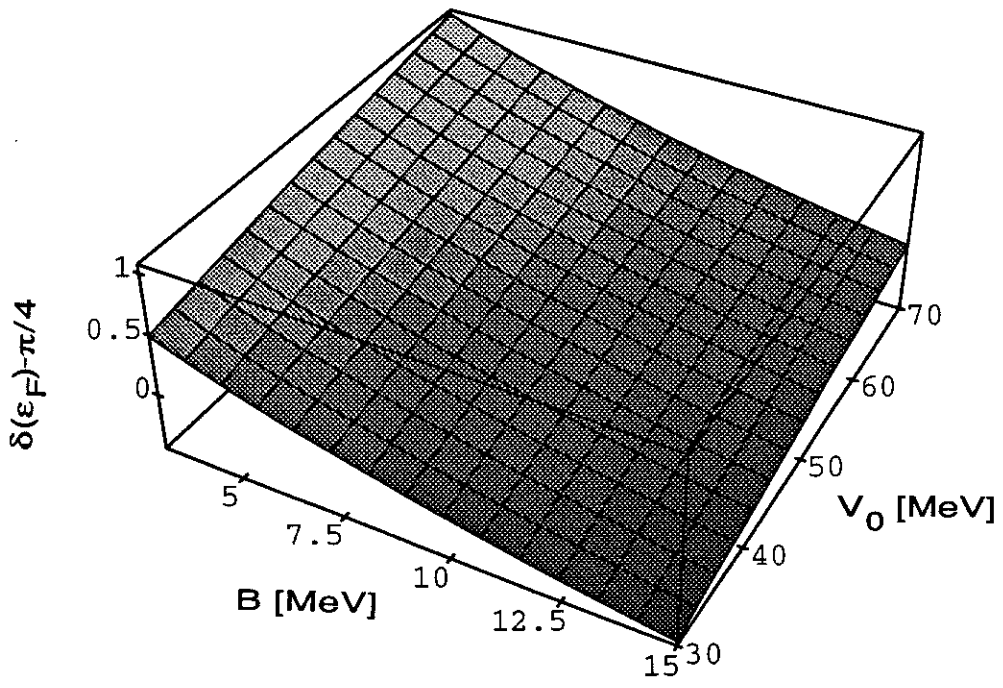

Figure A2. Plot of the phase shift $\delta(\varepsilon_F) - \frac{\pi}{4}$ for a Woods-Saxon potential as a function of the potential depth V_0 and of the nucleonic separation energy $\mathrm{B} = V_0 - \varepsilon_F$. The surface diffuseness parameter a is taken equal to 0.67 fm.

increasing diffuseness tends to reduce the surface contribution at the Fermi energy and can even change its sign. However, since realistic values of a are known to be confined in the approximate $0.55\,\mathrm{fm} \lesssim \mathrm{a} \lesssim 0.75\,\mathrm{fm}$ range (Handloser and Stocker, 1985), the a-dependence of the surface term is proportionally reduced. Therefore, we have neglected the a-dependence of the single-particle level density at the Fermi energy and considered an average value of $\mathrm{a} = 0.67\,\mathrm{fm}$.

Since for nuclear level density calculations, the quantity of fundamental importance concern the single-particle level density at the Fermi energy, we have plotted in Fig. A2 the phase shift $\delta_{WS}(\varepsilon_F) - \frac{\pi}{4}$ as a function of B and V_0. Fig. A2 clearly emphasizes the high sensitivity of the surface contribution $\tilde{g}_S(\varepsilon)$ to these two quantities. The B- and V_0-dependence of the phase shift can be approximated to a first approximation by the linear interpolation

$$\delta_{WS}(\varepsilon_F) - \frac{\pi}{4} = \alpha_s V_0 - \beta_s \mathrm{B} + \gamma_s \qquad (A8)$$

as suggested by Fig. A2. For the range of values $3\,\mathrm{MeV} \leq \mathrm{B} \leq 20\,\mathrm{MeV}$ and $30\,\mathrm{MeV} \leq V_0 \leq 70\,\mathrm{MeV}$ and for $\mathrm{a} = 0.67\,\mathrm{fm}$ and $D = 2$, a multiple regression fit within 8% can be obtained with the parameter set:

$$\begin{aligned} \alpha_s &= 1.3\ 10^{-2}\,\mathrm{MeV}^{-1} \\ \beta_s &= 6.6\ 10^{-2}\,\mathrm{MeV}^{-1} \qquad (A9) \\ \gamma_s &= 2.0\ 10^{-1} \end{aligned}$$

Expression $(A8)$ emphasizes how important the influence of the separation energy B on the surface contribution to the single-particle level density at the Fermi energy can be. The impact of B on the surface correction has already been considered by Kataria and Ramamurthy (1980), who suggested an empirical 1/B-dependence. However, such a relation is not confirmed by our treatment of the surface term—i.e. by the semi-classical approximation to the Woods-Saxon single-particle level density—nor has it been by other studies (e.g. Arnould and Tondeur, 1981).

Since it is known that the most general single-particle potential has to be both momentum and energy dependent, the influence of the non-localicity of the potential should also be considered.

Handloser and Stocker (1985) generalized expression ($A5$) to the non-local case. They obtained a similar expression to relation ($A5$), where the nucleonic mass m is simply replaced by the effective mass m*. While for deeply bound states it is well known that m* < m, it has been shown (e.g. Hodgson, 1983) that near the Fermi energy m* displays a narrow enhancement reaching a maximum value close to the bare mass m. Therefore, the introduction of an effective mass m* much smaller than m, which would reduce both the volume and the surface contributions to the single-particle level density, is not justified. The influence of the effective mass on the single-particle level density has also been discussed by Barranco and Treiner (1981) and Ormand et al. (1989).

In order to test the accuracy of expression ($A5$) to describe the smooth contribution to the single-particle level density, we have estimated the neutron single-particle number

$$N(\varepsilon) = \int_0^{\varepsilon} g(\varepsilon)\, d\varepsilon \qquad (A10)$$

in a Woods-Saxon potential for ^{208}Pb as a function of the single-particle energy. Fig. A3 compares the exact value ($A10$) with the smooth quantity obtained by integrating expression ($A5$) for the same potential parameters (the potential parameters can be found in Section II.2.4). Yet we have approximated the surface term by a simple quadratic function—fitting expression ($A6$)—in order to check the validity of the semi-classical approximation for levels above the neutron separation energy, i.e. for energies $E = \varepsilon - V_0 > 0$. As can be observed in Fig. A3, the agreement is excellent in the whole energy range. In particular, the surface correction appears to be non-negligible and to improve significantly the prediction of the single-particle level density (also shown in Fig. A3, is the approximation including the volume term only). Such a result enables us to put some confidence in the semi-classical description ($A5$) of the Woods-Saxon single-particle level density.

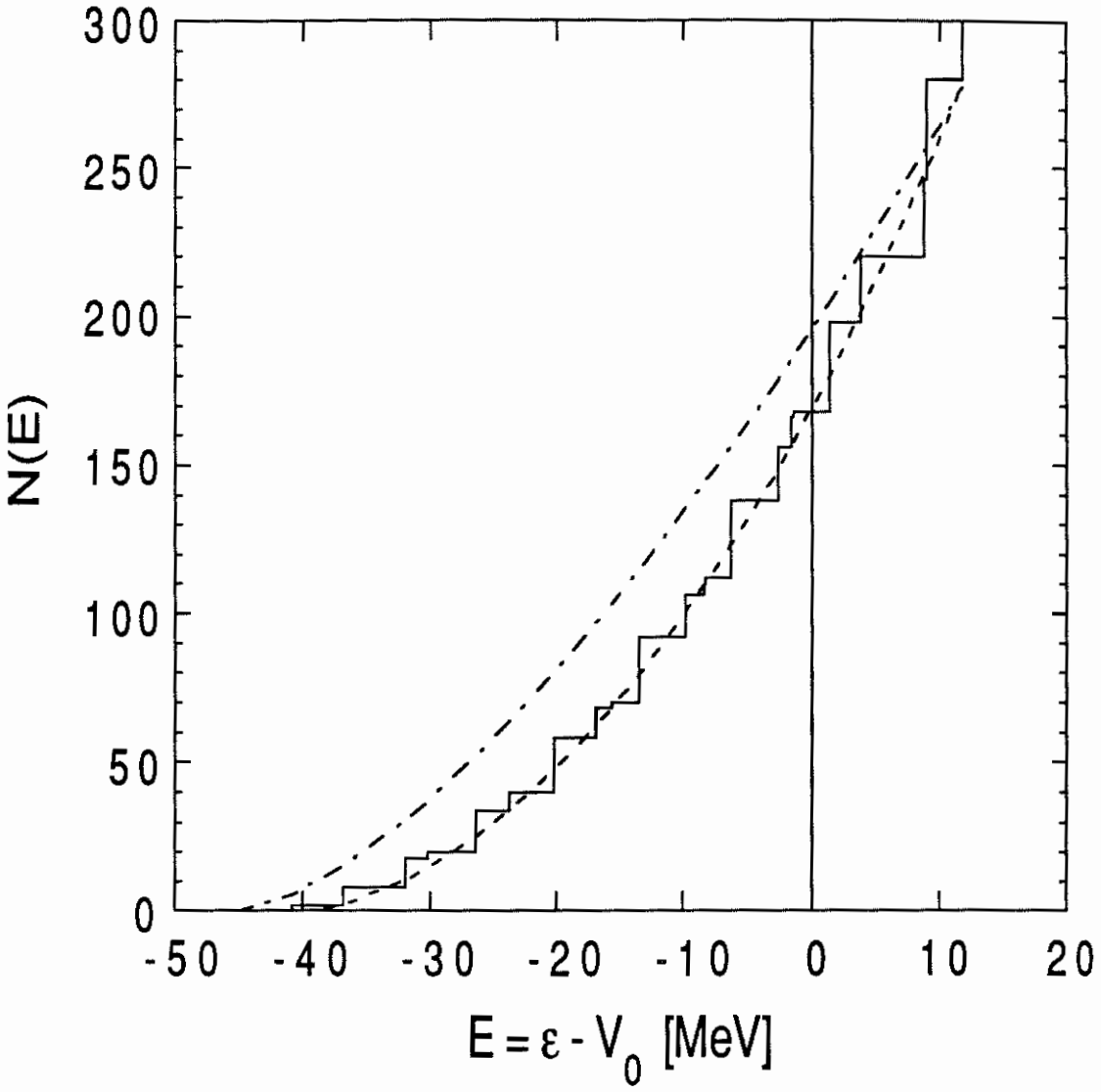

Figure A3. Neutron single-particle number in a Woods-Saxon potential for ^{208}Pb as a function of the single-particle energy $E = \varepsilon - V_0$ ($V_0 = 45\,\mathrm{MeV}$ is the potential depth). The dashed line corresponds to the semi-classical prediction including the volume and surface contributions. The dash-dot line corresponds to the volume term only. The parameters used are given in the text.

A.2 The oscillating single-particle level density in the infinite square well potential

As regards the non-zero length paths, it has been shown (Balian and Bloch, 1972; Berry and Mount, 1972) that only closed orbits (i.e. periodic orbits for which the system has the same momenta as well as the same coordinates at both ends of its trajectory) with energy ε contribute to the function $g_{osc}(\varepsilon)$ in expression $(A1)$. It has been shown (Strutinsky and Magner, 1976) that the amplitude of the oscillating function g_{osc}, or equivalently the intensity of the shell effect, is determined by the degree of degeneracy of the family of classical orbits, by the volume in the phase space occupied by the family of orbits and by some stability characteristics of the orbit. In the particular case of an infinite square well potential, the periodic orbits correspond to the regular polygons in diametral planes. Let us analyse the topology of these periodic paths.

Each orbit can be characterized by means of two integers (p,t): the number of vertices p and the number of turns t which they make around the origin in their plane (see Fig. A4). For $p = 2t$, the polygon contracts to a single diameter described t times in each direction, while for $p > 2t$, we have normal polygons repeated only once when p and t are prime with respect to each other. Starting from a basic polygon, described once, we may construct a family of polygons obtained by describing it n times. Taking R as the radius of the spherical nucleus, the length of the polygon (p,t) is given by

$$L(p,t) = 2pR\sin\phi \qquad (A11)$$

where $\phi = \frac{t\pi}{p}$ is half the angle to the centre of the polygon. Therefore, for a given t, the length $L(p,t)$ of a polygon tends when $p \to \infty$ to the limit $2\pi Rt$, corresponding to the perimeter of the circle covered t times. Thus all polygons with a given t form a family, called a band, in which the length L tends to a limit. It is also of interest to see that the $p = 2t$ and $p > 2t$ polygons must be treated differently as the stationary polygons $p > 2t$ depend on three continuous parameters (the orientation of the plane and the position of the polygon in the plane), whereas diameters depend on

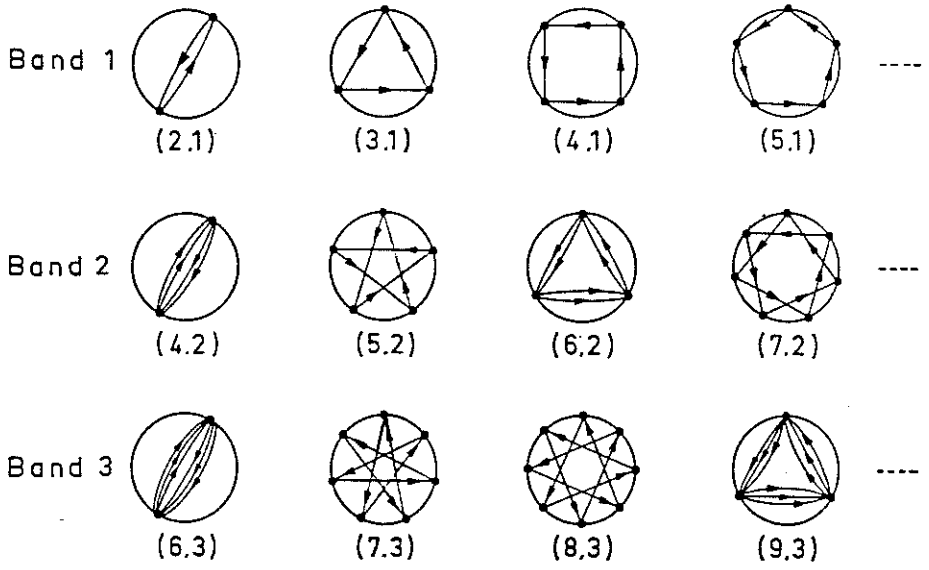

Figure A4. Closed orbits in a infinite spherical potential well. The first integer p is the number of vertices; the second t the number of turns around the centre. (from Balian and Bloch, 1972).

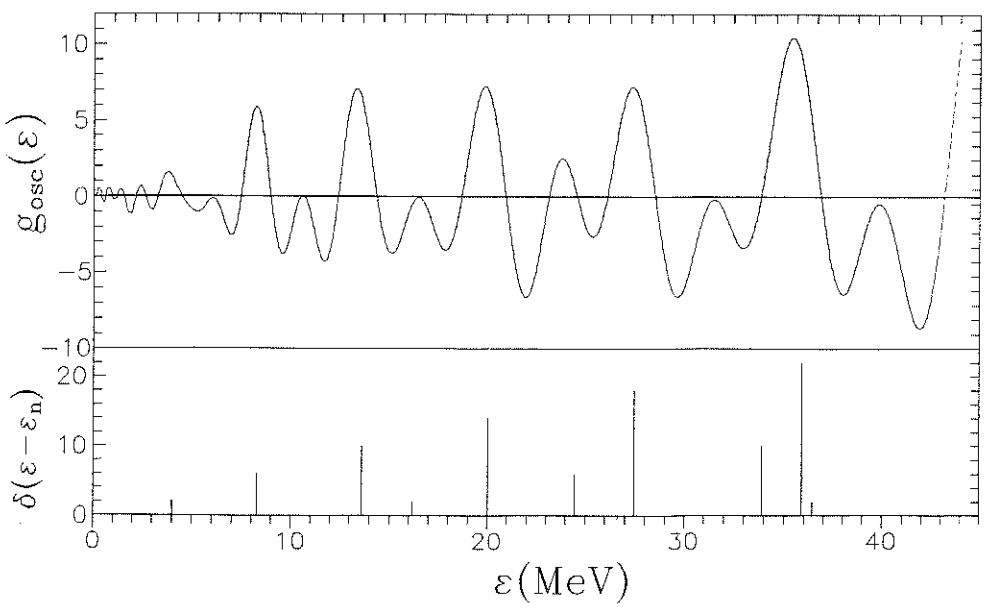

Figure A5. Comparison between the neutron single-particle level scheme of ^{208}Pb in an infinite spherical potential (lower part) and the semi-classical approximation to the oscillating contribution to the single-particle level density (upper part). The parameters are given in the text.

two parameters only. They will consequently lead to contributions of different orders of magnitude in expression $(A1)$, as shown by Strutinsky and Magner (1976).

In the case of an infinite spherical potential, it appears possible to express in a simple way the action integral for each orbit

$$S(p,t) = p(\varepsilon)\, L(p,t) \tag{A12}$$

where $p(\varepsilon)$ is the momentum of the particle. Expression $(A12)$ leads to a simple evaluation of the component of the Green's function corresponding to the regular polygons. Integrating equation $(A1)$ finally enables us to express the oscillatory contribution to the density of eigenvalues of an infinite square well potential as (Balian and Bloch, 1972; Strutinsky and Magner, 1976)

$$\begin{aligned} g_{osc}(\varepsilon) = 2\,(kR)^{1/2}\frac{2mR^2}{\hbar^2}\sum_{\substack{p>2t\\ t\geq 1}}\sum_{n=1}^{\infty}\sin 2\phi\sqrt{\frac{\sin\phi}{np\pi}}\,Im\exp\left[iknL(p,t)+iK(p,t,n)\right] \\ -\frac{2mR^2}{\hbar^2}\sum_{n=1}^{\infty}\frac{1}{2\pi n}\,Im\exp(i4knR) \end{aligned} \tag{A13}$$

where $k = \sqrt{\frac{2m}{\hbar^2}\varepsilon}$ is the wave number and where a factor of 2 has been included to take the spin degeneracy into account. The phases, also known as the Maslov indices, are given for each orbit by $K(p,t,n) = \frac{\pi}{4} - nt\pi + np\frac{\pi}{2}$. The final oscillating contribution can, consequently, be rewritten as

$$\begin{aligned} g_{osc}(\varepsilon) &= \sum_{t=1}^{\infty}\sum_{p=2t}^{\infty} g_0(p,t,\varepsilon) \\ &= \sum_{p>2t} g_1(p,t)\varepsilon^{1/4}\sin\left[g_2(p,t)\varepsilon^{1/2}+K(p,t)\right] + \sum_{p=2t} g_1(p,t)\sin\left[g_2(p,t)\varepsilon^{1/2}\right] \end{aligned} \tag{A14}$$

where the first summation is carried over the $p > 2t$ periodic orbits and the second one over the diameter orbits. The amplitude $g_1(p,t)$, the frequency $g_2(p,t)$ and the phase $K(p,t)$ of each contributing path depend on the two integers (p,t) characteristic of the path (if we include their n-dependence by considering multiples of the (p,t) pair) and are given by

$$\text{for} \quad p > 2t: \qquad g_1(p,t) = \left(\frac{2mR^2}{\hbar^2}\right)^{5/4}\sin\frac{2t\pi}{p}\sqrt{\frac{\sin t\pi/p}{\pi p}} \tag{A15}$$

$$g_2(p,t) = 2\left(\frac{2mR^2}{\hbar^2}\right)^{1/2} p \sin\frac{t\pi}{p} \qquad (A16)$$

$$\text{for} \quad p = 2t: \qquad g_1(2t,t) = -\left(\frac{2mR^2}{\hbar^2}\right)\frac{1}{2\pi t} \qquad (A17)$$

$$g_2(2t,t) = 4\left(\frac{2mR^2}{\hbar^2}\right)^{1/2} t \qquad (A18)$$

As regards the frequency $g_2(p,t) \propto L(p,t)$, it is of interest to emphasize the rapid convergence of g_2 for each band to the constant value of $2\left(\frac{2mR^2}{\hbar^2}\right)^{1/2} t\pi$. Each band is therefore characterized by a more or less constant frequency g_2.

For the paths $p = 2t$, characterized by a lower degeneracy, the amplitude $g_1(2t,t)$ is smaller than the amplitude of the $p > 2t$ paths by a factor $\sqrt{kR}$, so that for practical applications, their contributions can often be neglected. Moreover, when $p \to \infty$, the angle $\phi = t\pi/p \to 0$ and it follows that the series giving the total contribution of a band, obtained by keeping t fixed in $(A13)$ is convergent since each term is proportional to $1/p^2$. Similarly, when higher bands are considered, higher p polygons are concerned, so that the relative contribution of the high bands becomes rapidly negligible. Another feature which leads to an even lower contribution of the $t > 1$ bands relative to the $t = 1$ band, is contained in the rotating phase factor $K(p,t)$. In each band, two successive odd-p (or even-p) polygons will be characterized by an approximately identical frequency g_2, but also by an opposite phase and will tend to cancel out, especially for high p-values. This important factor leads to a much faster convergence of the double summation. Therefore, the main contribution to the oscillating single-particle level density can be expected to result from orbits of high degeneracy—i.e. that are not too near the surface—such as the triangle (1,3) and the square (1,4).

The function $g_{osc}(\varepsilon)$ has been computed in the special case of ^{208}Pb, i.e. for a potential radius $R \simeq 7.1\,\text{fm}$, by considering the contribution of the first 6 polygons of the first 2 bands ($t = 1,2$ and $2t < p < 2t+5$). The energy dependence of $g_{osc}(\varepsilon)$ is compared in Fig. A5 with the exact discrete eigenvalues spectrum of the corresponding infinite square well potential. The agreement

between the maxima of the oscillating function g_{osc} and the position of the nuclear shells appears to be relatively good. Instead of predicting the position of specific eigenvalues, the semi-classical approximation determines now the distribution of maxima of the level density. The first oscillations at low energy clearly describe individual eigenvalues, whereas at higher energies the oscillations correspond to the bunching of eigenvalues, i.e. the shell structure of the nucleus.

Appendix B: The single-particle state density with fixed angular momentum projection

As described by Magner et al. (1978), the single-particle state density $g(\varepsilon, m)$ with fixed angular momentum projection m can be expressed in the case of an axially symmetric potential in terms of the corresponding Green function $G(\rho' z', \rho z; \varepsilon, m)$ defined as the Fourier transform of the energy-dependent Green function over the angular variable. In the cylindrical coordinates system (ρ, z, φ)—where z corresponds to the symmetry axis of the potential—the state density $g(\varepsilon, m)$ is given by

$$g(\varepsilon, m) = -\frac{1}{\pi} Im \int G(\rho' z', \rho z; \varepsilon, m) \Big|_{\rho' z' \to \rho z} \rho \; d\rho \; dz \; d\varphi \qquad (B1)$$

A semi-classical approximation to G can be written in the form

$$G = G_0 + G_{osc} \qquad (B2)$$

where G_0 corresponds to the shortest classical trajectory from the point (ρz) to $(\rho' z')$ without reflection on the potential wall. Similarly, the oscillating component of the Green function G_{osc} is associated with the more complicated closed orbits (see Appendix A). The state density can then be expressed in the form

$$g(\varepsilon, m) = \tilde{g}(\varepsilon, m) + g_{osc}(\varepsilon, m) \qquad (B3)$$

where $\tilde{g}(\varepsilon, m)$ is the smooth part of the state density, related to the Green function G_0 and usually referred to as the Thomas-Fermi term. The oscillating component $g_{osc}(\varepsilon, m)$ corresponds to the quantity G_{osc} and is related to the gross shell effects. In the special case of an infinite square well potential, expression $(B1)$ can be reduced to a very simple analytical formula. Let us derive, in this simple case, the semi-classical approximations to the two contributions to $g(\varepsilon, m)$.

B.1 The smooth single-particle state density for the infinite square well potential

Berry and Mount (1972) show that in the case of a N-dimensional system governed by the isotropic Hamiltonian

$$H(\mathbf{r},\mathbf{p}) = \sum_{\alpha=1}^{\mathrm{N}} \frac{(p^{\alpha})^2}{2\mathrm{m}} + V(\mathbf{r}) \qquad (B4)$$

where $\mathbf{r}$ denotes the generalized coordinates and $\mathbf{p}$ the corresponding momenta of the particle of mass m, the Thomas-Fermi approximation to the spectral distribution—corresponding to the contribution from the paths of zero length in expression $(B1)$—is given by

$$\tilde{g}(E) = \left(\frac{\mathrm{m}}{2\pi\hbar^2}\right)^{\mathrm{N}/2} \int_R \frac{1}{\Gamma(\mathrm{N}/2)} [E - V(\mathbf{r})]^{\mathrm{N}/2-1}\, d\mathbf{r} \qquad (B5)$$

where the region R includes only the coordinates where $E > V(\mathbf{r})$ since in other regions no direct path exists.

The discussion will be restricted here to nuclear models involving a spin-independent central potential V. In this case, the projections along the z-axis m_l and m_s of the orbital momentum and of the spin of the nucleons are independent. Because of the straightforward treatment of the spin contribution to $g(\varepsilon, m)$, we will consider here the orbital term only.

To derive the smooth contribution to the state density $g(\varepsilon, m_l)$, we have applied expression $(B5)$ to the case of a particle subject to both a central potential and a centrifugal potential. By considering the radial wave equation, which is similar to the one-dimensional motion (N=1) of a particle of mass m in the potential

$$V(\mathbf{r}) = V(r) + \frac{l(l+1)\hbar^2}{2\mathrm{m}r^2} \qquad (B6)$$

we can write the spectral distribution for a fixed angular momentum l as

$$\tilde{g}^l(E) = D\left(\frac{\mathrm{m}}{2\pi^2\hbar^2}\right)^{1/2} \int_{r_0}^{r_1} \left[E - V(r) - \frac{l(l+1)\hbar^2}{2\mathrm{m}r^2}\right]^{-1/2} dr \qquad (B7)$$

where D takes the spin degeneracy ($D = 2$) into account and r_0 and r_1 are the classical turning points, i.e. r_1 is defined by the radius of the potential well R and r_0 by the relation

$$E = V(r_0) + \frac{l(l+1)\hbar^2}{2\mathrm{m}r_0^2} \tag{B8}$$

In the case of an infinite square well potential, a direct integration leads to

$$\tilde{g}^l(\varepsilon) = D\left(\frac{\mathrm{m}}{2\pi^2\hbar^2}\right)^{1/2}\frac{R}{\varepsilon}\left(\varepsilon - \frac{l(l+1)\hbar^2}{2\mathrm{m}R^2}\right)^{-1/2} \tag{B9}$$

where ε is the energy accounted from the bottom of the well. The density of states with projection m_l of l on the z-axis follows

$$\tilde{g}(\varepsilon, m_l) = \int_{|m_l|}^{l_{max}} \tilde{g}^l(\varepsilon)\, dl \tag{B10}$$

$$= \frac{D}{4\pi\varepsilon}\left[-(m_l+1/2)\sqrt{\frac{\varepsilon}{\varepsilon_0}+1/4-(m_l+1/2)^2} + (\frac{\varepsilon}{\varepsilon_0}+1/4)\cos^{-1}\frac{m_l+1/2}{\sqrt{\frac{\varepsilon}{\varepsilon_0}+1/4}}\right]$$

where l_{max} corresponds to the maximum possible value of l at a certain energy ε, i.e.

$$\varepsilon = \frac{l_{max}(l_{max}+1)\hbar^2}{2\mathrm{m}R^2} \tag{B11}$$

and where we have introduced the reduced centrifugal potential energy

$$\varepsilon_0 = \frac{\hbar^2}{2\mathrm{m}R^2} \tag{B12}$$

Note that $\tilde{g}(\varepsilon, m_l)$ is defined only for positive values of m_l, but also that $\tilde{g}(\varepsilon, m_l) = \tilde{g}(\varepsilon, -m_l)$

It is of interest to see that this expression can be obtained identically if use is made of the WKB formula approximating the total number of states for a nucleon with angular momentum l and energy ε (Bloch, 1954):

$$N_l(\varepsilon) = D\left(\frac{2\mathrm{m}}{\pi^2\hbar^2}\right)^{1/2}\int_{r_o}^{r_1}\left[\varepsilon - \frac{l(l+1)\hbar^2}{2\mathrm{m}r^2}\right]^{1/2} dr \tag{B13}$$

The density of states for fixed angular momentum l can then be obtained from

$$g^l_{WKB}(\varepsilon) = \frac{dN_l(\varepsilon)}{d\varepsilon} \tag{B14}$$

$$= D\left(\frac{\mathrm{m}}{2\pi^2\hbar^2}\right)^{1/2} \int_{r_0}^{r_1} \left[\varepsilon - \frac{l(l+1)\hbar^2}{2\mathrm{m}r^2}\right]^{-1/2} dr \tag{B15}$$

which is identical to expression $(B7)$

However, it is well known that application of the WKB method yields unsatisfactory results for singular potentials, such as the centrifugal potential $(B6)$. The defects of the WKB approximation, especially for small l, are usually eliminated by using the Langer substitution $l(l+1) \longrightarrow (l+\frac{1}{2})^2$ (Berry and Mount, 1972). Yet this substitution has a little influence on the distribution function $\tilde{g}(\varepsilon, m_l)$ since it leads to the cancellation of the factors $1/4$ appearing in expression $(B10)$. At a high energy ε and more particularly at the Fermi energy ε_F, we have $\varepsilon_F \gg \varepsilon_0$, so that the factor $1/4$ plays a negligible role even at low angular momentum.

Lastly, it can be verified that the smooth level density $\tilde{g}(\varepsilon)$, as defined in Chapter II.2 and Appendix A, can be derived from the state density $\tilde{g}(\varepsilon, m_l)$ via the relation

$$\tilde{g}(\varepsilon) = 2\int_0^{m_l^*} \tilde{g}(\varepsilon, m_l)\, dm_l \; - \; \tilde{g}(\varepsilon, 0) \tag{B16}$$

where m_l^* corresponds to the turning-point in the m-space (defined as $\varepsilon = \varepsilon_0 \; m_l^*(m_l^*+1)$) and where we have taken into account the fact that the $m_l = 0$ states contribute only once to the total number of states per level, unlike the $|m_l| > 0$ states.

After integrating expression $(B16)$, we obtain

$$\tilde{g}(\varepsilon) = \tilde{g}_V(\varepsilon) + \tilde{g}_S(\varepsilon) + \; \cdots \tag{B17}$$

$$= \frac{D}{4\pi^2}\frac{1}{\varepsilon_0}\left[\frac{4\pi}{3}\left(\frac{\varepsilon}{\varepsilon_0}\right)^{1/2} - 2\pi\, \cos^{-1}\frac{1}{2\sqrt{\frac{\varepsilon}{\varepsilon_0}+1/4}} + \cdots\right] \tag{B18}$$

$$\simeq \frac{D}{4\pi^2}\frac{1}{\varepsilon_0}\left[\frac{4\pi}{3}\left(\frac{\varepsilon}{\varepsilon_0}\right)^{1/2} - \; \pi^2 + \; \cdots\right] \tag{B19}$$

assuming that $\varepsilon/\varepsilon_0 \gg 1$ (a typical value of ε_0 being $\sim 0.5\,\mathrm{MeV}$).

Expression $(B19)$ is identical to expression $(A4)$, which was also obtained for an infinite square well potential. The difference between the surface terms in expressions $(B18)$ and $(A4)$ can be associated with the inaccurate treatment of integrals $(B10)$ and $(B16)$ for small angular momenta.

B.2 The oscillating single-particle state density for the infinite square well potential

Magner et al. (1978) studied in the framework of the quasi-classical theory the gross-shell effects in the nuclear single-particle spectrum for states with a fixed value of angular momentum. Using the semi-classical approximation of the Green function G_{osc}, they determined the oscillating component $g_{osc}(\varepsilon, m_l)$ of the state density in the case of a spherical potential. As suggested by equation $(B1)$, the oscillating state density receives contributions from the three-dimensional periodic orbits connecting the points (ρz). It has been shown (see Appendix A) that the periodic orbits reduce to two contributions: the planar orbits (β) and the diameters. It can be shown (Magner et al., 1978) that the contribution due to the diameter orbits can be neglected when dealing with quasi-classical accuracy, so that $g_{osc}(\varepsilon, m_l)$ can be expressed in terms of the planar orbits and of the energy-dependent single-particle level density associated with such orbits

$$g_{osc}(\varepsilon, m_l) = \sum_{\beta} \frac{1}{2l_\beta}\, g_{osc}^{(\beta)}(\varepsilon) \qquad (B21)$$

where the quantity $g_{osc}^{(\beta)}(\varepsilon) = g_0(p, t, \varepsilon)$ is given by expression $(A13)$ (see Appendix A). The summation includes β-families of planar orbits with angular momentum $l_\beta \geq |m_l|$ only. The orbital angular momentum for an orbit β is given by

$$l_\beta = \frac{1}{\hbar}\,[\mathbf{r}_\beta \times \mathbf{p}_\beta] \qquad (B22)$$

where $\mathbf{r}_\beta$ is the distance of the orbit to the centre and $\mathbf{p}_\beta$ the linear momentum of the particle on the orbit β.

When the angular momentum projection m_l increases, the contributions of orbits β with minimal angular momentum l_β disappear in the sum. Consequently, the quantity $g_{osc}(\varepsilon, m_l)$ decreases with increasing $|m_l|$. The amplitude of $g_{osc}(\varepsilon, m_l)$ differs approximately by a factor of $1/2l_\beta$ from $g_{osc}(\varepsilon)$ at not too large $|m_l|$ values. It is of importance to stress that this factor $1/2l_\beta$ is not related to the quantum mechanical degeneracy of the individual l-levels in the spherical potential. It appears in formula $(B21)$ because the full degree of degeneracy of the classical orbits is lower in the spherical case with a fixed projection m_l when compared with the corresponding problem with a free value of m_l. The oscillating component $g_{osc}(\varepsilon, m_l)$ is averaged over many quantum mechanical l-states in each gross shell.

We have calculated the quantities l_β in the case of an infinite square well, where the planar orbits are known to correspond to regular polygons in diametral planes. As already emphasized in Appendix A, the main contribution to the oscillating function $g_{osc}(\varepsilon)$ and consequently to $g_{osc}(\varepsilon, m_l)$, comes from the first band ($t = 1$) of polygons. The angular momentum relative to the centre of the orbit is given, for each orbit p, by

$$\begin{aligned} l_{p,1} &= kR \cos\frac{\pi}{p} \\ &= \left(\frac{\varepsilon}{\varepsilon_0}\right)^{1/2} \cos\frac{\pi}{p} \end{aligned} \qquad (B23)$$

It can be seen that the main contribution to $g_{osc}(\varepsilon, m_l)$ is due to the triangle and square orbits, since they are characterized not only by the lowest angular momenta but also by the highest amplitudes in the $g_{osc}^{(\beta)}(\varepsilon)$ function. This justifies the substitution of the $2l_\beta$ factor by the average value $2\bar{l}$, taken over the few contributing orbits only. Considering the angular momentum projections $|m_l| < l_{\beta min}$ ($l_{\beta min}$ is the minimal angular momentum for the first band, i.e. $l_{\beta min} = \frac{1}{2}kR$), we are finally left with the very simple expression

$$g_{osc}(\varepsilon, m_l) \;=\; \frac{1}{2\bar{l}}\; g_{osc}(\varepsilon) \qquad (B24)$$

where the oscillating single-particle level density $g_{osc}(\varepsilon)$ is given by expression $(A14)$ (see Appendix

A). The $\bar{l}$ factor can be parametrized by

$$\bar{l} = \iota \left(\frac{\varepsilon}{\varepsilon_0} \right)^{1/2} \qquad (B25)$$

where $\iota \simeq 0.6$ is an average value of $\cos \frac{\pi}{p}$ over the contributing orbits.

Appendix C: The semi-classical approximation to the ground-state shell correction energy

The semi-classical approach to the statistical properties of the nucleus enables us to express analytically the ground-state shell correction energy of a system of nucleons confined in an infinite square potential. It has been shown (see Section II.2.3) that it could be expressed as

$$\delta W = \delta W_1 + \delta W_2 \tag{C1}$$

where the two contributions are given by a double infinite sum carried over the periodic polygons (p,t) characterizing the closed orbits of the potential well (see Appendix A):

$$\delta W_1 = \sum_{t=1}^{\infty} \sum_{p=2t}^{\infty} a_1(p,t) \sin\Big[g(p,t) + K(p,t)\Big] \tag{C2}$$

$$\delta W_2 = \sum_{t=1}^{\infty} \sum_{p=2t+1}^{\infty} a_2(p,t) \cos\Big[g(p,t) + K(p,t)\Big] \tag{C3}$$

The amplitudes for non-diametral paths $(p > 2t)$ are given, respectively, by

$$a_1(p,t) = a_1^0 \, \frac{1}{p^{5/2}} \frac{\cos t\pi/p}{\sqrt{\sin t\pi/p}} = \frac{\pi^2}{3\sigma_a^2\sqrt{\pi}} \left(\frac{2mR^2}{\hbar^2}\right)^{1/4} \varepsilon_F^{5/4} \, \frac{1}{p^{5/2}} \frac{\cos t\pi/p}{\sqrt{\sin t\pi/p}} \tag{C4}$$

$$a_2(p,t) = a_2^0 \, \frac{1}{p^{7/2}} \frac{\cos t\pi/p}{\sin^{3/2} t\pi/p} = \frac{\pi^2}{6\sigma_a^2\sqrt{\pi}} \left(\frac{2mR^2}{\hbar^2}\right)^{-1/4} \varepsilon_F^{3/4} \, \frac{1}{p^{7/2}} \frac{\cos t\pi/p}{\sin^{3/2} t\pi/p} \tag{C5}$$

the frequencies by

$$g(p,t) = g_0 \; p \sin t\pi/p = 2 \left(\frac{2mR^2}{\hbar^2}\right)^{1/2} \varepsilon_F^{1/2} \; p \sin t\pi/p \tag{C6}$$

and the phases by

$$K(p,t) = \frac{\pi}{4} - t\pi + p\frac{\pi}{2} \tag{C7}$$

The other quantities appearing in expressions $(C1)$–$(C7)$ have been defined in Section II.2.2 and Section II.2.3. For the diametral paths, contributing to the sum $(C2)$, different expressions of the amplitudes must be derived and can be obtained from Appendix A.

The energies δW_1 and δW_2 can be considered as functions of the particle number because of their dependences on the potential radius ($R \propto A^{1/3}$) and on the Fermi energy ($\varepsilon_F \propto \left(\frac{N}{A}\right)^{2/3}$). Let us, first, analyse expression $(C2)$, corresponding to the energy δW_1, in detail.

Simplifications of the double infinite sum can be made as a result of the special behaviour of the amplitudes $a_1(p,t)$, frequencies $g(p,t)$ and phases $K(p,t)$, over the different contributing orbits:

- Neglect of the diametral paths contribution:

The diametral orbits in the potential well are characterized by the two integers t and $p = 2t$. It can be shown that the amplitudes $a_1(2t,t)$ are lower by a factor of $\sqrt{kR}$ (where k is the wave number of the nucleon) relative to the $p > 2t$ paths (see Appendix A), so that for our practical applications, their contributions can be neglected.

- Neglect of the $t > 2$ bands:

For each band t, the main contribution to the sum $(C2)$ comes from the path characterized by $p = 2t + 1$. Since $a_1(p,t)$ is a rapidly decreasing function of p and t, the $t > 1$ bands give rise to a relatively small contribution to expression $(C2)$ relative to the $t = 1$ band. In addition, the rotating phase factors $K(p,t)$ also lead to a fast cancellation of the high-p polygons in the $t \geq 1$ bands. Since in each band, the frequency $g(p,t)$ rapidly converges to the constant value $g_0 t\pi$, two successive odd-p (or even-p) orbits will be characterized by an approximately identical frequency and amplitude, but also by an opposite phase $K(p,t)$, so that for increasing p-values the different contributions tend to cancel each other out, two by two.

Yet the $t = 2$ band tends to affect the total behaviour of the δW_1 function in a non-negligible way. Although the amplitude of the $t = 2$ band is relatively small compare with the $t = 1$ contribution, the frequencies $g(p,2) \simeq 2g(p,1)$ have an important effect on the $t = 1$ band. As a matter of fact, the phase difference of the angle π between the two bands gives rise to a situation

where the minima of the $t = 1$ band correspond to the minima of the $t = 2$ band, but because of the double frequency of the $t = 2$ band, the $t = 2$ function is again at its minimum when the $t = 1$ contribution reaches its maximum. Since the $t = 1$ and $t = 2$ bands are functions oscillating around the zero value, the correction due to the $t = 2$ band leads to a total function δW_1 which is not about equally often positive as negative, but mainly negative. This characteristic of the shell correction energy has been emphasized phenomenologically by Myers and Swiactecki (1966). It now clearly appears to result from the contribution of the $t > 1$ bands and consequently to be associated with the constructive and destructive interferences in the nucleonic motions along the $t = 1$ and $t = 2$ periodic orbits.

- Simplification of the $t = 1$ band:

As already emphasized, above a value p^* of the integer p, the frequency $g(p,1)$ can be considered as p-independent (and equal to the high-p limit $g_0\pi$), so that the contribution of the polygons in the $t = 1$ band with $p \geq p^*$ can be reduced to

$$\begin{aligned} \delta W_1 \Big|_{p\geq p^*} &\simeq a_1^0 \; s_o \cos\Big[g(p^*,1) - \frac{3\pi}{4}\Big] + a_1^0 \; s_e \sin\Big[g(p^*,1) - \frac{3\pi}{4}\Big] \\ &\simeq a_1^0 \; s_o \; \frac{1}{2\sqrt{2}} \; \sin g(p^*,1) \end{aligned} \qquad (C8)$$

where the factors s_o and s_e corresponds to the summations over odd-p and even-p values, respectively:

$$s_o = \sum_{p\geq p^*}^{odd} (-1)^{\frac{p-1}{2}} \frac{1}{p^{5/2}} \frac{\cos \pi/p}{\sqrt{\sin \pi/p}} \qquad s_e = \sum_{p\geq p^*}^{even} (-1)^{\frac{p}{2}} \frac{1}{p^{5/2}} \frac{\cos \pi/p}{\sqrt{\sin \pi/p}} \qquad (C9)$$

Since the frequency $g(p,t)$ converges relatively quickly, the above approximation can be expected to be rather good for a value of $p^* \simeq 15$. It can be verified that $s_e \simeq -s_o$.

However, this accurate and simple expression cannot be easily generalized for the contribution of the polygons with $p < p^*$. The energy δW_1 is, in fact, given as an infinite series of oscillating functions with decreasing amplitudes and characterized by a given phase. This problem is well known in optical diffraction but is generally found in a simpler context where the phase difference

between two successive contributions remains constant and the amplitude follows a geometric series. We can write by analogy

$$\delta W_1 = Im\ \bar{a}_1^0\ \mathrm{e}^{-i\frac{3\pi}{4}} \sum_{p=3}^{\infty} r^p \mathrm{e}^{ip\delta} \qquad (C10)$$

where a good approximation to the p-dependence of the amplitude $a(p,1) = \bar{a}_1^0\, r^p$ is obtained for $r = 0.76$. Unfortunately, the phase $\delta = \frac{\pi}{2} + g_0 \sin \pi/p$ does not correspond to an additional constant phase shift obtained after the pth reflection on a surface of reflectivity r. Yet if we sum the odd and even terms separately, two by two, we are left with a summation of terms in the form $a \sin \frac{\Delta g}{2} \sin \bar{g}$ where the high frequency wave $\sin \bar{g}$ is modulated in amplitude by the low frequency wave $\sin \frac{\Delta g}{2}$. In addition, if we assume the low frequencies $\frac{\Delta g}{2}$ to remain fairly constant, we can reduce the phase in expression $(C10)$ to $\delta \sim \bar{g}$. The sum $(C10)$ has now become a geometric series which can easily be estimated. We finally obtain

$$\delta W_1 \simeq a_d\ \frac{1}{1 + \rho \sin^2 \delta/2} \qquad (C11)$$

where the factor $a_d \propto a_1^0 \sin \frac{\Delta g}{2}$ includes all the contributions to the total amplitude. In addition, if we consider the dependence of the Fermi energy and of the potential radius on the particular number and if we assume that $\sin \frac{\Delta g}{2} \sim \frac{\Delta g}{2}$ (i.e. $\frac{\Delta g}{2} \ll 1$), the total amplitude appears to be proportional to $N^{1/2}$ for the neutrons (or $Z^{1/2}$ for the protons)—if we neglect the small isospin dependence. Similarly, the average frequency δ is then proportional to $N^{1/3}$ (or $Z^{1/3}$ for the protons; for simplicity, only the case of the neutron system will be discussed here). Finally, if we take the contribution of the $t \geq 2$ bands into account, in a phenomenological way by introducing in expression $(C11)$ an over-all negative shift, we can write

$$\delta W_1 = s_1 N^{1/2} \left[1 - \frac{t_1}{1 + r_1 \sin^2 \left(\bar{g}_1 N^{1/3} + k_1 \right)} \right] \qquad (C12)$$

In these conditions, the quantity δW_1 appears to be reduced to a typical diffraction pattern, i.e. an oscillating wave reinforced at the minima or the maxima. Approximation $(C12)$ is compared

in Fig. C1 with the original quantity $(C2)$ obtained with an amplitude $a_1^0 = 75N^{1/6}\,\mathrm{MeV}$ and a frequency $g_0 = 4.33\,N^{1/3}$ (corresponding to an average potential radius $r_0 = 1.26\,\mathrm{fm}$ and a Fermi energy $\varepsilon_F = 38\,\mathrm{MeV}$). Expression $(C12)$ fitting the resulting function is characterized by the parameters: $s_1 = 1.5\,\mathrm{MeV}$, $t_1 = 1.75$, $r_1 = 2.0$, $\bar{g}_1 = 5.8$ and $k_1 = 0.26$. As can be observed, the approximate function follows the global trend of δW_1 fairly well in the whole range of N-values considered.

A similar analysis can be made for the quantity δW_2. Expression $(C3)$ defining the shell energy δW_2 differs from expression $(C2)$ corresponding to δW_1 in two respects:

- the faster decreasing p-dependence of the amplitude $a_2(p,t)$
- the additional $\frac{\pi}{2}$ phase in the trigonometric functions.

An equivalent simplification of the amplitudes, frequencies and phases for each orbits contribution leads to an identical expression, namely

$$\delta W_2 = s_2 N^{1/6} \left[1 - \frac{t_2}{1 + r_2 \sin^2\left(\bar{g}_2 N^{1/3} + k_2\right)} \right] \qquad (C13)$$

where the total amplitude is this time proportional to $N^{1/6}$ because of its different dependence on the potential radius. Figure C2 shows a comparison of expression $(C3)$ and $(C13)$ as a function of the neutron number N. The function $(C3)$ has been obtained with the parameters $a_2^0 = 95N^{-1/6}\,\mathrm{MeV}$ and the frequency $g_0 = 4.33N^{1/3}$ (corresponding to the same potential parameters as above; yet the amplitude a_2^0 has been multiplied by a factor of 5, because of the possible underestimate of expression $(C3)$, as shown in Section II.2.3). The fit displayed in Fig. C2 corresponds to the parameter set: $s_2 = 2\,\mathrm{MeV}$, $t_2 = 1.2$, $r_2 = 0.5$, $\bar{g}_2 = \bar{g}_1 = 5.8$ and $k_2 = k_1 + \frac{\pi}{4} = 1.04$.

In spite of the numerous approximations made to derive the phenomenological expressions $(C12)$ and $(C13)$, the agreement with the original functions $(C2)$ and $(C3)$, respectively is fairly close. Yet some systematic discrepancies can be observed. In particular, the energy δW_1 deviates locally from a smooth oscillating function because of the contributions of the $t > 1$ bands. These

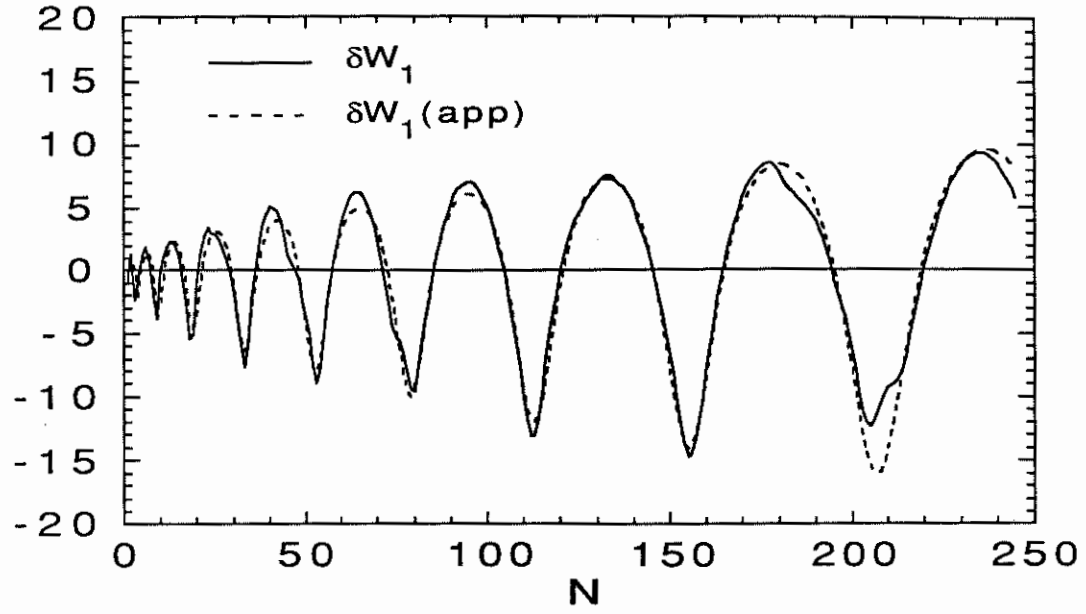

Figure C1. Comparison between the semi-classical expression ($C2$) of the shell energy ΔW_1 and the analytical approximation ($C12$) as a function of the nucleon number N. The parameters for the two curves are given in the text.

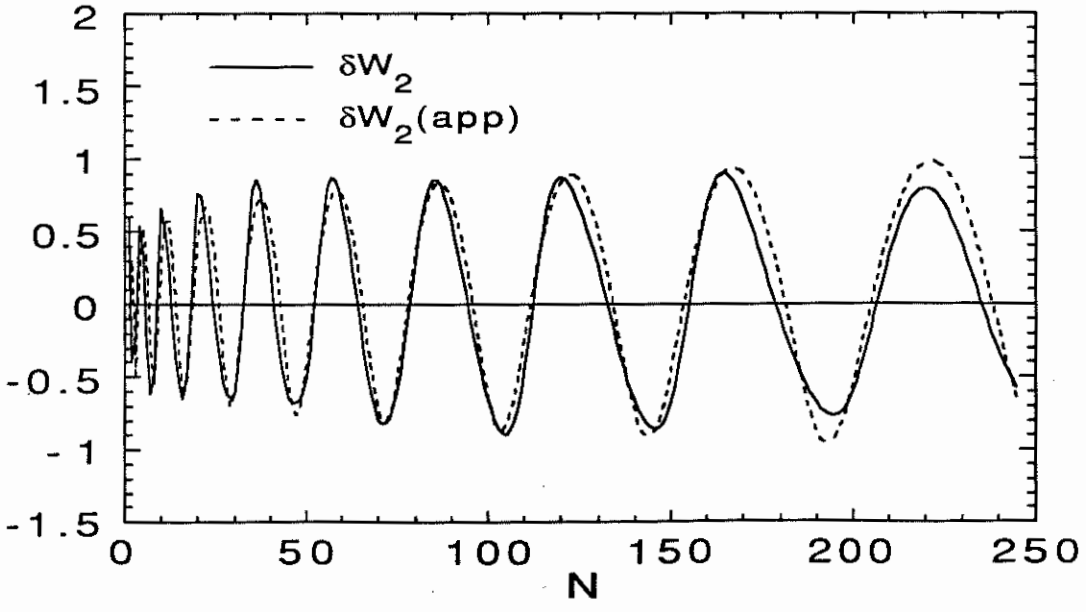

Figure C2. Same as Fig. C1 for the δW_2 contribution to the shell energy. The analytical approximation is given by ($C13$).

irregularities cannot be reproduced accurately by the oversimplified approximation $(C12)$. The semi-classical expressions also show at high N-values a decrease of the amplitudes, while the amplitudes of the approximate energies have been assumed to be monotonic increasing functions of N. This feature of the approximate shell functions results from the assumption made: $\sin \frac{\Delta g}{2} \sim \frac{\Delta g}{2}$, which is not confirmed at high N-values, especially in the $t > 1$ bands.

In order to take the contribution of $t > 1$ bands more accurately into account, another fit can be obtained by separating the $t = 1$ and $t = 2$ contributions and fitting both contributions separately. The $t = 1$ band appears to be well reproduced by the simple function

$$\delta W_1(t = 1) = a_{11} N^{1/6} \sin \Delta g_{11} N^{1/3} \sin \left(\bar{g}_1 N^{1/3} + k_{11} \right) \qquad (C14)$$

because of the small frequency $\Delta g_{11} N^{1/3}$ in the range of N-values considered. The uncertainty associated with Δg_{11} can consequently be compensated by a modification of the amplitude.

The $t = 2$ band is more difficult to fit because of its double frequency which also doubles the modulated frequency. The proposed approximation can be expressed as

$$\delta W_1(t = 2) = a_{12} N^{1/6} \left(2 - \cos \Delta g_{12} N^{1/3} \right) \sin \left(2\bar{g}_1 N^{1/3} + k_{12} \right) \qquad (C15)$$

The two contributions $(C14)$ and $(C15)$ as well as their sum are compared in Fig. C3 with the respective quantities derived numerically from expression $(C2)$. As can be observed, the fits have been significantly improved. However, they are now dependent on 7 parameters, compare to 5 in the previous approximation. The parameters used to fit expression $(C2)$ with the values $a_2^0 = 75 N^{1/6}\,\mathrm{MeV}$ and $g_0 = 4.33 N^{1/3}$ are

- for the $t = 1$ contribution: $a_{11} = 4.1\,\mathrm{MeV}$, $\Delta g_{11} = 0.3$, $\bar{g}_1 = 11.6$, $k_{11} = -\frac{\pi}{4}$
- for the $t = 2$ contribution: $a_{12} = 0.45\,\mathrm{MeV}$, $\Delta g_{12} = 3.0$, $k_{12} = 0$

In a completely similar way, the above result can be applied to the evaluation of the shell energy

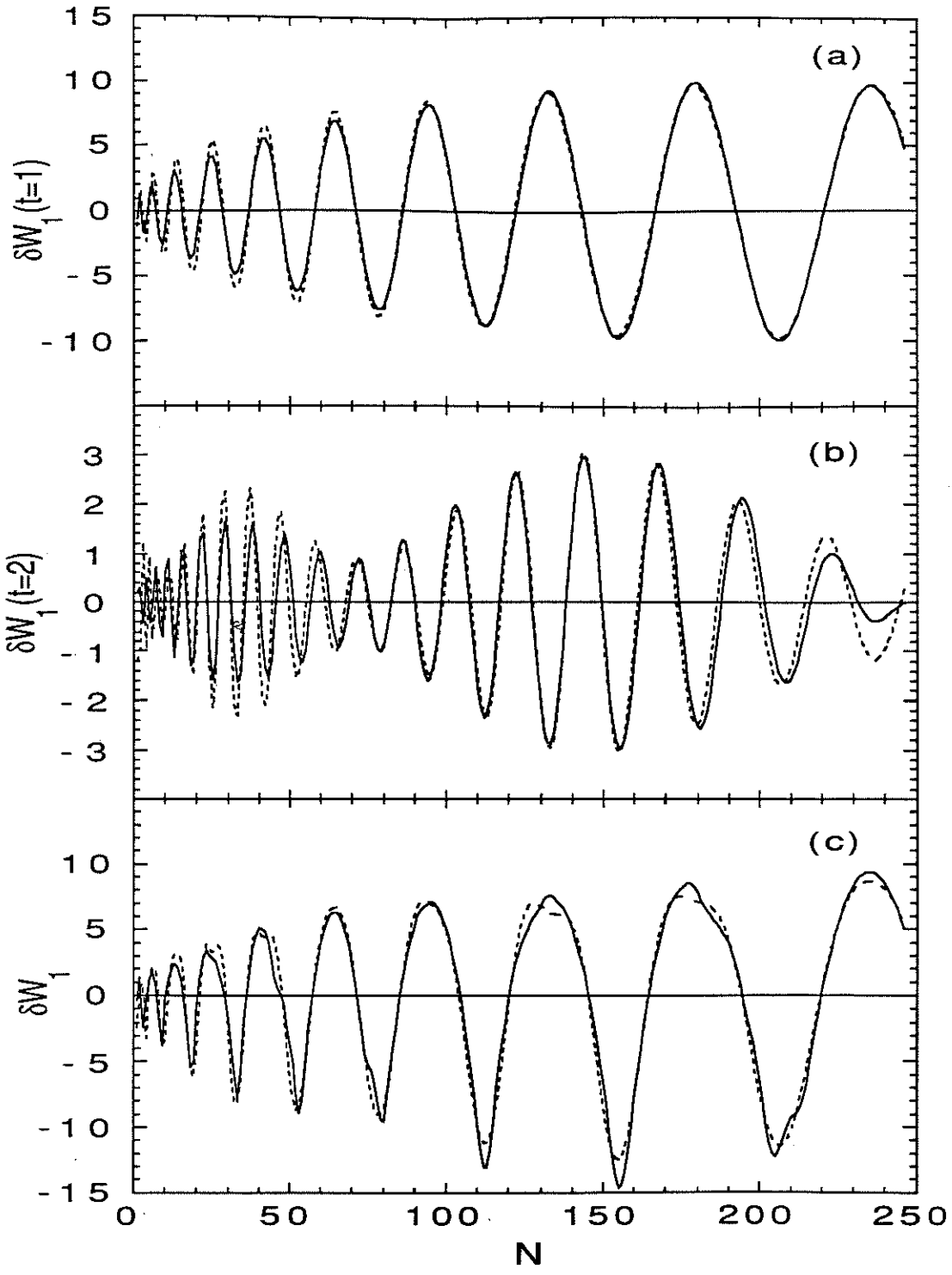

Figure C3(a) Comparison between the semi-classical contribution to the shell energy δW_1 corresponding to the $t = 1$ band (full line), and the analytical approximation (dashed curve) given by expression $(C14)$.

(b) same as (a) for the contribution of the $t = 2$ band to the energy δW_1. The analytical approximation corresponds to expression $(C15)$.

(c) same as (a) for the total energy δW_1. The parameters used are given in the text.

δW_2. We can write directly

$$\delta W_2(t=1) = a_{21} N^{-1/6} \sin \Delta g_{21} N^{1/3} \sin \left(\bar{g}_2 N^{1/3} + k_{21} \right) \qquad (C16)$$

$$\delta W_2(t=2) = a_{22} N^{-1/6} \left(2 - \cos \Delta g_{22} N^{1/3} \right) \sin \left(2\bar{g}_2 N^{1/3} + k_{22} \right) \qquad (C17)$$

the resulting functions are compared in Fig. C4 with the corresponding quantity derived from $(C3)$. The different contributions to δW_2 have been obtained with the parameters $a_2^0 = 95 N^{-1/6}$ MeV and $g_0 = 4.33 N^{1/3}$ in expression $(C3)$, while the parametrized approximation reproducing $(C3)$ is characterized by the parameters:

- for the $t = 1$ contribution: $a_{21} = 2.0\,\text{MeV}$, $\Delta g_{21} = 0.3$, $\bar{g}_2 = 11.6$, $k_{21} = \frac{\pi}{4}$
- for the $t = 2$ contribution: $a_{22} = 0.02\,\text{MeV}$, $\Delta g_{22} = 3.0$, $k_{22} = \frac{\pi}{2}$

It is of interest to note that the frequencies are identical in the semi-classical expression of both energies δW_1 and δW_2, so that the approximate expressions are characterized by the equalities: $\bar{g}_1 = \bar{g}_2$, $\Delta g_{11} = \Delta g_{21}$ and $\Delta g_{12} = \Delta g_{22}$. The additional $\frac{\pi}{2}$ phase in the δW_2 energy relative to the δW_1 energy is also reproduced.

This second fit to the energies δW_1 and δW_2 emphasizes the important influence of the $t \geq 2$ bands on the total shell energy. More specifically, it can be seen in Fig. C3 that the $t = 2$ band clearly shifts the δW_1 curve to more negative values. Moreover, it tends to sharpen the minima and to flatten the maxima. This special feature of the shell function has already been pointed out by Myers and Swiatecki (1967). Experimentally, it is observed that when positive, the shell function tends to *sag*, whereas theoretically it remains arched. This characteristic has been explained by Myers and Swiatecki (1967) as resulting from the reversal shell effects appearing when the nuclear deformation increases. The introduction of *wiggles* in the shell damping function for increasing deformations (see Section II.5.1) has been justified by a purely empirical observation of the debunching of levels with deformation, as schematized by Nilsson's diagram. However, Fig. C3(c) suggests that even in the spherical case, there exist wiggles at the maxima of the shell

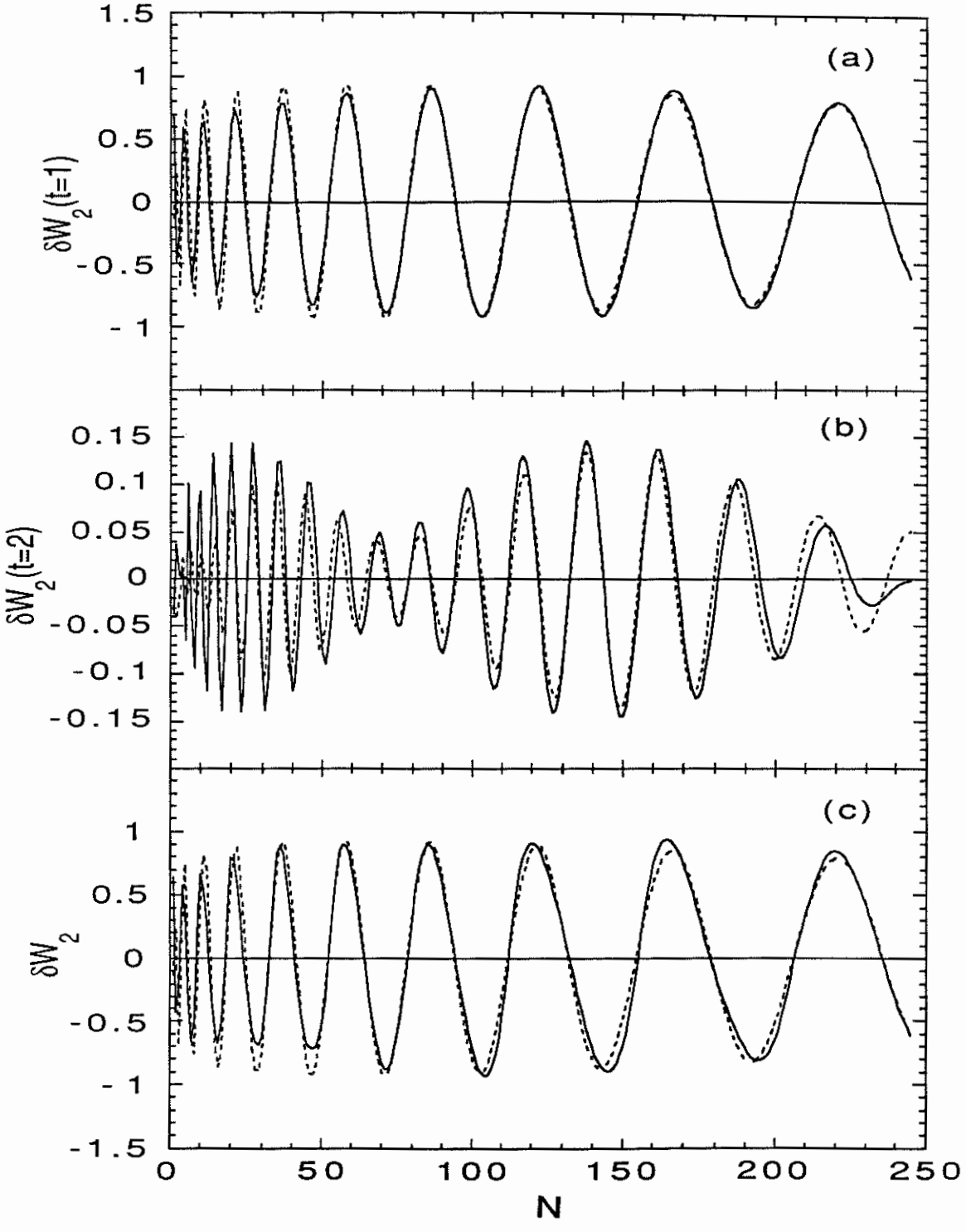

Figure C4(a) Comparison between the semi-classical contribution to the shell energy δW_2 corresponding to the $t = 1$ band (full line), and the analytical approximation (dashed curve) given by expression $(C16)$.
(b) same as (a) for the contribution of the $t = 2$ band to the energy δW_2. The analytical approximation corresponds to expression $(C17)$.
(c) same as (a) for the total energy δW_1. The parameters used are given in the text.

function. Consequently, their origin might not be associated with the redistribution of levels when the deformation increases, but with the destructive interferences in the nucleonic motions along the $t = 1$ and $t = 2$ periodic orbits.

It should be recalled that the shell energy $\delta W = \delta W_1 + \delta W_2$ derived in this appendix corresponds to the simple case of a system of nucleons confined to an infinite square potential. Therefore, it remains hazardous to draw conclusions about more realistic nuclear models, which, in particular, would include the effects of the spin-orbit potential. However, this analysis has the advantage of offering a clear insight into the different effects of the nucleonic motions on the ground-state shell correction energy of a spherical nucleus.

References

Aboussir, Y., Pearson J.M., Dutta, A.K., Nayak, R.C., Farine, M., Tondeur, F. 1991, unpublished

Akkermans, J.M., Gruppelaar, H. 1985, *Z. Phys. A* **321**, 605

Anders, E., Grevesse, N. 1989, *Geochim. Cosmochim. Acta* **53**, 197

Arcoragi, J.-P., Langer, N., Arnould, M. 1991, in preparation

Arnould, M. 1972, *Astron. Astrophys.* **19**, 82

Arnould, M., Rayet, M. 1990, *Ann. Phys. Fr.* **15**, 183

Arnould, M., Takahashi, K. 1990, *Astrophysical Ages and Dating Methods*, eds. Vangioni-Flam et al. (Editions frontières, Gif-sur-Yvette)

Arnould, M., Tondeur, F. 1981, *4th Conf. on nuclei far from stability*, Helsingør, CERN 81-09, Vol. 1, p. 229

Avrigeanu, M., Avrigeanu, V. 1991, *Int. Summer School*, Predeal, Romania

Baba, H. 1970, *Nucl. Phys.* **A159**, 625

Balian, R., Bloch, C. 1970, *Ann. Phys.* **60**, 401

Balian, R., Bloch, C. 1972, *Ann. Phys.* **69**, 76

Balian, R., Bloch, C. 1974, *Ann. Phys.* **85**, 514

Bao, Z.Y., Käppeler, F. 1987, *At. Data Nucl. Data Tables* **36**, 411

Barashenkov, V.S., Iljinov, A.S., Toneev, V.D., Gereghi, F.G. 1973 *Nucl. Phys.* **A206**, 131

Bardeen, J., Cooper, L., Schriffer, J. 1957, *Phys. Rev.* **108**, 1175

Barranco M., Treiner, J. 1981, *Nucl. Phys.* **A351**, 269

Beckerman, M. 1977, *Nucl. Phys.* **A278**, 333

Behkami, A.N., Huizenga, J.R. 1973, *Nucl. Phys.* **A217**, 78

Berry, M.V., Mount, K.E. 1972, *Rep. Prog. Phys.* **35**, 315

Bethe, H.A. 1936, *Phys. Rev.* **50**, 332

Bjørnholm, S., Bohr, A, Mottelson, B.R. 1974, *Physics and Chemistry of Fission*, Vol. 1, (IAEA, Vienna), p. 367

Bloch, C. 1954, *Phys. Rev.* **93**, 1094

Bohr, A., Mottelson, B.R. 1969, *Nuclear Structure*, Vol. 1 (Benjamin; New York)

Bohr, A., Mottelson, B.R. 1975, *Nuclear Structure*, Vol. 2 (Benjamin; New York)

Brack, M., Damgaard, J., Jensen A.S., Pauli, H.C., Strutinsky, V.M., Wong, C.Y. 1972, *Rev. Mod. Phys.* **44**, 320

Brack, M., Guet, C., Håkansson, H.-B. 1985, *Phys. Reports* **123**, 275

Burbidge, E.M., Burbidge, G.R., Fowler, W.A., Hoyle, F. 1957, *Rev. Mod. Phys.* **29**, 547

Cameron, A.G.W. 1958, *Can. J. Phys.* **36**, 1040

Cameron, A.G.W., Elkin, R.M. 1965, *Can. J. Phys.* **43**, 1288

Cameron, A.G.W., Cowan, J.J., Klapdor, H.V., Metzinger, J., Oda, T., Truran, J.W. 1983a, *Astrophys. Space Sci.* **91**, 221

Cameron, A.G.W., Cowan, J.J., Truran, J.W. 1983b, *Astrophys. Space Sci.* **91**, 235

Chu, Y. H., Jennings, B.K., Brack, M. 1977, *Phys. Lett.* **68B**, 407

Cowan, J.J., Cameron, A.G.W., Truran, J.W. 1983, *Astrophys. J.* **265**, 429

Cowan, J.J., Thielemann, F.-K., Truran, J.W. 1991, *to appear in Physics Reports*

Das Gupta S., Rhadakant S. 1974, *Phys. Rev.* **C9**, 1775

Decowski, P., Grochulski, W., Marcinkowski, A., Siwek, K., Wilhelmi, Z. 1968, *Nucl. Phys.* **A110**, 129

Dilg, W., Schantl, W., Vonach, H., Uhl, M. 1973, *Nucl. Phys.* **A217**, 269

Døssing, T., Jensen, A.S. 1974, *Nucl. Phys.* **A222**, 493

Dutta A.K., Arcoragi, J.-P., Pearson, J.M., Behrman, R., Farine, M. 1986a *Nucl. Phys.* **A454**, 374

Dutta A.K., Arcoragi, J.-P., Pearson, J.M., Behrman, R., Tondeur, F. 1986b *Nucl. Phys.* **A458**, 77

von Egidy, T., Schmidt, H.H., Bekhami, A.N. 1986, *Nucl. Phys.* **A454**, 109

von Egidy, T., Schmidt, H.H., Bekhami, A.N. 1988, *Nucl. Phys.* **A481**, 189

Engelbrecht, C.A., Engelbrecht, J.R. 1991, *Ann. Phys.* **207**, 1

Ericson, T. 1958, *Nucl. Phys.* **8**, 265

Ericson, T. 1960, *Advan. Phys.* **9**, 425

Facchini, U., Saetta Menichella, E. 1968, *Energ. Nucl.* **15**, 54

Flügge, S. 1971, *Practical quantum mechanics* (Springer, Berlin), p. 162

Ford, G.P. 1978, *Nuclear Science and Engineering* **66**, 334

French, J.B., Ratcliff, K.F. 1971, *Phys. Rev.* **C3**, 94

Gilbert, A., Cameron, A.G.W. 1965, *Can. J. Phys.* **43**, 1446

von Groote, H., Hilf, E.R., Takahashi, K. 1976, *At. Data Nucl. Data Tables* **17**, 418

Grossjean, M.K., Feldmeier, H. 1985, *Nucl. Phys.* **A444**, 113

Gutzwiller, M. C. 1967, *J. Math. Phys.* **8**, 1979

Handloser, G., Stocker, W. 1985, *Nucl. Phys.* **A441**, 491

Hansen, G., Jensen, A.S. 1983, *Nucl. Phys.* **A406**, 236

Hilf, E.R., von Groote, H., Takahashi, K. 1976, in *Proc. Third International Conference on Nuclei far from Stability* (CERN 76-13, Geneva), p. 142

Hill, D.L., Wheeler, J.A. 1953, *Phys. Rev.* **89**, 1102

Hillebrandt, W., Takahashi, K., Kodoma, T. 1976, *Astron. Astrophys.* **52**, 63

Hillman, M., Grover, J.R. 1968, *Phys. Rev.* **185**, 1303

Hodgson, P.E. 1983, *Contemp. Phys.* **24**, 491

Hodgson, P.E. 1990, *Contemp. Phys.* **31**, 295

Holmes, J.A., Woosley, S.E., Fowler, W.A., Zimmerman, B.A. 1976, *At. Data Nucl. Data Tables* **18**, 306

Howard, W.M., Mathews, G.J., Takahashi, K., Ward, R.A. 1986, *Astrophys. J.* **309**, 633

Huizenga, J.R., Vonach, H.K., Katsanos, A.A., Gorski, A.J., Stephan, C.J. 1969, *Phys. Rev.* **182**, 1149

Huizenga, J.R., Moretto, L.G. 1972, *Ann. Rev. Nucl. Sci.* **22**, 427

Ignatyuk, A.V., Stavinskii, V.S. 1970, *Sov. J. Nucl. Phys.* **11**, 674

Ignatyuk, A.V. 1975, *Sov. J. Nucl. Phys.* **21**, 10

Ignatyuk, A.V., Smirenkin, G.N., Tishin, A.S. 1975, *Sov. J. Nucl. Phys.* **21**, 255

Ignatyuk, A.V. 1985, IAEA report, INDC (CCP)–233/L

Ivascu M., Avrigeanu, V., Avrigeanu, M. 1987, *Rev. Roum. Phys.* **32**, 697

Jensen, A.S., Sandberg, J. 1978, *Physica Scripta* **17**, 107

Jorissen, A., Arnould, M. 1986, in *Advances in Nuclear Astrophysics*, eds. E.Vangioni-Flam et al. (Editions frontières, Gif-sur-Yvette), p. 419

Jorissen, A., Arnould, M. 1989, *Astron. Astrophys.* **221**, 161

Käppeler, F., Beer, H., Wisshak, K. 1989, *Rep. Prog. Phys.* **52**, 945

Kataria, S.K., Ramamurhty, V.S., Kappor, S.S. 1978, *Phys. Rev.* **C18**, 549

Kataria, S.K., Ramamurthy, V.S. 1980, *Nucl. Phys.* **A349**, 10

Kataria, S.K. 1985, *Nucl. Phys.* **A437**, 397

Kennedy, R.C. 1966, *Phys. Rev.* **144**, 804

Klapdor, H.V., Oda, T. 1980, *Astophys. J. Lett.* **242**, L49

Kodoma, t., Takahashi, K. 1973, *Phys. Lett.* **43B**, 167

Kodoma, t., Takahashi, K. 1975, *Nucl. Phys.* **A239**, 489

Lang J.M., Le Couteur, K.J. 1954, *Proc. Phys. Soc. Lond.* **A67**, 586

Lattimer, J.M.B., Schramm, D.N. 1974, *Astrophys. J. Lett.* **192**, L145

Lattimer, J.M., Schramm, D.N. 1976, *Astrophys. J.* **210**, 549

LeBlanc, J.M., Wilson, J.R. 1970, *Astrophy. J.* **161**, 541

Madland, D.G., Nix, J.R. 1988, *Nucl. Phys.* **A476**, 1

Magner, A. G., Kolomietz, V.M., Strutinsky, V.M. 1978, *Sov. J. Nucl. Phys.* **28**, 764

Mathews G.J., Mengoni, A., Thielemann, F.-K., Fowler, W.A. 1983, *Astrophys. J.* **270**, 740

Mayle, R.W., Wilson, J.R. 1988, *Astrophys. J.* **334**, 909

Merrill, P.W. 1952, *Science* **115**, 484

Meyer, B.S., Howard, W.M., Mathews, G.J., Takahashi, K., Möller, P., Leander, G.A. 1989a, *Phys. Rev.* **C39**, 1876

Meyer, B.S., Möller, P., Howard, W.M., Mathews, G.J. 1989b, in *50 Years with Nuclear Fission*, ed J. Behrens (American Nuclear Society), p. 587

Möller, P., Nix J.R. 1988, *At. Data Nucl. Data Tables* **39**, 213

Möller, P., Myers, W.D., Swiatecki, W.J., Treiner, J. 1988, *At. Data Nucl. Data Tables* **39**, 225

Möller, P., Nix, J.R. 1990, *Nucl. Phys.* **A520**, 369c

Möller, P., Randrup, J. 1990, *Nucl. Phys.* **A514**, 1

Moretto, L.G., Stella, R., Caramella Crespi, V. 1970, *Energ. Nucl.* **17**, 436

Moretto, L.G. 1972, *Nucl. Phys.* **A185**, 145

Moretto, L.G. 1972a, *Phys. Lett.* **38B**, 393

Moretto, L.G. 1974, *Nucl. Phys.* **A226**, 9

Moretto, L.G., Kataria, S.K. 1974, *Letterrer Al Nuovo Cimento* **9**, 190

Mughaghab, S.F., Divadeenam, M., Holden, N.E. 1981, *Neutron cross-sections* (Academic Press, New York)

Mühlschlegel, B. 1959, *Z. Phys.* **155**, 313

Myers, W.D., Swiatecki, W.J. 1966, *Nucl. Phys.* **81**, 1

Myers, W.D., Swiatecki, W.J. 1967, *Ark. Fys.* **36**, 343

Myers, W.D., Swiatecki, W.J. 1974, *Ann. Phys.* **84**, 186

Myers, W.D. 1976, *At. Data Nucl. Data Tables* **17**, 412

Nemirovsky, P.E., Adamchuck, Yu. V. 1962, *Nucl .Phys.* **39**, 551

Newton, T.D. 1956, *Can. J. Phys.* **34**, 804

Nilsson. S.G., Tsang, C.F., Sobiczewski, A., Szymanski, Z., Wycech, S., Gustafson, C., Lamm, I.L., Möller, P., Nilsson, B. 1969, *Nucl. Phys.* **A131**, 1

Ormand, W.E., Bortignon, P.F., Bracco, A., Broglia, R.A. 1989, *Phys. Rev. C* **40**, 1510

Pearson J.M., Aboussir, Y., Dutta, A.K., Nayak, R.C., Farine, M., Tondeur, F. 1991, *Nucl. Phys.* **A528**, 1

Prakash, M., Wambach, J., Ma, Z.Y. 1983, *Phys. Lett.* **128B**, 141

Prantzos, N., Arcoragi, J.-P., Arnould, M. 1987, *Astrophys. J.* **315**, 209

Prantzos, N., Arnould, M., Cassé, M. 1988, *Astrophys. J.* **331**, L15

Prantzos, N. 1989, in *Research Reports in Physics: Nuclear Astrophysics*, Eds M. Lozano, M. Gaillardo, J. Arias (Springer-Verlag), p. 1

Ramamurthy, V.S., Asghar, M., Kataria, S.K. 1983, *Nucl. Phys.* **A398**, 544

Reisdorf, W., Töke, J. 1981, *Z. Phys. A* **302**, 183

Rickayzen, G. 1965, *Theory of Superconductivity*, Interscience Monographs and Texts in Physics and Astronomy, Vol 14. (Interscience Publishers, New York)

Ring, P., Schuck, P. 1980, *The Nuclear Many-Body Problem* (Springer-Verlag, New York)

Rolfs, C., Rodney, W.S. 1988, *Cauldrons in the Cosmos* (The University of Chicago Press, Chicago)

Sano, M., Yamasaki, S. 1963, *Prog. Theor. Phys.* **29**, 397

Sano, M., Wakai, M. 1972, *Prog. Theor. Phys.* **48**, 160

Schmidt, K.H., Delagrange, H., Dufour J.P., Cârjan, N., Fleury, A. 1982, *Z. Phys. A* **308**, 215

Seeger, P.A., Fowler, W.A., Clayton, D.D. 1965, *Astrophys. J. Suppl.* **11**, 121

Siemens, Ph. J., Sobiczewski, A. 1972, *Phys. Lett.* **41B**, 16

Staudt, A., Bender, E., Muto, K., Klapdor, H.V. 1990, *At. Data Nucl. Data Tables* **44**, 79

Strutinsky, V.M. 1967, *Nucl. Phys.* **A95**, 420

Strutinsky, V.M., Magner, A.G. 1976, *Sov. J. Part. Nucl.* **7**, 138

Strutinsky, V.M. 1989, *Nucl. Phys.* **A502**, 67c

Symbalisty, E.M.D., Schramm, D.N., Wilson, J.R. 1985, *Astrophys. J. Lett.* **291**, L59

Symbalisty, E.M.D., Schramm, D.N. 1982, *Astrophys. Lett.* **22**, 143

Takahashi, K., Yamada, M. 1969, *Prog. Theor. Phys.* **41**, 1470

Takahashi, K., Yamada, M., Kondoh, T. 1973, *At. Data Nucl. Data Tables* **12**, 101

Thielemann, F.-K., Arnould, M., Hillebrandt, W. 1979, *Astron. Astrophys.* **74**, 175

Thielemann, F.-K., Arnould, M., Truran J.W. 1986, *Advances in Nuclear Astrophysics*, eds. E.Vangioni-Flam et al. (Editions frontières, Gif-sur-Yvette), p. 525

Töke, J., Swiatecki, W.J. 1981, *Nucl. Phys.* **A372**, 141

Tondeur, F. 1978, *Nucl. Phys.* **A303**, 185

Tondeur, F. 1979, *Nucl. Phys.* **A315**, 353

Tondeur, F. 1983, *Phys. Lett.* **123B**, 139

Tondeur, F., Dutta A.K., Pearson, J.M., Behrman, R. 1987, *Nucl. Phys.* **A470**, 93

Tondeur, F. 1991, private communication

Truran, J.W. 1972, *Astrophys. Space Sci.* **18**, 306

Vogel, P., Jonson, B., Hansen P.G. 1984, *Phys. Lett.* **139B**, 227

Vonach, H., Uhl, M., Strohmaier, B., Smith, B.W., Bilpuch, E.G., Mitchell, G.E. 1988, *Phys. Rev.* **C38**, 2541

Wapstra, A.H., Audi, G. Hoekstra, R. 1988, *At. Data Nucl. Data Tables* **39**, 281

von Weizsäcker, C.F. 1935, *Z. Phys.* **96**, 431

Woosley, S.E., Fowler, W.A., Holmes, J.A., Zimmerman, B.A. 1979, *At. Data Nucl. Data Tables* **22**, 371

Zeldes, N., Grill, A., Simievic, A. 1967, *Mat. Fys. Skr. Dan. Vid. Selsk.* **3**, No. 5